LANDSCAPE AND BIOTIC EVOLUTION OF THE KOCHKOR BASIN, KYRGYZSTAN

by

WIN NADIA FRANCIS MCLAUGHLIN

A DISSERTATION

Presented to the Department of Earth Sciences
and the Graduate School of the University of Oregon
in partial fulfillment of the requirements
for the degree of
Doctor of Philosophy

June 2018

DISSERTATION APPROVAL PAGE

Student: Win Nadia Francis McLaughlin

Title: Landscape and Biotic Evolution of the Kochkor Basin, Kyrgyzstan

This dissertation has been accepted and approved in partial fulfillment of the requirements for the Doctor of Philosophy degree in the Department of Earth Sciences by:

Samantha Hopkins	Chairperson
Edward Davis	Core Member
Stephen Frost	Core Member
Ray Weldon	Core Member
Stephen Dueppen	Institutional Representative

and

Sara D. Hodges	Interim Vice Provost and Dean of the Graduate School

Original approval signatures are on file with the University of Oregon Graduate School.

Degree awarded June 2018

DISSERTATION ABSTRACT

Win Nadia Francis McLaughlin

Doctor of Philosophy

Department of Earth Sciences

June 2018

Title: Landscape and Biotic Evolution of the Kochkor Basin, Kyrgyzstan

Kyrgyzstan is the single most seismically active country in the world. Accessing the past, and therefore future hazard of faults, necessitates a high-resolution understanding of the timing of different geologic events. With no radiometrically datable rocks from the Neogene of Kyrgyzstan, I herein present the first work formally describing Neogene vertebrate faunas from the Kochkor Basin of Kyrgyzstan. I utilize a combination of biostratigraphy and magnetostratigraphy to constrain the timing of when the vertebrate assemblages were emplaced, and have dated the three bone beds to all fall in the latest Miocene, spanning 9-5 million years ago. All four bone beds represent mass death assemblages, inferred to be from drought-caused mortality. The timing of the deposits corresponds to uplift in the Pamirs, Himalayan, and greater Tibetan Plateau, which would have blocked the Indian monsoon from reaching Central Asia, forever altering the climate and biota of the region. This change is reflected in the shifting mammals faunas, as evidenced by the novel rhinocerotid I describe in a phylogeographic context.

CURRICULUM VITAE

NAME OF AUTHOR: Win Nadia Francis McLaughlin

GRADUATE AND UNDERGRADUATE SCHOOLS ATTENDED:

University of Oregon, Eugene
University of the Pacific, Stockton, California

DEGREES AWARDED:

Doctor of Philosophy, Earth Sciences, 2018, University of Oregon
Master of Science, Geology, 2012, University of Oregon
Bachelor of Science, Environmental Science, 2010, University of the Pacific

AREAS OF SPECIAL INTEREST:

Vertebrate Paleontology
Neotectonics
Field Geology
Biogeography

PROFESSIONAL EXPERIENCE:

Instructor, University of Oregon, 2016-2017

Teaching Assistant, University of Oregon, 2012-2018

Condon Collections Curator, Museum of Natural and Cultural History, University of Oregon, 2012-2017

English Language Instructor, American Corners, U.S. Embassy Bishkek, Kyrgyzstan, February-October 2015

Osteological Consultant, SWCA Environmental Consultants, July-August 2012

GRANTS, AWARDS, AND HONORS:

Jackson Travel Grant, Society of Vertebrate Paleontology, 2017

Mountain Research Grant, American Alpine Club, 2017

Student Research Award, Geological Society of America, 2016

Ewart Baldwin Scholarship, University of Oregon, 2001, 2012, 2014, 2016

Best Student Proposal, Paleontological Society, 2015

Student Researcher Grant, Fulbright, 2014

1st in the 3-Minute Thesis, University of Oregon, 2014

Condon Scholarship, University of Oregon, 2014

Student Research Grant, Society of Sedimentary Geology, 2014

Welles Fund Travel and Research Grant, University of California Berkeley, 2013

Student Travel Grant, Geological Society of America, 2013

Theodore Roosevelt Grant, American Museum of Natural History, 2013

Student Research Grant, Department of Geological Sciences, UO, 2013

Research Grant, Evolving Earth, 2012

PUBLICATIONS:

McLaughlin, W.N.F., S.S.B. Hopkins, and M.D. Schmitz. 2016. A new Late Hemingfordian vertebrate fauna from Hawk Rim, Oregon, with implications for biostratigraphy and geochronology. Journal of Vertebrate Paleontology, 35(5); e1201095.

ACKNOWLEDGMENTS

I wish to express sincere appreciation to my adviser Samantha Hopkins and to Ray Weldon for becoming my bonus adviser. Thanks is also needed for all the rest of my committee for their advice, insight, and support throughout my graduate school education. Kanatbek Abdrakhmatov, my Kyrgyz collaborator, for both scientific advice and facilitating nearly all the fieldwork presented on herein. Thank you to all the collections managers who provided me with access to comparative specimens and great scientific discussions, such as P. Holroyd at the UCMP, Chris Conroy at the UCMVZ, Amanda Millhouse at the NMNH, Jan Ove R. Ebbestad at the Uppsala Universitat Museum of Evolution, and Judy Galkin at the AMNH. Pat Ward prepared the rhino skull and jaws featured in Chapter 4 and the juvenile *Hipparion* mandible in Chapter 2, and without his painstaking artistry reconstructing the fossils, much of this work would have been impossible. Liz White illustrated the rhinoceros in a beautiful reconstruction, and helped facilitate all opportunities thus far to display Kyrgyz mammal fossils to the public. A huge “thank you” is needed to all of my past and current lab mates for the support and scientific discussions, including John Orcutt, Meaghan Wetherell, John Jacisin, Kristen MacKenzie, Dana Reuter, Genevieve Perdue, Paul Barrett, Nick Famoso, Leonard Finkelstein, Kellum Tate Jones, Holley Flora. Thank you to the students whom I have had the privilege of helping advise, and especially for all of the too many hours you have spent gluing broken Kyrgyz fossils back together or stripping the flesh from roadkill, including Márti May, Selina Robson, Eva Bierdron, Caitlyn Boatman, Julien Royer, Adi Chainey, Rafael Newman, Dylan Carlini, Holley Flora. My family and friends are also deserving of thanks, especially my parents who encouraged me to pick up dead birds and

poke dead things on the beach. A ginormous thank you to all the people who have assisted me in fieldwork including Meaghan Wetherell, Ryan Seward, Zach Buehler, Brian Meyers, Michael Elizabeth, Kyle Haggart, Azat Moldobaev, Kyle Olsen, Rebecca Cramerus, Win Francis, Alana Francis, Ben Alldritt, Dylan Colón. Thank you to Azis Kubanychbek Uulu and Nazgul Ibraimova for help locating sites, and translation, as well as Elin Irgistseva and David Zakharov for translation. Thanks (I think) to Falling Sky, for opening a brewery across from my office and providing the writing and editing "fuel" needed to finish. The investigation was supported in part by a Fulbright Student Research Grant to the Kyrgyz Republic, a Sedimentary Geology Student Research Grant, the Paleontological Society Best Student Research Proposal, and significant funding from the Department of Earth Sciences at University of Oregon.

To Killian, who is just a cat, and that's all he has to be.

TABLE OF CONTENTS

Chapter Page

I. INTRODUCTION 1

II. TAPHONOMY OF FOUR MASS DEATH ASSEMBLAGES IN THE KOCHKOR BASIN KYRGYZSTAN; TEASING APART LANDSCAPE AND CLIMATIC CHANGE 7

Introduction 7

Neogene Mass Death Assemblages of Kyrgyzstan 8

Geologic Setting 10

Methods 11

Data and Analyses 17

Systematic Paleontology 24

Institutional Abbreviations 24

Faunal List and Count by Site 25

Results 54

Conclusions 65

Transition 70

II. BIOSTRATIGRAPHY AND MAGNETOSTRATIGRAPHY OF THE KOCHKOR BASIN KYRGYZSTAN; INSIGHTS INTO UPLIFT OF THE TIEN SHAN 72

Introduction 72

Methods 78

Geology 78

Magnetostratigraphy 79

Biostratigraphy 84

Chapter Page

Results 85

Geology 85

Magnetostratigraphy 89

Biostratigraphy 101

Disscussion and Conclusion 106

Transition 112

IV. A NEW CHILOTHERE (MAMMALIA, RHINOCEROTIDAE) FROM THE NEOGENE OF KYRGYZSTAN, WITH IMPLICATIONS FOR PHYLOGENY AND BIOGEOGRAPHY OF THE RHINOCEROTID FAMILY 113

Introduction 113

Materials and Methods 116

Paleontology 116

Phylogenetic Analysis 119

Systematic Paleontology 121

Description 122

Disscussion 132

Assignment to *Chilotherium* 132

Comparison to other *Chilotherium* Species 132

Comparisons to other Rhinocerotids 135

Phylogenetic Analysis 138

Paleoecology 142

Conclusions 144

Chapter Page

V. CONCLUSION 146

APPENDICES 148

A. VODKA BONE BED (UO-4603) 148

B. ORTOK BONE BED (UO-4605) 152

C. BONE HILL BONE BED (UO-4601) 158

D. DAM SITE BONE BED (UO-4604) 164

E. UNCORRECTED STRIKE AND SUN COMPASS READINGS 167

F. P-MAG SAMPLE COLLECTION FIELD DATA 170

G. SQR FILE FOR ORTOK WITH RATINGS 177

H. SQR FILE FOR KOCHKOR EAST (KSS) WITH RATINGS 180

I. DAM SITE (KDS) FIELD DATA AND RATINGS WITH FOLD TEST 182

J. KARA SUU (KSU) FIELD DATA AND RATINGS 185

K. SOURCES FOR MATERIAL INCLUDED IN COMPARISONS AND PHYLOGENETIC ANALYSIS 189

L. PHYLOGENETIC CHARACTERS AND DESCRIPTIONS 192

REFERENCES CITED 213

LIST OF FIGURES

Figure Page

1. Map of central and southern Asia, showing modern country boundaries for Kyrgyzstan 3
2. Cervidae (deer family) and Bovidae (antelope family) mandibles figures in Tarosov 1970. 4
3. Google Earth imagery of the Kochkor and Issyk Kul Basins 12
4. Simplified composite stratigraphic column for Kyrgyz bone beds 13
5. Examples of cervid dental material 32
6. Three teeth, the p2, p3, and m3, of a samothere giraffe 35
7. Palate of F-70400, a palaeomerycid 38
8. Proportions of vertebrate guilds represented at each site 55
9. Faunal representatives at a family level for each locality 56
10. *Hipparion* mandible and *Chilotherium* tibia as discovered in situ at the Vodka locality 58
11. Plot of element completeness, an indicator or weathering, transport distance, and degree of carcass processing 59
12. Length measurements (L1) for all elements 63
13. Plots of flatness (L3/L2) to columnarity (L3/L1) 64
14. Grouping the distribution of elements into rough body position categories more clearly illuminates gross trends in element distribution 65
15. Juvenile *Hipparion* mandible from Ortok 66
16. Global seismic hazard map of Asia, location of Kyrgyzstan shown 73
17. Google Earth imagery of the Kochkor Basin, Kyrgyzstan 74
18. Map of all documented occurrences of fossil localities in Kyrgyzstan and surrounding areas reported in the Paleobiology Database 77

Figure Page

19. Sampling methodology for collecting paleomagnetic samples in soft sediments . 80

20. Schematic and generalized stratigraphic column for the Cenozoic formations outcropping in the Kochkor Basin 85

21. Google Earth imagery of the Ortok 87

22. Geologic map of the Kochkor Basin..... 88

23. Example demagnetization pathways for four samples of varying quality..... 90

24. Stratigraphic section for the KSS section including the bone bed Bone Hill 92

25. Alpha 95 plots of the overprint (bottom) and primary (top) for the Kochkor East extension (KSS) 94

26. Stratigraphic section for the Kara Suu (KSU) section containing the Vodka bone bed locality..... 95

27. Stereonet plots of Kara Suu (KSU) showing the primary and overprint polarities..... 96

28. Fold test conducted at the base of the Dam Site (KDS) section 97

29. Alpha 95 plots of the overprint (top) and primary (bottom) for the Dam Site (KDS)..... 98

30. Stratigraphic section for the Dam Site fossil site..... 99

31. Stereonet plots of Ortok (KO) showing the primary and overprint polarities 100

32. Stratigraphic section for Ortok..... 101

33. Biostratigraphic ranges for each of the four bone beds 106

34. Fence diagram of the four measured stratigraphic sections..... 108

35. Outcrops with a clear relationship between the Chu Formation and the Sharplydak Formation..... 106

36. Temporal relationship of the four novel paleomagnetostratigraphic sections from this study and the two previously existing sections from the Kochkor Basin 107

Figure Page

37. Reinterpretations of both the geology in map view and the interpretation of both magnetochron and sedimentation rate 109

38. Composite column as this study reinterprets the Wack (et al., 2014) data, presenting a new and younger range for sections 110

39. Composite stratigraphic column of Neogene sediments in the Kochkor Basin, Kyrgyzstan, showing the stratigraphic ranges of rhinocerotid fossils 114

40. Google Earth imagery of the Kochkor Basin Kyrgyzstan, with an overlay of some geologic mapping 115

41. Distribution, both temporally and geographically, of Rhinocerotidae fossils 116

42. Google Earth view of the Kara Suu Valley denoting where the stratigraphic section was measured as well as the location of the Vodka bone bed 117

43. Top, dorsal view of the Vodka taxon skull in situ, after the projecting nasals had been removed. Bottom, Left mandible exposed after the removal of the right mandible, in situ 118

44. Skull of the Shamsi taxon 123

45. Ventral view of the dentition 124

46. Dorsal view of the skull 125

47. Lateral views of the posterior-most portion of the skull 126

48. Occlusal view of the better preserved right lower dentition 129

49. Side by side comparison of the radia from the Vodka taxon and the Chu taxon ... 130

50. Consensus tree 140

51. Life reconstruction of the Shamsi *Chilotherium* 143

LIST OF TABLES

Table Page

1. Five categories of bone surface weathering 18

2. Metatarsal measurements for the giraffid from Ortok, with comparisons against several candidate fossil taxa and two modern taxa 36

3. Degree of weathering for elements at each site, using the categories of Shipman, 1981 and Gifford, 1980 57

4. Relative proportions of articulated to disarticulated material 60

5. Distribution of elements between the four bone beds in this study and several micro and macro fauna comparatives 61

6. Percent of age-identifiable material assigned to juvenile verses adult age classes for the four bone beds from this study (1) and compared to several other modern and fossil assemblages 62

7. Rating system for accessing quality of samples 83

CHAPTER I

INTRODUCTION

Kyrgyzstan, located in the heart of Central Asia, lies in important geographical and biological crossroads. Kyrgyzstan is a small country of just shy of 200,000 km^2 (CIA, 2017) and a population around 6 million (Kyrgyz National Census, 2017). With a human history dating back to the dawn of pastoralism, and the likely site for several domestication events including dogs and sheep (Shannon et al., 2015, Tapio et al., 2006), Kyrgyzstan's contribution to modern civilization is unquestionable; in the 20^{th} century Kyrgyzstan shifted from Turkic control to being incorporated into the Soviet Union. Only then did Westernization and modern industrialization really come to the broader region. While cultural context may seem unrelated to the broader geology and biological evolution of the region, the two are intimately linked, with the geography, topography, and ecological setting controlled by uplift.

Famed for the Silk Road, linking the Far East to Europe, Kyrgyzstan's historic trade route mirrors the much older paths ancient faunas took to disperse from their evolutionary cradles in the Tibetan Plateau (Deng et al., 2011) and beyond. Despite the evolutionary story told by such well known Neogene faunas as the Siwaliks, the Hipparion faunas of the Chinese red clays, and the Samos faunas, little paleontological work exists from Central Asia, the obvious geographic route of faunal exchange across Eurasia. Both the physical geography and the geopolitical history of the region prevented early exploratory work as early as Eurasia's key Neogene localities were discovered.

This is not to say that no paleontological work was conducted in Kyrgyzstan and surrounding countries, only that said work is severely limited and often in need of

modern revision. In addition to a lack of modern work, the region also has a high degree of modern edemicity, which likely stems from the unique geologic history. The Soviet Union payed great geological attention to Central Asia in the 1950s through 1970s, mostly for the possibility of the region supplying the USSR with natural resources (Smith, 1995). When Kyrgyzstan failed to offer productive sources of oil or natural gas, like those discovered in Kazakhstan, little attention other than academic treatment of the incredible neotectonic record was taken (Tarosov, 1970), despite the later realization that Kyrgyzstan is the single most seismically active country in the world (Abdrakhmatov et al., 2001). The first published mention of Neogene fossil faunas from Kyrgyzstan came from an exploratory geologic mapping study, a 1970 Soviet dissertation published in Russian out of Bishkek Kyrgyzstan (Tarosov, 1970). Through the aim of mapping the high-angle thrust faults forming the Tien Shan, vertebrate fossils were discovered in the Kochkor basin of Kyrgyzstan (Figure 1).

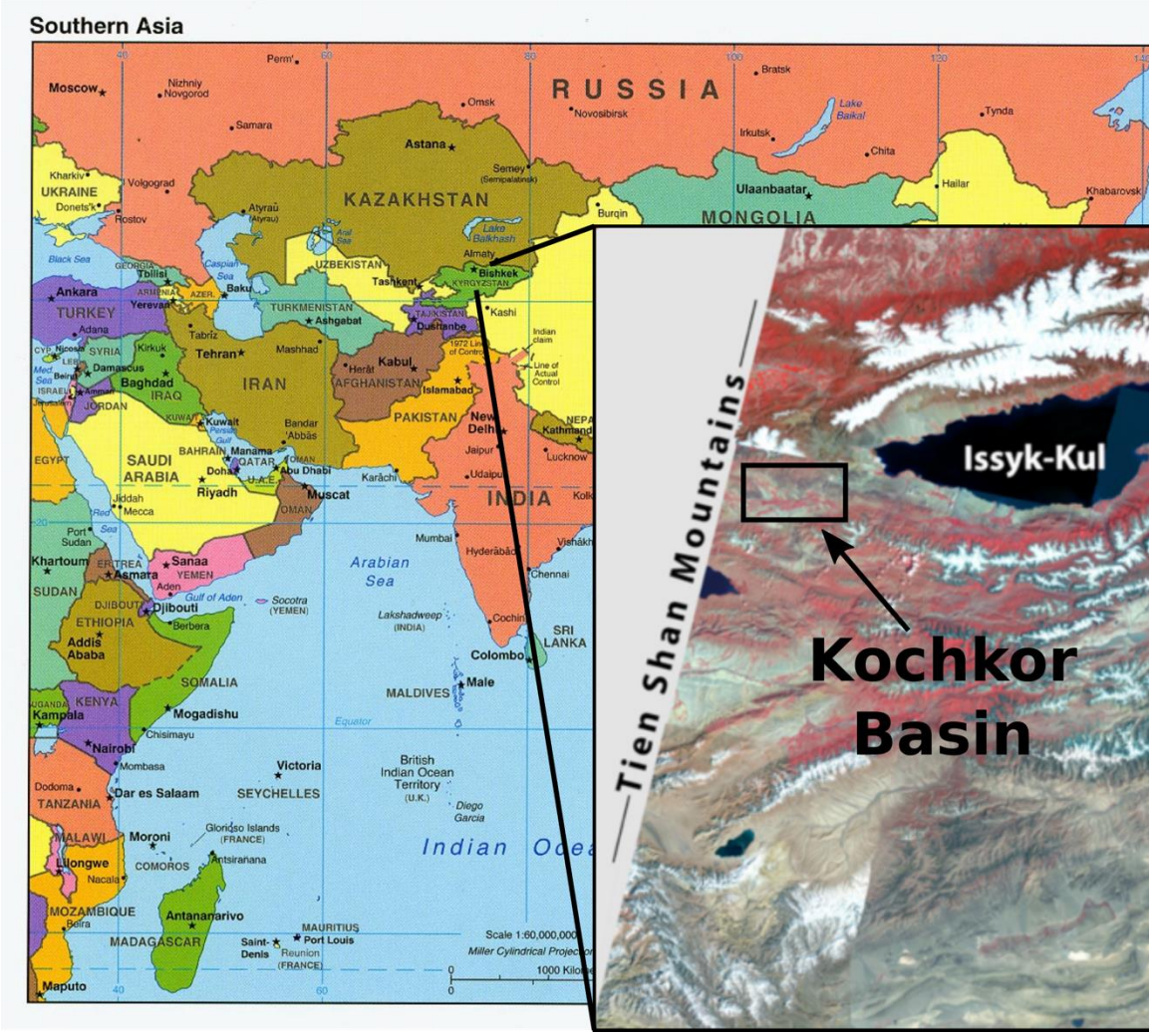

Figure 1: Map of central and southern Asia, showing modern country boundaries for Kyrgyzstan. False color LANDSAT image of the central Tien Shan range imposed on map, with the location of the Kochkor Basin indicated with a black rectangle. The low, and geologically recent, boundary between the Issyk-Kul Basin and Kochkor Basin seperates what was once a larger basin during the Neogene. Southern Asia (Political) 2004 map from UT Austin, and LANDSAT map modified from Paulson (2013).

This work included rough reference to localities ("in an area West of the Bijerty River", pp 60), identifications of taxa (though without description or justification of identifications), and some figured material in appendices (Figure 2).

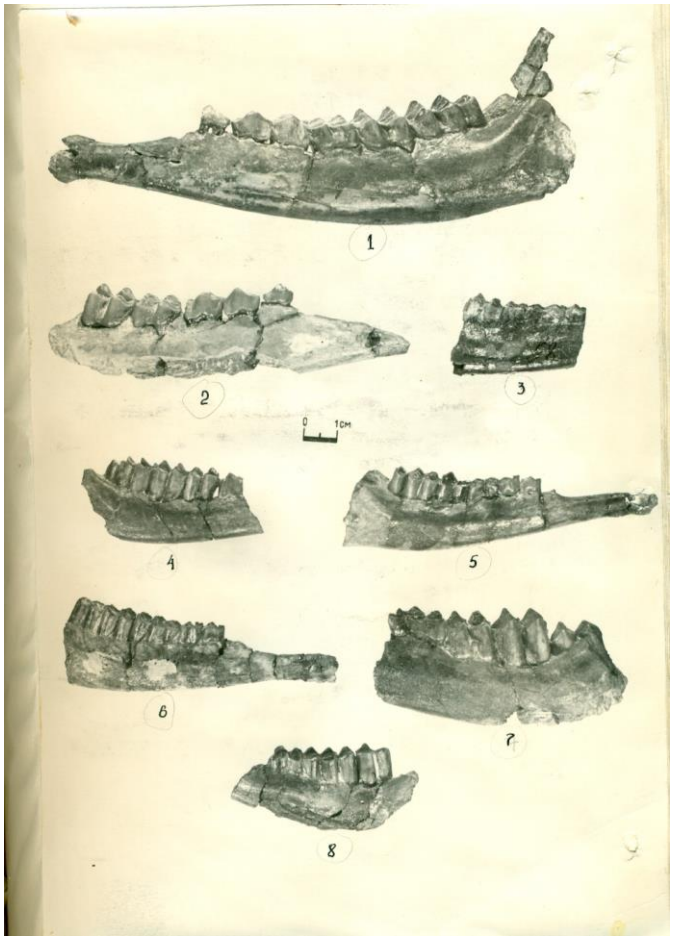

Figure 2. Cervidae (deer family) and Bovidae (antelope family) mandibles figure in Tarosov 1970. While figured, the specimens were never formally described, nor are the specimens reposited in an extant museum collection.

Little attention appears to have been paid to the fauna and the location or continued existence of the vertebrate material in question is now unknown, as it is not contained in the history museum in Bishkek, the paleontological collection in Almaty Kazakhstan, or in the Russian National collection in Moscow. In the 1960's two Eocene fossil localities were discovered, Toru Agur on the Northwest margin of Issyk Kul and Andarak, on the southwest Kyrgyz edge of the Fergana Valley. Some of the material was described and published (Belyaeva, 1962, Erfurt et al., 1999), although the location and continued existence of the fossil material from Toru Agur is also questionable. Material from the

more distant (to sites included in this study) locality Andarak, is largely reposited at the Zoological Institute, St. Petersburg. Finally, the formation of Kyrgyzstan as an independent nation in the 1990's resulted in increased Western collaboration and an attempt to synthesize some of the regional paleontological work (Averianov and Godinot, 2005, 1999, Erfurt et al., 1999). Sotnikova (et al., 1997) produced the first paleontological work, aimed at constraining regional biostratigraphy, although the work did not figure or describe any of the fossils discussed therein. Additionally, several Mesozoic vertebrates and Paleozoic invertebrate fossils were described in the past 25 years (Martin and Averianov, 2004, Gubanov et al., 1995, Averianov et al., 2007).

The increased post-Soviet Era Western attention, also led to extensive geologic mapping of Kyrgyzstan, with the aim of constraining uplift of the Tien Shan. Some of this data collection aims at constraining the large magnitude earthquakes driving the uplift. However, to predict initiation and modes of uplift, precise geochronology is vital. As the Tien Shan lie far from any volcanic center active the late Cenozoic, biostratigraphy offers one of the few geochronological options for temporally constraining the rest of the geological work. To the aim of providing a rough geochronological framework, American paleontologists were brought in on some of the larger-scale tectonics projects. Uplift also impacts regional climate, in turn impacting the deposition of sedimentary basin-filling sequences. Several large-scale gravel-progradation events seen across the Tien Shan are currently debated as either tectonic or climatic in origin. While the answer likely involves some of both factors, improved geochronology is also necessary to distinguish between causes, as tectonic-driven

progradation events would have transgressive boundaries depending on the sequence stratigraphy.

The work contained herein is a preliminary attempt to describe and diagnose Neogene faunas of the Kochkor Basin (Figure 1). Furthermore, the taphonomic work aims to provide context for such concentrated fossil deposits, as well as examine causal factors for mortality and how mortality pertains to changing landscapes and ecosystems. This record of change I temporally constrain using the combined geologic treatment of magneotstratigraphy and the biological approach of biostratigraphy. Finally, I delve into the taxonomy, evolutionary history, and biogeography of the most common family of mammals in the Kyrgyz fossil sites, the rhinoceros family.

CHAPTER II

TAPHONOMY OF FOUR MASS DEATH ASSEMBLEDGES IN THE KOCHKOR BASIN KYRGYZSTAN; TEASING APART LANDSCAPE AND CLIMATIC CHANGE

Introduction

Kyrgyzstan, in the heart of Central Asia, represents a transitional region from Asian ecosystems to European and Norther Asian steppe and woodland habitats not represented in the great Himalayan and Tibetan Plateaus. This frontier between markedly different climates, topographical settings, and biotic communities has existed back at least as far as the Miocene, and marks a narrow geographical area controlling the interchange of faunas between broad geographic areas. Vertebrate fossil assemblages therefore offer snapshots in time, illuminating the forces driving climate change, and biotic and landscape evolution. Taphonomic evaluation of these previously undescribed, or informally described, fossil assemblages showcases not only the rich Neogene faunas of Kyrgyzstan, but also the changing ecosystems driving many of the dispersal and turnover events within the region.

The Neogene vertebrate fossil assemblages of Kyrgyzstan have seen very little study since geologic survey work in the 1940-1960's revealed the presence of fossiliferous material (Tarosov, 1970, Balyaeva, 1948). While taxonomic evaluation of these new localities is needed and ongoing, taphonomy addresses why large bone bed deposits are cropping up throughout the Neogene stratigraphy. Taphonomic evaluation also filters our interpretations as to how communities changed through time in response

to shifting climates and mountain building events. With little previous work to build on, a taphonomic study is preliminary to understanding where and why fossils were accumulated in Kyrgyzstan, and potentially Central Asia as a gateway to and from the Tibetan Plateau and Central China.

Neogene Mass Death Assemblages of Kyrgyzstan: Previous publications on the Cenozoic paleontology of Kyrgyzstan is limited to descriptions of two Eocene localities (Averianov & Godinot, 1998, Erfurt et al., 1999), and some gray literature or unverified mentions of younger localities (Tarosov, 1970, Sotnikova et al., 2001, Balyaeva, 1948, Kuznetsov et al., 1964). While some preliminary fieldwork suggests most Kyrgyz basins produce Neogene vertebrate material, we have concentrated initial studies to the Kochkor Basin. Past work within this basin is limited to mentions of two Miocene localities in a Kyrgyz Soviet era PhD dissertation (Tarosov, 1970).

We have located numerous productive vertebrate localities throughout the Neogene deposits of Kyrgyzstan, some of which may be the same sites as visited by Tarosov. However, this study focuses on four bone bed localities that are thus far the most productive. The primarily mammalian fossil assemblages are dominated by large ungulate taxa, with representatives from Rhinocerotidae, Equidae, Cervidae, Bovidae, and Giraffidae forming much of the diversity. These bone bed localities have produced hundreds of specimens, and are far from quarried out.

Many geologic processes accumulate bones. Cave deposits and fissure fills, geomorphic features offering only one way in and no path of escape, are common features resulting in accumulation reflected in the fossil record (Shipman, 1981). Fluvial

processes, such as meander bend deposits, gravel bar accumulation, or over-bank flood deposits emplace fossil material in addition to sorting material by size, shape, and density (Shipman, 1981). Even progradation of alluvial fans provides the rapid accumulation of sediments necessary for fossilization. Biological methods of accumulating vertebrate material alter representation of elements and taxa, like carnivore dens or raptor roosts, yet these agents also concentrate material in terrestrial environments in volumes equivalent to geologic processes alone. Deducing the geologic or biotic mode of accumulation is important for deducing both the temporal and geographic range reflected in the bone bed. Does a bone bed represent slow attrition and accumulation within an environment or a more catastrophic mass death assemblage (Behrensmeyer et al., 2000)? For a bone bed to represent a true mass death assemblage, the input of carcasses into the system must overwhelm the environment's ability to process the carcasses (Behrensmeyer et al., 2000, Haynes, 1987), and "prime age", rather than aged, are most common (Hunt, 1990, Valli, 2005). Most of the modification and processing of bone is accomplished via carnivores and scavengers, with microorganisms and plants adding to alteration of bone surfaces. Evidence of scavenging, pre-fossilization weathering, degree of bone or skeletal completeness, age distributions, and several other factors are used to distinguish between accumulations of bones over great time and space and those from mass death assemblages. Different causes of death, such as drought (Haynes, 1987, Faith & Behrensmeyer, 2006), natural disasters (Haynes, 1987, Famoso & Pagnac, 2011), or carnivore accumulation (Haynes, 1987, Faith & Behrensmeyer, 2006, Maldonada et al., 2016) leave different taxonomic signatures as well.

Geologic Setting: The formation and uplift of the Tien Shan is derived from the collision of the Indian sub-continent into Asia. While the Himalayan mountains accommodate most the shortening, the continued convergence of the two plates generates more stress than the Himalayan mountains alone can accommodate (Sobel and Dumitru, 1997). Thus, the Tien Shan, the youngest result of the collision, has some of the highest uplift and convergence rates in the world (Abdrakhmatov et al., 2001). This convergence is accommodated across huge thrust faults, additionally resulting in the highest seismic hazard of any country in the world for Kyrgyzstan (Abdrakhmatov et al., 2001). The rapid uplift drives the Paleozoic-Mesozoic basement up and over the erosional deposits of the Cenozoic, with the older basement later eroding and providing the source material for the Neogene sedimentary sequences. High-angle thrust faults propagate into the larger basins, tilting and deforming the Cenozoic record. The resulting high-elevation basins produce nearly continuous records of deposition from the Eocene through the present. The rate of deposition into the basins reflects the rate of uplift, resulting in many kilometer-thick sequences exposed in most basins across the North to South transect of the Tien Shan. Currently the mode of uplift across the Tien Shan is heavily debated in modern tectonics literature. Whether the Tien Shan have uplifted as a geologic unit (Abdrakhmatov, et al., 2001) or with deformation and rates of uplift initiating at the margins and propagating inwards (Wack et al., 2014) is highly debated. The initial uplift model suggests transitional boundaries between widespread geologic formations is climatically driven, with the age of the formation boundaries being the same across like strata, while the propagating deformation model would suggest tectonically driven changes and thus different ages for similar lithological changes. While the work

presented in this study is limited to a single basin, and thus will not fully resolve this debate, both tectonic uplift rates and climatic change heavily impact the taphonomic signature of a site. Therefore, the first taphonomic studies of Kyrgyz Neogene fossil localities may have broader implications for tectonic processes.

Methods

With such a limited history of vertebrate fossil collecting in Kyrgyzstan, the total number of localities and distribution of fossiliferous material is still expanding and concentrated around areas with the most intensive fieldwork in the 2014 and 2015 seasons. As such, this study concentrates on only the four most fossiliferous of the total localities. Sites are primarily located through surface prospecting of geologically mapped (Abdrakhmatov et al., 2001, Paulson, 2013) Neogene strata. None of the localities discussed in this paper are "quarried out" and contain abundant material still *in situ*, and therefore the data presented herein should be considered preliminary and most importantly as a recommendation for continued collection in both the Kochkor basin and the Kyrgyz Neogene deposits. All five bone beds included in this study are within the Kochkor basin (Figure 3).

Most fossils included in this study are from large taxa, likely in part an artifact of our collecting techniques and the limited collection history in Kyrgyzstan. Small mammal taxa tend to be under sampled in sites that have not been screen washed, yet three of the four bone beds examined in this study do contain a few small mammal taxa. This difference in diversity is certainly not a reflection of paleoabundance, but a result of size-biased sorting in the geologic processes that accumulated the bones. Preliminary

geochronology based on biostratigraphy, magnetostratigraphy, and sequence stratigraphy (Chapter 3) suggests the fossil deposits discussed herein occur during a period of high sedimentation rate, resulting from rapid uplift, spanning several million years from the late Miocene through the Pleistocene. This places the Kyrgyz fossil localities not only in a crucial time range for constraining the possible acceleration of uplift in the Tien Shan, but also at a period of drastic climate change and shifting ecosystems. The bone beds included herein contain one locality from the Shamsi Formation (Vodka) and three (Bone Hill, Damn Site, Ortok) from the stratigraphically younger Chu Formation (Figure 4).

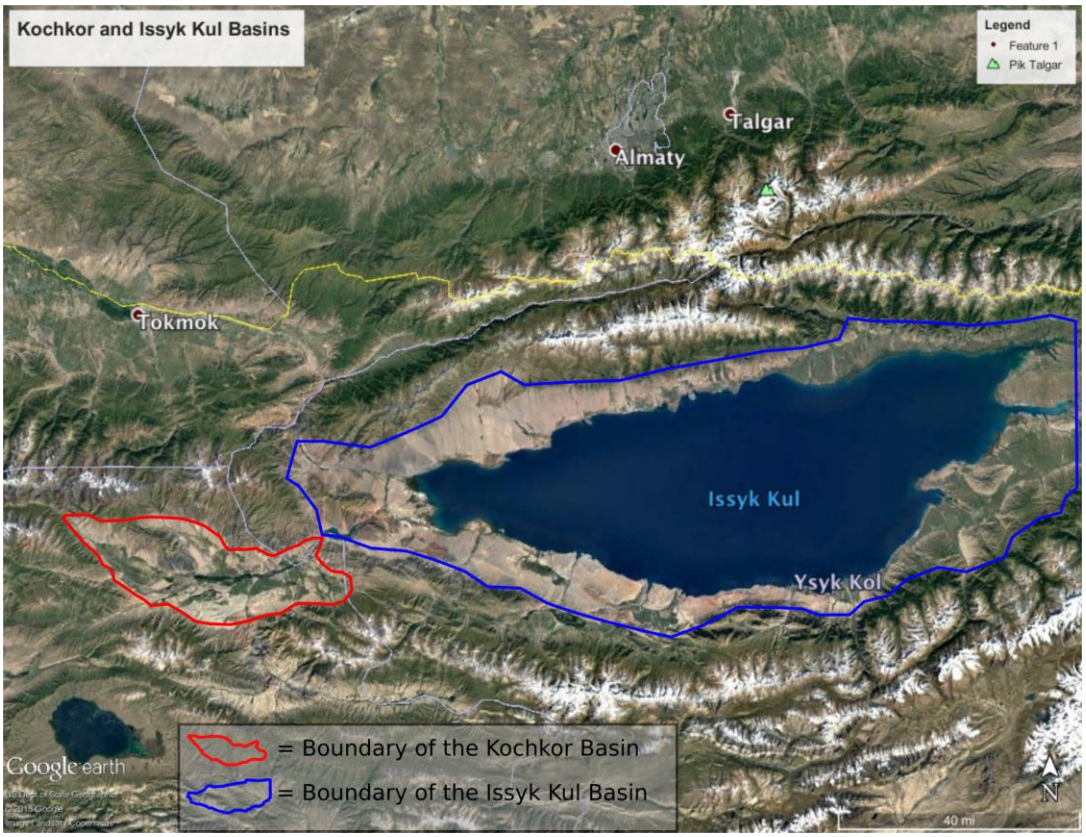

Figure 3. Google Earth imagery (accessed May 2018) of the Kochkor and Issyk Kul Basins. Likely, the Kochkor Basin was connected to the Issyk Kul Basin (the large lake in the figure) until geologically very recently, as shown by the low hills dividing the two basins. The Tien Shan mountains run roughly east-west, leaving high altitude basins infilled with Cenozoic sediments between each sub range. The Kochkor Basin is roughly 50 miles long and 15 miles wide.

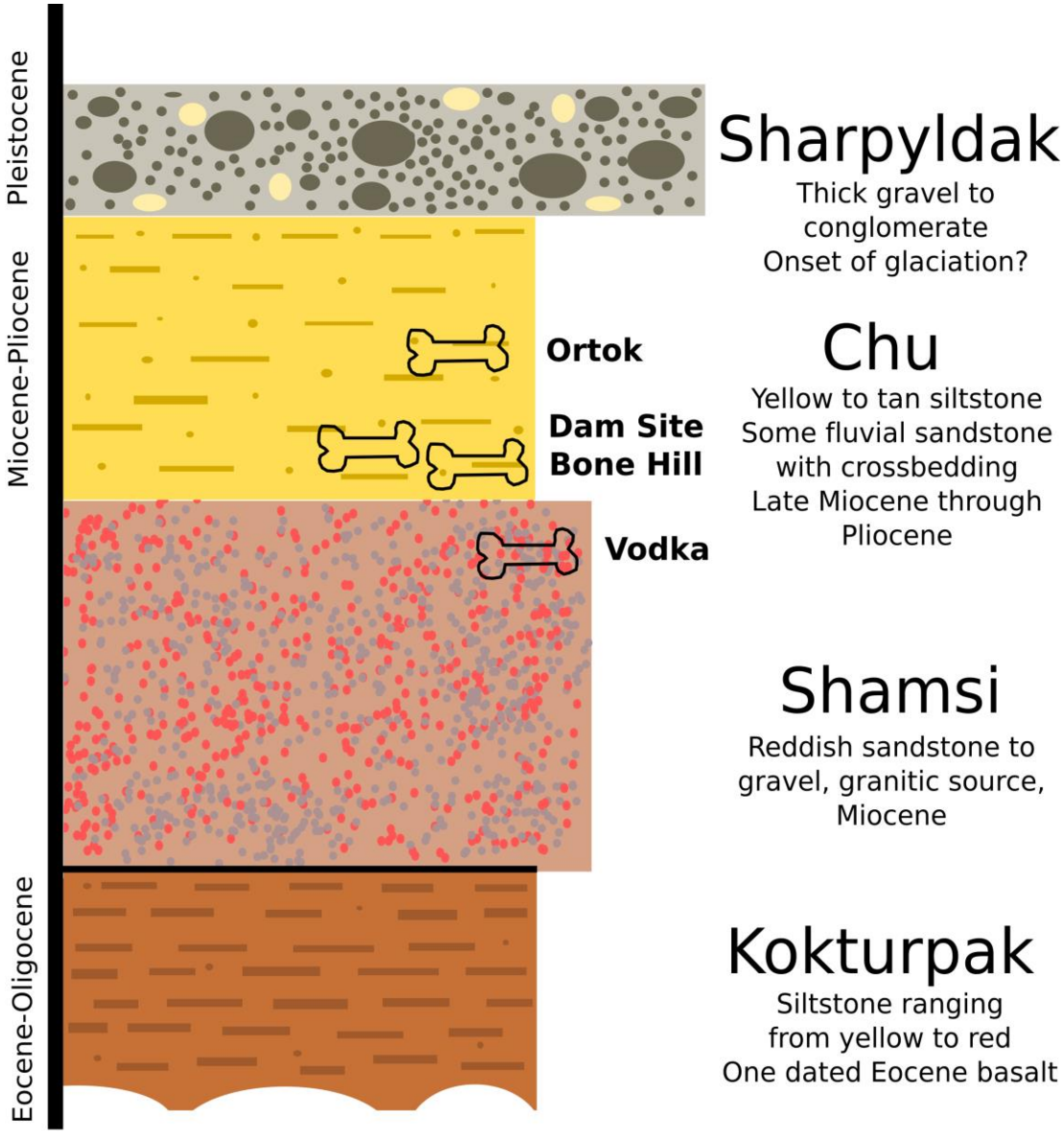

Figure 4. Simplified composite stratigraphic column for Kyrgyz bone beds. Most basins, including the Kochkor Basin, span the late Eocene to Pleistocene, with nearly continuous deposition. Most individual sections do not span the whole time period, but sections exist spanning each transitional boundary.

While the stratigraphic relationship of the three Chu Formation bone beds is also imperfectly constrained, previous geologic mapping in the basin (Paulson, 2013) and

ongoing paleomagnetic studies (Abdrakhmatov et al., 2001, Chapter 3) suggest a roughly contemporaneous age for Bone Hill and Dam Site, and a younger age for Ortok. As sampling at existing sites continues, and new localities are prospected, biostratigraphic resolution and therefore inferences into the paleoenvironment will improve.

Ortok, the only previously named locality, is referred to in both Tarosov (1970) and Sotnikova (et al. 2001), but in both cases the actual geographic location is vague. Sotnikova's map is on a regional scale, and Tarasov's description of the locality of fossiliferous Neogene deposits is "...North side of the basin, westerly… (in Russian)" (1970, pg. 60), leaving something to be desired in spatial precision. Ortok was relocated in 2012 by driving to the small village of Ortok, and then driving along the basin's northern margin westwards looking for outcrops of Neogene sediments. While the geographic extent and stratigraphic thickness of the locality is limited, Ortok represents the only outcropping Neogene stratigraphy on the Northern margin, thus we place reasonable certainty the locality is the same as referred to in Sotnikova and Tarosov. Tarosov further goes on to describe an additional fossiliferous outcrop "...West of the Bezjerty River…" (1970, pg. 60). Numerous days of fieldwork in 2014 yielded diffuse vertebrate material through much of the stratigraphy and one bone bed locality. The bone bed, Dam Site, was the only plentiful vertebrate material in the area, thus may represent the same locality as visited by Tarosov in the 1960's. Bone Hill was located by preliminary reconnaissance near previously published (Abdrakhmatov et al., 2001) paleomagnetostratigraphy sections in 2012, although was not realized to be a bone bed at that time. Quarrying at the site was conducted in 2014, although more material remains in situ at the locality. An additional bone bed, Rhino Party, was discovered in 2014 by

tracing the stratum containing Bone Hill over two ridges to the south, however this site has fewer fossils and very poor fossil preservation, and thus is not included in this study. Vodka was discovered by two Russian geologists mapping in the area in 2012 (E. S. Przhiyalgovsky, E. V. Lavrushina), when they discovered fragmented vertebrate material in a dry wash. The locality information, and fossiliferous material that had subsequently weathered into the wash facilitated locating the bone bed horizon in a cut bank in 2014, with excavations in both the 2014 and 2015 field seasons.

All bone beds were located or rediscovered via surface prospecting of Neogene deposits. Once the location of *in situ* material was determined, all bone beds referenced herein were quarried. The permitting and exportation requirements limited the field teams' ability to jacket fossil material, and difficulties in obtaining acetone for making conventionally used consolidants made it difficult to remove fossils intact from outcrops. At each quarry, all material identifiable to element was collected. Fragmentary material in close proximity to identifiable material was also collected, and even if deemed not associated, is included in this study. While an ideal taphonomic study would also include all fragmentary material for use in sorting analyses and for estimating transport, the limits imposed from transporting material from field sites to Bishkek and shipping to the USA resulted in our minimum collectable specimen standards. Wet screening for vertebrate microfauna has not yet been implemented at any Kyrgyz localities, although some microfaunal material is produced through quarrying and through later preparation of larger material out of matrix. While this certainly biases the fauna through underrepresentation of the microfauna, the authors' processing of matrix suggests microfauna are not a large percentage of any of the bone beds represented.

With few described faunas from Central Asia and many of the existing faunas in need of taxonomic reevaluation, little comparative material exists to facilitate identification of species, or in some cases even genera within the Kyrgyz faunas. Taxonomic descriptions of individual faunal units are further complicated by a high degree of endemicity in the greater Tibetan Plateau. Therefore, while diagnosis and description of the Kyrgyz faunas is vital and ongoing, it is at this time beyond the scope of the preliminary work presented here. Preliminary work suggests at least three of the taxa represent new species, namely the smaller hyena and both the Chu and Shamsi rhinocerotids (Robson et al., in prep, McLaughlin, chapter 4). For the sake of taphonomic analyses, taxa are diagnosed as possible species units within a family. For example, the equid present in the Shamsi Formation is smaller in stature, with less complicated plications in the enamel than the equid found in all Chu Formation localities. As both size and enamel folding complexity are frequently used to describe and diagnose equid taxa, it can thus be assumed that these represent different species, and will be treated as "Equid A" and "Equid B" for the time being. Headgear-possessing artiodactyls present a particular problem, when headgear and dental material are not found directly associated. While some risk of misdiagnosis is possible or even probable, artiodactyl material is lumped into taxonomic units at first a family level and then a size class level. In defense of this consolidation, each bone bed has only produced headgear from a maximum of one bovid, cervid, and giraffid, suggesting the assignment of dental material to more than one species in each family is also unlikely. The one exception is the presence of two different size classes of bovid present at Ortok. The very small stature (muntjac-sized) bovid is less than half the size of

the larger bovid, making distinguishing between the two size classes of bovids possible with all skeletal elements.

The diversity of taxa represented in a fauna is informative not only of paleoecological structure, but clues as to cause of death (Badgley, 1986). The makeup of faunas can be further broken down by guild, comparing ratios of carnivores to herbivores, a ratio useful for several paleoecological inferences (Van Valkenburgh, 1988). Body size of taxa represented are not a reflection of actual paleo community structure, but are informative of transport and depositional settings.

Data and Analyses:

Bone preservation illuminates both geologic and biologic processes related to the paleoecology of a site. Bone surface modification indicates how long individual elements weathered before final deposition, and therefore, taken across a bone bed, the length of time recorded in a single deposit. Weathering of bone pre-fossilization is characterized by cracking or spalling of bone, broken into five categories of weathering (see Table 1) (Shipman, 1981, Gifford, 1980).

	I	*II*	*III*	*IV*	*V*
Description of weathering state	Bone surface is smooth, lacks cracks, no sign of weathering	Bone surface has small cracks, less than 5mm in length, root traces possible less than 1mm in width	Cracks over 1 cm in length, root traces with a greater width or depth than 1mm, some cracks may be beginning to spall and peel away	Parallel cracks common, reaching length greater than 10 mm, spalling common, where sections of the bone surface are missing	Spalling is extensive, little of original bone surface remains, more interior levels of bone begin to develop a powdery texture
Inferred time on surface	0-6 months	6-12 months	1-2 years	2-3 years	Greater than 3 years

Table 1. Five categories of bone surface weathering from Shipman, 1981 and Gifford, 1980. All bones or bone fragments are assigned to one of the categories for each bone bed. Assessing the difference between stages I and II usually requires a hand lens or dissecting microscope to see depth and width of cracks and root traces.

This is useful on a first order for helping to distinguish between a mass death assemblage and other modes of bone accumulation, but also useful when paired with sedimentological rates of deposition to constrain any depositional hiatuses. Total time over which bones accumulated can also rule out certain types of deposition or paleoenvironments. Also included within the bone preservation category is abrasion, or physical damage resulting from transportation, such as rounding or polishing. Degree of abrasion is an indicator of transport distance, especially when combined with some of the other factors discussed like cylindricity. Additionally, abrasion (or lack thereof) is needed to rule out the possibility of reworking older bone or fossil material. Bone preservation was determined using a hand lens or dissecting scope to distinguish between pre-fossilization and post-fossilization bone wear, as root damage pre and post fossilization

leave different patterns on bone surfaces (Behrensmeyer, 1978, Cardoso et al., 2010), and many of the fossils displayed dendritic surface patterns resulting from plant roots exploiting the bones for phosphate. Only pre-fossilization bone-wear was considered for the weathering categorization.

Completeness of bones constrains the amount of time sampled from death to burial of elements, but also relates to degree of scavenging, rate of deposition, mode of transport and deposition, and causes of death. Completeness was evaluated by comparing a particular element to the same element from a modern representative of the family. The degree of completeness was assigned to the nearest 10%, rather than the 5% scale used in other studies (Calede, 2016, Moore and Norman, 2009), as preservation of the fossil material was worse than the comparative assemblages in terms of clay-mineral replacement of fossil material, and completeness was frequently impacted by both excavation and shipment despite the author's best efforts to conserve fossil material or at least record original degree of completeness. Fossils were grouped into three completeness categories: fragmentary (less than 50% complete), partial (50-90% complete), and complete (greater than 90% complete). This roughly follows Coombs and Coombs (1997), to fully characterize the average completeness of each deposit and differences and among taxa and bone beds. The degree of completeness was evaluated on an element assignment level. For example, while a maxilla is part of the skull, a complete maxilla would be rated as 100%, whereas a skull with only one maxilla present, but also parts of the basacrania, might be rated as 50%, following the element assignments of Calede (2016) and Lloveras et al. (2012). Completeness was assessed on all fossil

material assignable to a family level, but excluded fragmentary material only assignable to order or element without taxonomic distinction.

Finally, the shape and size of individual elements, when treated as particle or clast size, are important factors when determining mode of deposition, as well as climatic factors driving deposition. Shape and size were roughly, but uniformly, determined using three orthogonal measurements. The longest dimension became L1, a proxy for size, after work by Blob and Fiorillo (1996). While Blob and Fiorillo (1996) discussed element orientation in the context of microfaunal assemblages, Hanson's (1980) flume work suggests the longest dimension is most likely to determine transport distance and resting orientation during deposition of skeletal material, during fluvial processes, regardless of overall size of taxa. Shape was approximated with two other linear measurements to determine columnarity and flatness (Moore and Norman, 2009, Calede, 2016). Shape, in the general categories of flat, columnar, or compact, influences transport distance and therefore also sorting of skeletal material in bone beds (Boaz and Behrensmeyer, 1976). L2 is the longest measurement perpendicular to L1, and L3 is the shortest axis perpendicular to L2. Columnarity is measured as a ratio of the shortest axis (L3) to the longest axis (L1), with smaller values corresponding to more column-shaped bones or bone fragments. Flatness is measured as the ratio of the shortest axis to the median axis, or L3/L2, with smaller values corresponding to flatter bones or bone fragments. Measurements were collected with Mitutoyo Digimatic CD-8" CX calipers for all measurements under 8" and were rounded to the nearest millimeter. Measurements greater than 8" were collected with a meter stick, rounding to the nearest millimeter. These shape ratios were used to categorize the fossils into flat (specimens that have a

depth less than or equal to half their width), columnar (specimens that have a length at least 1.5 times their width), or compact (fit neither of the previous categories). If a specimen fit both the columnar and flat categorical test, then the larger ratio value was used for the categorical assignment.

The representation of different skeletal elements is important for determining both cause of mortality, but also mode of transport and deposition (Shotwell, 1955, Behrensmeyer, 1991). Elements were grouped into Cranial, Axial + Limb Girdles, Autopod, Zeugopod, and Stylopod categories. Therefore, data on distribution of skeletal elements was collected for each bone bed. Comparison to both modern and fossil large-animal-dominated faunas is included (Faith & Behrensmeyer, 2006, Haynes, 1988), as well as one microfauna site (Calede, 2016) as comparisons. Screen washing has not yet been possible with the Kyrgyz deposits, so the percentage of microfauna may increase with time and additional sampling. Within the modern comparatives, large mammal communities impacted by a variety of mass mortality events (Haynes, 1988) are included in an attempt to distinguish between accumulation agents. While many studies use minimum number of individuals (MNI), the preliminary nature of this study precludes sufficient sample sizes for this method to yet be meaningful, so we instead utilize NISP, or number of individual specimens present. Therefore, numbers of individual elements, regardless of siding on elements, is used in this study. The number of each skeletal element for each bone bed was used to calculate the relative abundance of the respective elements.

Skeletal elements were grouped by region of the body, following general categorization from other taphonomic studies (Haynes, 1988, Calede, 2016). Some

categories were further grouped for comparison, such as “long bones” after Faith & Behrensmeyer (2006) for comparison with large African drought killed faunas. Metacarpals and metatarsals were grouped together into metapodials, as incompleteness of the specimens frequently prevented an assignment to front or hind feet. Likewise, phalanges were grouped together. All carpals and tarsals, with the exclusion of the calcaneum and astragalus, were included in podials, with the addition of non-knee joint sesamoids for this study. While some of the comparative studies (Haynes, 1988) do not include sesamoids, they represented a relatively common skeletal element in the Kyrgyz material and thus were included in the podials category. All isolated sesmoids were compared to modern taxa, and if sesmoid position was not definitively from the distal portions of the limb, they were not included as an identified element. In keeping with other published studies (Haynes, 1988), maxillary fragments and horn cores were included in cranial elements, while mandibular fragments were counted individually. Isolated teeth or tooth fragments are treated as their own category, with no distinction made between upper and lower dentition, even when such a distinction was possible. As fragmentary remains of Rhinocerotidae teeth were so common in some of the Kyrgyz bone bed localities (Ortok especially) in the weathered surface material, the tooth fragments are grouped by field number rather than treating each fragment as an individual specimen. Lastly, the authors acknowledge the difficulty in assigning fragmentary ribs to taxon or even correctly placing the element, may have biased the selective sampling of the Kyrgyz bone beds away from this element. If elements were found in articulation, they have been given a single specimen number, yet for analysis of representation of different skeletal elements each individual element is counted even if

they belong to the same specimen number. Looking as representation of element or element categories does not necessitate assigning material to a taxon, thus it includes a higher total number of specimens than taxon based analyses.

All elements were categorized by approximate age at time of death. The categories used were juvenile and adult, although additional information such as fetal or aged individuals were noted when possible to assess, such as in the case of dental material. We used modern representatives of each family to compare tooth eruption sequences and tooth eruption age and order and age of epiphyseal fusion. This somewhat arbitrary breakdown biases our ability to compare age categories for some elements. For example, as the astragalus lacks epiphyseal plates, we are unable to assign the element to the juvenile category unless the element is found in articulation with elements distinguishable by age, and therefore elements lacking epiphyseal plates or dental elements were not assigned an age category. In the case of arthritic development, the degree and cause of arthritis was assessed before assignment. As nearly all Rhinocerod taxa possesses arthritic development by 7 million years ago (Stilson et al., 2016), and the bone beds span an estimated 6.5-8.5Ma, arthritic development on Rhinocerotidae bones was not deemed grounds for assignment to the adult category in those taxa. While the ability to assess age does vary from taxon to taxon, generally we looked for unfused epiphyses in long bones, unworn or excessively worn dentition, juvenile dentition, and in the case of some of the Artiodactyla the stage of horn or antler development. While we used fewer age classes than Voorhies (1969) or Valli (2005), we found the distinction between juvenile and adult animals a useful comparison, as average age, or over representation of juveniles is characteristic of certain agents of mortality and

accumulation. However, few elements other than dentition can be assigned to “aged adult” verses “prime adult”, thus we did not distinguish this category. Additionally, modern studies (Haynes, 1988, Faith & Behrensmeyer, 2006) suggest that juvenile material is common in mass mortality events, and a higher percentage of elderly adults than prime adults does not distinguish attritional deposits driven by large carnivores from mass death deposits as postulated by Palmqvist et al. (1996) relating proportion of juveniles to estimated body mass of adults as a marker of large predator kills. Differences in age distributions are important in distinguishing between mass death assemblages and other modes of carcass accumulation (Haynes, 1988).

While degree of completeness has already been discussed, the degree of articulation also matters in the Kyrgyz deposits. The presence (or absence) of articulated material offers information regarding rate of accumulation, degree of transport, mode of transport, and environmental conditions at time of deposition (Haynes, 1988, Behrensmeyer et al., 2000). Degree of articulation was assessed for each bone bed by specimen number to number of elements.

Systematic paleontology

Institutional Abbreviations: University of Oregon Museum of Natural and Cultural History, (UOMNH), Museum of Evolution Uppsala Universitet, Sweden (UUZM), University of California Berkeley, Museum of Paleontology (UCMP), Smithsonian Institute of Natural History, (NMNH), Texas Memorial Museum, and The University of Texas at Austin (TMM).

Faunal lists and count by site:

Site	Class	Order	Family	Genus	Spec. Count
Vodka					
	Mammalia	Artiodactyla	Bovidae	*Gazella*?	1
			Cervidae		9
			Indet.		3
		Perissadactyla	Equidae	*Hipparion*	4
			Rhinocerotidae	*Chilotherium*	47
		Rodentia	Cricetidae		1
		Indet.			24
	Reptilia	Testudines	Testudinidae		1
Dam Site					
	Mammalia	Artiodactyla	Bovidae	*Gazella*	11
			Giraffidae		1
			Indet.		2
		Lagomorpha	Ochotonidae		2
			Leporidae		4
		Perissadactyla	Equidae	*Hipparion*	2
			Rhinocerotidae	*Chilotherium*	13
		Indet.			4
Bone Hill					
	Mammalia	Artiodactyla	Bovidae		3
			Cervidae		27
			Indet.		3
		Perissadactyla	Equidae	*Hipparion*	14
			Rhinocerotidae	*Chilotherium*	21
			Indet.		1
		Indet.			25
	Reptilia	Squamata	Varanidae	*Varanus*	2
Ortok					
	Mammalia	Artiodactyla	Bovidae	*Gazella*	7
				Indet.	5
			Cervidae		6
			Giraffidae	*Samotherium*?	5
			Palaeomerycidae		1
			Indet.		4
		Perissadactyla			
			Equidae	*Hipparion*	12
			Rhinocerotidae	*Chilotherium*	49
			Indet.		4
		Carnivora			1
		Indet.			40

Class MAMMALIA Linnaeus, 1758

Order ARTIODACTYLA Owen, 1848

Family BOVIDAE Gray, 1821

Specimens: UOMNH F-70325 small distal metapodial, UOMNH F-70327 small right astragalus, UOMNH F-70328 small right astragalus, UOMNH F-70329 small distal phalanx, UOMNH F-70339 medium horn core, UOMNH F-70346 medium distal calcaneum, UOMNH F-71406 medium horn core, UOMNH F-71407 medium horn core, UOMNH F-71408 medium horn core, UOMNH F-71409 medium horn core, UOMNH F-71410 medium horn core, UOMNH F-71411 medium horn core (from UO-4605 Ortok). UOMNH F-64560 medium mandible section with p2-p3 (from UO-4603 Vodka). UOMNH F-64509 medium horn core base, UOMNH F-64639 medium mandible fragment with m1, UOMNH F-65618 medium base of horn core, UOMNH F-64457 medium horn core, UOMNH F-71402 medium horn core, UOMNH F-70340 medium horn core, UOMNH F-64539 medium horn core, UOMNH F-71404 medium horn core, UOMNH F-71403 medium horn core, UOMNH F-71405 medium horn core, UOMNH F-64462 medium horn core, UOMNH F-64463 tooth fragment, UOMNH F-70326 medium mandible fragment with m1-3 (from UO-4604 Dam Site). UOMNH F-64449 medium horn core, UOMNH F-64495 medium proximal metapodial, UOMNH F-64376 tooth fragment, UOMNH F-64384 medium mandible fragment with m3, UOMNH F-64373 medium mandible with p2-m1 (from UO-4601 Bone Hill).

Localities: UO-4605 Ortok, UO-4603 Vodka, UO-4604 Dam Site, UO-4601 Bone Hill.

Description: Fossil material represents two size classes of bovids, one being very small (muntjak-sized) and the other medium (gazelle-sized). The smaller post crania, the only

material currently assignable to the very small size-class bovid, is only found at Ortok, whereas the gazelle-sized material is produced at Ortok and The Dam Site primarily, with two partial horn cores from Bone Hill, and a mandibular section with two premolars from Vodka in the same size class, if not the same taxon. The horn cores are all roughly uniform in size and are ovate in cross section at the base. Each horn core curves slightly and uniformly tapers from the base to tip. The horn cores are covered in ridges running from the base to the tip, with each ridge remaining separate from neighboring ridges until at least half the total length of the horn core (as compared to the sole complete horn core), with the depth of individual ridges ranging from 1-2 millimeters at the base of the horn core and shallowing towards the tip. One specimen, UOMNH F-71410, preserves the complete horn core length and is the also the sole example to preserve attached cranial material. Part of the orbit is preserved, displaying the relationship of the horn cores to the orbits. The horn core is positioned dorsal to the orbit, with the anterior edge growing from the frontal bone after the anterior-most third of the orbit. The base of the horn cores is smooth, with the ridges beginning within 1 cm of the orbit and ending all along the same point on the horn core circumference. The rugose portion of the horn core does not project proximally, with no incision under the boss of the horn core as is seen in some bovids.

The astragali exhibit two keeled trochleae, parallel with the dorsal-ventral orientation for the bone. The trochlear keels are strongly pronounced, and the whole bone is rectangular. The two complete astragali are very small, with lengths of 22.4 and 20.2 mm. The metapodials are roughly “D-shaped” in cross section, with paired spools on the distal end. The distal spools have a strongly pronounced medial trochlea, each of which is

oriented parallel to the other, with uniform spacing between. The preserved portion of the phalanx (distal) is elongate and relatively gracile. It most likely represents a 1st phalanx, although without the proximal portion, this is difficult to positively establish. The dental material from Vodka preserves one mandibular section (UOMNH F-64560) with the p2-p3, as well as a small portion of the diastema. The premolars are small, lack rugosity in the enamel texture, and are mesodont. Dam Site dental material is limited to molars, and thus is difficult to compare to the premolars from other sites. Molars are hypsodont, lack rugosity, and are mediolateraly compressed.

Discussion: Even fragmentary horn cores could be assigned to Bovidae, as the ridges are far more linear and more deeply incised than those seen in cervid antler material, and the headgear of Giraffidae and Palaeomerycidae have a smooth surface texture lacking any ridges. The more complete horn cores also lack the pedicle seen in cervid antlers. The astragali were not only much smaller in size than any cervid material collected from Kyrgyzstan, the medial trochlea possesses a sharper edge than seen in even comparatively small cervids. The distal metapodial lacks the strong groove in the center of the anterior edge of the shaft seen in cervids, as well as being from a far smaller taxon than any of the cervid cranial or dental material. Because the smallest giraffid taxon in the family's evolutionary history is orders of magnitude larger than the largest material discussed in this section, that artiodactyl family can also seems highly unlikely.

Comparison to both modern and fossil material precludes the possibility of all bovid material belonging to a single taxon. The size differences between the horn cores and postcranial material is too great of a difference. The limited previous paleontological work in Kyrgyzstan notes the occurrence of *Gazella dorcadoides*, however this

assignment is given without description or justification. The horn cores are consistent in rough size class and curvature with the figured *Gazella dorcadoides* material figured in Tarosov (1970), but are larger than the type specimen's horn cores (Schlosser, 1903) and are more ovate in cross section (Zhang & Yang, 2016). The lack of associated dental and cranial material makes positive diagnoses difficult, as few quantitative approaches to categorizing or diagnosing interspecifc and intraspecfic variation currently exist (Chainey et al., in prep, Zhang & Yang, 2016). More complete material will be necessary for a conclusive assignment beyond *Gazella*, especially as the genus is one of the most diverse in *Hipparion* faunas (Zhang & Yang, 2016), and needs associated dental and horn core material.

No bovid material of a size class smaller than *Gazella* was previously reported from Ortok (Sotnikova et al., 2001), nor any of the Southern Kazakh localities (Sotnikova et al., 2001). Thus, the lack of cranial or dental material associated or even occurring at the site precludes even a generic level discussion at this point.

Family CERVIDAE Goldfuss, 1820

Specimens: UOMNH F-70333 two antler fragments, UOMNH F-70334 antler pedicle, UOMNH F-70356 antler fragment, UOMNH F-70380 antler fragment, UOMNH F-70390 antler fragment, UOMNH F-70423 radius (from UO-4605 Ortok). UOMNH F-64520 maxillary fragment with P4-M1, UOMNH F-64532 mandible fragment with fragments of two molars, UOMNH F-64533 mandible with p3-m3, UOMNH F-64534 scapula, UOMNH F-64535 metapodial, UOMNH F-64536 phalanx, UOMNH F-64537 proximal scapula, UOMNH F-64538 proximal femur and articulated acetabulum,

UOMNH F-64539 distal tibia (from UO-4603 Vodka). UOMNH F-70451 carpal, UOMNH F-64565 mandible fragment with p2-3, UOMNH F-70458 astragalus, UOMNH F-64443 proximal phalanx, UOMNH F-70456 antler fragment, UOMNH F-70471 two proximal phalanges, UOMNH F-64353 mandible with p2-m3, UOMNH F-64445 podial, UOMNH F-64402 antler fragment, UOMNH F-70446 mandible fragment with m3, UOMNH F-64372 phalanx, UOMNH F-64441 maxilla with P4-M2, UOMNH F-70452 antler fragment, UOMNH F-70463 mandible with m1-3, UOMNH F-70439 metapodial, phalanges, sesamoids, UOMNH F-70457 mandible with p2-m3, UOMNH F-64392 antler fragment, UOMNH F-64375 antler pedicle, UOMNH F-64346 phalanges, UOMNH F-64484 maxilla mold with M1-3, UOMNH F-64488 maxilla with P2-M3, UOMNH F-64545 mandible with m1-2, UOMNH F-70454 distal metapodial, UOMNH F-79443 distal humerus, radius, carpals, UOMNH F-64638 mandible with p2-m3, UOMNH F-64348 partial metapodial and phalanges, UOMNH F-70432 metapodial, phalanges, sesamoids (from UO-4601 Bone Hill).

Localities: UO-4605 Ortok, UO-4603 Vodka, UO-4601 Bone Hill.

Description: Material positively assignable to Cervidae at Ortok was primarily composed of antler fragments. One sample, UOMNH F-70334, preserves the entire pedicle, with no bone extending ventrally from the pedicle base. This implies the antler was shed, rather than representing the death of the animal. The pedicle extends approximately 5mm out from the antler base circumference, and has a very rounded surface texture across the relatively broad antler base. While all fragmentary, two antler fragments preserve tine-branches off the main shaft of the antler. Assuming similarities to modern cervids, this implies individuals were fully adult in age. Each antler fragment preserves a textured

outer surface, with low ridges across the surface. These ridges are not parallel to each other or the direction of growth, and frequently merge and divide. Antler material preserved at Bone Hill that contained pedicle also projected into the frontal bone, suggesting all proximal antler material at least was from mortality events. The frontal bone extends approximately 4 cm below the pedicle before broadening out to form the brain case.

The radius (UOMNH F-70423) is nearly complete, although heavily eroded, as it was found in-situ in a channel base. Diagnosis as cervid was facilitated via comparison to UOMNH B-21672, a modern black-tailed deer (*Odecoileus hemionus*). The proximal humeral head is fully fused, and as this is the last epiphysis to fuse in modern cervids (Purdue, 1983), it can be assumed the fossil material also represents an adult individual. The fossil radius is 3/4 of the length of the *O. hemionus* radius and proportionately smaller in diameter. The postcranial material from Vodka was also primarily identified via comparison to UOMNH B-21672 (*Odecoileus hemionous*) and to UOMNH B-21672 (*Ovis aries*). The morphology of the articular surfaces was most similar to the *Odecoileus hemionous*, yet had very little similarity to the modern bovid, thus this postcranial material was assigned to Cervidae. All postcranial material was of a consistent size class and was consistent with dental and antler material.

The metapodials possessed a roughly D-shaped cross section with a deep trough in the posterior side. The anterior distal portions have a strongly pronounced groove ending in a fenestra, about ½ cm from the distal medial portion of the bone. The trochlea are strongly keeled and parallel to each other. Phalanges taper distally and are mediolaterally compressed.

Dental material uniformly contains rugose enamel, with greater rugosity labially than lingually (Figure 5). Molars have a cervine fold, where a complete conulid of enamel, separate from either tooth loph, is situated labially. Dentition is brachyodont and selenodont. P4 is molariform, while p4 is not. Lower premolars are “W” shaped.

Figure 5. Examples of cervid dental material. Top and middle are left mandible UOMNH F-64520 from UO-4603 Vodka, bottom is left mandible UOMNH F-64533 from UO-4601 Bone Hill. Note the differences in the labial profile of the premolars, the labial groove present in the premolars of the Bone Hill specimen. Both taxa do however have a “cervine fold” in the molars, most visible on the m2.

Discussion: Antler fragments were distinguished from other bone fragments or horn core material in two ways: the smaller portion of the total diameter occupied by cortical bone on the interior, including a more gradual transition with progressive fining of the vesicle size towards the exterior of the bone cross section, and the irregular ridges on the exterior of the bony material, as opposed to the smooth surface seen in the giraffid ossicones or the parallel lineations seen in the bovid horn cores. This facilitated the diagnosis of even very fragmentary material as belonging to Cervidae.

Several candidate taxa exist for the Kyrgyz cervid material, which represents at least two species (or genera), with the dental material from Bone Hill having significantly different morphology in the premolars than the mandible from Vodka (Figure 5). The Miocene represents a crucial period in cervid evolution, with morphological transitions from more archaic lineages to the more modern cervine type deer, the Pliocervinae, with complete antler pedicles and three-tined antlers (Dong, 1993). The completely formed pedicles imply that at least the deer present at Ortok and Bone Hill were true cervines, as opposed to earlier such lineages as "crown of thorns" Lagomerycinae clade (Dong, 1993). However, despite the importance of the Miocene in cervid evolution and biogeography, cervids are poorly studied and in need of dramatic taxonomic revisions (Pitra et al., 2004, Azanza et al., 2013). This makes diagnosis of a taxon extremely difficult. While the antler, postcranial, and dental material is found in the same bone beds, none has been found in articulation. Thus, positively associating cervid material is currently impossible, although the fact that each bone bed possesses cervid material from only one size class implies that the localities each contain only one cervid taxon. The Kyrgyz faunas superficially seem to have the most faunal similarities with the

"*Hipparion* Faunas" of the Chinese red clays. However, the very morphologically similar fossil material from those sites is described by Zdansky (1925) as *Pliocervus,* which may no longer be considered a valid taxon (Petronio et al., 2007). While this material (UUZM-M868, UUZM-M991, UUZM-M992, UUZM-M993, UUZM-M886-891) seems to be the same taxon represented in the younger Kyrgyz bone beds, the original Chinese material has not been redescribed or assigned to a new taxon besides "*Pliocervus*". The few specimens assignable to Cervidae from Vodka, the older Kyrgyz bone bed, are not enough material to speculate on its identity, other than that the dental morphology is different enough from both the other Kyrgyz material and the Chinese *Hipparion* Fauna "*Pliocervus*" material as to represent different species and possibly a different genus. The p4 is less molariform than the p4 in the Chu Formation cervids.

All cervid material from Bone Hill, Rhino Party, and Ortok were consistent in morphology of the dental and cranial material; however the Vodka material differed signifficantly in morphology of the premolars. While belonging to the same size class, the Vodka material had premolars with greater folding of the lateral cusps changing the shape from the "E shape" seen in the other material, to a premolar with the paraloph folded so that the axis of the loaf is parallel to the axis of the jaw and the paraconid is posterior to the protoconid. The hypoconulid and entoconid are reduced, when compared to both *Odocoileus hemionus* and the Chu Formation cervid taxon. As Vodka is stratigraphically lower than other bone beds, this finding is not particularly surprising and is reflected across a variety of other taxa.

Family GIRAFFIDAE Gray, 1821

Specimens: UOMNH F-64478 left p2, p3, and m3, UOMNH F-64481 metapodial, cubonavicular, carpal, UOMNH F-67907 ossicone fragment, UOMNH F-70341 tooth fragment, UOMNH F-70382 distal metapodial (from UO-4605 Ortok). UOMNH F-64541 upper molar and associated tooth fragments (from UO-4604 Dam Site).

Localities: UO-4605 Ortok, UO-4604 Dam Site

Description: The dental material all possesses clearly defined selenes, is of a large artiodactyl, and is overall robust in morphology. The p3 and p2 is not molariform (Figure 6).

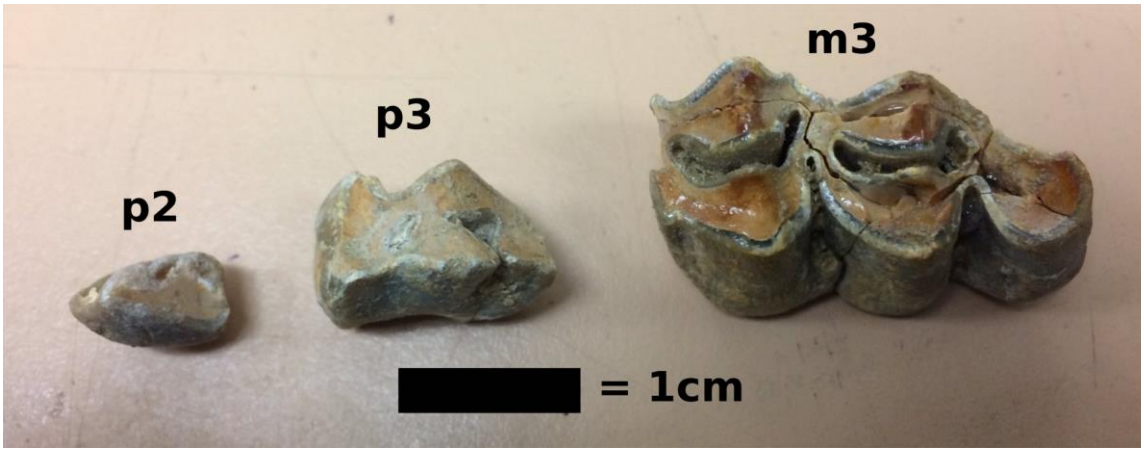

Figure 6. Three teeth, the p2, p3, and m3, of a Samothere giraffe. While the teeth were found in close association with each other, they are missing several teeth in between the premolars and molars. The teeth are consistent with *Samotherium* in morphology, however are smaller than all comparative specimens of the genus. Likely the Kyrgyz specimens represent an endemic species of *Samotherium*, however most material is needed to facilitate a positive diagnosis.

The exterior enamel is slightly rugose in texture. All teeth are relatively wide compared to their length, with m1-m2 being almost square in shape and the p3 being wider that it is long. The selenes have very rounded ends and have a wider space between the medial and lateral enamel bands in the center than at the anterior and posterior ends of the selene. The metapodial and articulated tarsals are large but relatively gracile. The posterior

groove is quite deep and the proximal end of the metatarsal lacks a foramen (Ríos et al., 2016). All epiphyses are fused, representing adult individuals. Diagnosis as giraffid material was facilitated via comparison to fossil material from Uppsala (UUZM-M3869, mandible of *Palaeotragus decipiens*, UUZM-M10786, cubonavicular of *Samotherium* c.f. *mumayri*, UUZM-M10814-10815, p3-4 of *Samotherium* sp., UUZM-M1157, metatarsal, cubonavicular, astragalus of *Palaeotragus microdon*) as well as comparison to modern giraffid material from University of California Berkeley (MVZ-M-216048, partial skeleton of *Giraffa camelopardalis*).

Discussion: While the metapodial is closer in length to *Palaeotragus* than other fossil giraffid (Table 2) (Ríos et al., 2016, 2017), the material is distinctly more robust in cross-section than any described taxa of Palaeotragus (Ríos et al., 2016, 2017).

TAXON	TOTAL LENGTH	ANTERIOPOSTERIOR WIDTH	MEDIOLATERAL WIDTH
KYRGYZ GIRAFFID	~400mm	47.19mm	37.08mm
SAMOTHERIUM MAJOR	400mm	-	47.45mm
PALAEOTRAGUS ROUENII	400mm	-	26.7smm
DECENNATHERIUM REX	405mm	42.06mm	46.03mm
DECENNATHERIUM PACHECOI	375mm	-	31.47mm
BIRGERBOHLINIA SCHAUBI	390mm	-	50.33mm
BOHLINIA ATTICA	580mm	-	43.33mm
OKAPIA JOHNSTONI	310mm	-	27.70mm
GIRAFFA CAMELOPARDALIS	575mm	-	43.31mm

Table 2. Metatarsal measurements for the giraffid from Ortok, with comparisons against several candidate fossil taxa and two modern taxa (Okapia and Giraffa). Standardized measurements taken from Ríos et al., 2016, with measurements taken from Ríos et al., 2016, 2017.

When scaled to a smaller overall size, the morphology of the proximal articular surface and the morphology of the cubonavicular bone are extremely like comparative examples of *Samotherium* (UUZM-M10786, cubonavicular of *Samotherium* c.f. *mumayri*, UUZM-M764, metapodial of *Samotherium* sp., UUZM-M773, cubonavicular of *Samotherium* sp., UUZM-M659 metapodial *Samotherium sinense*) and are more boxy in the proximal surface and with a deeper and wider groove to the posterior side of the shaft than all compared metapodials of the similarly sized *Palaeotragus* (UUZM-M1158 distal metapodial *Palaeotragus microdon*, UUZM-M1157 metatarsal, cubonavicular *Palaeotragus microdon*). Thus, it is likely, given the geographic extent and isolation of Central Asia, that the Kyrgyz giraffid material represents a new species of *Samotherium*; however, the material is too fragmentary at this point to describe a new taxon.

Family PALAEOMERYCIDAE Lydekker, 1883

Specimens: UOMNH F-70400 palate with L and R P2-M3 (from UO-4605 Ortok).

Localities: UO-4605 Ortok.

Description: Complete palate preserving the P2-M3 on both sides, broken ~1-1.5 cm dorsally to the enamel dentine junction, and broken ~2cm anteriorly to the P2s, lacking the toothless premaxillae (Figure 7). Specimen also includes the palatine bones, and shape of the anterior portion of the opening to the sinuses in the palatine and vomer. Teeth are in a moderate stage of wear, representing an adult individual. Teeth are rugose on exterior enamel margins, with greater rugosity on the lingual side of the teeth. The P4 is molariform, while the P3-P2 are not. The M1-M3 contain palaeomerycid folds, forming a complete tubule between the primary lophs of the molars. The molars also

contain enamel lakes between the clearly developed selenes in the M1-M3. Each tooth is robust, with a greater width than length in the P4-M2. The tooth row is curved, narrowing towards the anterior portion considerably.

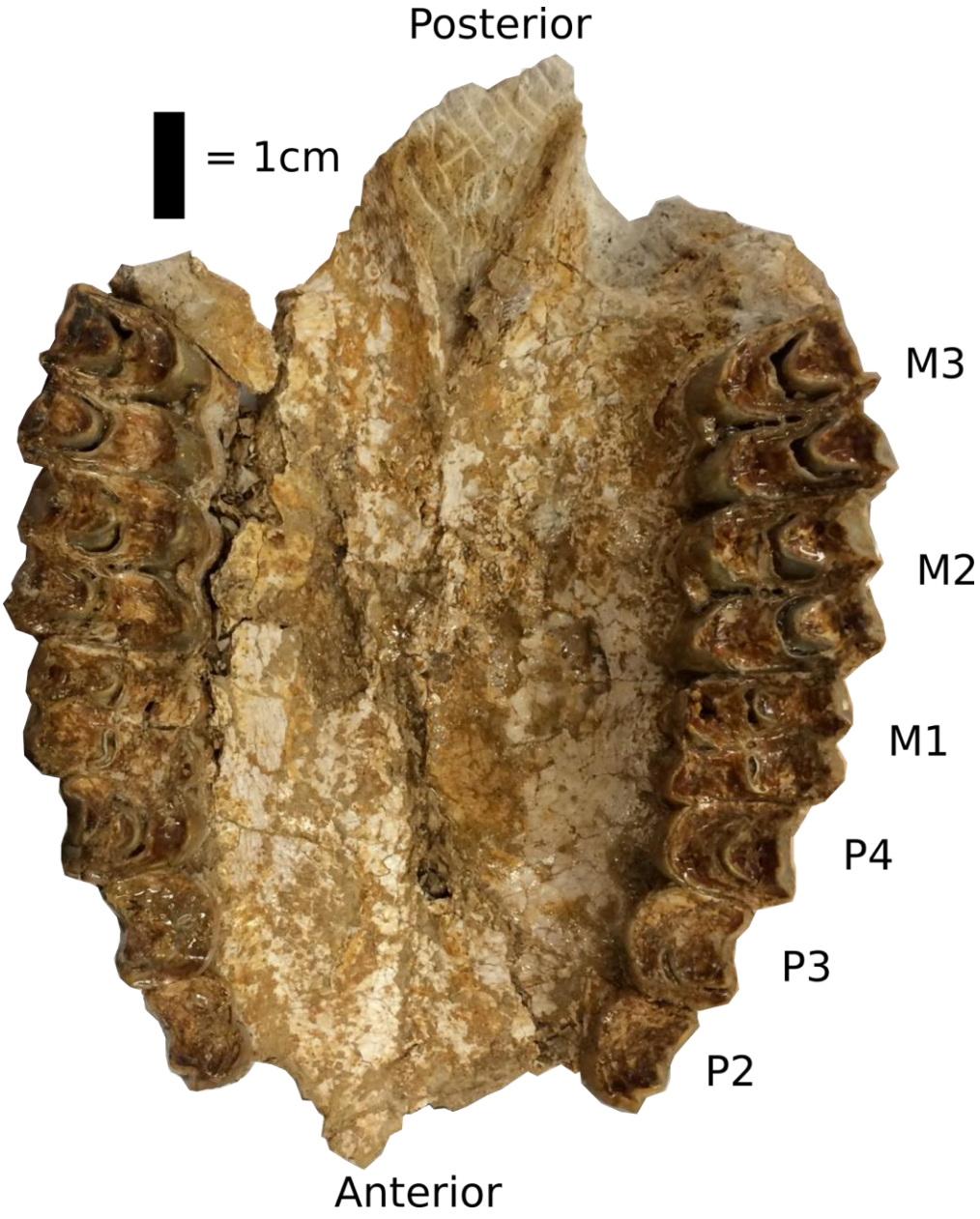

Figure 7. Palate of F-70400, a palaeomerycid. The medial edge of the molars, between the lophs, has the palaeomerycid fold, and while a similar feature is seen in cervids, it is not couples with the enamel lakes in between the selenes. The premolars are all molariform, another feature differing from cervids.

Selenes are angled lingual, and narrow from the medial portion to almost a point on both the anterior and posterior sides. The P3 make a distinct “E” shape, where the limbs are roughly parallel to each other, even in wear.

Discussion: Few artiodactyls possess the conule of enamel between loaphs of the molars. Notably, the Cervidae and Palaeomercidae do possess this feature. However, the internal enamel lakes seen in this specimen are rarely (but occasionally) seen in bovids, and are not seen in giraffids or cervids. The rugosity seen in the external surfaces of the enamel is also present in cervids, but not in bovids. While a moderately-sized artiodactyl, this specimen is still smaller that all but one giraffe taxon: *Palaeotragus microdon*. However, *P. microdon* lacks both the palaeomerycid fold between the lophs and lacks the internal enamel lakes seen in the Kyrgyz specimen. In addition to morphological differences in the tooth structure, the Kyrgyz specimen is also significantly larger in size than contemporarily aged cervids. Contemporary deposits in the Siwaliks produce palaoemerycids, indicating the presence of this family in the region both temporally and geographically, yet this material is morphologically quite distinct (Sánchez et al., 2015). This family is uncommon in Eurasian deposits of any age, particularly by the late Miocene.

ARTIODACTYLA indet.

Specimens: UOMNH F-70343 tooth fragments, UOMNH F-70364 calcaneum fragment, UOMNH F-70372 distal phalanx, UOMNH F-70384 astragalus fragment (from UO-4605 Ortok). UOMNH F-64517 distal radioulna, UOMNH F-64524 frontal with base of head-gear, UOMNH F-64553 sesamoid (from UO-4603 Vodka). UOMNH F-70474 tooth

fragments, UOMNH F-70482 metapodial fragment, UOMNH F-64350 headgear fragment (from UO-4601 Bone Hill).

Localities: UO-4605 Ortok, UO-4603 Vodka, UO-4601 Bone Hill.

Description: The tooth fragments contained selenes, characteristic of artiodactyls. The enamel was relatively thin, and the labial profile had high medial points to each loph. The calcaneum fragment, the posterior portion, was bulbous in shape at the far most posterior portion, and tapered to a narrow ovate cross-section for the shaft portion. The distal phalanx has a greater dorsoventral length than width and is asymmetrical. The trochlea are well developed, with pronounced keels on the ventral surface, and a strong groove between the two halves. The astragalus preserves only half of the bone, but would fit a roughly rectangular bone if whole. The skull fragment with the base of headgear preserved only preserved the basal most outward projection of the headgear. Therefore, it was impossible to distinguish if the material was horn core or antler, especially given the extension of the frontal bone ventral to the pedicle seen in some of the cervid antlers. The headgear has undergone significant diagenic alteration, removing any surface texture to the bone. The smoothness of the surface would be consistent with ossicones, however the degradation made bovid horn cores also a possibility.

Discussion: As the cervid and larger bovid material are of comparable size, some of the postcranial material is not diagnostic for differentiating between the two families. Likely the material belongs to one of these two taxa, however not all elements are easily distinguished between bovids and cervids.

Order CARNIVORA Bowdich, 1821

Family HYENIDAE Gray, 1821

Specimens: UOMNH F-64466 p4 (from UO-4601 Bone Hill).

Localities: UO-4601 Bone Hill.

Discussion: See Robson et al. in prep for taxonomic discussion.

Family MUSTELIDAE Fischer von Waldheim, 1817

Specimens: UOMNH F-70506 m1 (from UO-4601 Bone Hill).

Localities: UO-4601 Bone Hill.

Description: Mustelid material is limited to a single lower carnassial tooth. The tooth represents a small carnivoran. The talonid has a well-developed basin. Shearing blades are very pronounced across the tooth, suggesting hypercarnivory. While broken, the bases of two roots are preserved. Little wear is evident on the tooth.

Discussion: The well-developed talonid basin precludes feliforms, such as Herpestidae and Viveravidae, and the small size precludes Hyenidae and Felidae. However, the length of the talonid is slightly less than one quarter of the total tooth length, a degree of reduction typically not seen in even small canids. In both gross morphology and size, the tooth is consistent with *Martes*, however this generic level assignment is tentative with only one tooth. Additionally, *Martes* is currently a very broadly defined genus, containing a large temporal range and degree of morphological diversity, although it is known from Eurasian faunas of the late Miocene (Nakaya, 1994).

CARNIVORA indet.

Specimens: UOMNH F-67906 canine tooth (from UO-4605 Ortok).

Localities: UO-4605 Ortok.

Description: Unidentified carnivore material from Ortok is limited to a single worn canine. Specimen UOMNH F-67906 is a very weathered canine tooth, preserving all but the base of the tooth root. The tooth is triangular in lateral view, with a thick base quickly tapering to a worn surface. At the base the cross section is slightly ovate, but not significantly mediolateraly compressed. Dorsal to the enamel-dentine junction, the posterior edge of the tooth is straight, while the anterior margin curves posteriorly. The tip of the tooth exhibits grinding wear, exposing the internal dentine. In addition to this lifetime wear, the tooth displays evidence of fluvial transport, with extensive pitting and abrasion of the enamel. Where the base of the root is broken off, the edges are rounded slightly, suggesting fluvial transport.

Discussion: Because canine teeth are simple and single-cusped, this tooth is similar in gross morphology across a wide range of taxa. This factor, exacerbated by the fluvial modification to the tooth surface, precludes positively assigning the tooth to family level. The lack of mediolateral compression makes Felidae, or barberofelids, unlikely candidates. Hyenidae material is known from two other localities in the Kyrgyz Neogene sequences, and comparison to modern examples suggests this would be a plausible assignment; however, the morphology of canid canines is too like late Miocene hyenids to preclude this possibility as well. The high degree of lifetime wear is consistent with a carnivoran processing some amount of bone along with softer tissues.

Order LAGOMORPHA Brandt, 1855

Family LEPORIDAE Fischer von Waldheim, 1817

Specimens: UOMNH F-64542 tooth fragments, UOMNH F-70321 incisor, UOMNH F-64363 mandible with p3-m2, UOMNH F-64460 left and right humeri, left calcaneus, left tibia, left femur UOMNH F-64452 distal humerus (from UO-4604 Dam Site).

Localities: UO-4604 Dam Site.

Discussion: Taxonomic discussion in Flora et al. in prep.

Family OCHOTONIDAE Thomas, 1897

Specimens: UOMNH F-70320 left upper incisors, nasal bone, premaxillary bone (from UO-4604 Dam Site).

Localities: UO-4604 Dam Site.

Discussion: Specimen described in Flora et al. in prep.

Order PERISSODACTYLA Owen, 1848

Family EQUIDAE Gray, 1821

Genus *HIPPARION* de Christol, 1832

Specimens: UOMNH F-64481 tooth fragment, UOMNH F-64482 upper cheek tooth fragment, UOMNH F-65583 partial astragalus, UOMNH F-70323 distal metapodial fragment, UOMNH F-70334 distal metapodial fragment, UOMNH F-70338 tooth fragment, UOMNH F-70355 distal femur fragment, UOMNH F-70373 tooth fragments, UOMNH F-70381 upper cheek tooth fragment, UOMNH F-70396 upper left deciduous tooth row, UOMNH F-70398 incisor and associated incisor fragments, UOMNH F-70424

tooth fragment, UOMNH F-70431 mandible with left and right di1-dp4 (from UO-4605 Ortok). UO-64492 R upper cheek tooth, UOMNH F-64493 mandible with i1-m2, UOMNH F-64521 carpal sesamoid, UOMNH F-70316 tooth fragment (from UO-4603 Vodka). UOMNH F-64453 mandible with four cheek teeth, UOMNH F-64501 mandible with two cheek teeth, UOMNH F-64502 tooth fragment, UOMNH F-64504 distal tibia (from UO-4604 Dam Site). UOMNH F-70472 tooth fragments, UOMNH F-64548 incisor, UOMNH F-64438 two deciduous incisors and deciduous cheek tooth, UOMNH F-64608 upper cheek tooth, UOMNH F-64609 partial mandible with remains of several cheek teeth, UOMNH F-70460 mandible with left and right p2-m3, UOMNH F-64463 lateral metapodial, UOMNH F-64393 tooth fragment, UOMNH F-70467 distal metapodial, UOMNH F-64379 podial, UOMNH F-70495 upper cheek tooth, UOMNH F-70465 calcaneum, UOMNH F-70492 distal tibia, UOMNH F-70444 calcaneum (from UO-4601 Bone Hill).

Localities: UO-4605 Ortok, UO-4603 Vodka, UO-4604 Dam Site, UO-4601 Bone Hill.

Description: Teeth and tooth fragments contained weak perikymata in the cross sections of the enamel. Tooth exteriors also contained significant deposits of cementum. More complete dental material contained complicated infolding of the enamel, with a protocone forming a distinct loop of enamel, separate from the two primary lophs of the teeth. Incisors were ovate in cross section, narrowing towards the roots. Complete incisors were strongly curved and generally contained enamel lakes. Astragali were roughly equant in height and width, with slanted trochlear keels. Phalanges had strong bilateral symmetry and were robust in nature.

Discussion: While perikymata were more weakly developed than in the Rhinocerotidae fragments, it was present in all dental material, distinguishing the equid material from artiodactyl material. The incisors from Ortok did not contain internal enamel lakes, but the only associated with cheek teeth were deciduous, and deciduous incisors lack enamel lakes (Silver, 1963). Distinguishing adult and deciduous incisors is possible, but must be established at a species level with associated material (Silver, 1963). The incisors in the partial jaw from Vodka do contain enamel lakes. The complete mandible from Ortok (UOMNH F-70431) belongs to a juvenile individual. No adult teeth are erupted, but adult teeth are visible in the interior of the mandible. The mandible is very narrow through the diastema. As the protocone is separated from the primary lophs, these specimens can be confidently assigned to the genus *Hipparion*. A species-level diagnosis is more difficult, however. The genus needs taxonomic revisions, with potential consolidation of some species. Comparative material from the Chinese *Hipparion* fauna possesses at least 15 species (Qui et al., 1987, Bernor et al., 1990). As important taxonomic information comes from the depressions anterior to the orbits, but this feature is only poorly preserved in one specimen from Bone Hill. The overall size of material, as well as degree of complexity in lower tooth enamel infolding implies the smaller and less complicated enamel material from Vodka is likely a different species of *Hipparion* that the material present at all other bone beds. As all dental material is assignable to *Hipparion*, with no evidence of other genera at any site, postcranial material from Equidae was also assigned to *Hipparion*.

Family RHINOCEROTIDAE Gray, 1821

Specimens: UOMNH F-64479 astragalus fragment, UOMNH F-64480 podial, UOMNH F-64481 tooth fragments, UOMNH F-64482 astragalus fragment, UOMNH F-64483 carpal, UOMNH F-64484 tooth fragment, UOMNH F-64485 partial astragalus, UOMNH F-64486 tooth fragment, UOMNH F-64487 unworn tooth fragments, UOMNH F-64488 distal tibia fragment, UOMNH F-64489 tooth fragments, UOMNH F-70324 tooth fragment, UOMNH F-70335 humerus, UOMNH F-70337 tooth fragment, UOMNH F-70342 tooth fragments, UOMNH F-70345 tooth fragments, UOMNH F-70347 tooth fragments, UOMNH F-70348 astragalus fragment, UOMNH F-70349 distal femur fragment, UOMNH F-70350 distal metapodial, UOMNH F-70351 carpal, UOMNH F-70354 astragalus fragment, UOMNH F-70357 proximal humerus fragment, UOMNH F-70359 tooth fragments, UOMNH F-70360 radius, UOMNH F-70362 tooth fragment, UOMNH F-70363 tooth fragment, UOMNH F-70365 tooth fragments, UOMNH F-70374 astragalus fragment, UOMNH F-70375 tooth fragments, UOMNH F-70385 tooth fragments, UOMNH F-70386 tooth fragments, UOMNH F-70387 podial fragment, UOMNH F-70388 distal femur fragment, UOMNH F-70389 tooth fragment, UOMNH F-70391 tooth fragments, UOMNH F-70394 tooth fragments, UOMNH F-70395 radius, UOMNH F-70397 tooth fragments, UOMNH F-70399 tooth fragments, UOMNH F-70401 tooth fragment, UOMNH F-70402 distal femur fragment, UOMNH F-70403 proximal femur fragment, UOMNH F-70404 patella, UOMNH F-70405 calcaneum, UOMNH F-70406 podial, UOMNH F-70407 podial, UOMNH F-70425 tooth fragments, UOMNH F-70427 tooth fragment (from UO-4605 Ortok). UOMNH F-64514 distal radius, UOMNH F-64515 distal radius, UOMNH F-64522 distal metapodial, UOMNH F-

64523 tibia, UOMNH F-64527 carpal, UOMNH F-64529 partial tibia, UOMNH F-64530 partial calcaneum, UOMNH F-64534 podial, UOMNH F-64537 astragalus, UOMNH F-64551 tarsal, UOMNH F-64552 distal humerus, UOMNH F-64553 partial pelvis, UOMNH F-64554 occipital, UOMNH F-64555 radius, UOMNH F-64556 proximal tibia, UOMNH F-64557 skull, UOMNH F-64558 acetabulum, UOMNH F-64559 distal metapodial, UOMNH F-64560 carpal, UOMNH F-65461 carpal, UOMNH F-64562 tarsal, UOMNH F-64563 tarsal sesamoid, UOMNH F-64564 sesamoid, UOMNH F-64566 mid-shaft tibia, UOMNH F-64567 distal metapodial, UOMNH F-64568 carpal, UOMNH F-64569 vertebra fragment, UOMNH F-64570 humerus fragment, UOMNH F-64572 ungal phalanx, UOMNH F-64573 metapodial fragment, UOMNH F-64575 tibia, UOMNH F-64576 tarsal, UOMNH F-64577 fibula, UOMNH F-64578 atlas fragment, UOMNH F-64579 sesamoid, UOMNH F-64580 tooth fragments, UOMNH F-64581 thoracic vertebra fragment, UOMNH F-70303 carpal, UOMNH F-70304 podial, UOMNH F-70305 calcaneum, UOMNH F-70306 calcaneum, UOMNH F-70307 podial fragments, UOMNH F-70312 carpal, UOMNH F-70314 metapodial (from UO-4603 Vodka). UOMNH F-64423 tooth fragment, UOMNH F-64540 metacarpal fragment, UOMNH F-64544 distal metapodial, UOMNH F-70462 patella, UOMNH F-64617 ulna fragment, UOMNH F-70461 proximal radius, UOMNH F-64637 proximal tibia, UOMNH F-64489 distal radius, UOMNH F-64624 distal tibia and astragalus fragment, UOMNH F-64526 radius, UOMNH F-64638 proximal radius, UOMNH F-64490 several fragmentary carpals, UOMNH F-64491 proximal humerus, UOMNH F-64500 right astragalus and right calcaneum, UOMNH F-64505 distal radius, UOMNH F-64506 left astragalus, UOMNH F-64626 mandibles with c1-m3, UOMNH F-70301 mandibles with

c1-m3, UOMNH F-70501 astragalus, UOMNH F-70502 proximal radius (from UO-4604 Dam Site). UOMNH F-64425 tooth fragments, UOMNH F-64428 proximal radius, UOMNH F-64493 femoral head, UOMNH F-70503 distal femur, UOMNH F-70500 scapula, UOMNH F-64614 distal radius, UOMNH F-64554 articulated distal femur and proximal tibia, UOMNH F-64371 tooth fragments, UOMNH F-64397 tooth fragments, UOMNH F-70447 tooth fragments, UOMNH F-70499 tooth fragments, UOMNH F-70469 sesamoid, UOMNH F-70466 vertebral zygapophesis, UOMNH F-70478 tooth fragments, UOMNH F-70438 deciduous lower molar, UOMNH F-70433 proximal metapodial, UOMNH F-64499 navicular, UOMNH F-70437 distal metapodial, UOMNH F-70464 carpal, UOMNH F-70468 podial, UOMNH F-70502 pelvis (from UO-4601 Bone Hill).

Localities: UO-4605 Ortok, UO-4603 Vodka, UO-4604 Dam Site, UO-4601 Bone Hill.

Description: Teeth and tooth fragments all possess thick enamel with well-developed parallel banding (perikymata). Podial elements were robust and exhibited extensive pathology, with subchondral cysting and remodeling of the surfaces adjacent to the joint surfaces. Astragali are roughly box-shaped, with slanted trochlea forming two keels. The patella is large, with two deeply-developed grooves parallel to each other. Metapodials have an asymmetrical proximal end, a thick shaft, ovate in cross section with an anterior/posterior plane of compression, and a symmetrical distal end with a small keel developed in the center of the articular surface. The skull has an un-ossified nasal septum, with a retracted and elevated nasal bone. The premaxilla and the front the maxillary bones are missing. The M3s are both present and one side has a partial M2 preserved. (see chapter 4 for additional description)

Discussion: Dental material was diagnosed both by the thickness of the enamel, which is thicker than anything except proboscideans present in the Eurasian Miocene, and by the very strongly developed perikymata. Labial enamel surfaces also had a corrugated texture. The banding in the enamel, while seen in equids, is much more pronounced in rhinocerotids (Prothero, 2005). Most postcrania were identified via the large size, extreme robusticity (Prothero, 2005), and by the presence of extensive pathology in distal limb elements, which is widespread across rhinocerotids in the late Miocene (Stilson et al., 2016). Distal tibiae and astragali had robust but slanted trochlea characteristic of perissodactyls, yet with broader trochlea than equids. The skull represents a large rhinocerotid, lacking horns, and with two protruding tusks from the lower jaw. While this description is like *Chilotherium*, one of the more common late Miocene taxa regionally, the skull profile and shape of the nasals and basacrania are markedly different than any previously described species. Taxonomic diagnosis and description of this skull is the subject of a later publication (McLaughlin, chapter 4). The rhinocerotid present at Vodka is of different size and proportions than the rhinocerotid present in all Chu Formation localities. The Vodka taxon is larger, but of more gracile proportions overall, as evidenced by a comparison of the complete radii (see chapter 4). The radii from Vodka and Dam Site have the same midshaft diameter, yet the Vodka radius is 25% longer in total length. Differences also exist in the shape of the distal articular surfaces, confirming the assignment to two different taxa (Prothero, 2005).

Order PERISSODACTYLA indet.

Specimens: UOMNH F-70344 tooth fragments, UOMNH F-70353 distal tibia fragments, F-70368 sesamoid, UOMNH F-70377 tooth fragment (from UO-4605 Ortok). UOMNH F-70442 radius fragment (from UO-4601 Bone Hill).

Localities: UO-4605 Ortok, UO-4601 Bone Hill.

Description: Tooth fragments possessed moderately thick enamel with weakly developed perikymata. Distal tibia fragment preserved a small portion of the joint surface, but enough to distinguish a slanted slot for the trochlear keel of the astragalus. The sesamoid was similar in shape to a sesamoid from UOMNH F B-8701, *Ceratotherium simum*, but smaller in size.

Discussion: The sesamoid likely belongs to a rhinocerotid because of gross morphological similarities, however the small size precludes positive diagnosis. It could therefore belong to a juvenile rhinocerotid or an equid. The dental fragments likewise could exhibit thinner enamel than typically seen in rhinocerotid because they are juvenile material, or could represent very fragmentary material from an equid.

Order RODENTIA Bowdich, 1821

Specimens: UOMNH F-70318 incisor (from UO-4603 Vodka).

Localities: UO-4603 Vodka.

Description: Small curved incisor with open roots. Single groove along anterior surface.

Discussion: The size, shape, and single groove are consistent with Cricetidae, however as other less common candidate families are known from other Asian faunas, the specimen is currently assigned only to Rodentia.

Class MAMMALIA indet.

Specimens: UOMNH F-64482 bone fragments, UOMNH F-64483 bone fragment, UOMNH F-64484 mandibular fragment, UOMNH F-70330 carpal fragment, UOMNH F-70331 periotic capsule, UOMNH F-70332 bone fragment, UOMNH F-70336 bone fragment, UOMNH F-70352 bone fragment, UOMNH F-70358 bone fragment, UOMNH F-70361 tooth fragment, UOMNH F-70366 bone fragment, UOMNH F-70367 bone fragment, UOMNH F-70369 bone fragment, UOMNH F-70370 bone fragment, UOMNH F-70371 bone fragment, UOMNH F-70376 proximal metapodial fragment, UOMNH F-70378 proximal metapodial fragment, UOMNH F-70379 podial fragment, UOMNH F-70383 podial fragment, UOMNH F-70392 periotic capsule fragment, UOMNH F-70393 bone fragment, UOMNH F-70408 bone fragment, UOMNH F-70409 bone fragment, UOMNH F-70410 bone fragment, UOMNH F-70411 bone fragment, UOMNH F-70412 bone fragment, UOMNH F-70413 bone fragment, UOMNH F-70414 bone fragment, UOMNH F-70415 bone fragment, UOMNH F-70416 bone fragment, UOMNH F-70417 bone fragment, UOMNH F-70418, UOMNH F-70419 bone fragment, UOMNH F-70420 bone fragment, UOMNH F-70422 bone fragment, UOMNH F-70426 bone fragment, UOMNH F-70428 bone fragment, UOMNH F-70429 bone fragment, UOMNH F-70430 bone fragment (from UO-4605 Ortok). UOMNH F-64518 pelvis fragment, UOMNH F-64519 carpal fragment, UOMNH F-64557 articulated ribs, UOMNH F-64558 bone fragment, UOMNH F-64559 bone fragment, UOMNH F-64560 bone fragments, UOMNH F-64561 bone fragments, UOMNH F-64562 pelvis fragment, UOMNH F-64563 proximal phalanx, UOMNH F-64564 two associated podials, UOMNH F-64566

rib fragment, UOMNH F-64567 carpal fragment, UOMNH F-64568 rib fragment, UOMNH F-64569 rib fragment, UOMNH F-64570 sesamoid, UOMNH F-64571 bone fragments, UOMNH F-64572 bone fragment, UOMNH F- 70308 bone fragment, UOMNH F-70309 scapula fragment, UOMNH F-70310 pelvis fragment, UOMNH F-70311 bone fragments, UOMNH F-70313 fragment, UOMNH F-70315 bone fragments, UOMNH F-70317 bone fragment (from UO-4603 Vodka). UOMNH F-64557 bone fragment, UOMNH F-64620 bone fragment, UOMNH F-64619 proximal metapodial fragment (from UO-4604 Dam Site). UOMNH F-64439 caudal vertebra, UOMNH F-70448 proximal ulna fragment, UOMNH F-70487 tooth root, UOMNH F-70484 bone fragment, UOMNH F-70470 epiphyseal plate, UOMNH F-70480 bone fragment, UOMNH F-70479 bone fragment, UOMNH F-70475 phalanx fragment, UOMNH F-70493 bone fragment, UOMNH F-64349 proximal scapula, UOMNH F-70496 periotic, UOMNH F-70473 bone fragment, UOMNH F-70445 bone fragment, UOMNH F-70494 bone fragment, UOMNH F-70436 vertebra fragment, UOMNH F-70477 bone fragment, UOMNH F-70434 podial, UOMNH F-70491 bone fragment, UOMNH F-70489 bone fragment, UOMNH F-70435 podial fragment, UOMNH F-70490 bone fragment, UOMNH F-70497 bone fragment, UOMNH F-70476 bone fragment, UOMNH F-70440 bone fragment, UOMNH F-70441 scapula fragment (from UO-4601 Bone Hill).
Localities: UO-4605 Ortok, UO-4603 Vodka, UO-4604 Dam Site, UO-4601 Bone Hill.
Description: Material is all highly fragmentary. Material has a clearly developed cortical bone, with a gradual transition to the exterior portion of the bone in cross-section.
Discussion: Material was assigned to Mammalia based on the surface structure of the bone and the cross-sectional gradient from the cortical bone. Reptilian bone has a more

fibrous surface texture and different cross sectional relationship of the porous and dense bone (Chinsamy, 1997). Bone that was assignable to element could not be definitively assigned to an order.

Class REPTILIA Laurenti, 1768

Order SQUAMATA Oppel, 1811

Family VARANIDAE Merrem, 1820

Specimens: UOMNH F-64341 posterior portion of mandible, UOMNH F-70505 tooth (from UO-4601 Bone Hill).

Localities: UO-4601 Bone Hill.

Description: The isolated tooth was found in close proximity to the posterior portion of the jaw, and therefore may belong to the same specimen. They were not however found in direct association. The mandible fragment has a very low coronoid process, and a medial groove with the mandibular foramen far towards the anterior of the element. The tooth is a single cusp, of very simple morphology, and it lacks serration. The tooth is concave lingualy and convex labially.

Discussion: The texture of the bone was more fibrous than that seen in Mammalia. Additionally, the highly reduced articular morphology was consistent with squamates. Identification was largely made via comparison to a *Varanus gouldii* specimen (TMM M-1295) on Digimorph. Several members of the genus are found in modern Central Asian assemblages (Böhme, 2003), and fossil representatives are found in the broader region dating back to the early Miocene (Rage & Bailon, 2005). Many comparably large

squamates have serrations on the teeth, and of non-serrated groups, most have conical teeth without the lingual concavity (Rage & Bailon, 2005).

Order TESTUDINES Batsch, 1788

Family TESTUDINIDAE Batsch, 1788

Specimens: UOMNH F-70319 carapace fragment (from UO-4603 Vodka).

Localities: UO-4603 Vodka.

Description: Carapace fragment, with some suture lines preserved.

Discussion: General shape coupled with fiberous exterior bone texture and different cross sectional density of this bone fragment led to the assignment to testudines. The further assignment to tortoises was because of the overall size and thickness of the fragment. Fragment was assigned to carapace based on the degree of curvature of the sample, rather than plastron comparative material. The edges of the specimen evidenced fluvial wear unlike most specimens throughout all bone beds.

Results

All localities are mammal-dominated assemblages, with only three specimens of reptiles (two lizards and one tortoise) out of the 500+ included specimens. Additionally, ungulates compose most of each fauna (Figure 8). While ungulates dominating a fauna in part reflects a typical trophic structure, the Kyrgyz bone beds represent an even more extreme overrepresentation of ungulates and other herbivores to carnivores or omnivores than typical fossil mammal assemblages (Behrensmeyer, 1991). Despite spanning an

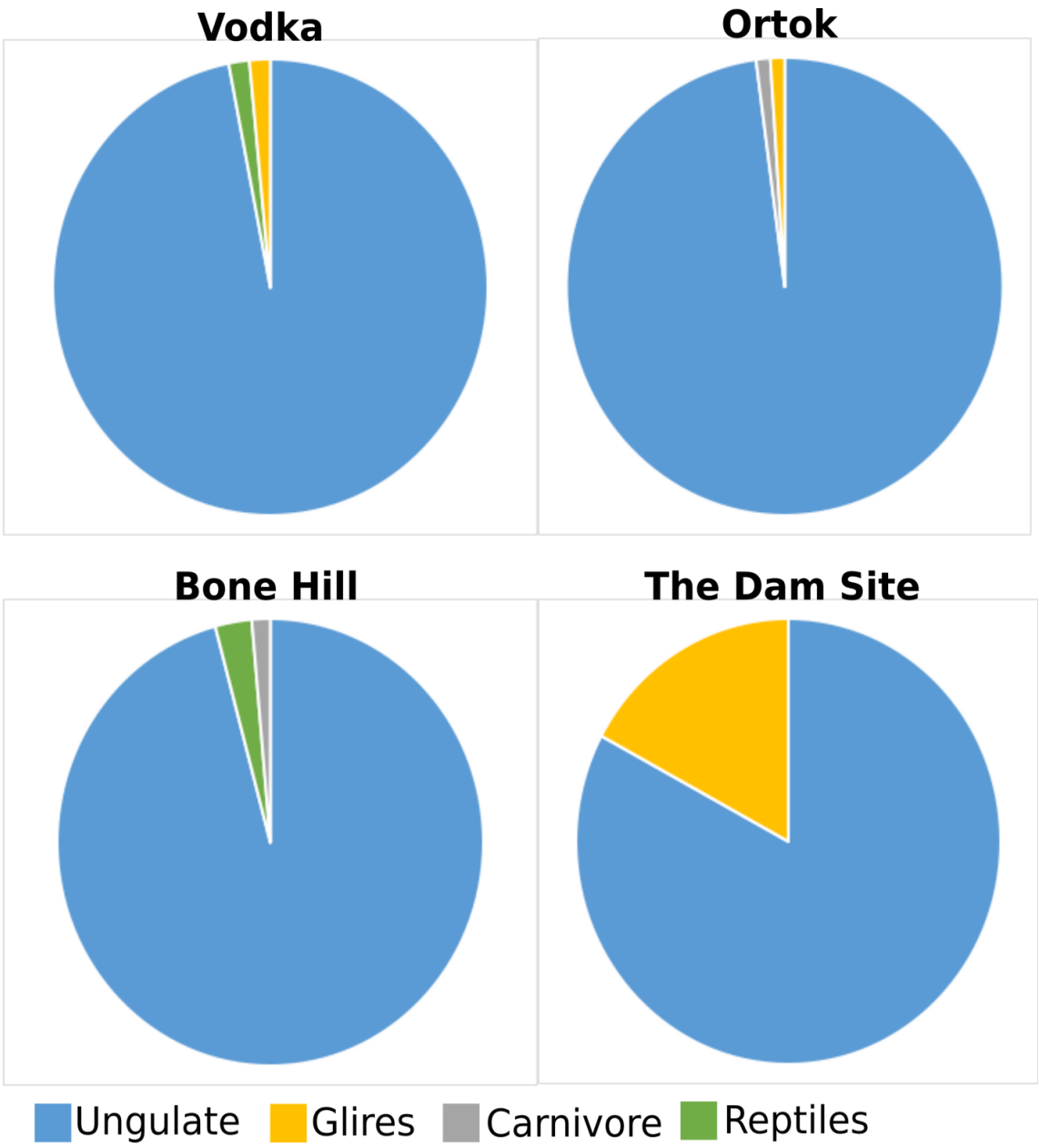

Figure 8. Proportions of vertebrate guilds represented at each site. While carnivores are rarely common, the relative percentage to more abundant ungulates is still informative, as it differs between agents of fossil accumulation and causes of mass mortality events.

estimated five million years, and variation between each of the faunas, each bone bed is rhinoceros dominated. Percentage of the fauna occupied by rhinoceros range from 31% to 74%, with Vodka bone bed having the highest percentage (Figure 9). This

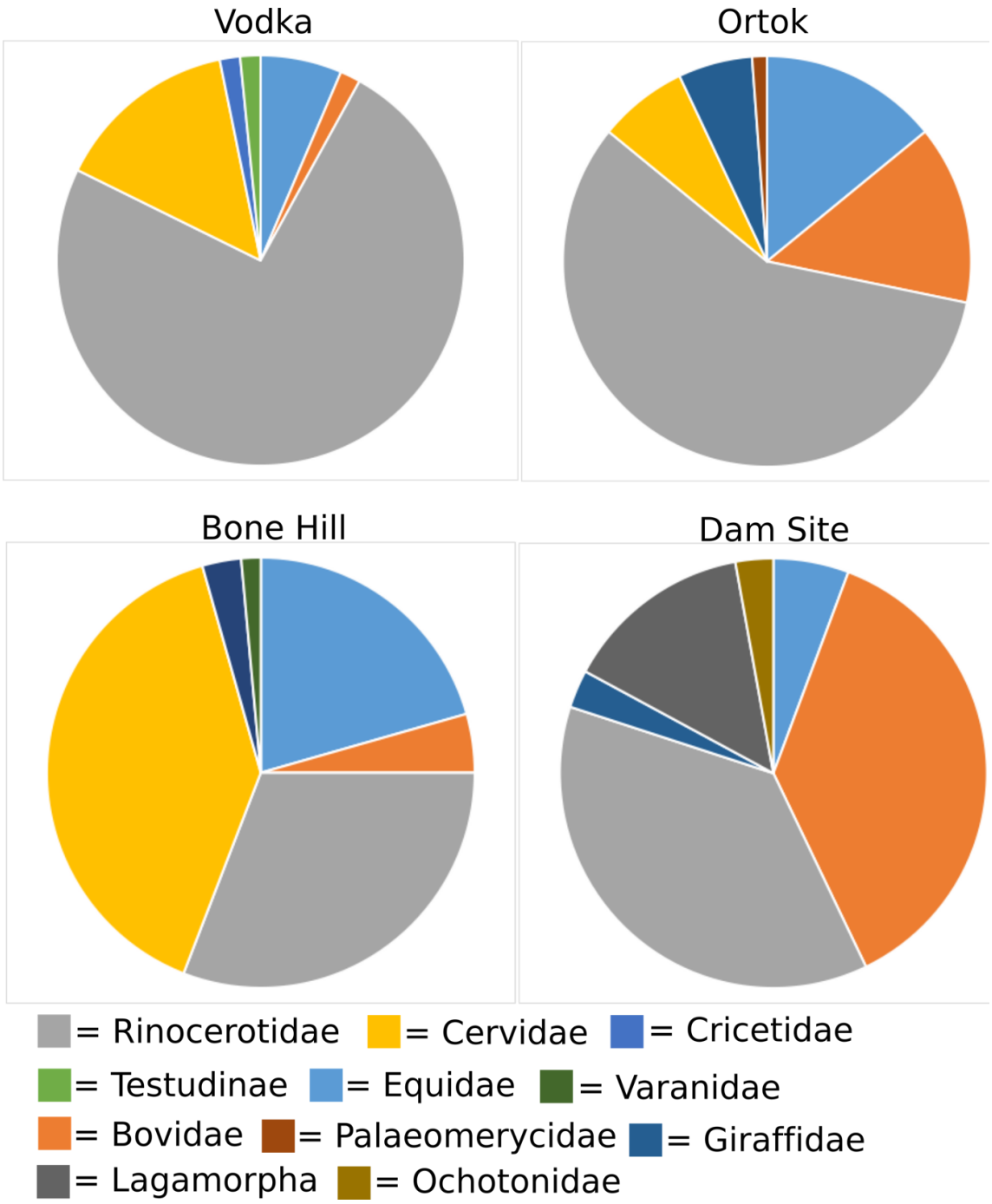

Figure 9. Faunal representatives at a family level for each locality. Vodka and Ortok are rhinocerotid dominated, while rhinocerotids tie for most common with bovids at the Dam Site. Only Bone Hill has rhinocerotids as not the most common family, with cervid material being the most common.

overrepresentation suggests differences in either mode of accumulation, in cause of death, or differences in behavior or social structure of fossil taxa.

Differences in bone preservation were present at each of the five bone beds. Weathering categories (Shipman, 1981, Gifford, 1980) were generally low, with little to no pre-fossilization surface wear (Table 3). While some bones were broken pre-deposition (Figure 10), no bones showed evidence of abrasion or polishing at any locality.

Bone Bed	*I*	*II*	*III*	*IV*	*V*
Vodka	49	28	6	0	0
Ortok	80	41	8	0	0
Bone Hill	89	10	3	0	0
Dam Site	34	4	0	0	0

Table 3. Degree of weathering for elements at each site, using the categories of Shipman, 1981 and Gifford, 1980 explained in Table 1. Most elements showed no surface weathering, implying carcasses spent less than 6 months from death to burial.

Degree of bone completeness and presence of articulation also varied between sites. Articulation was most common at Bone Hill, and less common, but present at Ortok, Vodka, and Dam Site. Degree of element completeness for each bone bed is listed in Figure 11. All sites were biased towards large elements, with greater size bias towards large material seen at Rhino Party than at other sites, although this could be in part a factor of sample size (smallest sample size) and preservation (objectively worst bone quality, limiting what could be identified or collected). The preservation of articulated rhinoceros material at Bone Hill and Ortok increases the maximum size of transported material.

Figure 10. *Hipparion* mandible and *Chilotherium* tibia as discovered in situ at the Vodka locality. This illustrates the mixed completeness, with the equid mandible broken and the rhinocerotid tibia complete, neither in articulation, and clearly deposited together. In the upper right portion of the photo large angular rock clasts can also be seen, characteristic of a poorly sorted, short transport distance with quick deposition deposit derived from a fanglomerate. This rapid deposition and short transport distance, combined with the lack of surface weathering, is consistent with fluvial deposition after a period of drought.

The bone beds varied both in the range of L1 and the median values for L1. As length is the greatest factor in total transport distance, these differences do imply some difference in transport distance. The largest length value for any site was that of the articulated partial rhinoceros skeleton present at Bone Hill. Articulation increases total length of transportable units, therefore articulation is not only a sign of quicker burial, but

also of less transport of elements (Table 4). Microvertebrates were only present at Ortok, Vodka, Dam Site, and Bone Hill, although never in great concentrations.

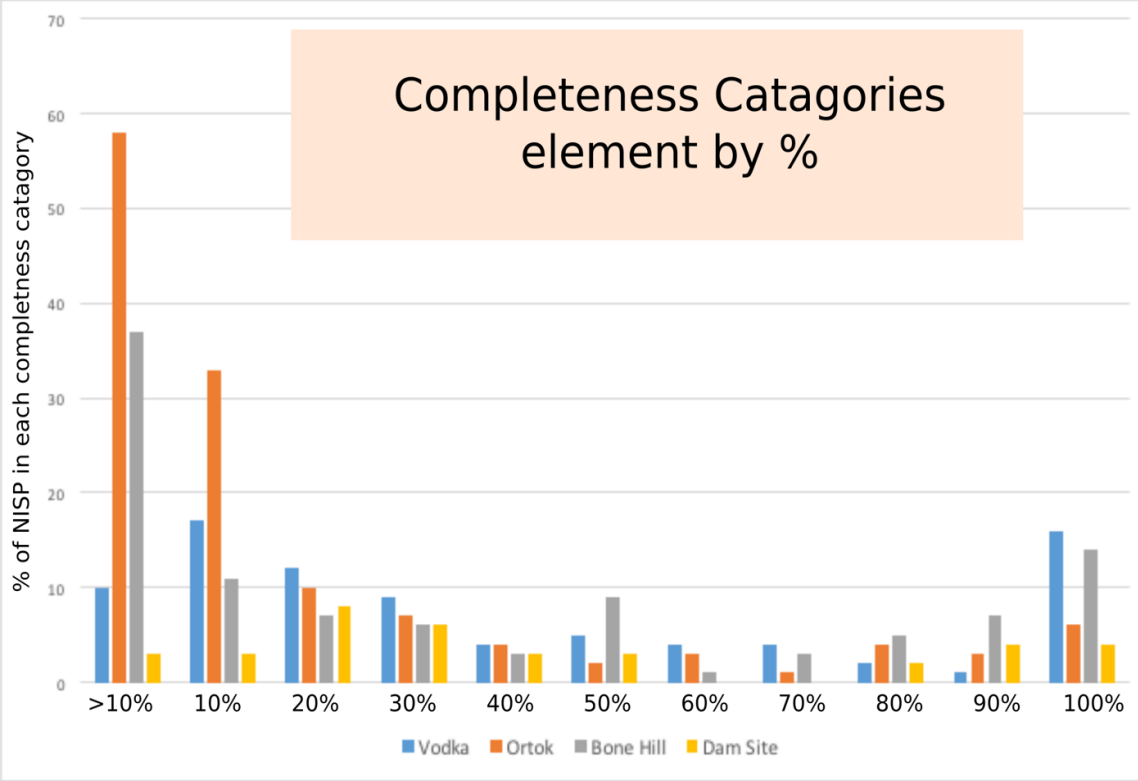

Figure 11. Plot of element completeness, as completeness is an indicator or weathering, transport distance, and degree of carcass processing. Individual elements were categorized on completeness when compared to a whole element from a related modern taxon. Completeness was assigned to a 10% standard to account for difficulty in accessing initial completeness resulting in poor fossilization or transportation and excavation wear. Vodka and Bone Hill had the most complete elements, while Ortok and Bone Hill had the most incomplete elements. The Dam Site has the most even distribution of individual element completeness.

Length values for all individual specimens, differentiated by locality, reported in Figure 12. Shape also varied slightly, with more compact or cylindrical elements than flat elements. No notable differences in shape existed between bone bed localities (Figure 13). Distribution of skeletal elements is more variable between localities. Ortok has cranio-dental material as the most common elements, whereas mid limb bone like the radius and tibia were most common at the Dam Site (Figure 14) (Table 5). Overall, the

total length and non-flat shapes imply little to no transport occurred before deposition. We infer this to be carcasses on the surface being transported very short distances in a fanglomerate setting before rapid burial.

Locality	*Articulated*	*Disarticulated*	*% Articulated*	*% Disarticulated*
Vodka	4	78	4.87	95.12
Ortok	2	124	1.58	98.41
Bone Hill	10	92	9.80	90.19
Dam Site	5	30	14.28	85.71

Table 4. Relative proportions of articulated to disarticulated material. While most material was disarticulated, all localities possessed some articulated material, a feature missing in modern sites with significant transportation or with greater than 1 year of surface weathering (Faith & Behrensmeyer et al., 2006). Thus, the presence of articulation implies rapid accumulation of material and quick burial with little to no transportation.

Assemblage	phalanges	dentaries	head gear	podials	skulls	teeth	humeri	metapodial	scapula	femora	radii/ulnae	vertebra	tibia/fibula	pelvis	rib	Source
Vodka	2.8	6.9	1.4	31.9	2.8	6.9	2.8	9.7	4.2	1.4	5.6	4.2	9.7	5.6	4.2	1
Ortok	1.9	1.0	13.6	23.3	2.9	36.9	2.9	7.8	0.0	4.9	2.9	0.0	1.9	0.0	0.0	1
Bone Hill	11.0	9.9	5.5	19.8	4.4	20.9	0.0	11.0	3.3	3.3	4.4	3.3	2.2	1.1	0.0	1
Dam Site	0.0	9.8	24.4	14.6	2.4	12.2	4.9	7.3	0.0	0.0	17.1	0.0	7.3	0.0	0.0	1
C0173	13.2	9.1	0	6.7	4.3	25	5.8	10.4	1.3	3	5.5	7.7	5	3	0.3	2
C0174	17	8.7	0	1	5.8	28.6	2.4	8.3	1.0	3.9	4.4	13.6	3.4	1.5	0.5	2
C1704	8.5	5.1	0	3.4	3.4	60.8	1.7	4.4	0.7	0.7	1	8.9	0.3	0.7	0.3	2
C1707	16.7	6.1	0	4.5	1.5	28.8	1.5	12.1	0.0	7.6	4.5	10.6	3.0	1.5	1.5	2
C1721	13.5	9.6	0	5.8	0.5	50	2.9	3.8	1.0	2.9	1.9	6.2	1.0	0.0	1.0	2
C1708	7.6	12.1	0	2.7	3.3	61.5	1.5	2.4	0.0	1.5	0.9	4.5	0.9	0.6	0.3	2
Siwalik I	9.1	4.2	inc. w/ skull	6.9	6.2	27.9	2.7	10.1	1.6	2.9	5	7.7	3.9	2.4	9.4	3
Siwalik II	2.9	4.4	inc. w/ skull	2.7	5.8	31.3	2.2	8.7	2.0	4.2	2.2	9.6	3.6	2.2	8.2	3
Siwalik III	3.9	2.9	inc. w/ skull	3.5	7.6	21.4	2.5	5.9	1.1	3.9	3.5	13.5	2.8	2.8	24.7	3
Siwalik IV	5.0	6.8	inc. w/ skull	3.3	6.8	36.2	3.0	4.7	2.7	3.0	5.3	11.6	2.7	1.2	7.7	3
Modern fluvial	5.0	5	inc. w/ skull	3.7	7.4	5.4	8.4	7.7	4.0	6.7	9.1	13.8	9.4	4.7	9.7	4
Amboseli 1975	not inc	3.9	not inc	not inc	2.2	not inc	3.7	6.2	3.1	3.0	3.5	40.9	3.1	13.3	7.5	5
Amboseli 02-04	not inc	10.3	not inc	not inc	8.7	not inc	8.2	7.4	7.6	5.6	9.5	20.3	6.1	5.6	10.8	5

Table 5. Distribution of elements between the four bone beds in this study (1) and several micro and marcro fauna comparatives. Assemblages beginning with C (2) are microvertebrate faunal from the Cabbage Patch from Calede (2016). Siwalik (3) assemblages are from four stratigraphic layers, with I and II inferred as attritional assemblages and III and IV as mass death assemblages from Badgley (1986). The modern fluvial (4) assemblage is an attritional grouping of modern bones via fluvial transport from Aslan & Behrensmeyer (1996). Finally, the Amboseli assemblages (5) are modern African drought killed mass mortality faunas from Faith & Behrensmeyer (2006).

Site	Adult NISP	Juvenile NISP	% juvenile	% adult	Mass mortality or attritional	Study source
Vodka	27	3	10.00	90.00	Attritional?	1
Ortok	34	9	20.93	79.07	mass mortality	1
Bone Hill	47	13	21.67	78.33	mass mortality	1
Dam Site	30	1	3.23	96.77	attritional?	1
Siwalik I	-	-	1	99	attritional	2
Siwalik II	-	-	1	99	attritional	2
Siwalik III	-	-	12	88	mass mortality	2
Siwalik IV	-	-	16	84	mass mortality	2
Akkasdagi Protoryx laticeps	-	-	12	88	mass mortality	3
Akkasdagi Microstonyx major	-	-	22	78	mass mortality	3
Akkasdagi Hipparion	35	16	31.37	68.63	mass mortality	3
Valley of Shavart	27	13	32.5	67.5	mass mortality	4
Brazil cave deposit	-	-	0	100	attritional	5

Table 6. Percent of age-identifiable material assigned to juvenile verses adult age classes for the four bone beds from this study (1) and compared to several other modern and fossil assemblages. Other studies include Neogene fossil assemblages from the Siwalik hills (2, Badgley, 1986), Turkish Neogene fossil assemblages (3, Valli, 2005), modern death assemblage from a mud pit forming over one drought season in Mongolia (4, Berger et al., 2001), and a Quaternary cave deposit where all bones were deposited from fluvial transport (5, Maldonado et al., 2016).

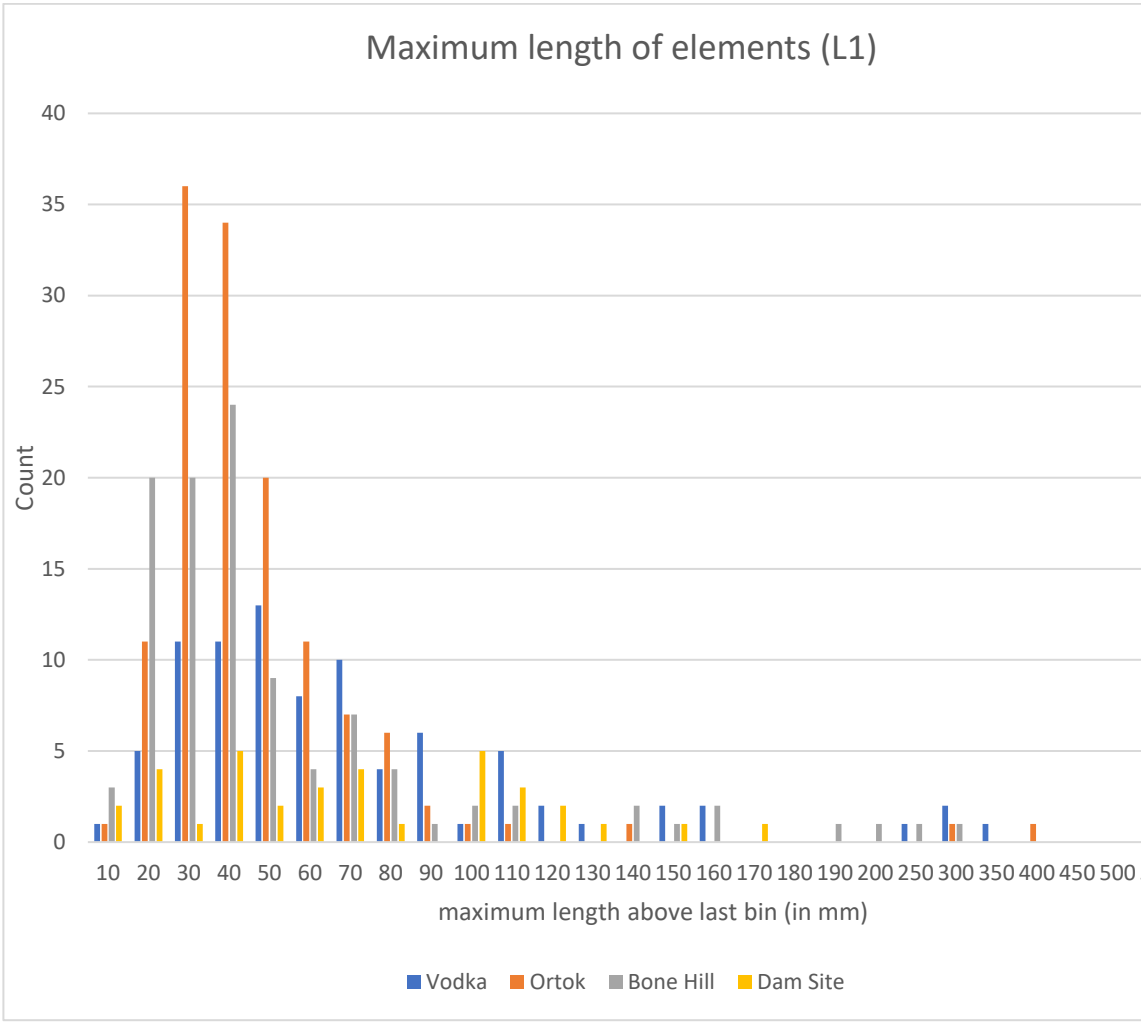

Figure 12. Length measurements (L1) for all elements. Maximum length is the single greatest predictor of total transport distance, with long elements being the least likely to be transported. Therefore, the longer the total length of the longest elements in each assemblage, the less likely transport of any noticeable distance.

Age distribution was varied between the four sites, ranging from 10-21% of the assemblages. While Palmqvist (et al., 1996) suggests the presence of any juveniles in a fossil assemblages makes mass mortality unlikely, none of the studies of modern mass death assemblages support this claim, with known mass mortality events producing high numbers of juveniles (Badgley, 1986, Aslan & Behrensmeyer, 1996, Faith &

Behrensmeyer, 2006, Valli, 2005, Berger et al., 2001) and attritional events producing low percentages of juveniles (Badgley, 1986, Maldonado et al., 2016). The high percentage of juveniles is in keeping with other mass mortality events, rather than attritional sites (Table 6) (Figure 15). Paired with the lack of any carnivore tooth marks, or breakage consistent with scavenging on any bones in all four assemblages, the presence of juveniles is instead attributed to young animals being less likely to survive environmental perturbations.

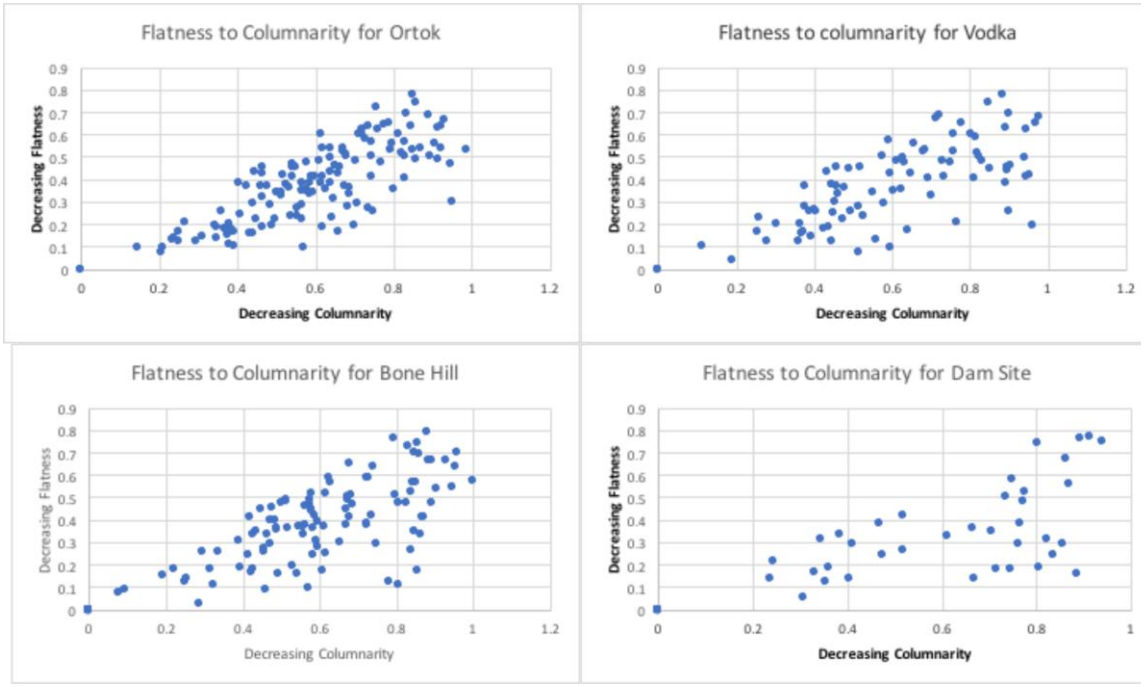

Figure 13. Plots of flatness (L3/L2) to columnarity (L3/L1) after methods of Calede (2016). Ortok had the most "box shaped" elements, while flatter elements were common in the other three sites. As flatness is a predictor of transport, after total length, this may imply that elements at Ortok were not transported as far as other sites.

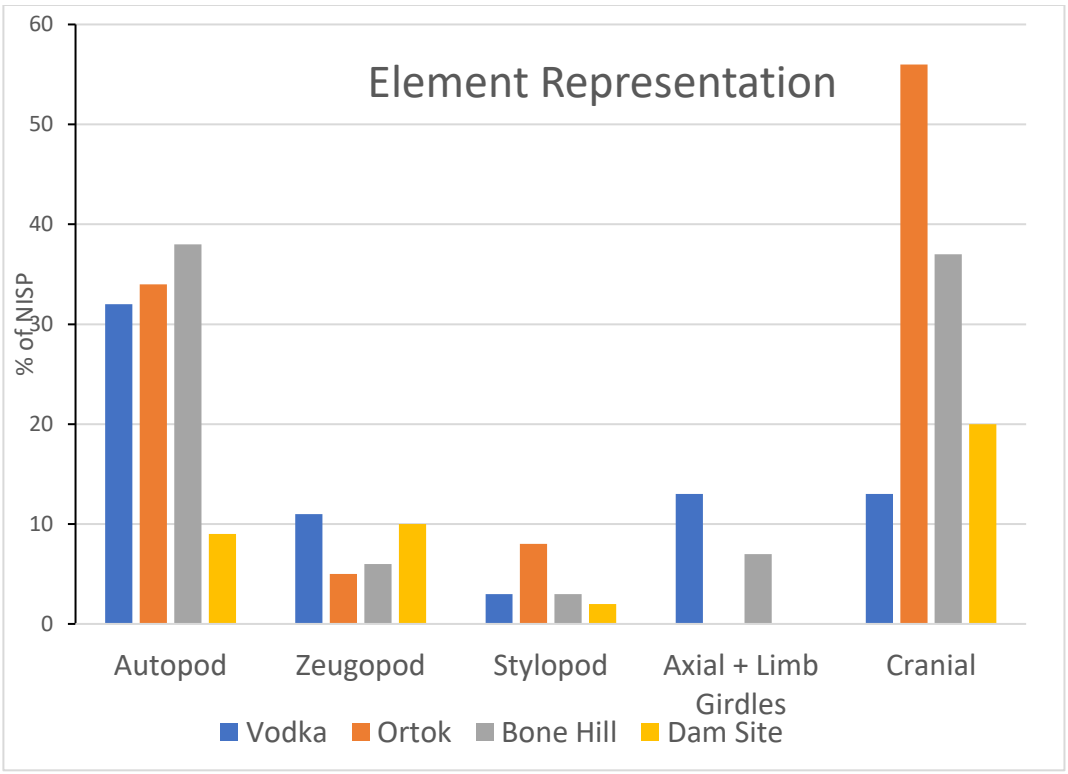

Figure 14. Grouping the distribution of elements into rough body position categories more clearly illuminates gross trends in element distribution. Ortok has the highest representation of cranial material by percent of total material. Vodka, Ortok, and Bone Hill were all highly represented in distal limb elements (autopod). This could represent local deposition or transport taken alone, however the lack of evidence of transport suggests little total transport distance driving the abundance of many small hand and foot elements.

Conclusion

Bone beds in the Kochkor basin uniformly represent mass death assemblages, despite spanning approximately five million years (McLaughlin, chapter 3). The relatively quick accumulation of vertebrate material, the very high density of material, general lack of bone surface weathering, lack of evidence of carnivore processing, high percentage of juveniles (at two localities), and mix of bone and skeleton completeness are indicative of assemblages where the prevalence of dead vertebrates overwhelms the ability of

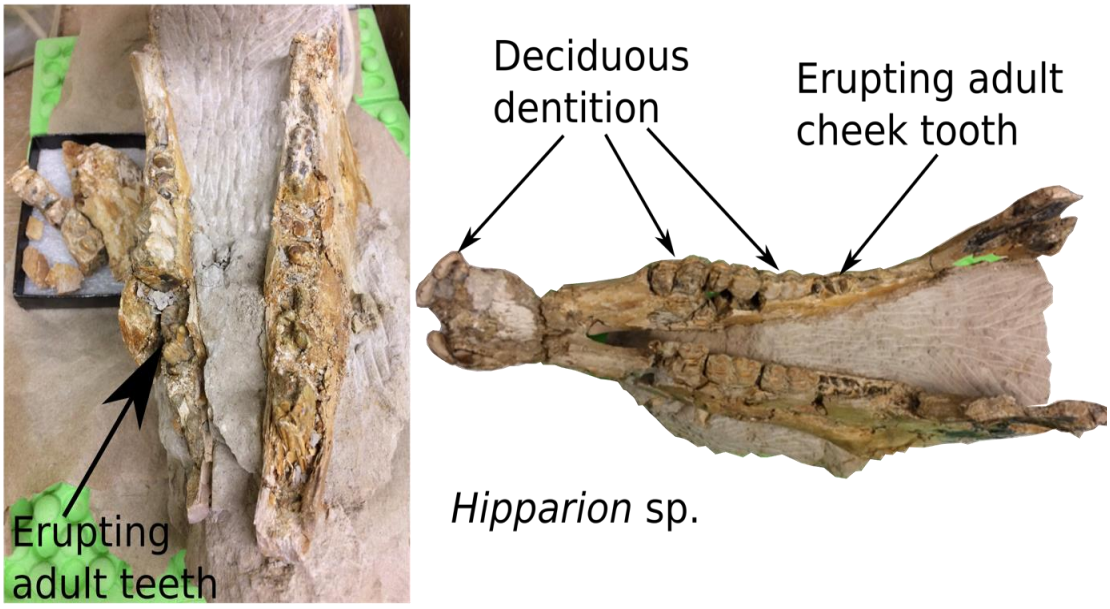

Figure 15: Juvenile Hipparion mandible from Ortok. Given tooth eruption rate in modern horses, the individual was likely 1-2 years old. The image on the left was taken during preparation of the specimen and gives a cross sectional view through the tooth row. Adult dentition is seen in the jaw just below the shallow caps of the juvenile dentition. The erupting adult dentition clearly contains a distinct protocone, facilitating the diagnosis as a hipparonine equid.

carnivores or scavengers to process the corpses (Behrensmeyer & Hill, 1980). As the bone beds uniformly show low levels of physical transport, minimal to no bone surface weathering, no processing by carnivores or rodents, and sedimentary indicators of rapid deposition, it can therefore be assumed that mode of accumulation is not to blame for the lack of carnivore or omnivore material. We propose that the large-vertebrate death assemblages most consistent as an analogue, are those resulting from large drought events (Haynes, 1988).

Low levels of surface weathering at all bone beds ((Shipman, 1981, Gifford, 1980) (Table 3) indicate quick accumulation of bones, likely on the weeks to months timescale. Additionally, the mix of element completeness and articulation is consistent

with accumulated corpses being transported short distances fluvialy and quickly deposited in flashflood onto proximal flood plains or fanglomerate type events, as opposed to attritional events or long periods of weathering (Faith & Behrensmeyer, 2006). Sediments associated with the bone beds are also fluvialy derived. The transition from the braided stream deposition of course materials in the Shamsi Formation, to the finer grained fluvial channel and overbank deposits is consistent with a drier climate in the younger formation. Additionally, the dense red paleosols of the Shamsi, characterized elsewhere as weathered soils in a monsoonal climate (Ding et al., 1999), disappear continuing up section into the Chu Formation. All Chu Formation localities are siltstone, with some clastic material, consistent with sudden deposition in an over bank or fan type sudden deposition of suspended material. The lack of articulation at Vodka implies that skeletal elements at Vodka may have spent longer between time of death and time of accumulation than other localities. The higher, but still low overall, degree of surface weathering present at Vodka corroborates this, as additional time allows for degradation of connective tissues and more chances for biological or mechanical disarticulation. The complete lower rhino dentition from Vodka is however one of the best examples of "drought wear" (Kaiser et al., 2013) seen at any locality, although equid dental material from Bone Hill also displays macro wear associated with browsing rather than grazing.

Quick deposition of minimally transported corpses of varyingly disarticulated skeletons is consistent with a large-scale drought event. In a drought to fluvial depositional event, we would expect corpses to accumulate on a landscape over weeks to months as individuals died and desiccated. When precipitation events eventually occurred, desiccated and partially disarticulated vertebrate material would quickly wash

downgradient until deposited. Therefore, L1, being the factor most related to transport distance, also ends up being a measure of articulation, and how long material stayed at the surface to weather and disarticulate. Longest elements were always articulated material, if articulated material was present. Vodka had little articulated material (one ribcage of a rabbit-sized animal), thus the rhinoceros skull was the largest single element at the site. Distribution of skeletal elements corroborates the previously mentioned hypothesis of more weathering time and greater transport at Vodka, with mid limb elements, and not fragile distal elements or cranio-dental elements, being the most commonly represented at Vodka. Along this reasoning, Ortok likely represents the lowest degree of transport, as evidenced by the most common skeletal element being cranio-dental material. Despite proboscidean material as a common part of nearly all comparative late Miocene Eurasian faunas (Koufos, 2003, Barry et al., 2001, Deng, 2006B), proboscidean material is lacking form all Kyrgyz mass death assemblages. In the case of proboscideans, this absence may derive from their documented ability to survive droughts in significantly higher rates relative to other fauna (Dudley et al., 2001, Haynes, 1988).

Overall the faunas contained similar taxa between localities, yet several potentially environmentally informative differences in both taxa richness and evenness exist. While a notable proportion of the ungulate faunas of Bone Hill, Ortok, and Vodka, no cervid material is currently produced by the Dam Site or Rhino Party. Rhino Party has the lowest number of specimens, and the least work conducted at the locality, so this may reflect a sampling bias rather than actual prevalence. The Dam Site, however, is well

sampled, with a greater total number of samples than Vodka, yet still does not produce cervid material.

With the most evidence of transport, and the lowest percentage of juveniles, Vodka may represent an attritional event, rather than a classic mass death assemblage. However, at 13% juveniles, Vodka still contains more juveniles than typically seen in purely attritional assemblages (Badgley, 1986, Maldonado, 2016, Calede, 2016). However, other factors, such as the still very low degree of surface weathering and "drought wear" on the rhinocerotid dentition, coupled with the fanglomerate deposit, still suggest drought as a possible cause of mortality. The uniformly high percentage of juveniles, wide distribution of elements, element completeness, presence of articulated elements, and over representation of herbivores in the three Chu Formation bone beds is consistent with other fossil mass mortality deposits (Badgley, 1986, Coombs & Coombs, 1997, Hunt, 1990, Valli, 2005, Voorhies, 1969) and modern drought-killed bone assemblages (Dudley et al., 2001, Haynes, 1988, Behrensmeyer, 1978, Faith & Behrensmeyer, 2006).

Transition

Central Asia in the Miocene was a period of rapid landscape, climate, and biotic change. Dating the onset and rate of these changes is crucial not only for constraining seismic hazard, but also to understand how shifting biomes impact a much broader region. As the Silk Road acted as a geographic filter for human civilization, so to have the Tien Shan acted as a filter for Eurasian faunas. Work from Kazakhstan, Inner Mongolia, and the Siwaliks of India and Pakistan hold similar records of climate change in the late Miocene. In the following chapter I aim to temporally constrain the timing of uplift and related climate change in the central Tien Shan utilizing a combination of vertebrate biostratigraphy and magnetostratigraphy. While these techniques are used in concert elsewhere across the globe, combining them in Kyrgyzstan is a novel approach. Previous paleontological work in the country is limited, and existing magnetostratigraphic work has largely lacked temporal constraints beyond sequence stratigraphy and some thermochronology.

Without a taxonomic examination of the fauna, as in the last chapter, the fauna cannot be used for geochronology. The lower the taxonomic level taxa are diagnosed to, generally the shorter the temporal range occupied. Therefore, the taxonomy is constantly being refined and updated as new material increases the faunal list or facilitates identification of key taxa to lower taxonomic levels. This is not to say broadly identified taxa cannot still be of great biostratigraphic utility, as will be discussed in Chapter 3.

Taphonomy, as examined in the last chapter also neatly integrated into the geologic and geochronological work presented in the next chapter. As outlined in the conclusions, the best hypothesis for cause of mortality in the bone beds is drought. This

local to regional scale climate change is driven and controlled by the tectonics examined in the next chapter. Without the tectonically active setting, dating back throughout much of the Neogene, Kyrgyzstan's biota would likely not have changed as quickly or as totally. The shifting environments in turn inform geologic discussions, where geologists debate if climate or pure tectonics drive the lithologic differences between formations.

CHAPTER III

BIOSTRATIGRAPHY AND MAGNETOSTRATIGRAPHY OF THE KOCHKOR BASIN KYRGYZSTAN; INSIGHTS INTO UPLIFT OF THE TIEN SHAN

Introduction

Kyrgyzstan, a country rapidly developing, is now facing the challenges posed by intense seismic hazard across the country, and notably proximal to population centers. Kyrgyzstan, in fact, has the highest seismic hazard of any country (Figure 16) (Abdrakhmatov et al., 2001). Seismic hazard impacts the populace not only directly, in a country with very limited building codes (Halvorson and Hamilton, 2007) and largely Soviet era buildings, but also indirectly by increasing landslide risk (Kirschbaum et al., 2010), the second largest geologic hazard in the country (Abdrakhmatov et al., 2003).

Properly accessing seismic risk necessitates a deep understanding of geologic processes driving regional seismicity. On a broad scale, seismicity in Kyrgyzstan is driven by the collision of the Indian subcontinent into Asia. The Himalayas are the primary result of this collision, initiating ~50 million years ago (Rowley, 1996), but the Tien Shan and Pamir are younger records of the regional impacts of crustal collision (Burbank et al., 1999). As the total amount of shortening across the Tien Shan is known, the relative rate of uplift over time comes into question. Dating this initiation of uplift, and rate of early uplift, is usually a matter of radiometric assessment of sytectonic sediments or primary volcanic material. However, the youngest radiometrically datable rocks in the country date from the Paleocene, possibly relating to crustal delamination events in the Himalayas (Zabelina et al., 2013).

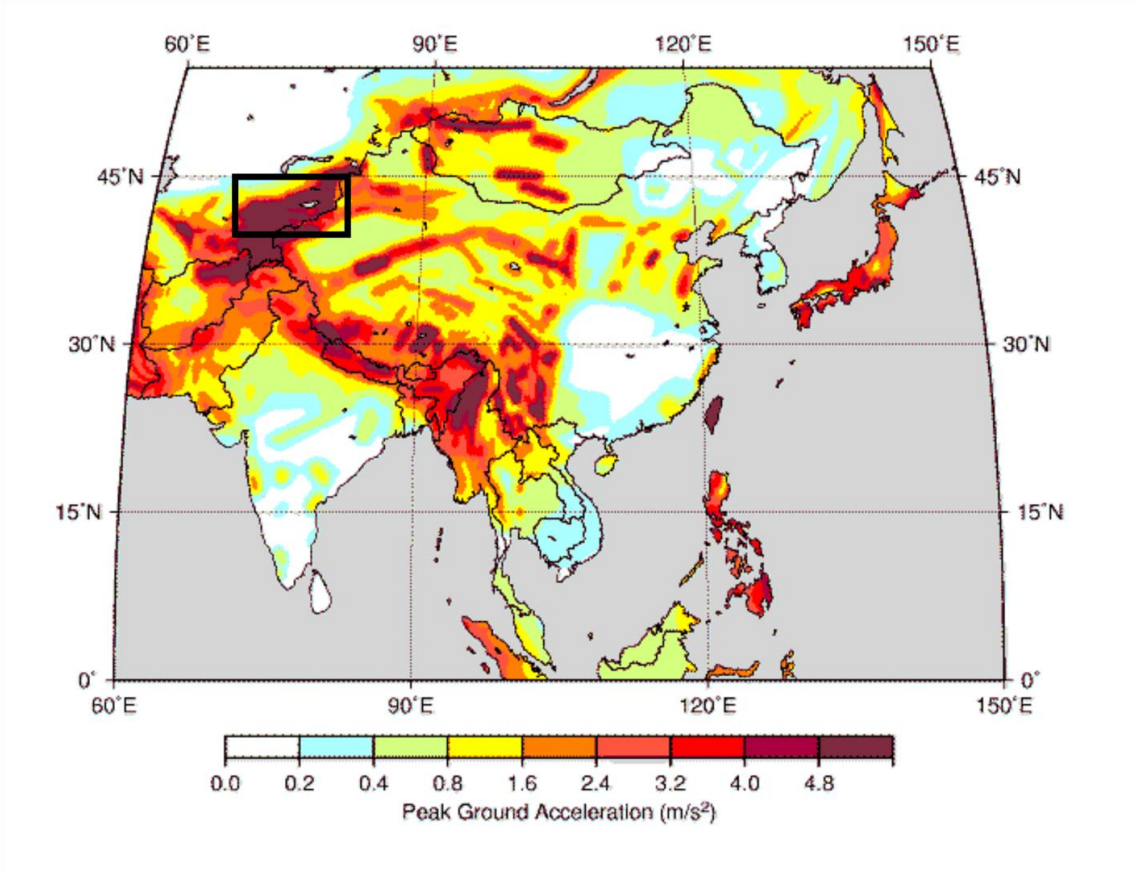

Figure 16: Global seismic hazard map of Asia, showing peak ground acceleration probability. Location of Kyrgyzstan shown with black box, exhibiting the uniformly highest seismic hazard in the region. Map annotated from the Global Seismic Hazard Assessment Program (1999). Seismic hazard is derived from the Indian subcontinent's collision with the Asian continent. Most of the current rate of convergence is accounted for in shortening in the Tien Shan, as shown in modern GPS rates (Abdrakhmatov et al., 1999).

The work contained herein concentrates on a single basin, Kochkor (Figure 17), that was likely connected to the greater Issyk Kul basin in the recent geologic past (Macaulay et al., 2016, Burgette et al., 2017).

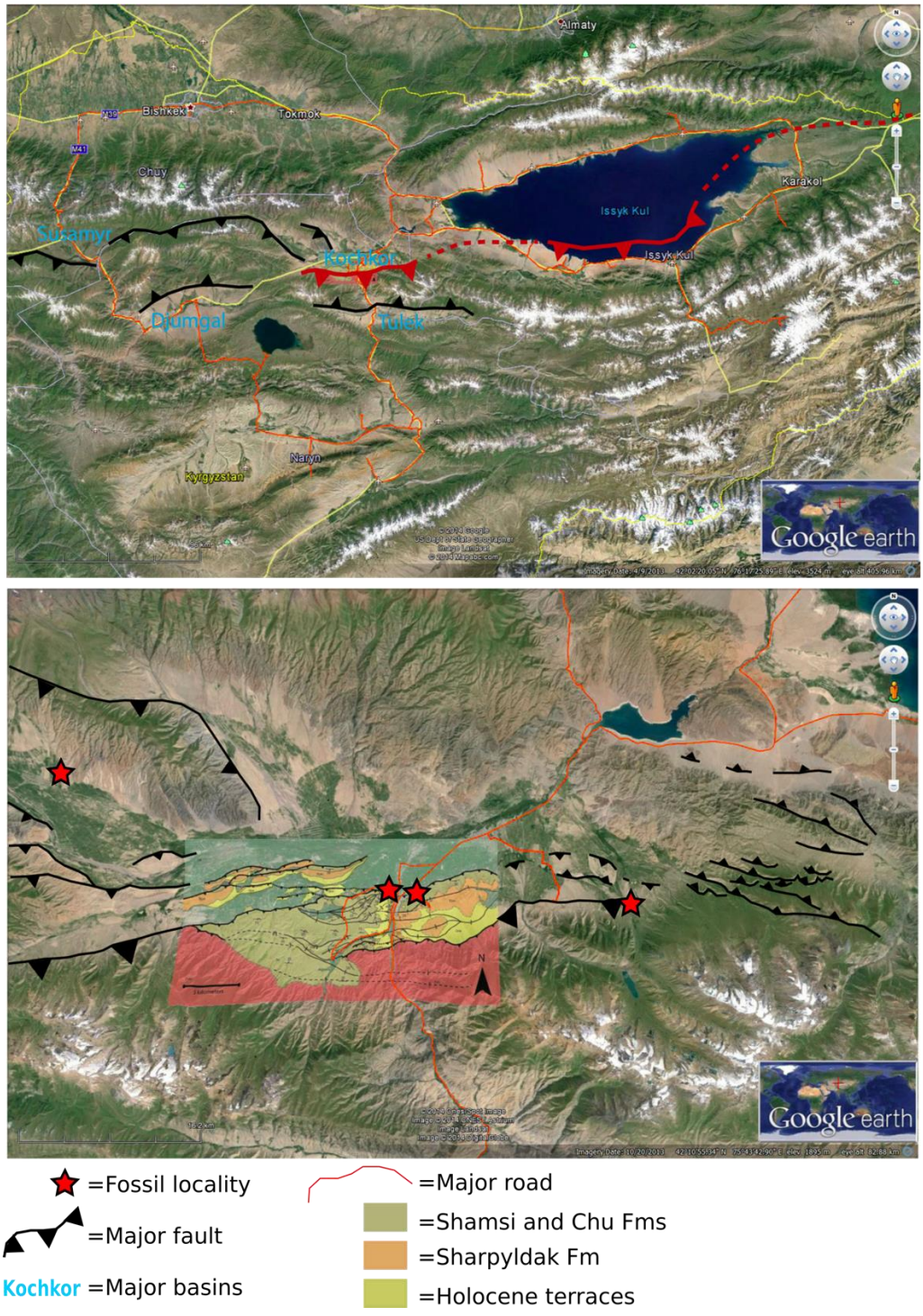

Figure 17: Google Earth imagery of the Kochkor Basin, Kyrgyzstan, with the Paulson (2013) map overlaid. Fossil localities, also sampled for magnetostratigraphy in this study, are shown with stars on the lower image. From left to right localities are Ortok, the Dam Site, Bone Hill (at the base of the previous Kochkor East section), and the Vodka fossil locality in the Kara Suu Valley.

While further interpretation of the data is needed to determine if uplift patterns in Kochkor Basin are representative of the Tien Shan, the location one basin to the south of the Ala Too range places the study sites in the central portion of uplift and deformation. Despite over two decades of fieldwork in the Kochkor, Naryn, and Issyk Kul basins (Abdrakhmatov et al., 1996, 2001), no rocks or sediments yielding radiomentrically datable minerals from the Cenozoic have been located. Previous geochronology attempting to date uplift has either been thermochronology or palaeomagnetostratigraphy (Abdrakhmatov et al., 1996, 2001, Wack et al., 2014, Sobel at al., 2006). Unfortunately, these methods largely do not seem to agree with each other. Without absolute dates to pin the stratigraphy on, magnetostratigraphy produces multiple possible correlations.

The initiation of uplift has major implications for the severity of continued seismicity (Burbank et al., 1999). If the Tien Shan began uplifting in only the last 10-12 million years, deformation would be relatively consistent throughout uplift, and with strain accumulation and uplift rates like those seem today (Makarov, 1990, Goryachev, 1959, Makarov, 1977, Sadybakasov, 1990, Abdrakhmatov, 1988, 1996, 2001, Chediya, 1986). If instead uplift initiated earlier, in the Oligocene to early Miocene, uplift rates would need to increase through time to match the slip and GPS rates seen today (Wack et al, 2014, Macaulay et al., 2016, Sobel & Dumitru, 1997, Burbank et al., 1999). This difference in mode of uplift is addressable via determining if boundaries between formations are coeval (climate driven) or occurred at different times (local scale tectonics), as well as determining absolute dates. If the Tien Shan uplifted rapidly in the last 10-12 Ma, that uplift would have to occur across the range, necessitating the formation boundaries being synchronous (Abdrakhmatov, 1996). If the Formation

boundaries are not synchronous, then the Tien Shan could have conceivably began uplift at the margin in the more distant past, with deformation propagating inwards through time. Additionally, absolute dating of the syntectonic strata, and comparing temporal ranges to sedimentation rates and current rates of uplift, slip, and GPS rates of deformation, illuminates if current rates of deformation are sufficient to explain the amount of uplift seen today (Thompson et al., 2002, Abdrakhmatov et al., 1996). GPS rate give the overall amount of convergence, but not the rate on individual faults. Therefore, to determine slip rates on individual faults, a longer time interval must be examined.

Biostratigraphy offers a yet unutilized method of dating the Neogene strata. However, little previous paleontological work in Central Asia, much less within the boundaries of Kyrgyzstan currently exists. A small amount of work exists from the Soviet era, including the recognition and description of a few taxa from the Eocene of the Fergana Valley region (Belyaeva, 1962). The Eocene of Kyrgyzstan has received continued attention, primarily centered in the Fergana Valley (Averianov and Godinot, 1998 & 2005), but with one site redescribed in the Issyk Kul Basin (Erfurt et al., 1999), representing the only formally described Cenozoic sites in the greater Issyk Kul/Kochkor basin. Several Paleozoic (Geyer et al., 2014) and Mesozoic (Averianov et al., 2007) fossil localities have also been described in the last thirty years, but no formal description of Cenozoic fossils younger than the Eocene exists. (Figure 18)

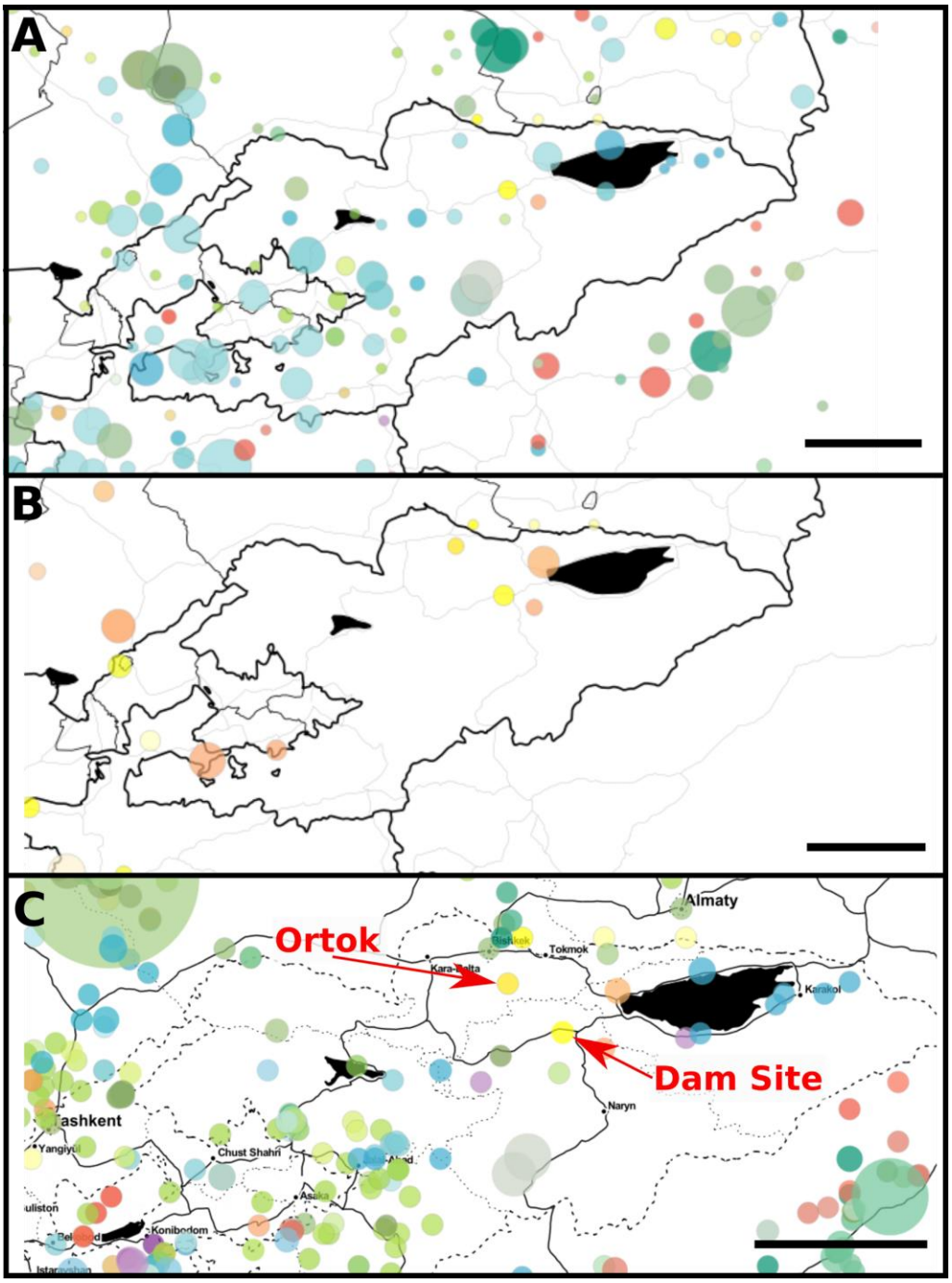

Figure 18: A. Map of all documented occurrences of fossil localities in Kyrgyzstan and surrounding areas reported in the Paleobiology Database (PBDB), B. Cenozoic fossil localities in Kyrgyzstan and surrounding areas, C. fossil localities in or near the Kochkor Basin. Light orange and yellow denote the Paleogene and Neogene respectively. All other colors are Paleozoic to Mesozoic localities. Size of circles denotes number of specimens or taxa. Localities include sites not formerly described, or most commonly listed in Belyaeva, 1948. All maps and data retrieved from the PBDB. Scale bar approximately 100 miles.

However, fossils from the later portion of the Cenozoic are widely present in Kyrgyzstan, as evidenced by undescribed fossils figured in the appendices of Tarosov's 1970 dissertation (shown as the two marked yellow circles in Figure 18C), mapping the faults of the Kochkor Basin, and several gray literature localities included in the biostratigraphic work of Sotnikova et al. (2001). As the rapid uplift of the Tien Shan provides a nearly continuous record of syntectonic sediments, fossils contained herein provide a novel method in Kyrgyzstan for calibration of other geochronological models.

Methods

Geology: Fossil-bearing localities were located via surface prospecting of previously geologically mapped Neogene stratigraphy in the Kochkor Basin for the Bone Hill and Dam Site assemblages (Figure 17). Once fragmentary vertebrate material is produced, further prospecting has yielded rich bone-bed deposits in five cases in the Kochkor basin thus far. Stratigraphic sections were measured using a Jacob's staff, Abney Level, and Brunton compass through all fossil bearing strata. Sections were measured to either connect to previously paleomagnetically sampled stratigraphy, or to collect new paleomagnetic samples included in this study. Lithostratigraphic data was collected from each stratum, such as grain size, sorting, composition, roundness, and test pits were dug to a depth of 20-30cm to produce unweathered material. A Munsell soil color chart was used to access color of strata and substrata. Paleosol structure was also noted when present, such as ped structure, presence of cutans (ped surface), and pedological structures such as root traces, gley, and slickensides (Retallack, 2008). Grain size was assessed with a hand lens and comparison to a mm scale card.

Magnetostratigraphy: Palaeomagnetic samples were collected with an impact sampler (see Figure 19) only, as sediments were either too poorly consolidated or vulnerable to disaggregation when wet, which prohibited drilling oriented samples. Instead the loose weathered material was cleared from the surface of each sampling site (see part A in Figure 19), and the impact sampler (technique and instrumentation modified from Weldon, 1986) was hammered into the outcrop 1-4 inches, or until stable, using a hand sledge. The concussive cap to the sampler is then removed, and a plastic and aluminum or brass (non-magnetic) platform is inserted into the now-open top of the impact sampler. The platform is grooved, so as the align a Brunton Compass or Sun Compass (see part C of Figure 19). Strike and dip is then recorded, with the Brunton compass placed on the rear of the sampler in the groove, while still in-situ in the outcrop to record orientation of the core. Rotation off the vertical orientation mark (see part B of Figure 19) is checked via the built-in level and noted for later correction of the sample. If weather and angle of the sample permitted it, a Solar Compass (see part C of Figure 19) was also used to check in-situ orientation of the core, with reading later converted using the SunAzm program (see APPENDIX E). The sampler, and internally contained oriented core, is then broken off the outcrop and the sample is extruded into a quartz glass sample holder using a "pusher" rod, or a steel rod slightly smaller than the internal diameter of the impact sampler, marked to preserve the known orientation from collection. Alternatively, samples were collected with a different impact sampler, with an internal plastic cartridge (see Figure 19).

A.

B.

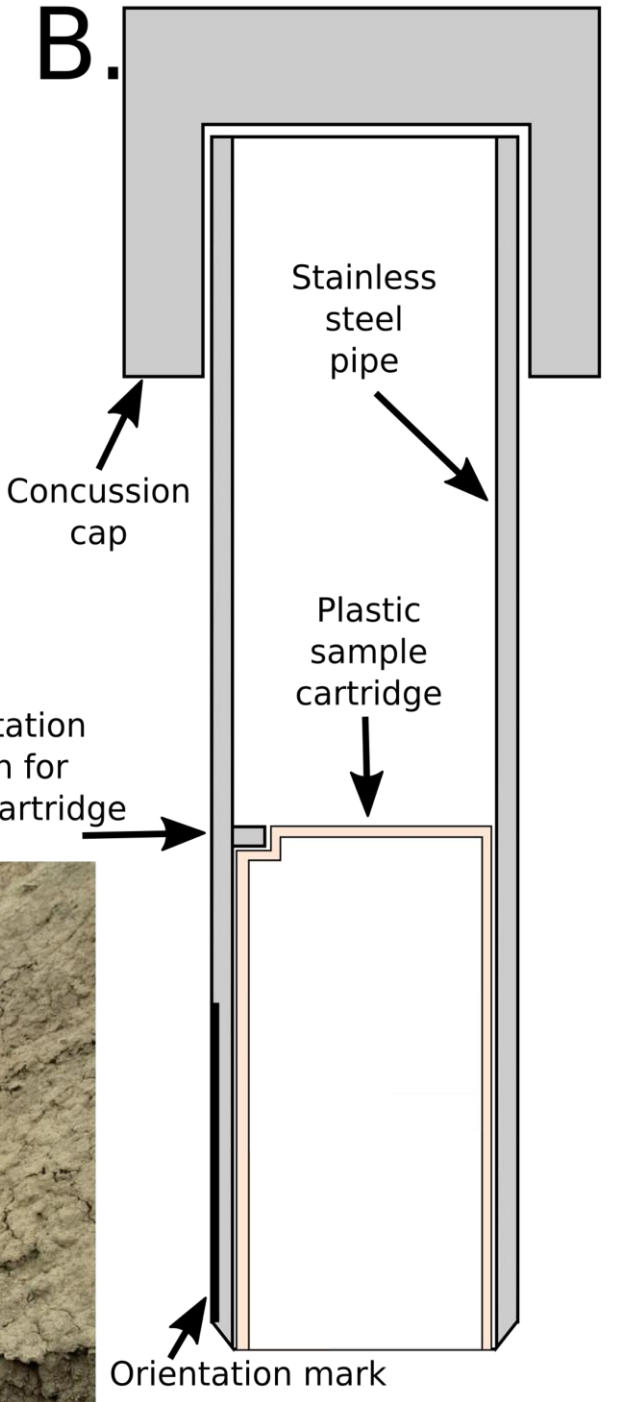
Stainless
steel
pipe
Concussion
cap
Plastic
sample
cartridge
Orientation
notch for
plastic cartridge
Orientation mark

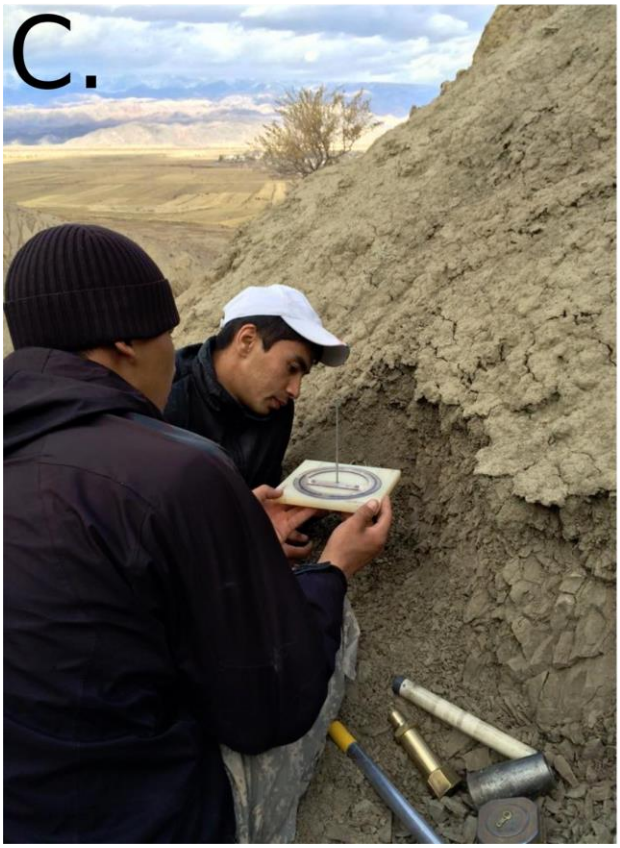

C.

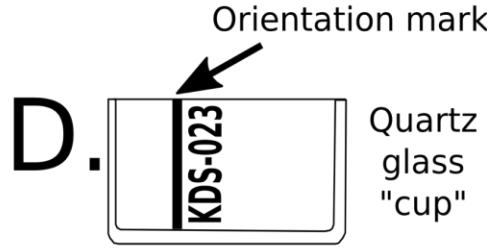
Orientation mark
D.
KDS-023
Quartz
glass
"cup"

Figure 19: Sampling methodology for collecting paleomagnetic samples in soft sediments. (A) Once weathered surface material is cleared, the impact sampler is positioned with the orientation line vertical, and hammered into the outcrop at an angle via direct blows with a hand sledge to the concussive cap. (B) Cross sectional diagram of the impact sampler, concussive cap, and plastic sample cartridge. Material shown in grey is steel, cream is clear plastic 2mm thick. (C) Two students from the Kyrgyz Institute of Seismology collecting core orientation data using a Sun Compass. The Sun Compass is fitted into a brass core inserted into the top of the impact sampler. On the ground in the right of the image is the concussive cap, plastic orientation cartridge for inserting the plastic sample cartridge, metal "pusher" for extruding the sample, and Brunton Compass. (D) Quartz glass sample cup in cross sectional view. Impact sample for quartz glass cups is same as figured, with the subtraction of the internal notch. Sample is in direct contact with internal diameter of the sampler tube and is extruded with the "pusher" rod. Orientation mark on the quartz glass cup is held lined up with orientation mark on sampler.

This cartridge, fitted into a notch on the upwards internal surface of the sampler chamber, also preserves the orientation of the sample, but holds enough core to load several quartz glass samples at a later date back in the lab. Samples, either in quartz glass cups or in plastic cartridges, were then labeled with a unique set of initials (see part C of Figure 19 for example) for each section and an individual number relating to stratigraphic position. Samples were sealed into cups with Parafilm. From the time of sample collection sample collection, the samples were shipped to the University of Oregon and immediately transferred to a μ-metal hutch. Samples spent three to four weeks in transit between collection and being placed into a fieldless environment.

In the lab at University of Oregon, specimens were stored in a fieldless environment, other than when samples were loaded into quartz glass from plastic cartridges or prepared for analysis. Poorly consolidated or broken samples were strengthened with a solution of sodium silicate. Sodium silicate was diluted with deionized water, as undiluted samples experienced crystal growth during the higher temperature thermal demagnetization steps (generally above 400° C. The sample surface

exposed at the open end of the sample cups was leveled with a hacksaw blade and course grit sandpaper if the sample height extended above the level of the sample holder. Space below the sample holder rim was infilled with Zircar Alumina Cement Type AL-CEM and cured under a heat lap within a μ-metal hutch. Most samples took two to three applications of Zircar cement to fill space, leaving 3-4 openings to allow for degassing and expansion of material. Course-grit sandpaper was again used to level the surface of the samples on the Zircar extending above the quartz glass sample holder. A White-Out pen was used to label the specimen numbers and redraw the orientation line on the quartz glass cups, as Sharpie marker (used in the field) burns off at approximately 300° C in the thermal demagnetization process.

Samples were run at the Occidental Paleomagnatism Laboratory in California. Samples are analyzed and stored in a fieldless environment. Transportation to the laboratory was also done in a μ metal hutch. Samples were divided into four sets for analysis, so that samples could be alternatingly analyzed while another set received thermal treatment, and limited by the 44 samples that would fit into the oven at one time. For all samples the Natural Remnant Magnetization (NRM) was measured first, to make sure samples recorded a magnetic signature and to measure a baseline to compare demagnetization paths against. All samples underwent four step-wise alternating field demagnetization (25 Oe, 50 Oe, 75 Oe, 100 Oe) followed by thermal demagnetization steps starting at 150°C up to 650°C, by 50° to 100° increments depending on volume of magnetization remaining in samples. We used a computer controlled superconducting moment magnetometer, with a conveyor sampling. The program Cithead was used to create “SAM” files, while PaleoMag 3.1 was used to conduct least-squares regression

models (Kirschvink, 1980) with most samples being fit to a line with variation in the

RATING	*DESCRIPTION OF ASSIGNMENT BASIS*
A1	At least 2 distinct lines formed in de-mag path. Primary inclination and declination within 30° of North and 60° for "normal" or South and 60° for "reversed" respectively.
A2	At least 2 distinct lines formed in de-mag path. Primary inclination and declination within 60° of North and 60° for "normal" or South and 60° for "reversed" respectively.
A3	At least 2 distinct lines formed in de-mag path. Primary inclination and declination within 90° of North and 60° for "normal" or South and 60° for "reversed" respectively.
B1	Only 1 line or there is more than 1 statistically significant component, but the last component removed is a plane. Primary inclination and declination within 30° of North and 60° for "normal" or South and 60° for "reversed" respectively.
B2	Only 1 line or there is more than 1 statistically significant component, but the last component removed is a plane. Primary inclination and declination within 60° of North and 60° for "normal" or South and 60° for "reversed" respectively.
B3	Only 1 line or there is more than 1 statistically significant component, but the last component removed is a plane. Primary inclination and declination within 90° of North and 60° for "normal" or South and 60° for "reversed" respectively.

Table 7: Rating system for accessing quality of samples

measured angle below 10°. Some samples were fit with a plane, but again, resulting polarity and directions were only included if the variation in angles was less than 15°. Samples fit with a plane were then fit with a line from the first and last points included in the plane to the origin, to determine the vector direction of demagnetization. Samples

with a variation of 10-15° were included as possible interpretations, but were not taken as sole indicators of polarity. To this end, a rating system of A1, A2, A3, and B1, B2, B3 was applied to each sample as an indication of quality (see Table 1).

A minimum of two samples from each strata and sampling site, with three run from some strata. While three samples were collected at each site, the third sample has only been run time permitting, and thus many strata currently contained unanalyzed samples. Lines or planes were fit for all components removed in a sample.

Biostratigraphy: Fossil material was quarried out of outcrop, with taphonomic data and sedimentary transport data also collected. Material underwent laboratory preparation to facilitate taxonomic identification. All vertebrate material is identified to the lowest taxonomic level possible, however in many cases this is still limited to subfamilies or genera. With little Neogene comparative material from Central Asia, and a high degree of endemicity, much of the Kyrgyz fauna represent novel species still in need of taxonomic description. While this will improve future biostratigraphic studies, it does limit the geochronological usefulness of some taxa.

Estimates of biostratigraphic range were generated from both the Palaeobiology Database (PBDB) (PBDB, 2017) and the New and Old Worlds Database of Fossil Mammals (NOW) (NOW, 2017). Temporal ranges were then verified, and in some cases modified, by referencing source literature from both databases. Taxa occurrences outside of Eurasia were not included, as biotic interchange at a continent level is relatively limited. When occurrences were questionable, the maximum temporal range verified by

at least two localities was taken. Age estimates for each site used only the taxa found in concurrence in each bone bed, to negate time averaging.

Results

Geology: Three full stratigraphic sections were measured, at the Kara Suu valley (KSU), Ortok fossil locality (KO), and west of the Chu River across the Dam Site fossil locality (KDS), with three from the Chu Formation (Figure 20) and one from the Shamsi Formation (Figure 20).

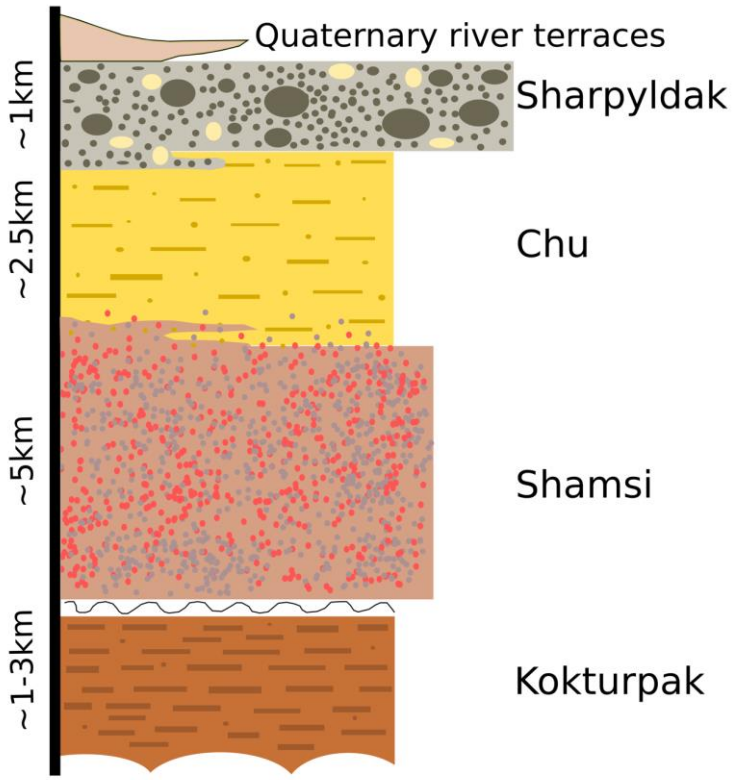

Figure 20. Schematic and generalized stratigraphic column for the Cenozoic formations outcropping in the Kochkor Basin. Relative average grainsize is indicated by the X axis, while stratigraphic position is related on the Y axis. Herein I use the figured names for formations, although other published works refer to some formations as "groups" and some formations by completely different names, as is discussed in the text. As this study concentrates on the Kochkor Basin, I use the nomenclature previously applied to sediment packages in the basin.

Although the sections are short, they stratigraphically correlate with much thicker sections from previous works (Abdrakhmatov et al., 2001, Weldon unpublished data). Additionally, they all also contain bone bed fossil localities, which narrows the age range possible, and the polarity of each bone bed facilitates correlating the fauna. A thinner section was measured as the base of the previous Kochkor P-mag East Section (KSS) (Abdrakhmatov et al., 2001), to extend the section down stratigraphy to include the Bone Hill fossil locality. Sedimentological evaluation, as well as comparison to previous geologic maps, places the Kara Suu section in the upper portion of the Shamsi Formation (Figure 20), possibly extending into the gradational zone connecting the older and stratigraphically lower Shamsi Formation into the finer-grained Chu Formation. This section is dominated by potassium feldspar-rich granite clasts, in sandstone to conglomerates (Mikolaichuk et al., 2008). The Chu Formation sections are more variable in parent material and color, but are averaged out as much smaller grain sizes, with primarily siltstones (Mikolaichuk et al., 2008). It is worth noting that existing literature variably refer to both the Chu and Shamsi formations as either formations or "Groups" (Mikolaichuk et al., 2008).

Exposure in the Kara Suu valley is limited to dry washes and gullies. Most of the exposure is sandstone to conglomerates, with a potassium feldspar-rich granite as the primary source rock, likely from the Paleozoic basement rock thrust over the Neogene sequences (see Thompson et al., 2002, Paulson, 2013, Mikolaichuk et al., 2008). Grains and clasts are rounded to sub-rounded, suggesting a degree of fluvial transport. Several exposures contain abundant imbrication of pebble to cobble sized clasts, pointing towards the center of the existing Kochkor basin, suggesting the current areas of topographic

highs as higher elevation dating back to at least deposition of the Shamsi Formation in the Miocene.

Lithostratigraphically, the largely finer-grained material of tan to reddish and greenish silts (Mikolaichuk et al., 2008) present at Ortok and the Dam Site confirm their affinity with the Chu Formation. Ortok is the smallest extent of exposure in terms of stratigraphic thickness, but is also the most consistently fine-grained. The entire sequence is siltstone to claystone and additionally is uniformly tan to cream in color (Figure 21).

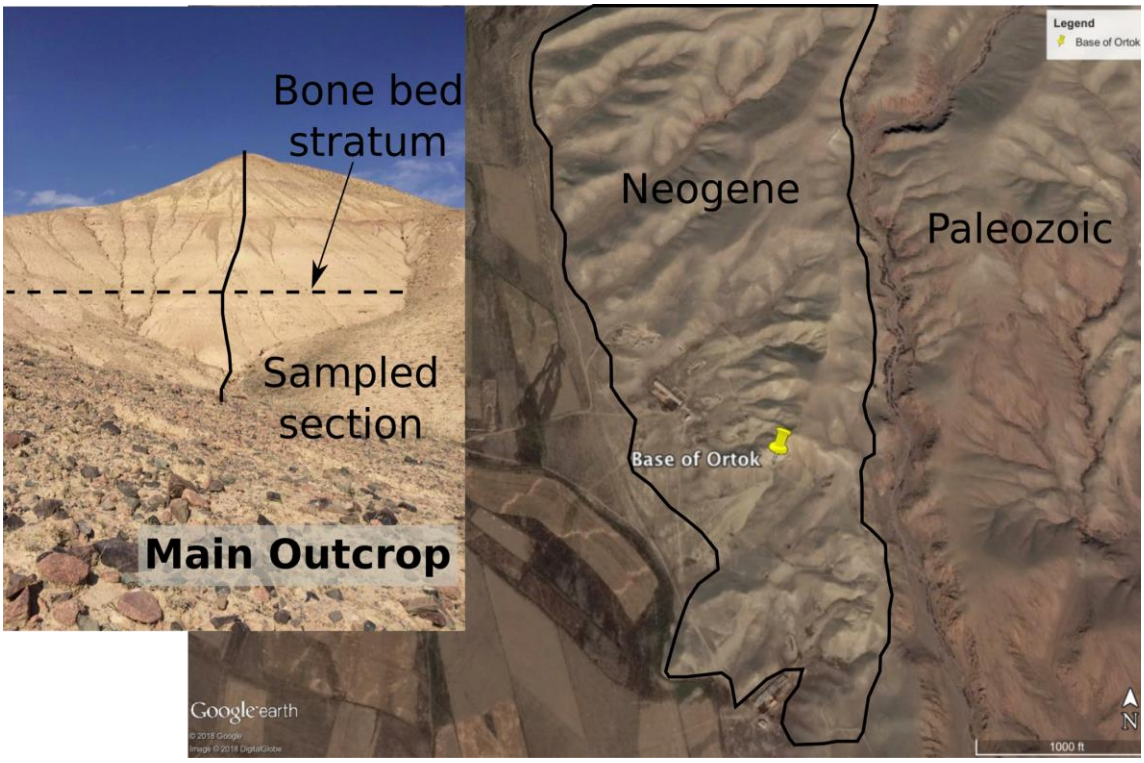

Figure 21. Google Earth imagery of the Ortok. Base of measured stratigraphic and paleomagnetostratigraphy section marked with "pin". Fossiliferous outcrop extends to east and north of the "pin" in the pale tan exposure. To the east, a gorge cut into reddish Paleozoic granite with the thin layer of Chu unconformably resting on it. Strata at Ortok are dipping very gently to the north and are the least deformed structurally of any site included in this study. Additionally, the fossils are the least diagenically altered, indicating little to no diagenic alteration to the site as well.

Ortok is also the only exposure of the Chu Formation on the Northern edge of the Kochkor Basin (Figure 22).

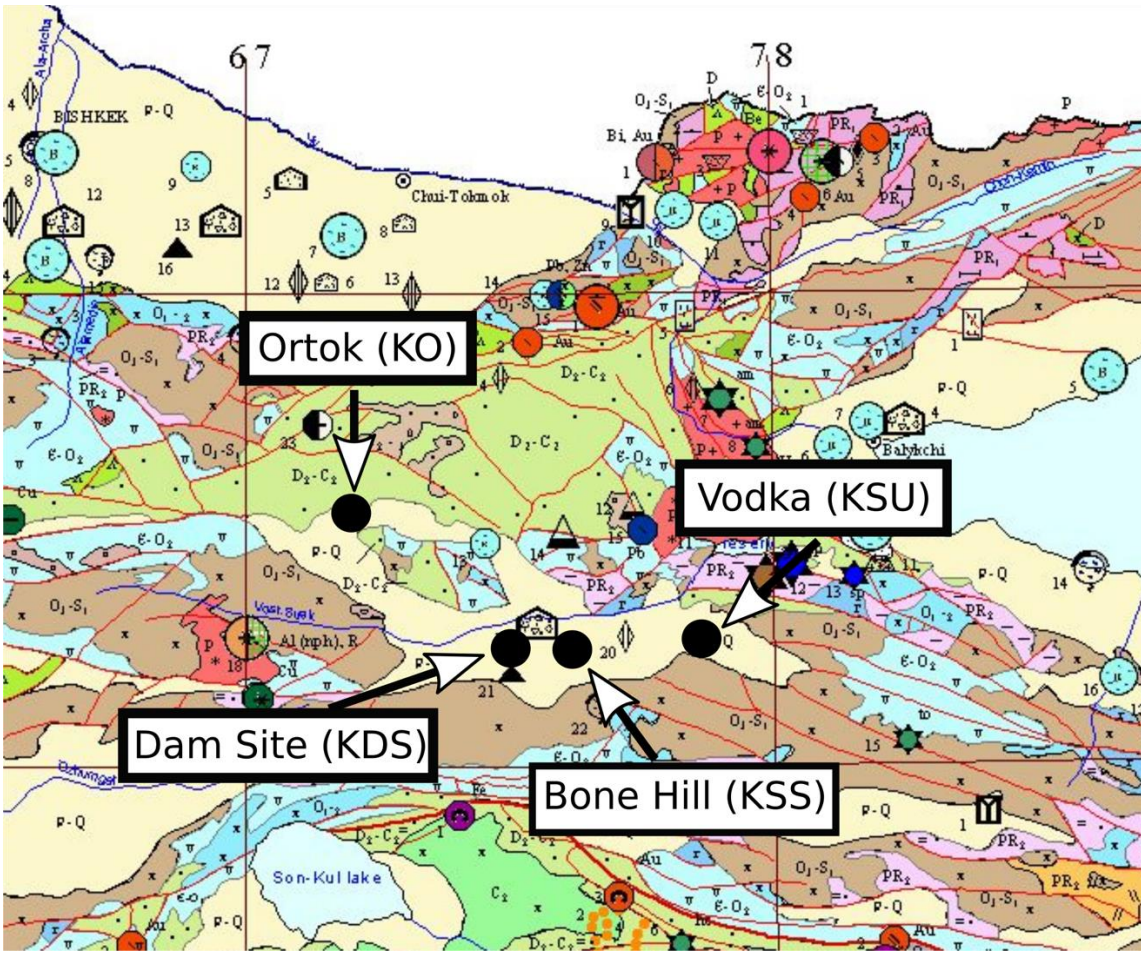

Figure 22. Geologic map of the Kochkor Basin. Major faults shown in red, very pale blue is water such as the lakes Son-Kul and Issyk-Kul. Light tan colored areas are Cenozoic sediments. Four fossil/paleomagnetic sites shown with black circles. Map highlights the narrow area of deformation separating the Kochkor Basin from the Issyk-Kul Basin (area of water on far east of map). Map annotated from Nikonorov (et al., 2000).

As the mountain range to the south provides the primary source (as evidenced by paleocurrent directional indicators in courser grained material), the formations are inferred to thin northwards as they onlap with the exposed Paleozoic to Mesozoic basement rocks.

Bone Hill fossil bed in the KSS section is continuing the Kochkor P-Mag East section stratigraphically lower, and thus is also part of the Chu Formation. Given the possible correlations of the section previously published (Abdrakhmatov et al., 2001), the

section lies in the lower extent of the Chu Formation, but above the gradational zone between the Shamsi and Chu Formations. Lithostratigraphic similarities, geologic mapping (Paulson, 2013), and the same magnetostratigraphic polarities between the fossiliferous strata of Bone Hill and Dam Site suggest these two localities are correlates of each other, despite several km separation and significant geologic structure separating the two sections.

While a fault clearly runs along the path of the Chu River, separating the stratigraphy to the east and west (Thompson et al., 2002, Paulson, 2013), we interpret little horizontal offset across the fault.

Magnetostratigraphy: Samples underwent Natural Remnant Magnatization (NRM) measurements, four steps of alternating frequency (AF) current, and thermal demagnetization. Thermal demagnetization was initiated at 150˚C and were heated by 50˚C increments to either 600˚ or 650˚C, depending on how much magnetic signal remained. Inclination and declination, in both geographic and tilt corrected values, is reported in the supplementary SQR files for each of the four sections (see appendix G-K). An example of a typical demagnetization path from the progressive AF and thermal demagnetization resulting in a strong overprint and primary path is shown in Figure 9. Some samples had an intermediate demagnetization pathway, primary from the Kara Suu (KSU) section, and an example from the Dam Site (KDS) is shown in Figure 10. These

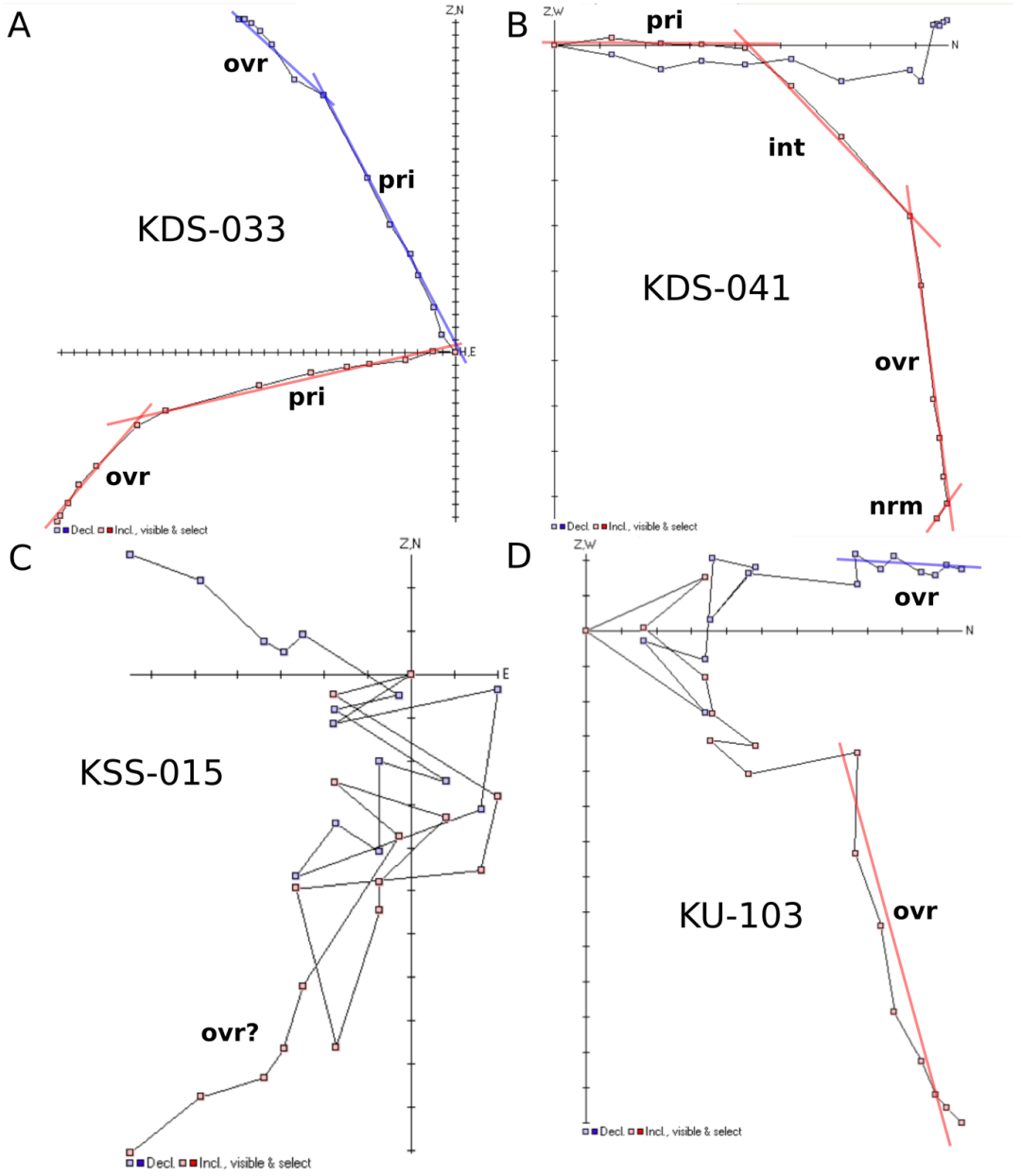

Figure 23: Example demagnetization pathways for four samples of varying quality. All plots shown are hyperbolic views of the Zeigerfield plot shown in geographic orientation. Red/pink points are inclination and blue points are declination of the sample at each progressive demagnetization step, with approximations of linear fit shown in red or blue lines. The points farthest from the origin are the NRM, the subsequent four points are the AF steps, and the remaining points are thermal steps. A demonstrates a typical sample with a clear overprint (ovr) and primary (pri) demagnetization pathway. B has a viscus remnant magnetization visible in the step from the NRM measurement to the first AF point. Then in addition to the ovr and pri, there is also an intermediate step, where more than one vector is being removed at once potentially. C is an example of a sample I was unable to extract any meaningful data from. D has a clear overprint (ovr), but lacks a clear signal for the primary component.

intermediate pathways may be additional overprints that occurred during deformation of the beds post the diagenic development of the primary magnetic signature and before the modern orientation and magnetic overprint. Other samples, within the "B" grades, displayed a clear overprint signal, but lost clarity in the primary pathway (Figure 23). Finally, some samples lacked any clear signal, and therefore couldn't be accurately analyzed, or received the lowest of the possible grades (B3) (sample figure of demagnetization pathway shown in Figure 23).

As samples uniformly turned red at high temperatures, and retained significant amount of magnetization above 500°C (Levy et al., 2012), magnetization is inferred to come from hydrated iron oxides produced diagenically shortly after deposition. The hydrated iron oxides appear to be primarily forming the cement between grains. While chemical analyses were not performed to precisely determine mineral identity, likely candidates include hematite (Fe_2O_3) or maghemite (γ-Fe_2O_3). Magnetic components are primarily contained in the cement, and not the original detrital clasts themselves. While Curie temperatures are often a range of temperatures for complete remagnetization, the lowest temperature end of Curie temperature for hematite is 500°C (Levy et al., 2012), implying the host rocks would have to have undergone a greater depth of burial or significantly more hydrothermal alteration than any of the Kyrgyz samples underwent to fully demagnetize the primary magnetic signal.

The detailed stratigraphic columns, paleomagnetic sampling sites, and inferred polarities for each measured stratigraphic column are presented in the following figures and the ratings for each sample, the SQR file values, and collection orientation data are

presented in appendices. Both the overprint and the primary demagnetization pathway α-95 values are presented after the stratigraphic columns.

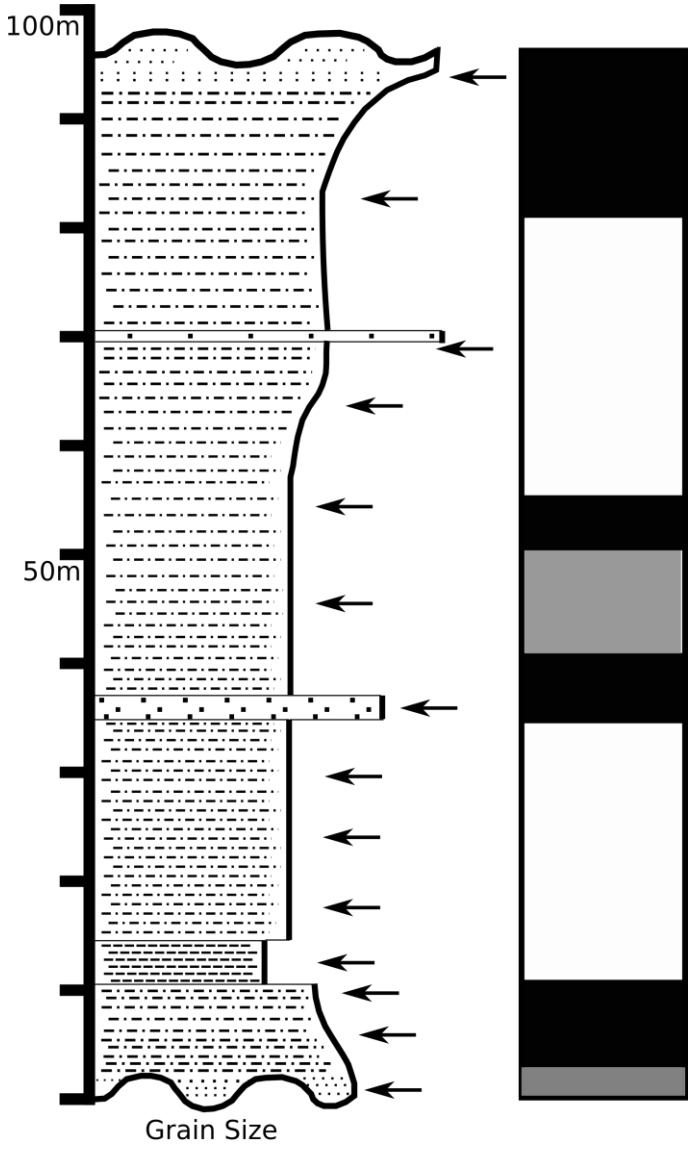

Figure 24. Stratigraphic section for the KSS section including the bone bed Bone Hill. This section is overlapping with the lowermost portion of the Abdrakhmatov (et al., 2001) Kochkor East section. Lithology is more varied in this section, ranging from siltstone to conglomerates. Paleomagnetostratigraphy sampling locations are denoted with black arrows, and three samples were collected at each location. Inferred primary polarity for each locality is shown to the right, with black bars representing normal polarity and white bars representing reversed polarity. If samples from the same strata were not in agreement, the polarity is shown as gray. When polarity changed, the change was inferred to occur at a stratigraphic level halfway in-between sample

localities. As samples were collected in a high density, actual boundaries could only move 1-2 meters in stratigraphic placement.

Measured stratigraphic section, with paleomagnetic sampling and reversals noted, for the Bone Hill fossil locality and Kochkor East section (KSS) is presented in Figure 24. This section overlaps with the previous Kochkor East section of Abdrakhmatov (et al., 2001), extending the section downwards to include the stratum bearing the bone bed. The lower percentage of "A" grade samples from this site is likely owning to the site being the first sampled, and thus the site with the greatest variation in sampling technique. Overprint and primary demagnetization pathway α-95 values are presented in Figure 25. SQR Files for all fits are reported in the Appendices G-K, with rating values of each samples also reported.

The Vodka fossil site, in the Kara Suu Valley (KSU) is the thickest stratigraphic section measured and sampled in this study. It is also the only section beginning in the stratigraphically lower Shamsi Formation, and extending to either the upper portion of the formation, or even the gradational zone between the Shamsi and Chu formations. A stratigraphic section, with paleomagnetic sample sites and inferred polarity is shown in Figure 26. The overprint and primary demagnetization pathway α-95 plots are presented in the following figure (Figure 27). The SQR File, with geographic and tilt-corrected demagnetization pathways is presented in appendix H, with A/B grade rating also reported.

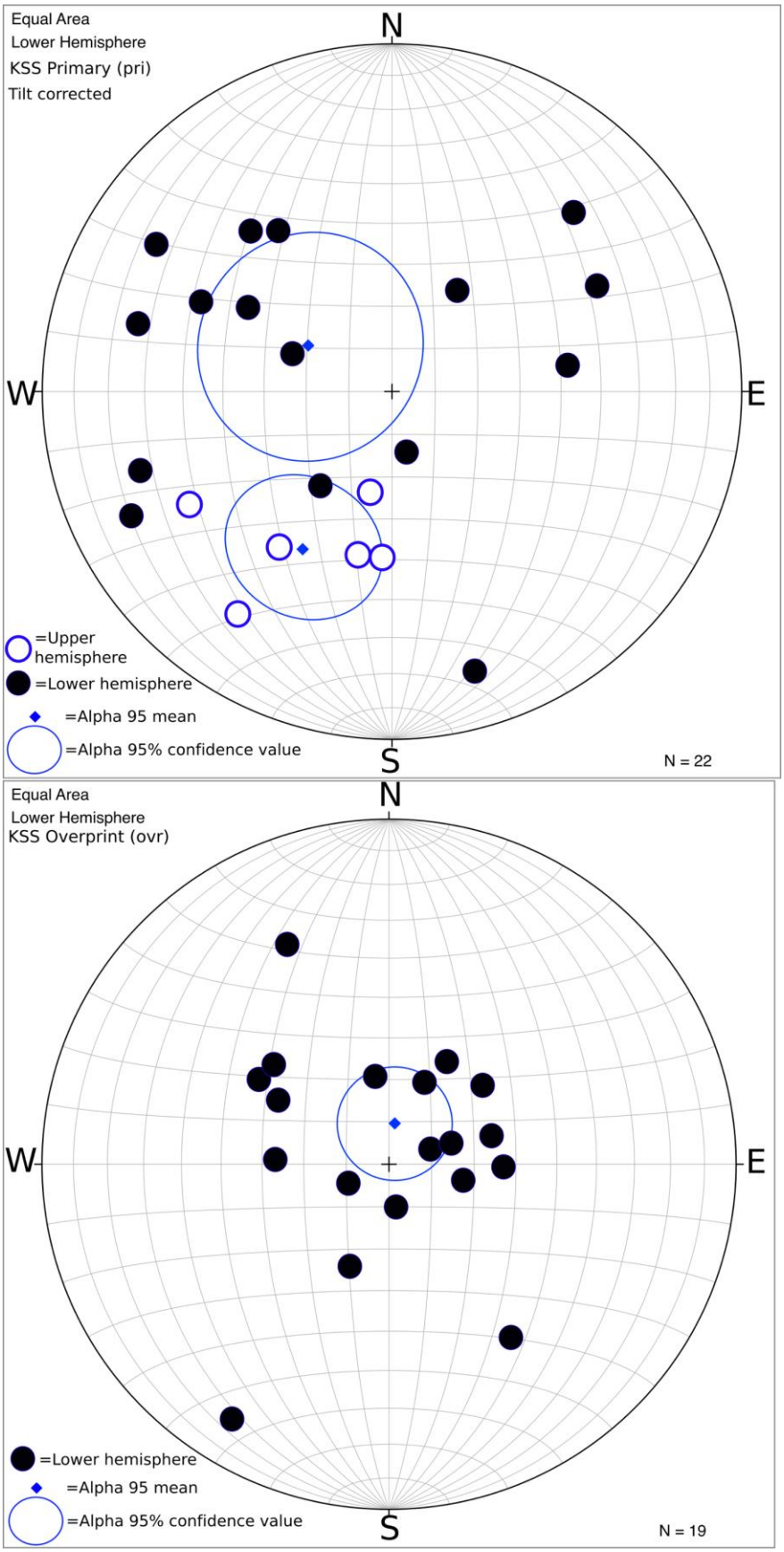

Figure 25: Alpha 95 plots of the overprint (bottom) and primary (top) for the Kochkor East extension (KSS). Each point is the average line for a demagnetization pathway plotted on a stereonet. The ovr plot is in geographic view, and the pri plot is in tilt corrected view.

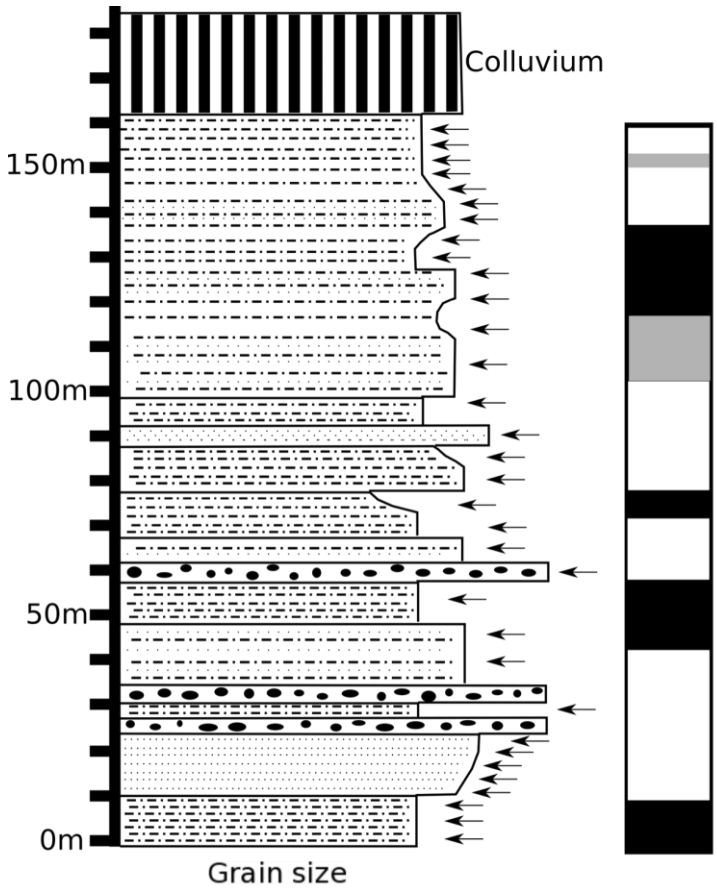

Figure 26: Stratigraphic section for the Kara Suu (KSU) section containing the Vodka bone bed locality. Palaeomagnetostratigraphy sampling locations shown with black arrows, and three samples were collected at each sampling locality. Lithology ranged from silty sandstone to conglomerate. Black bars denote normal polarity, white is reversed polarity, and gray is when samples were not in agreement as to the polarity.

Finally, the Dam Site (KDS) is the second thickest stratigraphic section presented herein. Located in the Chu formation, it is inferred to be correlative with the Bone Hill (KSS) section to the East, across the Chu River. This is also the section where we measured a fold test, on a highly-folded layer at the base of the stratigraphic section (Figure 28). The fold test was measured on two distinct strata, a grey shale layer, and a red paleosol, separated by course sandstone layer. The α-95 plot for the fold test is

presented in Figure

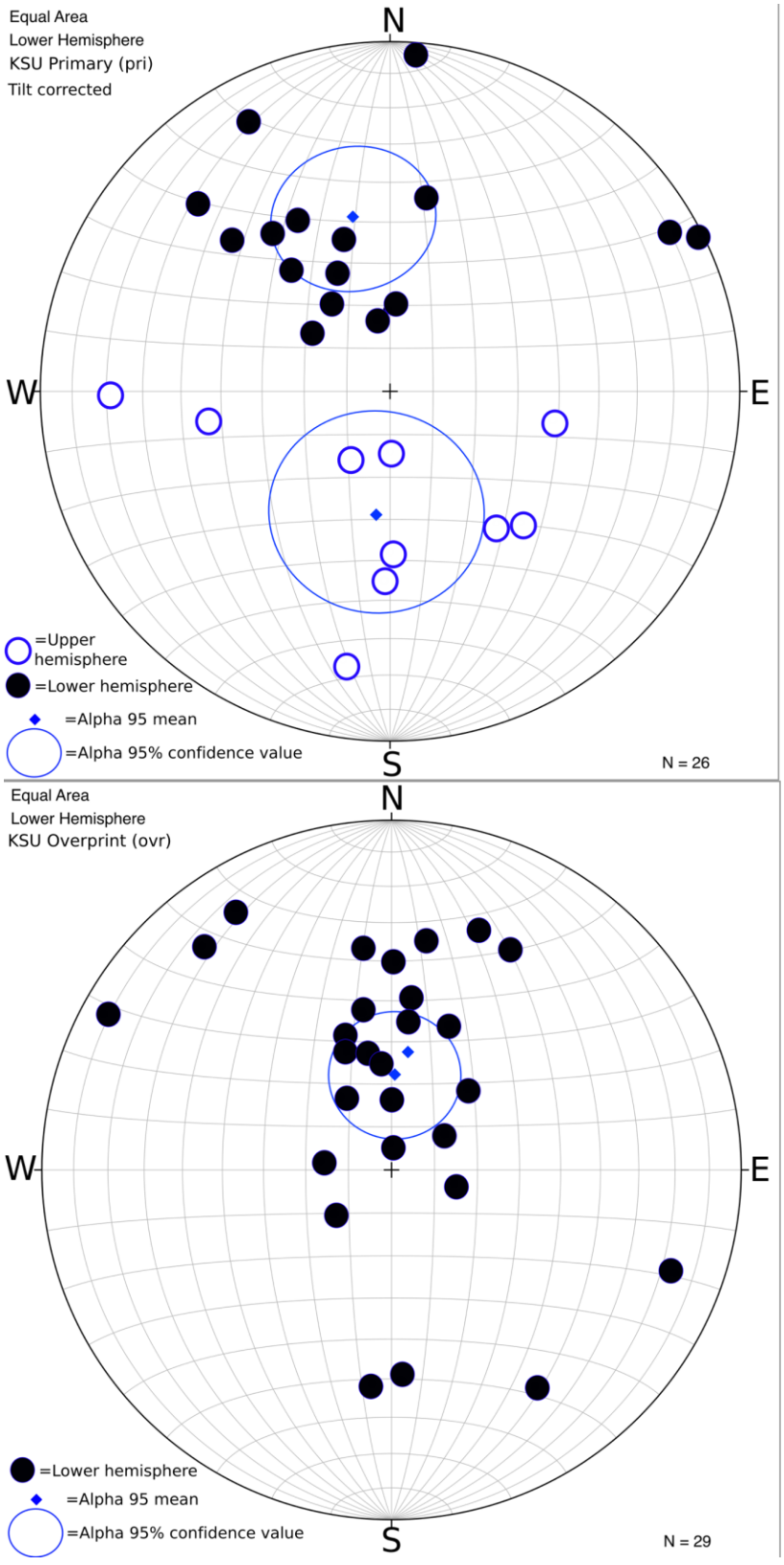

Figure 27. Stereonet plots of Kara Suu (KSU) showing the primary and overprint polarities. Blue circles show the 95% cone of confidence from the alpha 95 mean values (blue dots). Primary values are tilt corrected.

29, while the stratigraphic column, paleomagnetic sampling sites, and inferred polarities

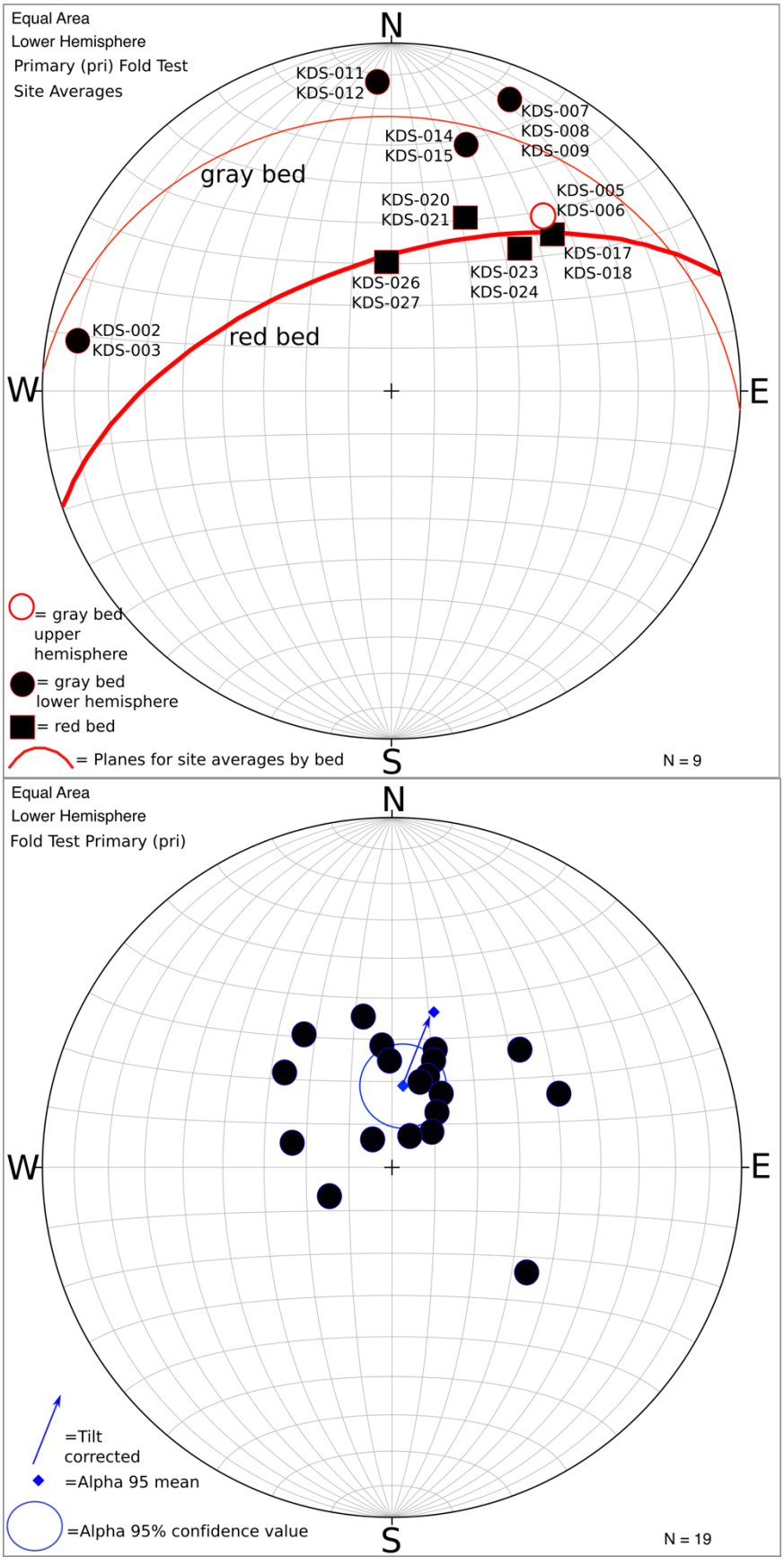

Figure 28: Fold test conducted at the base of the Dam Site (KDS) section. Two beds less than 1m apart stratigraphically were both sampled for the fold test. The upper plot is site averages of both analyzed samples in each site, plotted against other samples from the same bed. Both beds fit similar great circles. Individual values were tilt corrected prior to averaging. The lower plot is primary values for all sample from the fold test, prior to tilt correction. The alpha 95 median value is shown with a blue diamond, with an arrow denoting how the overly steep value is corrected for tilt.

are presented in Figure 30. The SQR files for all samples are reported in Appendix K.

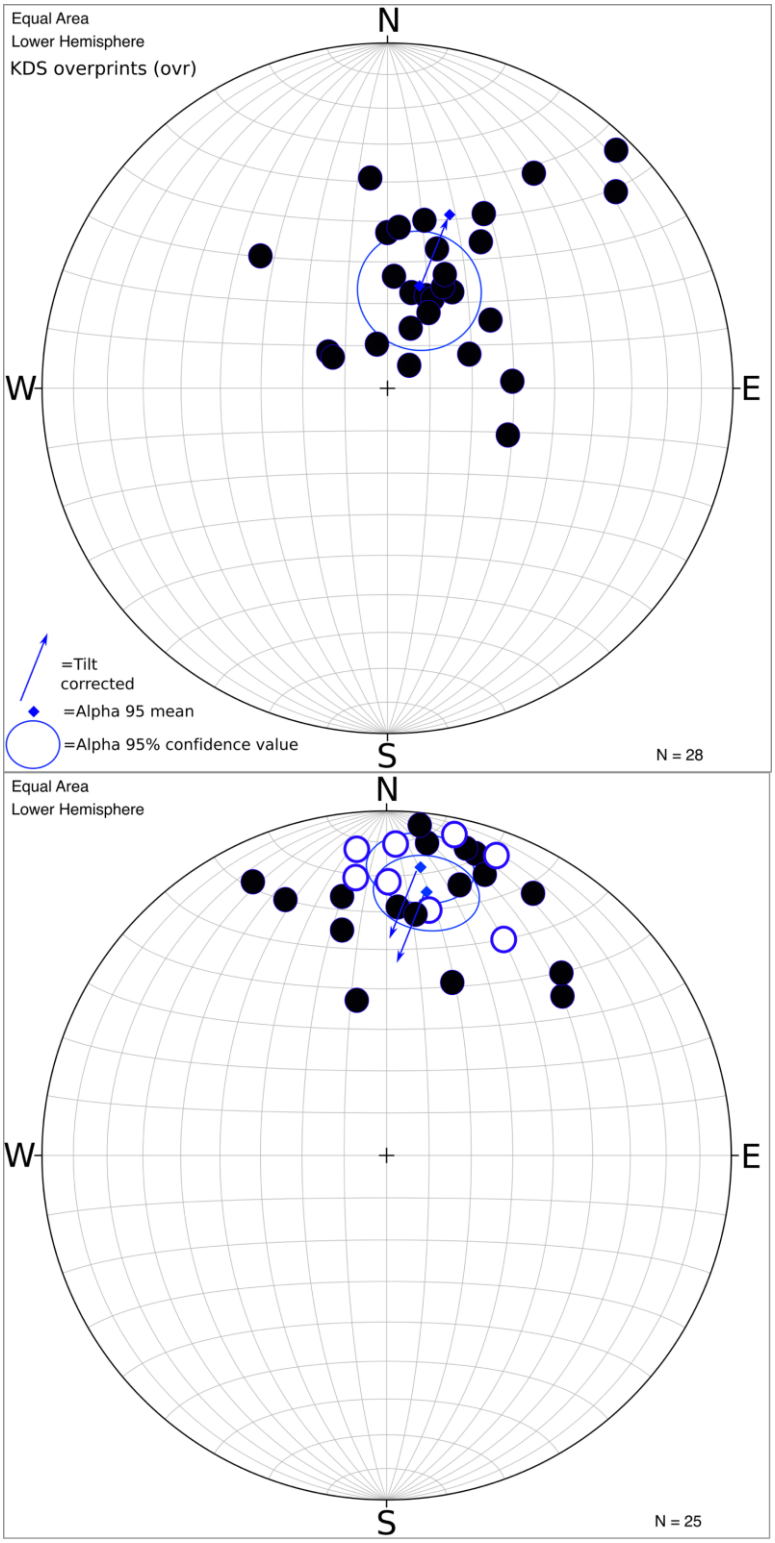

Figure 29: Alpha 95 plots of the overprint (top) and primary (bottom) for the Dam Site (KDS). Each point is the average line for a demagnetization pathway plotted on a stereonet. Both plots are in geographic view, with the blue arrows showing the tilt corrected data. While the overprint is North and Down, it is quite steep before correction. The Pleistocene-Holocene river terraces are also tilted, and indicate the site continues to undergo structural deformation in modern times. The primary pathways are all normal polarity in this section, as shown by the upper and lower hemisphere alpha 95 value circles. The number of samples varies, as only samples with a clear demagnetization pathway were included, thus not all analyzed samples can be included.

Figurers for Ortok (Figure 31 and Figure 32) follow. As Ortok is almost flat lying, the

plots are not tilt corrected. Ortok is the thinnest section, but also the most fine grained and the only section on the northern boundary.

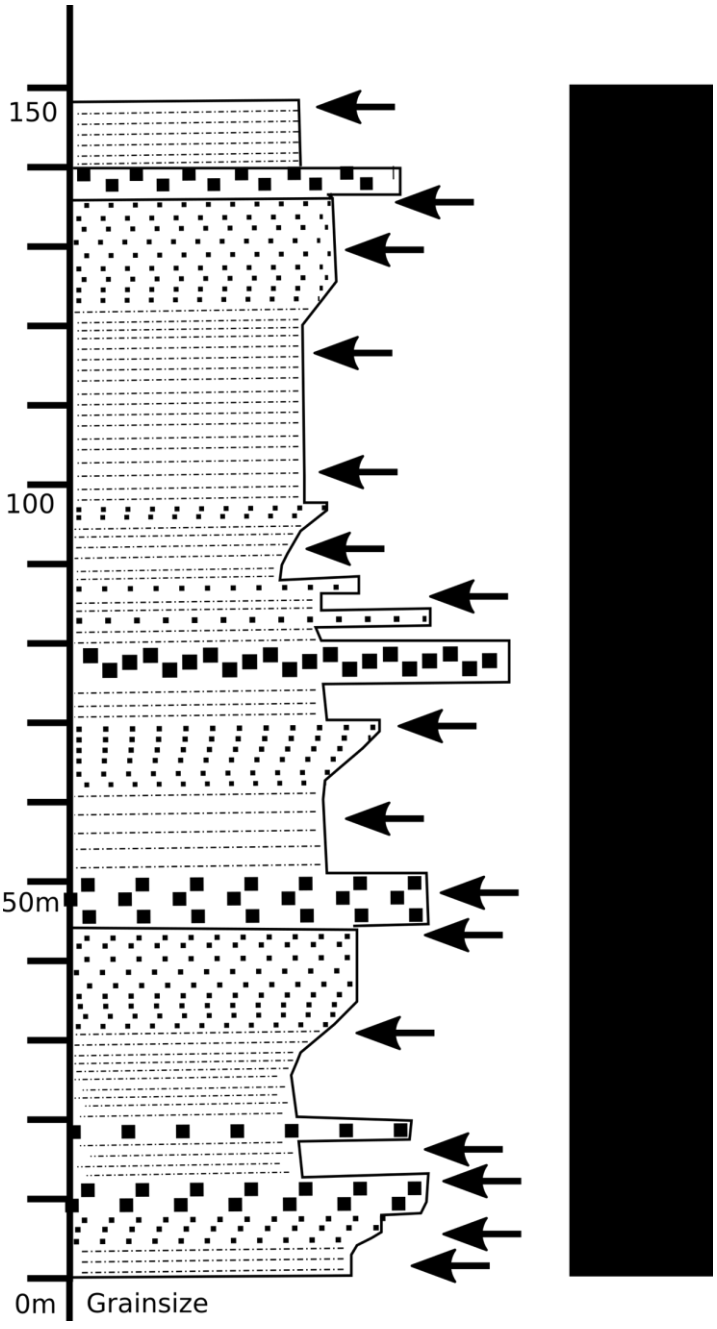

Figure 30. Stratigraphic section for the Dam Site fossil site. Paleomag sampling sites noted with arrows. The whole section is normal polarity.

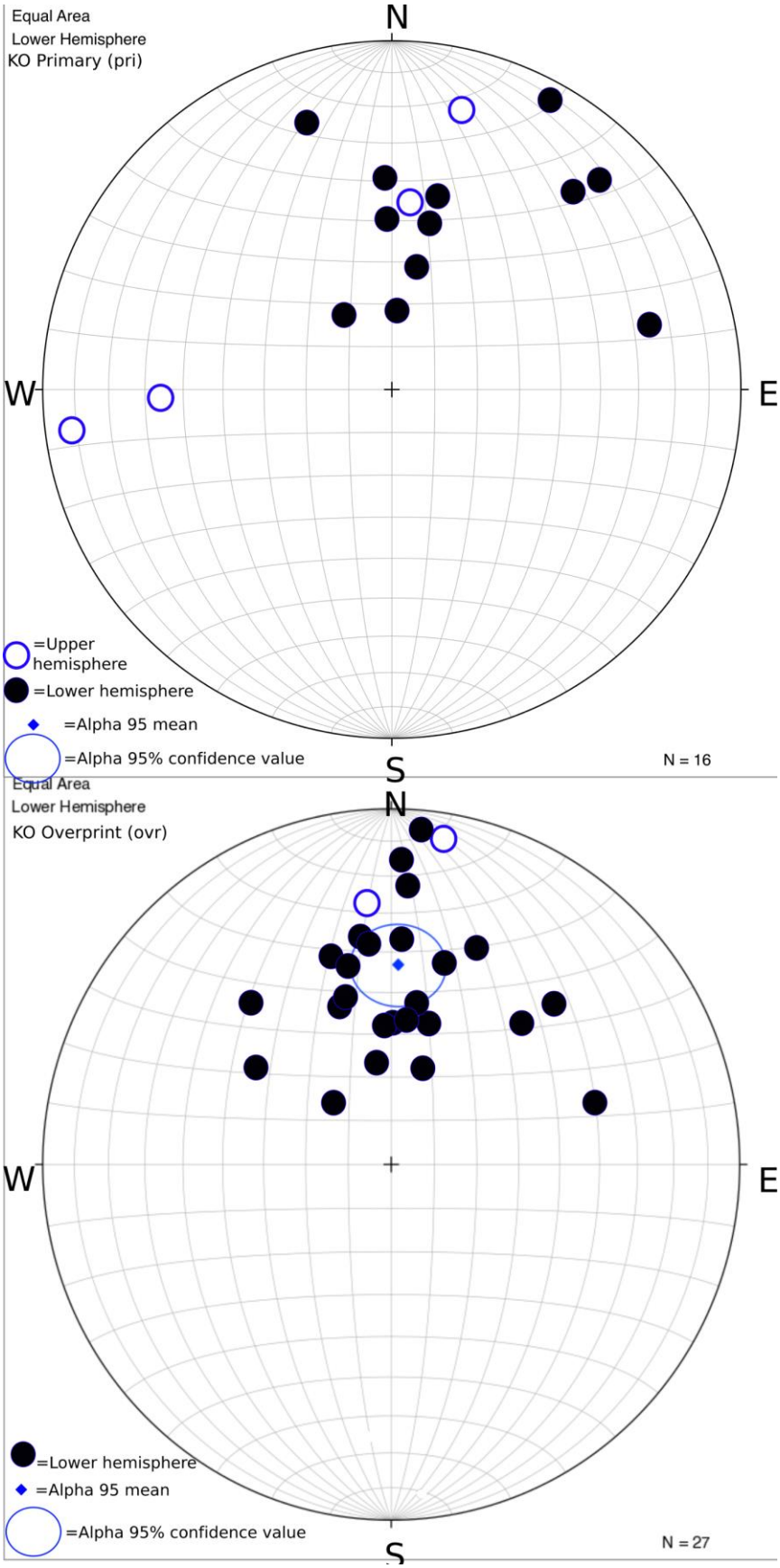

Figure 31: Stereonet plots of Ortok (KO) showing the primary and overprint polarities. Blue circles show the 95% cone of confidence from the alpha 95 mean values (blue dots). Primary values are tilt corrected. Because the tilting is so minimal (less than 15%), plots are geographic and not tilt corrected.

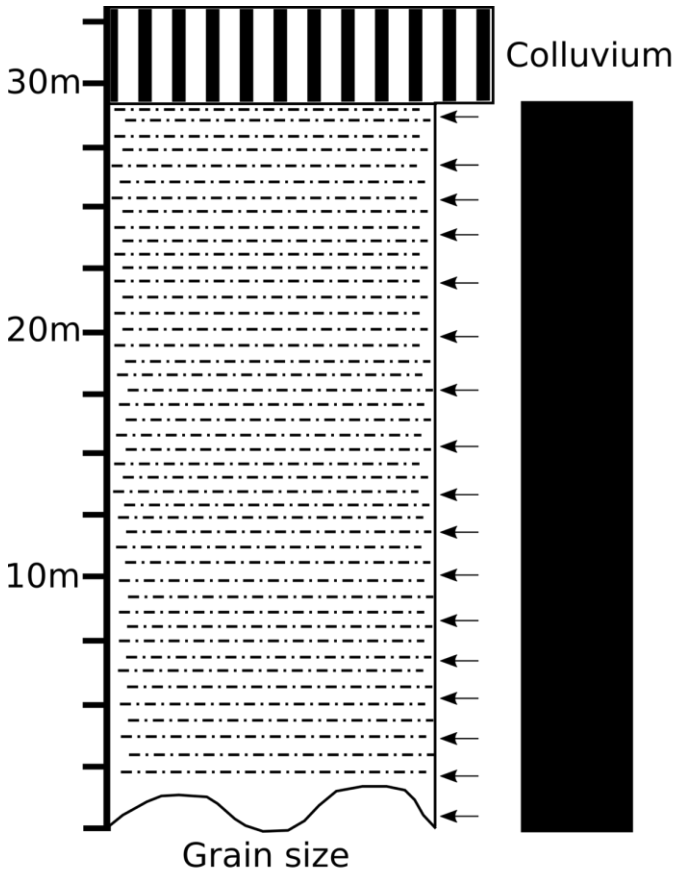

Figure 32: Stratigraphic section for Ortok. Magnetostratigraphy sampling locations shown with arrows. Three samples were collected at each site.

Biostratigraphy: Vodka, the oldest fossil locality, is within the age range of 5.3 to 9.6 Ma (Figure 33). Primarily constraining this site is the genus *Chilotherium* and the clade Cervinae, or modern-type deer. The *Chilotherium* is unfortunately material from a new species, and thus a species age range is not known (see chapter 4). This new species is however phylogenetically nested well within the genus, thus the taxon is unlikely to have evolved prior to previously published member of the genus. Regionally, one of the phylogenetically closest relatives *Chilotherium kowalevskii*, appears in Greece, Moldova, and Turkey from 9.5 to 7.3 Ma (NOW, 2017, Heissig, 1996, Güleç et al., 2007). True cervine deer, as evidenced by the complete formation of the antler pedicle and

development of the cervine fold in molars, are not seen till 9.6 Ma (Breda, 2001, Pitra et al., 2004, Azanza et al., 2013, Vislobokova et al., 2003), adding a more concrete lower limit on the age estimates. The oldest *Hipparion* horses in Asia do not appear before 12 Ma (Sen, 1990), with most invasions closer to 10 Ma (Vilobokova et al., 2003), providing a hard lower-limit to corroborate the slightly younger range of the cervine deer.

Bone Hill fossil bed generates a possible age range of 5.3-7.3 Ma for the stratum (Figure 33). The lower age limit is constrained by the presence of a premolar from the genus *Hyenaictitherium*, and while it is not enough material to assign to a species, the lower limits of the genus lie at 8.2 Ma (Ginsburg, 1999), with most representatives of the genus, and possibly more reliable geochronology, younger than 7.1 Ma (Andersson & Werdelin, 2005, Zhu et al., 2008). The upper age limit is again confined by the genus *Chilotherium*, which only regionally makes it to 5.3 Ma (Heissig, 1996, Zhu et al., 2008, Deng, 2002), before being replaced by more modern-type rhinocerotids, as evidenced by fossil *Coelodonta* material on display, but unpublished, in the Karakol Museum in Karakol Kyrgyzstan.

The Dam Site has a lower age limit of 7 Ma, as constrained by the presence of a modern-form leporid, or rabbit. While the order Lagomorpha dates back considerably earlier, true rabbits do not appear in Asia until 7 Ma at the oldest localities (Flynn et al., 2013). Again, the presence of *Chilotherium* offers an upper constraint of 5.3 Ma (Heissig, 1996, Zhu et al., 2008, Deng, 2002). These leaves one of the narrowest possible age ranges for the Dam Site (Figure 33). Other taxa present include an ochotonid (pika), gazelle, equid, and giraffe.

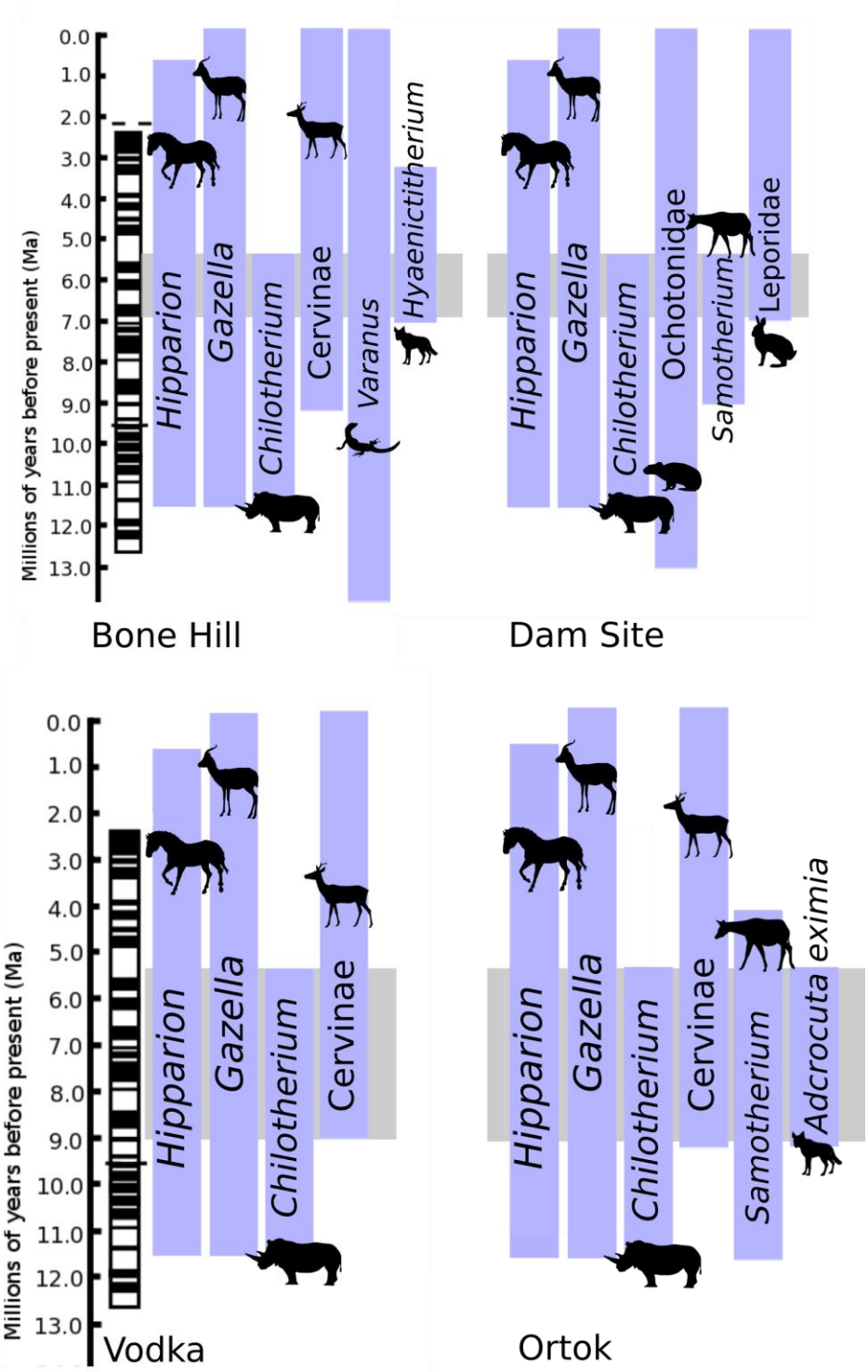

Figure 33. Biostratigraphic ranges for each of the four bone beds. Genus or clade ranges shown in purple bars, relative to the absolute time scale. Possible age range given only the fauna for each bone bed shown in gray bar.

Finally, the stratigraphically youngest bone bed, Ortok has a possible age of 4.9 to 7.7 Ma (Figure 33). Temporal constraint at this site rest on a single well-known species, *Adcrocuta eximia,* a large hyenid (Turner et al., 2008). This also demonstrates the improved utility of vertebrates as biostratigraphic indicators, if a species level assignment is possible. Corroborating the age estimate, although with known older age ranges, are the true cervine deer (Azanza et al., 2013) and the giraffe *Samotherium* (Kostopoulos, 2009).

Discussion and Conclusion

With three sections containing bone beds within the Chu Formation, and one within the Shamsi section, the relative age of Vodka is older, but relating the three Chu sites is more difficult (Figure 34). The Bone beds at the Dam Site and Bone Hill seem to be correlatives, or at least the fossils beds both lie in a band of normal polarity, with a younger fauna at Ortok. Ortok is also the finest grained, and in general the Chu formation seems to fine upwards until interfingering with the Sharplydak (Figure 35). Given the youngest biostratigraphic age of 5.3 Ma for all three Chu localities, and the extent of the Chu formation exposed up section from our measured sections, we place all three measured Chu sections in the lower portion of the Chu Formation. While the boundary between the Chu and Shamsi Formations is certainly transitional and may span some thickness, we place the entire Kara Suu section within the Shamsi Formation, given our preferred match with the global time scale and biostratigraphic constraints.

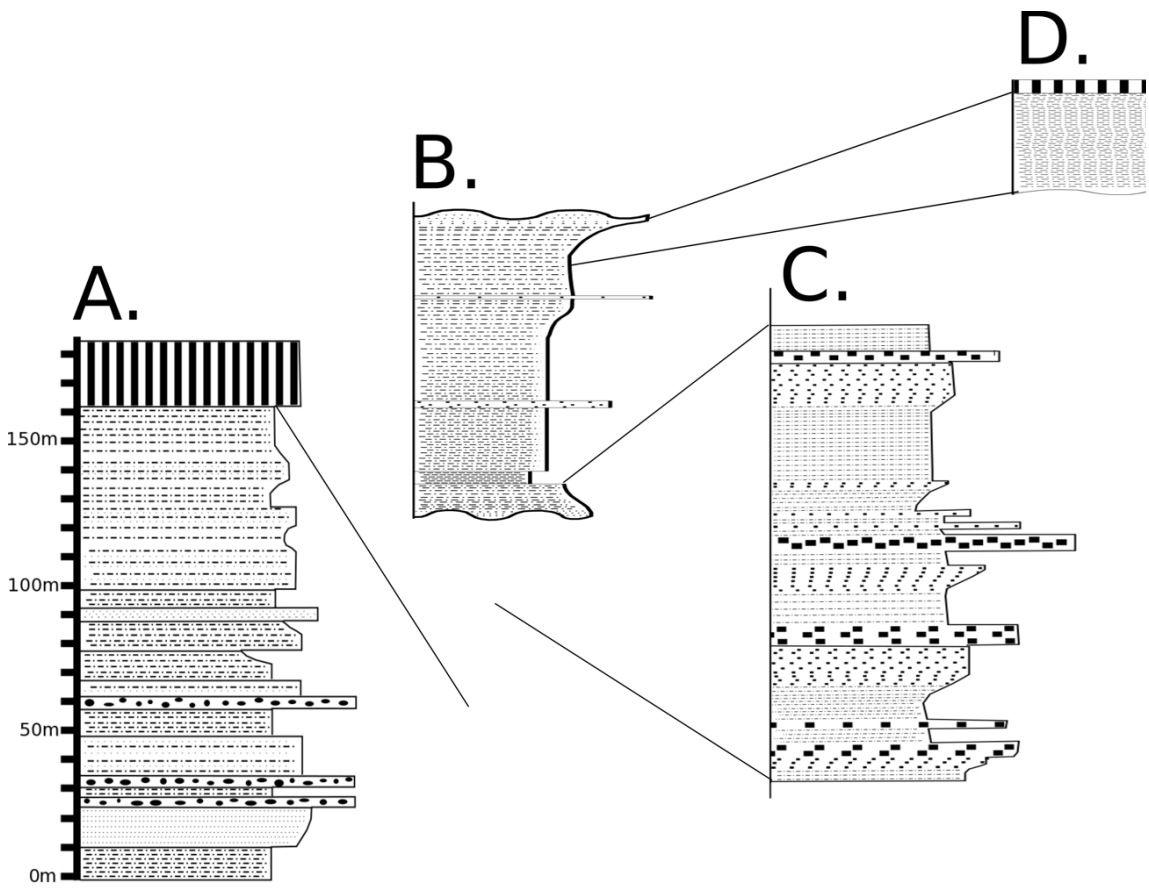

Figure 34: Fence diagram of the four measured stratigraphic sections. A-D is Vodka (KSU), Bone Hill (KSS), Dam Site (KDS), and Ortok (KO). Grain size is shown in thickness on the x axis, vertical thickness is scaled relative to one another, with true thickness shown in meters for Vodka. Vertical bands as fill denotes colluvium.

Given the possible temporal ranges of each fossil bone bed in the context of the magnetostratigraphy, we present the following as our preferred interpretation for each section (Figure 36). The additional section at the Kochkor East section, with the addition of biochronological constraints, causes us to select an interpretation of the Kochkor East section differing from the published Abdrakhmatov et al., (2001), placing the base of the section about one and a half million years younger than the authors' previously preferred interpretation. While previous work in the Kochkor Basin is limited, the Issyk Kul and Kochkor Basins were likely connected until geologically recently, as shown by the low topography of late Neogene sediments separating the two basins (Nikonorov et al., 2000).

Figure 35: One of the few outcrops with a clear relationship between the Chu Formation and the Sharplydak Formation. Red lines denote the contact between the two formations and illustrate that while the contact it sharp, the two formations do interfinger, and thus were presumably conformable. The pictured outcrop lies to the south of Ortok, but farther west than the Dam Site.

We therefore find direct comparisons to magnetostratigraphy studies from the Issyk Kul Basin to be useful. Most recently is the Wack et al. (2016) study, examining two sections on the southern shore of Issyk Kul. These sections sample primarily the Kyrgyz Group, which is equivalent to the Shamsi Formation (Wack et al., 2014, Nikonorov et al., 2000).

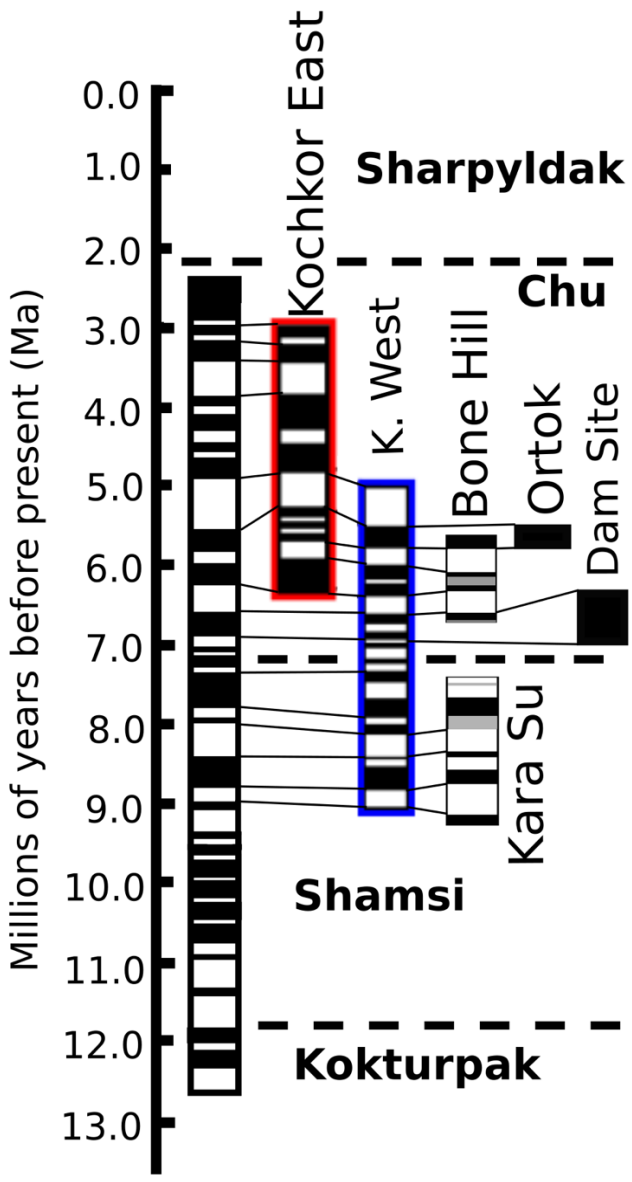

Figure 36: Temporal relationship of the four novel paleomagnetostratigraphic sections from this study and the two previously existing sections from the Kochkor Basin. Absolute time scale taken from Cande and Kent (1995). Formation boundaries placed relative to the sections measured.

After ground checking the same sections as sampled in the Wack et al. (2014) study, we suggest a reinterpretation of both the temporal match and some of the underlying geology. One of the main geochronological constraints on the study was two vertebrate fossils of a single taxon, however the biostratigraphic and paleontological

conclusions based on the fossils are questionable for several reasons. The fossils are testudine, or tortoise, with the only from within the sampled stratigraphy from approximately one quarter of the way up section in the JO section (Wack et al., 2014, Figure 10). The presence of *Stulemys karaklensis* supposedly constrains that portion of the section as Oligocene to Early Miocene, as published in Ryabinin (1927). Whereas the second testudine, *Testudo djetyogus* was found "above [the] JO section", and is dated to the Middle Pliocene (Kuznetsov et al., 1964). Notably, neither fossil is reposited in an existing collection, and thus neither can be diagnosed to any currently accepted nomenclature. Owing to the poor description of *S. karaklensis* in the initial publication, lack of other referred material, lack of geochronology in the original work, and lack of images of the original publication, subsequent testudine taxonomic studies do not recognize the species, nor place any confidence in the temporal assignment as Oliocene-Early Miocene (Danilov et al., 2006). Furthermore, while *Testudo* is still a genus in use, no subsequent use of the species name can be found beyond the original publication, calling any temporal range into doubt.

Given this lack of a calibration point, we reexamined best fits for the magnetostraigraphy presented in the two Wack et al., (2014) sections. We find one section to miss a significant portion of stratigraphy in the Shamsi equivalent Kyrgyz Group, and the other section actually begins in the Kokturpak Formation, without accounting for a hiatus in deposition (Figure 37). Additionally, given the absolute time match presented in the study, the rates of deposition vary widely between reversed and normal polarities (Figure 37, upper right portion). Given the mix of normal and reversed polarities in some sampled strata, we also interpret some portions of the

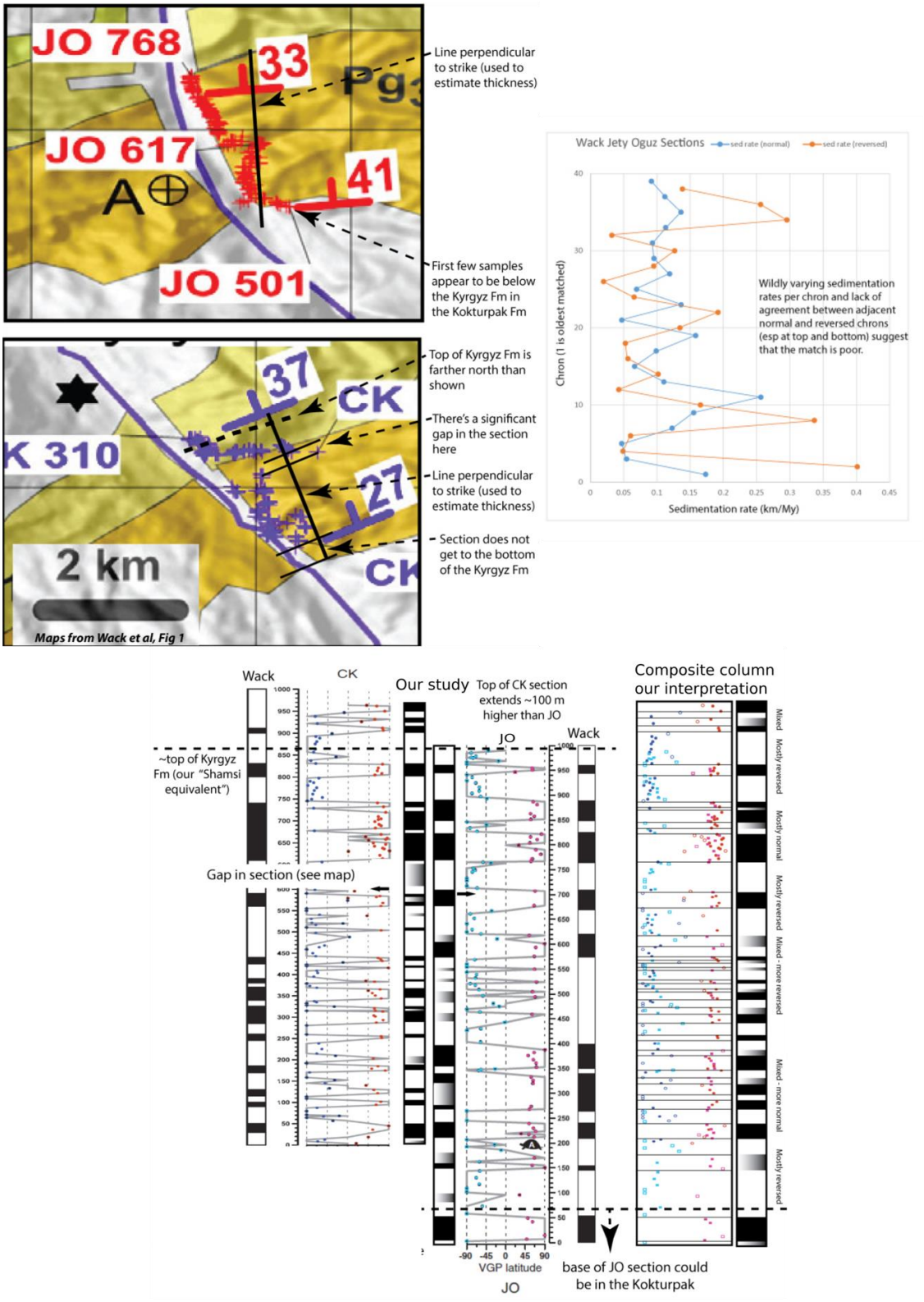

Figure 37: Reinterpretations of both the geology in map view as it relates to Wack et al., 2014 samples and the interpretation of both magnetochron and sedimentation rate.

magnetostratigraphy as “mixed polarity”, or gray bar for uncertainty. Given these differences, we find a preferred match for the sections with a much younger age range (7.5-11Ma), not including the lower portion possibly from the Kokturpak Formation (Figure 38). This differs from the preferred match in Wack et al. (2014) of ~10-25Ma. Not only do we find the section to be much younger, we also find it to span a shorter time, alleviating some of the issues with the sedimentation rate discrepancies.

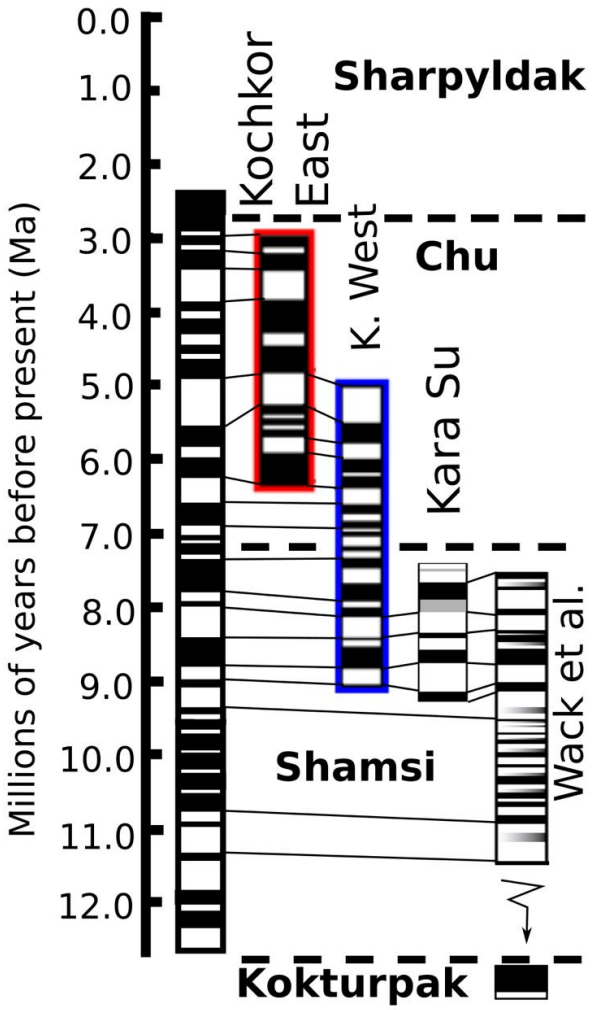

Figure 38: Composite column as this study reinterprets the Wack (et al., 2014) data, presenting a new and younger range for sections. Note the divided paleomagnetostratigraphy column for the Wack et al. study, recognizing the unconformable relationship between the samples in the Kokturpak and the rest of the section in the Shamsi Formation or Kyrgyz Group.

Our preferred match of both our data and the Wack et al., (2014) with the global time scale places the transitional boundary between the Shamsi and Chu Formations around 7-7.5 Ma. As this temporally matches changes in monsoonal climate patterns seen in both the Siwaliks (Quade et al., 1989) at 7-7.4Ma, the Tibetan Plateau (Wang et al., 2006, Molnar, 2005) 7-8Ma, and the Kazakh Shield (Abrajevitch, 2008, Miao et al., 2012) at 7-8Ma, we further suggest the boundary between the two formations is climatic in origin, and not tectonic as some authors have previously proposed (Wack et al., 2014, Macaulay et al., 2016). However, it should be noted, that tectonic change, namely uplift in the Himalayas, Tibetan Plateau, and Pamirs, drives much of the broader regional climatic change. While we did not extend our sections into the Sharpyldak Formation in this study, upwards extrapolation of our sections and correlation with the existing sections spanning that boundary in the Kochkor Basin place the boundary around 2.2 Ma, or consistent with the onset of Pleistocene glaciation. Furthermore, this implies rapid and recent uplift of the Tien Shan, consistent with modern rates of uplift and deformation (Abdrakhmatov et al., 1996, Abdrakhmatov et al., 2001, Thompson et al., 2002).

Transition

Studying the taphonomy of the Kyrgyz bone beds highlighted one family of taxa above all others: the rhinocerotids. This megafauna family is represented by two species, one from the older Shamsi Formation and one from the younger Chu Formation. Sotnikova et al., (2001) attributed the previously collected material from Ortok to the genus *Chilotherium*. Initially I assumed this previous diagnosis to be correct, however further examination calls the assigned species into question. In the following chapter I set out to describe the rhinocerotid material and diagnosis the taxonomic identity of the Kyrgyz taxa. As comparative material is generally from outside of Central Asia, preliminary work made it clear a phylogenetic analysis is necessary to properly access the identify and familial placement of the Kyrgyz taxa. The findings of my phylogeny also have major impacts on the presumed biogeography of the family. I present ideas as to the relationships between Eurasian and North American rhinocerotids, highlighting that similarities in body shape may be from relatedness rather than convergence.

CHAPTER IV

A NEW CHILOTHERE (MAMMALIA, RHINOCEROTIDAE) FROM THE NEOGENE OF KYRGYZSTAN, WITH IMPLICATIONS FOR PHYLOGENY AND BIOGEOGRAPHY OF THE RHINOCEROTID FAMILY

Introduction

While today herd behavior in rhinoceroses is limited, rhinoceros are presumed to exhibit herd behavior far back into the fossil record (Prothero, 2005, Milhbachler, 2005). Modern white rhinoceros (*Ceratotherium simum*) travel in mixed sex herds of up to 14 individuals (Shrader & Owen-Smith, 2002), while modern Indian rhinoceros (*Rhinoceros unicornis*) form female herds and sub-adult male herds (Laurie, 1982), although some historical accounts suggests most modern species were more gregarious before crippling population declines (Hutchins & Kreger, 2006). Fossil rhinocerotids are conclusively shown to travel in even larger herds, thanks to catastrophic mass death assemblages such as the *Teleoceras* herds of Ash Fall Fossil Beds National Monument (Prothero, 2005). While behavior can be hard to establish in the fossil record, the overabundance of rhinocerotids in all Kyrgyz bone beds examined in this study at least suggests that these large-bodied ungulates were both one of the more common organisms and were likely traveling in large groups. Additionally, rhinoceros' material comes from a wide age range of individuals, and tusks suggest the presence of both male and females, further indicating the presence of some sort of social structure.

The Kyrgyz rhinocerotid material is produced from two Neogene formations, the Chu and Shamsi groups, spanning the latest Miocene into the Pliocene (Figure 39). Both

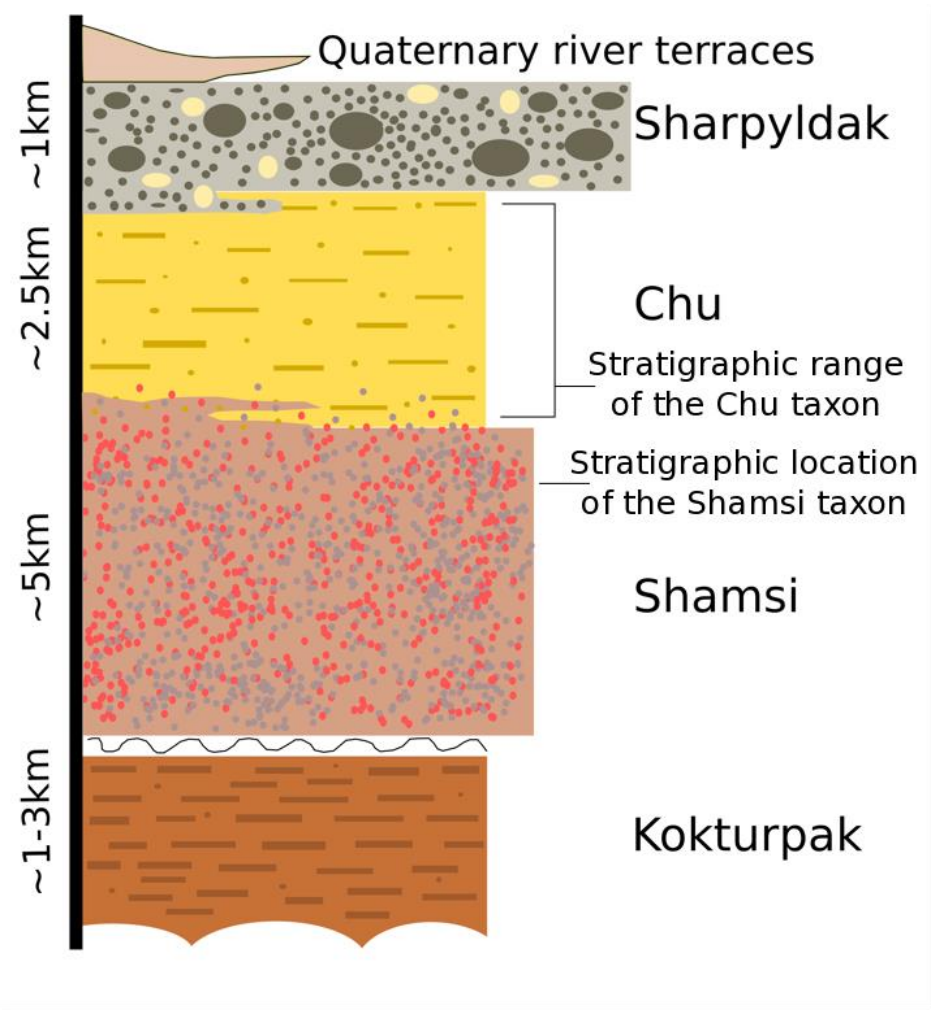

Figure 39: Composite stratigraphic column of Neogene sediments in the Kochkor Basin, Kyrgyzstan, showing the stratigraphic ranges of rhinocerotid fossils. The Kokturpak contains one dated basalt, placing the formation across the Eocene. The Shamsi and Chu formations are syntectonic, and generally finning upwards with a gradational contact. Capping the Neogene section is the Sharpyldak, a thick conglomerate presumed to be Pleistocene in origin. Rhinoceros included in this study span the upper Shamsi and throughout the Chu, although only the Shamsi rhinocerotid is described in detail.

formations are syntectonic basin filling sequences, primarily composed of fluvial and alluvial sediments, with a general fining upwards. Regional geologic and paleoclimatic data suggests Central Asia underwent uplift and climatic shifts in the late Miocene-Pleistocene to reach the semi-arid steppe ecosystems of today. Climate became both drier

and colder as the monsoon effect ceased to reach Central Asia (Wang et al., 2006). As topography and climate remodeled, corresponding faunal turnovers resulted in the evolution of both ice age and modern cold-adapted faunas (Deng et al., 2011).

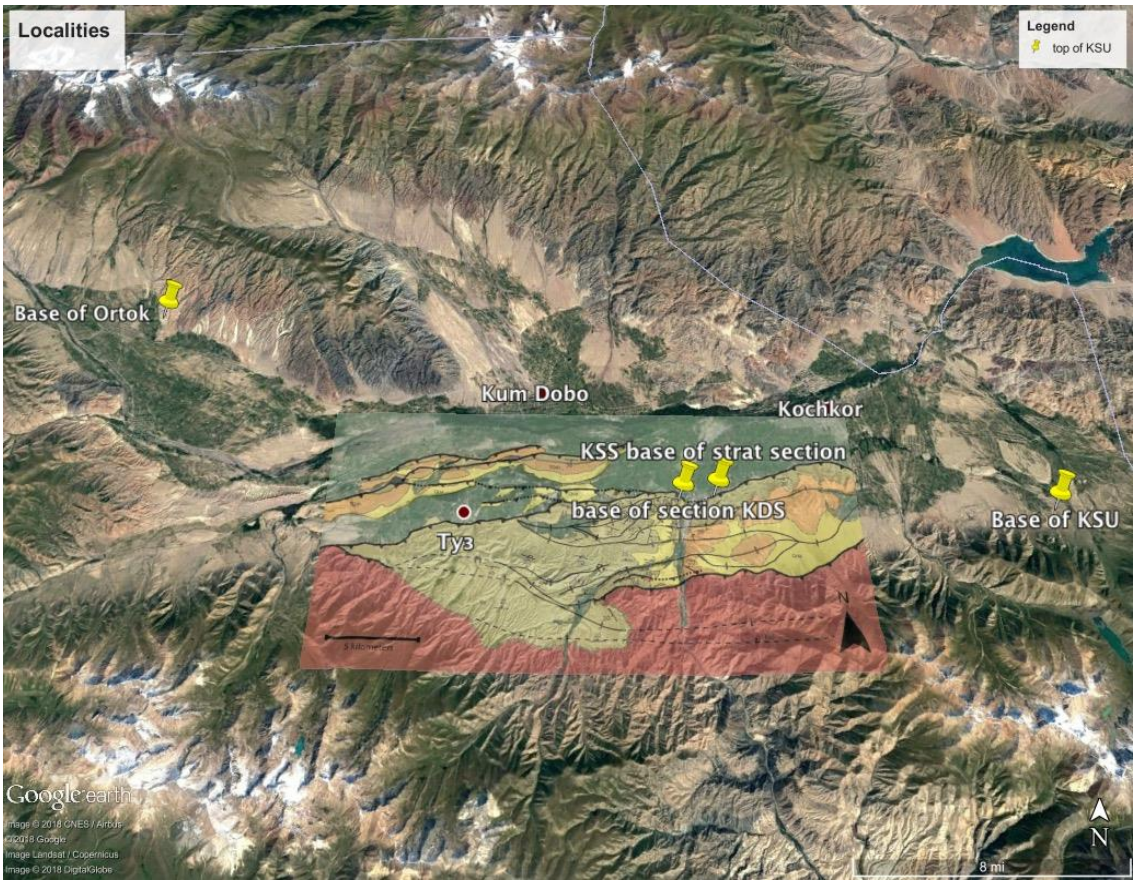

Figure 40: Google Earth imagery (accessed January 2018) of the Kochkor Basin Kyrgyzstan, with an overlay of some geologic mapping (Paulson, 2013). Pin represent bone bed localities, all of which produce rhinocerotid material. The novel taxon described in this work is from the KSU section on the far east of the map. Rhinocerotid material is produced throughout the section and is not confined to the bone beds, although all of the specimens included in coding characters for the phylogenetic analysis are from the four labeled bone beds.

Located in the heart of Central Asia (Figure 40), Kyrgyz fossil deposits therefore offer a unique opportunity to observe rhinoceros evolution over not only several million years, but at a key location for geographically and temporally understanding the paleobiogeography and phylogeny of this family (Figure 41). While the family evolved in

North America, previous authors suggest significant faunal interchange between North America and Eurasia, throughout the Cenozoic history of the family (Prothero, 2005, Lu, 2012). While this study concentrates on two species from Kyrgyzstan, the inclusion of North American Neogene taxa suggests strong phylogeographic connections between Asia and North America in the Miocene.

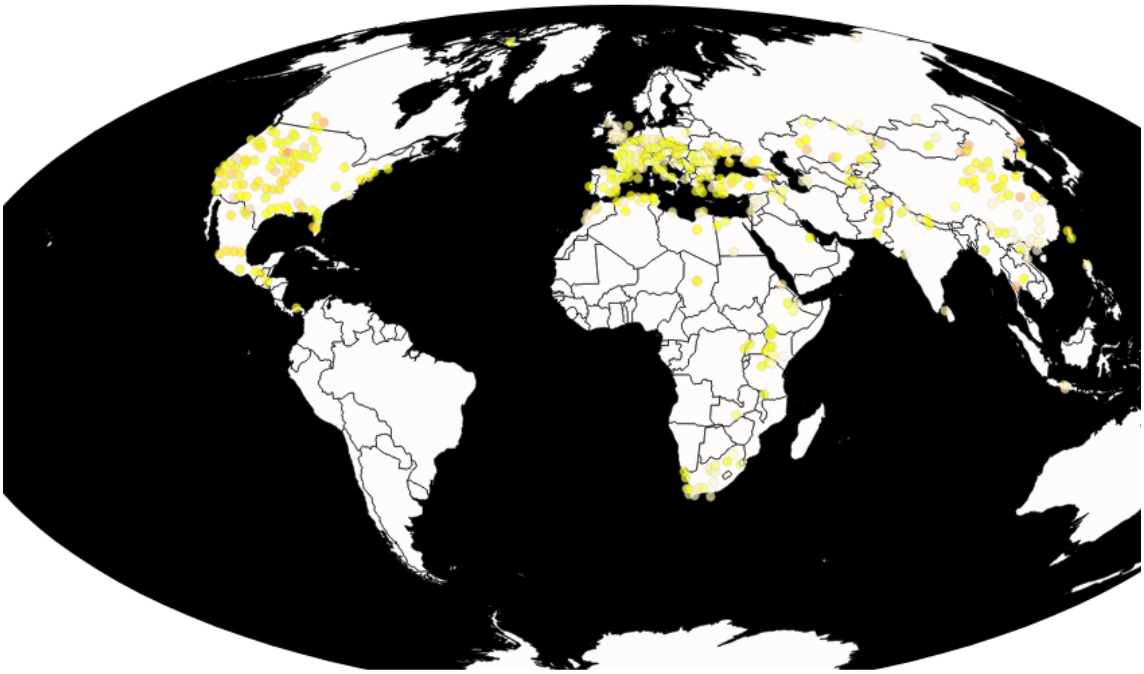

Figure 41: Distribution, both temporally and geographically, of Rhinocerotidae fossils. Data and graphic taken from the Paleobiology Database, search <Rhinocerotidae> on January 6th, 2018. Peach colors are Paleogene fossil localities publishing the occurrences of rhinocerotids, while the Neogene localities are shown in yellows. Rhinocerotids are first found in the Eocene of North America, but appear to have quickly spread to Asia, as evidenced my numerous Eocene localities in China. The PBDB search returns 2,347 localities with rhinocerotids, illustrating the wide-spread nature of this family throughout the Cenozoic.

Materials and Methods

Paleontology: The rhinoceros fossils described herein are all from a single bone bed outcrop, Vodka UO-4603, located along the southeastern margin of the Kochkor Basin,

Kyrgyzstan (Figure 42). Locally, the larger drainage containing the fossil locality is called the Kara Suu valley, as the closest village draws the name (meaning “black water” in Kyrgyz) from the numerous springs along the fault scarp. South of the South Kochkor Fault trace, the sediment packages are Neogene sequences in turn underlying the over-thrust Mesozoic basement rocks.

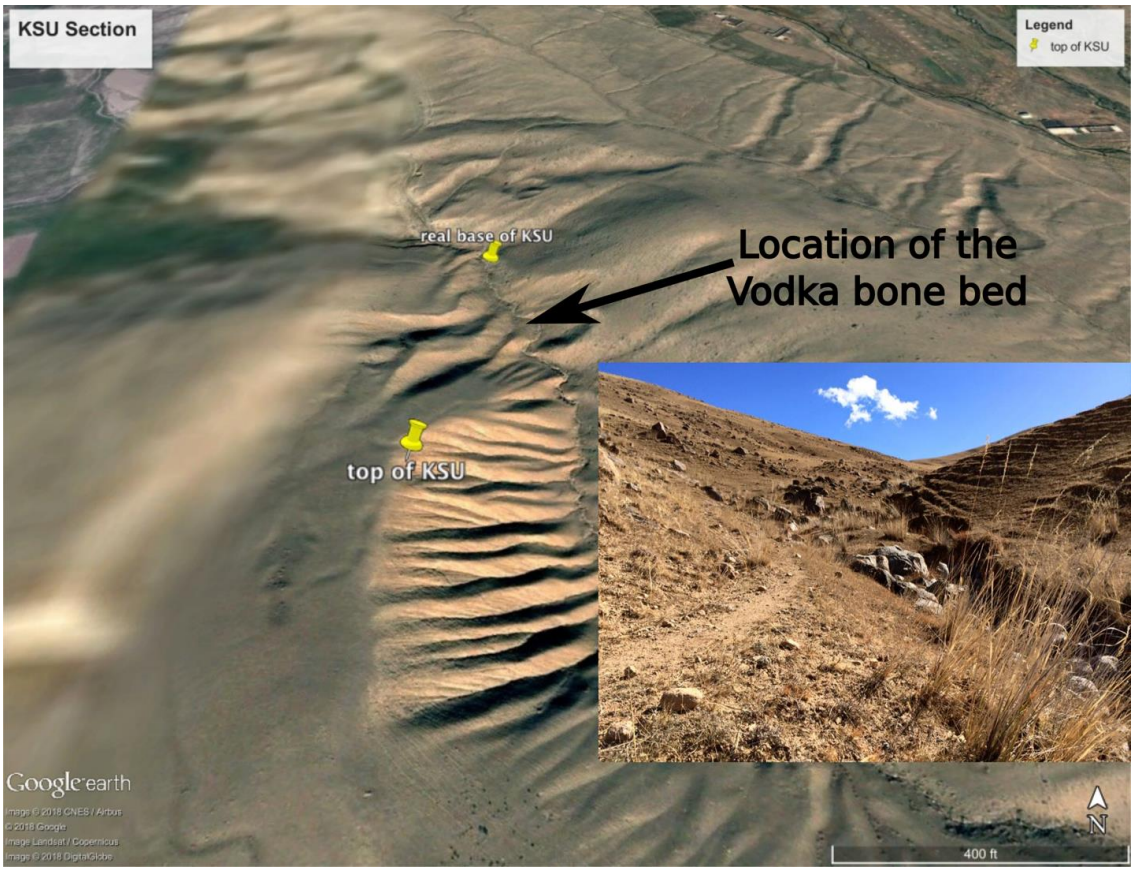

Figure 42: Google Earth view of the Kara Suu Valley denoting where the stratigraphic section was measured as well as the location of the Vodka bone bed. Inset image is looking south, from just north of the bone bed. The fossil bearing stratum outcrops in the dry wash.

The locality was discovered in 2012 by E.S. Przhiyalgovskiy and E.V. Laurushina of the Geological Institute of the Russian Academy of Sciences, two structural geologists who were conducting geologic mapping of the area. Initial collection was limited to fragmentary material weathered into the dry wash below the cut bank exposing the

fossiliferous stratum. In 2014, the outcrop was excavated by a field crew from the University of Oregon, producing most of the postcranial material. Again in 2015 the outcrop was quarried by a joint expedition from University of Oregon and the Kyrgyz Institute of Seismology, this time producing both the skull and complete mandibles (Figure 43).

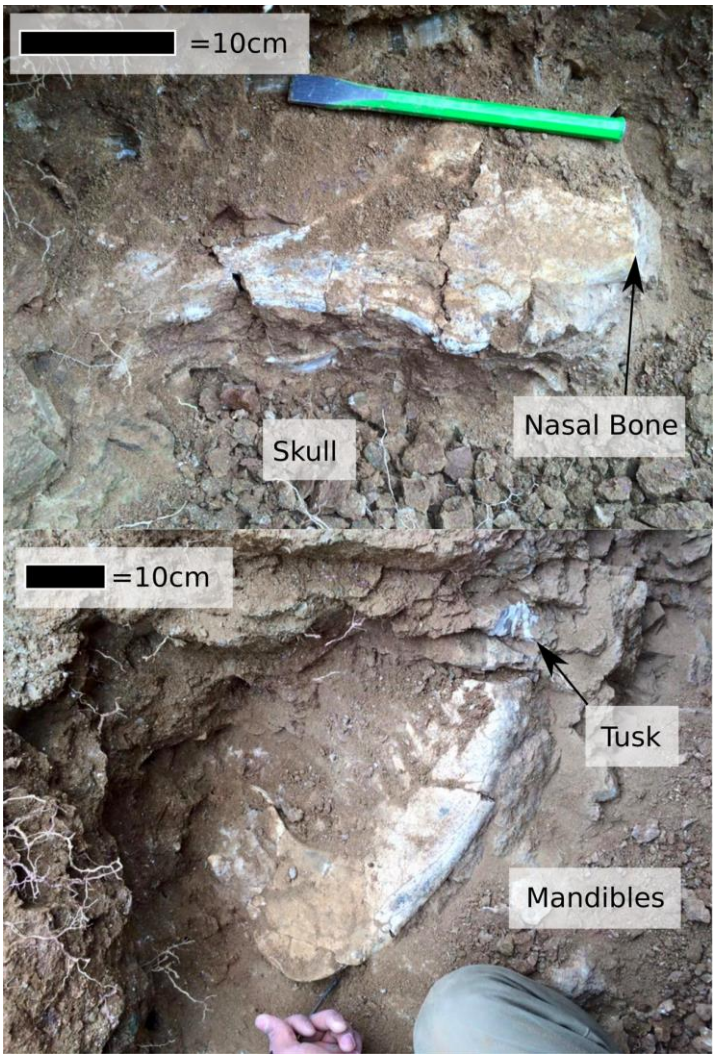

Figure 43: Top, dorsal view of the Vodka taxon skull in situ, after the projecting nasals had been removed (far right of image). Bottom, Left mandible exposed after the removal of the right mandible, in situ. Less than 1.5 meters separates the two specimens, and they lie at the same stratigraphic level.

A stratigraphic section and palaeomagnetic samples were also collected at the locality; however, stratigraphic and geochronologic placement will be discussed in another work (Chapter 3). Most of the exposure in the Kara Suu valley appears to belong to the Shamsi Group, and gradationally changes to the younger and finer grained Chu Group. This geologic assignment places the locality in the mid to late Miocene. The aforementioned work currently estimates the Vodka bone bed to be 8.6 Ma (although biostratigraphically it could range from 9.6-5.3 Ma).

The specimens were compared with the only previously attributed rhinocerotid species in Kyrgyzstan, *Chilotherium* cf. *chabereri* (Sotnikova, 1997), although the previous material is attributed to the presumably younger locality of Ortok, and is not reposited in an extant collection for comparison. Complicating comparisons is the high diversity of rhinocerotids in the late Miocene. Thus far, the Kyrgyz faunas share the most faunal similarities with the Hipparion faunas of China, which have the highest diversity of rhinocerotids in the Late Miocene (MN 9-12) over any other time period (Deng, 2006), with over two dozen species. In the Chinese to Mongolian Late Miocene, *Chilotherium wimani* is the dominant species (Deng, 2006).

Phylogenetic Analysis: I performed a cladistic analysis to evaluate the phylogenetic placement of the Kyrgyz rhinocerotid craniodental material. Taxa included in the analysis followed the published matrix of Pandolfi et al. (2015), which is based on characters developed in Lu (2013) and Antoine (2002, 2003, 2010). Pandolfi (2015) significantly expanded the number of included taxa, although narrowed the taxonomic breadth as compared to Antoine (2010). I include all taxa used in the Pandolfi (2015) analysis, as well as incorporate several novel taxa. I also recoded the basal North American

rhinocerotid *Subhyracodon occidentalis*, as a check on coding the characters. This taxon is already included in the Pandolfi (2015) phylogeny, and my recoding serves to check my interpretation of characters as similar to the previously published matrix. I also used different, more complete, specimens to code the species than those used by Pandolfi (2015), with both a male and female skull from the NMNH. The basal North American rhinocerotid *Trigonias osborni* was retained as the outgroup in the study. New taxa added to the analysis included both rhinoceros taxa from Kyrgyz Neogene fossil deposits, three additional species of *Chilotherium*, and several more North American rhinocerotids, notably three species of *Aphelops* and two of *Teleoceras* from the Neogene. Previous work suggests significant dispersal events in the history of the family, yet little work addresses the timing and exact nature of these relationships (Prothero, 2005). We therefore included North American rhinocerotids, North American temporal contemporaries of the Kyrgyz rhinos with similar "barrel bodied" morphologies, as a test if the morphology in the overall body shape is derived from relatedness or convergence. New taxa (see SI T1 for full list of taxa and morphological sources) were primarily coded from museum-reposited specimens at University of Oregon, Uppsala University, and the Smithsonian National Museum of Natural History, although some morphological data, including all juvenile dentition except for the Chu rhino, were coded from the literature (also in Apendix K).

Characters were coded into Mesquite (http://mesquiteproject.org/), and the full character matrix is available in the Apendix L. Detailed descriptions of each character are also available in the Apendix L. Trees were generated using "Tree analysis using New Tecnology" (TNT) (Goloboff &Catalano, 2016) using a normal run, although other run

types were tested and did not yield reduced numbers of trees or improved resolution. We completed 10,000 runs of the matrix, generating 5 most parsimonious trees using the entire character list of Pandolfi (2015), which is primarily taken from the character list of Lu (2013) and Antoine (2002). Characters were not weighted, but were designated as single vs. multistate, and ordered and non-ordered multistate. There were 53 ordered multistate characters, and an additional ten multistate, but not ordered, characters. Owing to poor resolution in some aspects of the tree, possibly derived from uninformative characters, we propose conducting future analyses with a pruned set of characters, as well as the future inclusion of postcranial characters.

Systematic Paleontology

Order PERISSODACTYLA Owen, 1848

FAMILY RHINOCEROTIDAE Owen, 1845

Tribe ACERATHERIINI Dollo, 1885

CHILOTHERIUM Ringström, 1924

CHILOTHERIUM sp. nov.

Holotype—UOMNH F-64557 skull, missing premaxillary bones and part of the maxillary bones.

Paratypes—UOMNH F-70507 mandible with m3-i2 both left and right, UOMNH F-64522 distal lateral metapodial, UOMNH F-64523 tibia, UOMNH F-64527 carpal, UOMNH F-64537 astragalus, UOMNH F-64552 distal humerus, UOMNH F-64555

radius, UOMNH F-64577 fibula, UOMNH F-70305 calcaneum, UOMNH F-70314 metapodial.

Referred material— UOMNCH-64514 distal radius, UOMNCH-64515 distal radius, UOMNCH-64554 bascranium, UOMNCH-64575 tibia.

Type locality—UO-4603 Vodka.

Diagnosis—Chilotherium sp. nov. is a medium sized, barrel-bodied rhinocerotid, but with more gracile limb proportions than other members of the genus. Like other members of the genus, it possesses a concave ventral surface in the mandibular symphysis, an anteroposterior widened symphysis, and two large lower tusks projecting laterally and formed from the i2. The nasal notch is broad, with horizontally projecting blunt-tipped nasals and lacking a nasal horn. The skull profile is slightly concave in the posterior portion of the skull. The posttympanic process and postglenoid process are in contact, but not fully fused into a pseudomeatus, although are separated ventrally, with the postglenoid process curving anteriorly. The teeth lack cementum, and the occlusal shape of the M3 is trapezoidal.

Description

Skull

The skull is largely complete (Figure 44), although lacking the premaxilla and much of the maxilla. Only the left and right M3 and partial left M2 are present for the upper dentition (See Figure 45). The nasals are widest posterior and narrow anteriorly, ending in a blunt tip. The ventral surface of the nasals is flat rather than vaulted. The anterior portion of the nasal bones is not notched and is fully sutured. The entire dorsal surface of the nasal bone and into the frontal bones is smooth, with no surface

roughening, indicating a lack of any horns. The nasal septum is not ossified and the dorsal profile is slightly very slightly curved downwards, with the anterior portion of the nasals almost parallel to the plane of the upper dentition. This profile continues back into the unvaulted frontal bones, which are nearly flat in profile until extending dorsally into the parietals. The posterior-most portion of the nasal notch opening is broad and U-shaped, with the nasal notch relatively posterior, leaving a small distance from the posterior-most portion of the opening to the orbits. The nasal notch is dorsal to the M2, making the nasal notch set relatively posterior in the skull and the unattached portion of the nasals moderately long as compared to other rhinocerotids.

Figure 44: Skull of the Shamsi taxon, left lateral view. Note the missing premaxillary bone and most of the upper dentition.

The skull narrows gradually posterior to the orbits, which are somewhat projecting with dorsal boney “hoods” over the orbits. When viewed dorsally, the zygomatic arches project directly posteriorly until the anteroposterior midpoint where they extend slightly laterally in a gently convex shape while also increasing in thickness and height. The parietal crests do not connect, but converge briefly before immediately diverging again, forming a split “X”, and failing to make a distinct sagittal crest. Throughout the extent of the parietal crests they are low in profile. Viewed dorsally (Figure 46), the occipital crest makes a gentle “M” shape, with the parietal crests connecting into the lateral limbs of the “M”. Viewed from the posterior, the occipital crest and the occipital surface are trapezoidal. The occipital surface forms a plane roughly vertically, with the surface inclined posteriorly through the occipital crest, which forms a rounded knob shape in profile, where the posterior edge of the occipital crest overhangs the occipital condyles.

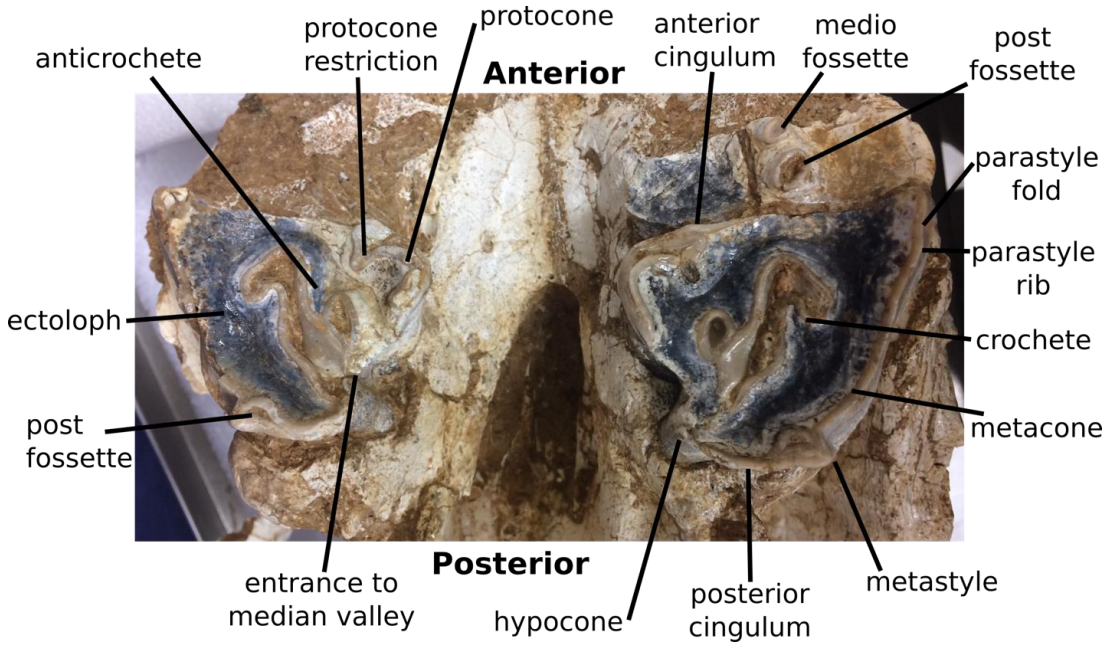

Figure 45: Ventral view of the dentition, showing the upper M3s and partial left M2. Major dental features visible in the Vodka taxon labeled.

Figure 46: Dorsal view of the skull with character 48 highlighted. The skull is widest across the posterior portion of the zygomatic arches, and the brain box is relatively narrow. Also note the gentle "M" shape of the paraoccipitals. Additionally, the nasals are fully fused and lacking any rugosity.

The posttympanic and postglenoid processes are in contact but not fused, before separating again ventrally, but form a pseudomeatus (Figure 47). The posttympanic process is enlarged and is of equal length as the postglenoid process, and as in other tapirids and all rhinocerotids, the paraoccital process and posttympanic process are completely and fully fused (Parker & Haswell, 1910). The postglenoid process is ovate in cross section and hooks anteriorly. Both the posttympanic and the postglenoid processes terminate ventrally before becoming even with the most ventral extent of the occipital condyles. On the ventral side of the skull, the anterior border of the choanae is rounded, but much more laterally constricted than other aceratheres. While the palatine spine is not well preserved, it also appears to be a weakly developed feature and does not

continue significantly posterior in the palate. The pterygoids are also damaged, but appear to project horizontally, or at least nearly horizontally.

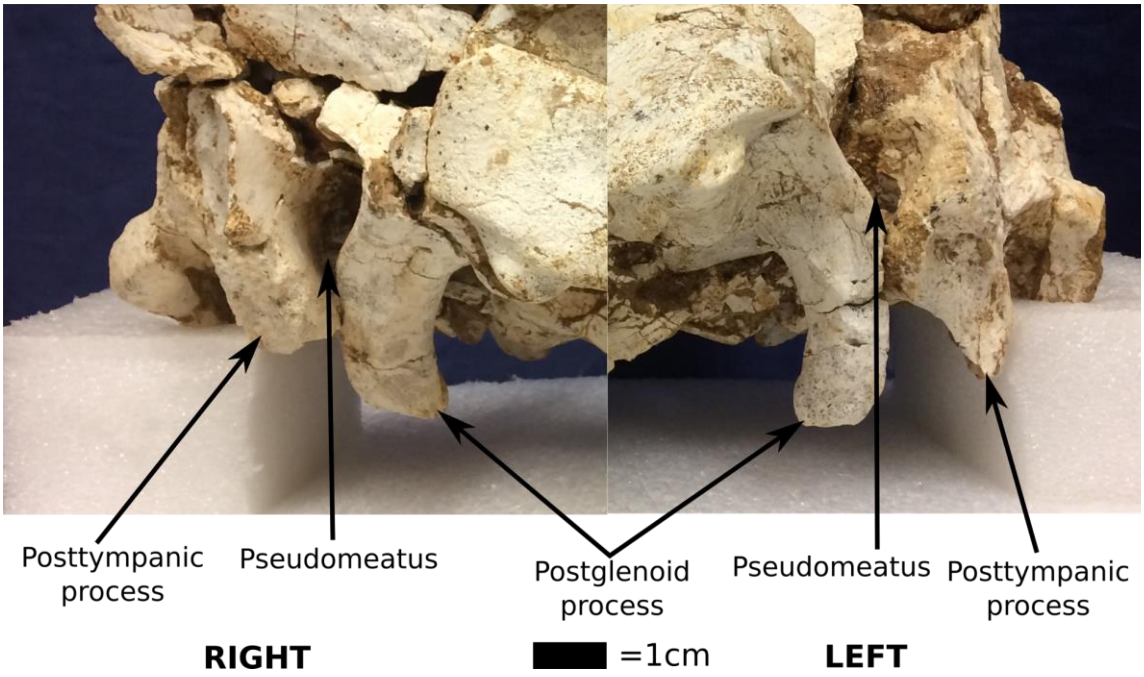

Figure 47: Lateral views of the posterior-most portion of the skull highlighting several important features. Because of diagenic deformation, combined with structural damage that occurred during excavation, the degree of closure on the pseudomeatus is variable between sides. Clearly there was not a complete suture, although contact can be clearly seen on the left side, and alteration of the surface of the postglenoid where contact previously occurred can be seen just to the right of arrow head on the right side. This character is touted as a defining character of Chilotherium, although is not coded on many species, including the several most basal. Note that in rhinocerotid and tapirids, the posttympanic process and paraoccipital process are completely fused together (Parker & Haswell, 1910).

The orbits are placed high in the skull, directly posterior to the posterior of the nasal notch. Both the supraorbital tubercle and postorbital tubercles are present and robust, with the surpraorbital process being slightly rugose. The orbits themselves are circular and slightly forward facing. Compared to other rhinocerotids, the orbits are moderate in size. The infraorbital foramina are not visible with the degree of damage and bone alteration displayed in the specimen.

Little remains of the upper dentition, other than the M3 on both sides and the posterior portion of the M2 on the left side (see Figure 45 for occlusal view of dentition). The teeth are very worn, indicating an old individual and an abrasive diet. The labial edge of the molars is wavy and complicated, even worn to less than one centimeter of enamel. No evidence of cementum is present in preserved teeth. In occlusal view, the shape of the M3 is trapezoidal. The M3 retains a paracone rib and parastyle fold (see Figure 45) on the labial surface. The protocone is strongly restricted, and a medifossette is present. There is also a strong antecrochet on both M3. Interestingly, the paracone rib and parastyle fold are characters considered basal in *Chilotherium*, while the restricted protocone, midifossette, and antecrochet are all considered derived characteristics in the genus. The M3, where not worn below the enamel-dentine junction, also have a strong lingual cingulum, although no labial cingulum is present.

Mandibles

The mandibles are robust and connected via a stout symphysis. The symphysis is anteroposteriorly thickened, with the dorsoposterior surface angling upwards at an intermediate angle. Anteriorly to the premolars, the mandibles constrict and have indented dimples on the ventral most portion of the lateral surface directly posterior to the base of the tusks. The tusks project laterally on an angle not in line with the tooth row. They are quite circular in cross section, with wear facets spanning the exposed length of the tusk. While worn, the tusks do not show evidence of a medial flange at the base. The smaller size in length and diameter, as well as the cross-sectional shape implies the preserved individual to be female (Mihlbachler, 2005, Chen et al., 2010), a character noted in another *Chilotherium* species, *Chilotherium wimani*. All species of *Chilotherium*

with sufficient sample size are sexually dimorphic in tusk cross-sectional shape, and no other taxa have circular cross sections (Chen et al., 2010).

The ventral surface of the mandibles is relatively flat, and only projects upwards immediately posterior to the base of the tusks. The mandible is robust both in thickness and in height. Within the mandible, the tooth row is offset on an angle compared to the axis of the mandible. Despite some diagenic deformation to the fossil, the ascending rami are both vertical, and therefore it looks to be a true character of the specimen.

The teeth are extremely worn and exhibit wear commonly associated with drought (Kaiser et al., 2013). While premolars wear before molars, from a combination of the chewing pattern and eruption pattern (Prothero, 2009, Kaiser et al., 2013), the molars are typically worn more progressively from the m3 forward. Other than fragmentary labial scraps of enamel, all premolars are worn below the enamel dentine junction. All remaining enamel lacks cementum on any surface. As the bone is somewhat eroded perimortem around the roots of the teeth, splaying double roots are visible for all teeth, except for the possibly single rooted p2. While the mandible does not appear to have an alveolus anterior to the remaining portion of the p2, the bone is worn, and this disappearance of presumably previously occupied alveola is present in several of the *Teleoceras* mandibles examined in this study. The degree of root formation and splay angle of the roots suggests that while an aged individual, the teeth were likely never approaching hypsodont. In the molars, particularly the m3 as it is least worn, the ectoconid and metaconid are well developed, with the m3 metaconid larger and extending lingually more than the metaconid (Figure 48). Only the m3 preserved the talonid basin, and therefore gives an accurate estimate of relative cusp extent internal to the tooth

margin. The p3-m1 are wider than they are long, indicating some degree of shortening in the tooth row.

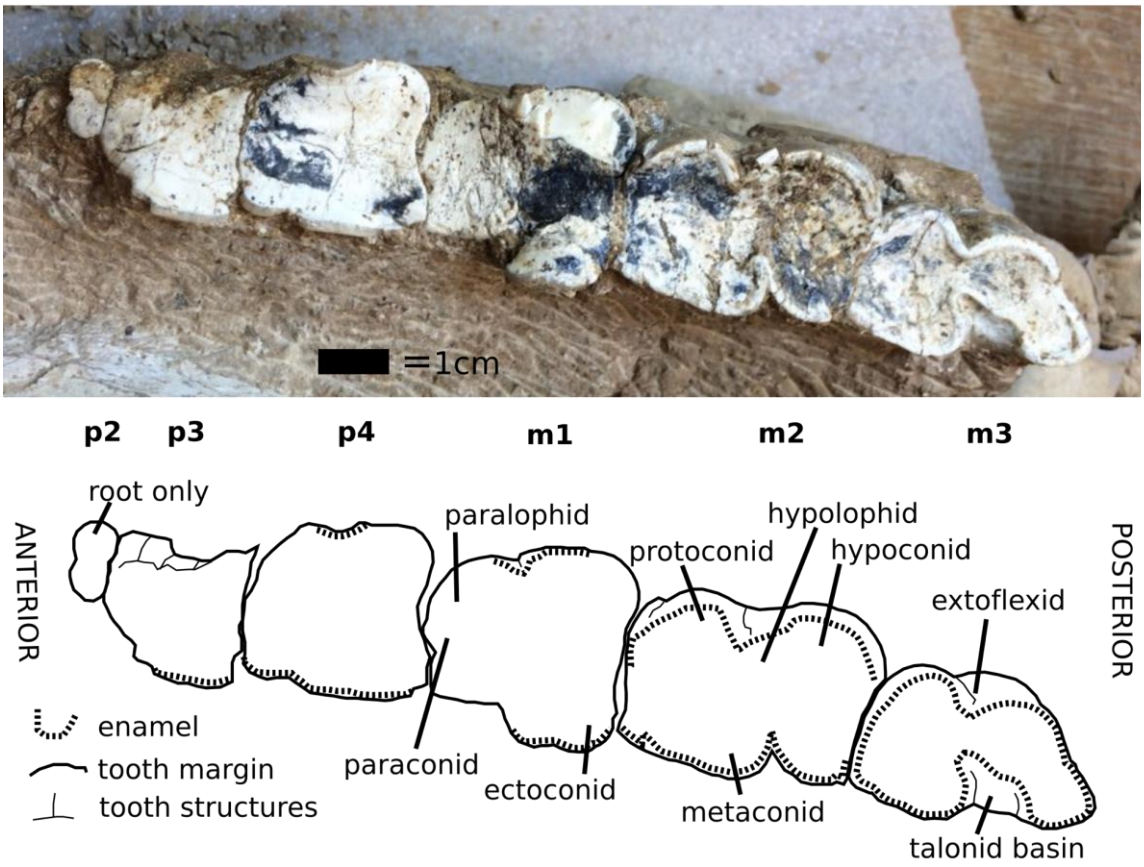

Figure 48: Occlusal view of the better preserved right lower dentition. While extremely worn, the chewing surface is not broken or otherwise diagenically altered. The m3 is least worn and preserves the best estimate of the relationship of interior cusps. Internal part of each tooth is dentine, while cross-sections of enamel are shown with a dashed line.

Radius

The radius is relatively elongate compared to other *Chilotherium* (see Figure 49), although limb length may respond more plastically than many other features. Some previous studies have associated more gracile distal limb elements with adaptation to open steppe environment (Deng, 2006, Guérin, 1980, Ringström, 1924). There is some dorsoventral flattening, with an ovate cross-section. Still robust compared to a modern

white rhinoceros (UOMNH B-8701), the radius is also more curved, another feature seen in “barrel-bodied” rhinocerotids (Prothero, 2009).

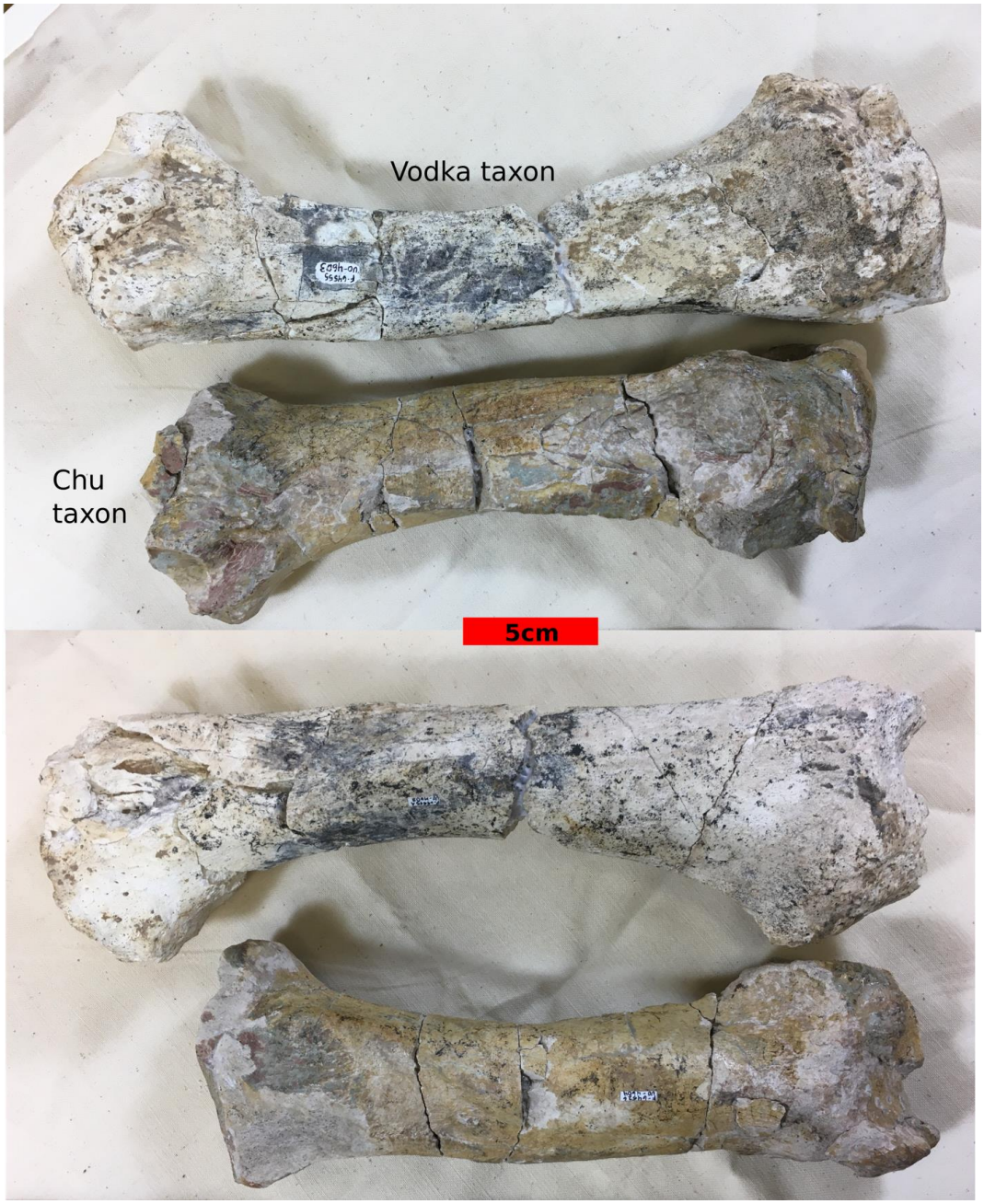

Figure 49: Side by side comparison of the radia from the Vodka taxon (top in both images) and the Chu taxon (lower in both images). Both are robust; however the older Vodka taxon is proportionately longer.

Astragalus

The astragalus is more strongly keeled than either *Teleoceras* or *Aphelops*. Wider than long, the astragalus also has a pronounced medial bulge. The articular surface constricts around the groove between trochlea, although the groove itself is shallow. Some of the head is damaged, but the head overall projects out from the trochlea more than modern white rhinoceros (UOMNH B-8701).

Metacarpal III

While the majority of the third metacarpal is preserved, the proximal surface is broken and missing. The bone exhibits good symmetry across a central axis, and is slightly curved dorsally at the distal-most end. Ovate in cross section, the metapodial is quite compressed dorsoventrally. The distal end is robust, with a very pronounced trochlear keel that is also narrow in lateral extent. The dorsal surface has a thin ridge projecting towards the proximal end of the bone and extending from the trochlear keel. Limited cysting (Stilson, 2017) is present just proximal to the joint surface.

Tibia and fibula

The tibia is shortened and robust compared to a modern white rhinoceros (UOMNH B-8701). The proximal end is mediolaterally wider than it is antioposteriorly, with 0.5 centimeter depression in each articular surface for the distal condyles of the femur. The articular surface is heart shaped, with a medial projection. Some evidence of "lipping" (Stilson, 2017) is shown on the lateral and posterior edges of the proximal articular surface. The distal end is strongly keeled, with deeper keels than seen in comparatives. The cross section is slightly tear-drop shaped, with a pronounced ridge

forming the anterior edge. The radius only preserves the distal end, but it is also quite robust in form.

Discussion

Assignment to *Chilotherium*

In the skull, the fused posttympanic and postglenoid processes are seen in all other species of *Chilotherium*, but are lacking in more basal aceratheres (Deng, 2006). While this character is unfortunately on a gradient (Fortelius et al., 2003), the Shamsi specimen has closure of the opening, although the sutured fusion between the posttympanic process and postglenoid process is lacking. This could place the Shamsi taxon just outside of *Chilotherium*, or as a more basal member of the taxon. However, the nasals project outwards, rather than curving ventrally, and there is no evidence of a horn on the nasals or frontal (Ringström, 1924). In the mandibles, the ventral surface of the symphysis is concave, and the symphysis in general is robust and thickened anteroposterior (Deng, 2006). The limb length, while longer than some *Chilotherium* species, is still proportionately short and robust compared to the overall body size. The metapodials are also dorsoventrally flattened (Prothero, 2009).

Comparison to other *Chilotherium* species

Chilotherium wimani is a similarly medium-sized rhinoceros, with a trapezoidal occipital; however, the occipital ridge possesses a prominent notch unlike the Shamsi taxon. Additionally, the dorsal profile of the frontal and parietal is almost perfectly horizontal, with only a slightly concave profile in *C. wimani*, whereas the Shamsi taxon is upturned sharply through the posterior portion of the parietal. *Chilotherium wimani* is one

of the only *Chilotherium* species with a prominent supraorbital tubercle (Deng, 2006); however, this does illustrate the possible presence of this feature in the genus, as it is also seen the Shamsi taxon. This taxon also shows sexual dimorphism in both size and cross-sectional shape of the i2 tusks (Chen et al., 2010), which we believe the Shamsi taxon shows, as no non-sexually dimorphic rhinocerotids have circular cross-sections to the tusks (Chen et al., 2010)\.

Chilotherium anderssoni was originally diagnosed largely by the broadly separated parietal crests (Ringström, 1924), however Deng (2001) showed this character is variable in several Chilotherium species and can also be impacted by ontogenetic development, with older individuals displaying greater distance between the parietal crests. The Shamsi specimen has widely separated parietal crests, but is also clearly an old individual given the wear stage on the teeth, so if that character is impacted by ontogenetic development it may be a poor method for comparison. *Chilotherium anderssoni* also has a nearly flat labial surface to the molars and lacks a lingual cingulum in the molars (Deng, 2006), while the Shamsi skull has a complicated labial profile on the M3 and partial M2 and a strong lingual cingulum.

Chilotherium persiae has a well-developed antecrochet on the upper molars (Pandolfi, 2015), like that seen in the Shamsi taxon. However, the nasals on C. persiae are quite short. *Chilotherium killasi*, a taxon not included in the phylogenetic analysis at this time, has a far more refined mandible where the ventral surface curves upwards and lacks the robusticity seen in the Shamsi taxon, or any other *Chilotherium* species (Fortelius et al., 2003).

Not included in previous discussion or phylogenies is *Chilotherium orlovi*. While an extremely limited number of specimens are attributed to this species, a comparison is needed, as the taxon is known from and described from southeast Kazakhstan (Bayshashov, 1982). The dorsal profile of the skull is quite different, with a more gradual slope angled anteriorly from the elevated paraoccipital ridge and a slightly ventrally projecting nasal (Bayshashov, 1982). Additionally, the nasals are quite short, similar to *C. persiae*.

Chilotherium habereri, the only rhinocerotid previously attributed to the Kyrgyz Neogene (Sotnikova, 2001) has a more level profile to the skull, with less dorsoposterior extension to the occipital crest. This taxon also has very short nasals compared to the Shamsi taxon or any other species of *Chilotherium* examined. While Sotnikova (2001) lists *C. chabereri* instead of *C. habereri*, this difference is presumed to be a translation error, as no other record of *C. chabereri* exists. If the nasals are indeed the most differentiating feature, the misattribution could have resulted from the sole figured skull in Tarosov (1970) lacking any of the dorsal portion of the skull. While the Shamsi specimen has extremely worn dentition, the degree of root formation and angle of the roots suggests the taxon was not particularly hyposodont, while *C. habereri* is reported to be one of the most hypsodont species of *Chilotherium* (Fortelius et al., 2003). The lower dentition also differs in the p4-m1 being much longer than they are wide (Fortelius et al., 2003), a character lacking in the Shamsi taxon.

Comparisons to other rhinocerotids

Within the previously proposed tribe or subtribe "Chilotheriini" (Qiu, Xie & Yan, 1987), although more appropriately assigned to Acerarthiini, *Acerorhinus hezhengensis* is another common large-bodied Asian rhinoceros present in *Hipparion* faunas (Deng, 2006). However, unlike the Shamsi taxon, *A. hezhengensis* has a posttympanic process projecting ventrally to the condyles. Another species in the Late Miocene of China is *Acerorhinus yuanmousensis* from the Yuanmou Basin, although the genus is known across Eurasia in the Late Miocene (Lu, 2013). *Acerorhinus yuanmousensis* has a nasal notch only extending to the M1, and has an undulating profile to the extremely short nasals (Lu, 2013). All Acerorhinus species have a prominent supraorbital tubercle like the Shamsi taxon and unlike most *Chilotherium* species, and the feature is considered more primitive (Deng, 2006). Additionally, *Acerorhinus* has vaulted ventral surfaces to the nasals with drooping lateral margins. *Acerorhinus* is also typically larger than the medium-sized Shamsi taxon, and the outline of the skull quickly constricts posterior to the orbits, unlike the more gradual narrowing seen in most *Chilotherium* species and the Shamsi taxon.

One of the more basal members of the Aceratheriini, *Persiatherium rodleri*, is also a medium-sized rhinocerotid from the edges of Central Asia (Iran). Like the Shamsi taxon, it also lacks a labial cingulum on the upper molars, but contrasting in the absence of cristae and absence of the antecrochet on the upper molars (Pandolfi, 2015). The lingual cingula are only present on the M1-M2 in *P. rodleri*, whereas it continues to the M3 in the Shamsi taxon. Lastly, the M3 on *P. rodleri* is triangular is shape (Pandolfi, 2015), unlike the trapezoidal form in the Shamsi taxon.

Within the Elasmotheriini, *Hispanotherium matritense* is another middle to late Miocene rhinocerotid known from Chinese *Hipparion* faunas, although more common in Iberian Peninsula sites. However, *H. matritense* is a small-bodied rhinocerotid with a nasal horn and significant amounts of cement in the upper molars (Deng, 2006). Like the Shamsi rhinocerotid, the limb proportions are more gracile, and the protocone of the upper molars is highly constricted (Deng, 2006). *Parelasmotherium simplum* and *Parelasmotherium schansiense* are additional Miocene rhinocerotids documented in correlative sites in China. Both taxa have only rudimentary crista in the upper molars, unlike the well-developed crista remaining even in advanced wear in the Shamsi taxon. *Parelasmotherium simplum* is also a small rhinocerotid, while *P. schansiense* is closer in size to the Shamsi taxon. *Parelasmotherium* (including *Paralasmotherium linxiaense*, another Chinese species of the genus) also have strong anterior and posterior cingula on the lower molars, a feature lacking in the Shamsi mandibles. An additional related candidate is *Sinotherium*; however, this taxon has lower molars angled anteriorly, and premolars angled posteriorly, so that the teeth wear in a bevel (Deng, 2006). *Sinotherium* also has a large frontal horn.

Also within the Elasmotheriini is *Iranotherium morgani*. Initial runs of the phylogeny, before cleaning and checking some of the character coding, placed the Shamsi taxon as sister to *I. morgani* in two out of 12 returned trees. However, this is more of an argument for reanalyzing the characters, as we have done, than actual phylogenetic affiliation, as the two taxa are quite different in gross morphology. *Iranotherium morgani* is quite large bodied, although body size is a potentially quickly evolving character, and hardly grounds for exclusion. Notably, *I. morgani* has a huge

nasal horn, and presence/absence of horns and relative position of horns is a more constrained feature within lineages (Prothero, 2005). The skull is also a very different shape in dorsal profile, with much of the skull forming a significantly convex profile and the nasals dipping ventrally sharply (Deng, 2006, Deng, 2005). The occipital crest, when viewed dorsally, is strongly "V" shaped, with the notch pointing anteriorly and is indented along the axis when viewing the occipital surface (Deng, 2005). Male *I. morgani* have roughened posterolateral zygomatic arches, indicating a degree of sexual dimorphism. The orbits are placed far posterior relative to the posterior portion of the nasal notch. In the mandible, *I. morgani* has a narrow mandibular symphysis. All teeth, both lowers and uppers, have significant amounts of cement (Deng, 2005, Pandolfi, 2015), a trait lacking in the Shamsi rhinocerotid. In the upper M3 the crochet is still strong on the Shamsi taxon, while weak on *I. morgani*, and the occlusal surface of the M3 is triangular-shaped (Deng, 2005). In the lower dentition, the premolars are more reduced in total tooth row portion in *I. morgani* and are overlapping in the p2-p4, and there are no enlarged tusks, as are prominently featured in the robust symphysis of the Shamsi taxon. *Iranotherium morgani* is also inferred to have evolved in Northwest China and dispersed through what would now be Kyrgyzstan to get to western Central Asia (Deng, 2005, 2006).

Within the Rhinocerotini, *Dicerorhinus* is one of the most frequent Asian genera from the Miocene. The nasal bones are much longer and wider than the Shamsi taxon, and contain a well-developed horn boss. The nasal notch extends only as far as the P3-4 making the distance from the orbit to the nasal notch also much greater than seen in the Shamsi taxon. The skull roof is concave, with a barely raised occipital, and the frontal is

quite concave, differing from the level to slightly concave surface of the Shamsi taxon. In the occipital, *Dicerorhinus* has an anteriorly inclined occipital surface, as opposed to the upright surface in the Shamsi skull, and the occipital crest has a strong notch at the median point. The M3 occlusal surface in *Dicerorhinus* is triangular, as opposed to the trapezoidal shape seen in the Shamsi taxon's M3s. *Dicerorhinus ringstromi* is very large in body size, far larger than the Shamsi taxon, but is notable in that it had cursorial limb bones, similar in degree of gracility, to those seen in the Vodka bone bed. Ringström (1924), Guérin (1980), and Deng (2006) propose a correlation between open steppe habitat and these more gracile limb proportions. All members of Rhinocerotini are characterized by the presence of at least one horn, nasal or frontal (Antoine, 2002, Pandolfi, 2015), ruling out less common members of this tribe as well.

All European members of Teleoceratini included in this study (the genus Brachypotherium) lack lingual cingula on the upper molars and have a pronounced labial cingulum on the upper molars (Pandolfi, 2015). The Shamsi taxon is the opposite of this, with lingual, but not labial cingula on the M2-M3.

Phylogenetic Analysis: Our analysis in TNT returned 5 most parsimonious trees from the cladistic analysis. Our preferred tree, the consensus tree, is shown in Figure 49. We retain the same definitions and included taxa for Aceratheriini as Pandolfi (2015), although we find a more complicated and possibly nested relationship between *Chilotherium* and *Acerorhinus* than Pandolfi (2015). In all trees returned, not just the consensus tree, *Chilotherium* is not returned as a monophyletic genus. Several authors, notably Fortelius (et al., 2003), imply many of the characteristics used to unite

Chilotherium may be pleisiomorphic traits. Not only were both new Kyrgyz taxa included within the *Chilotherium* clade, but also *Teleoceras*, *Aphelops*, and consistently *Aceratherium porpani*. While the preserved material for the Chu rhinocerotid was limited, and therefore limited the characters that could be coded, the taxon still consistently nested with *C. kowalevskii* and *C. schlosseri*. Likely, the entire tribe Aceratheriini is in need of taxonomic revision, although future alalyses should include postcranial characters and a revised set of craniodental characters.

Our inclusion of Neogene North American rhinocerotids is novel compared to previous studies. As proposed in Prothero (2005), both *Teleoceras* and *Aphelops* are supported in having an Asian origin. We retain Prothero's (2005) assignment of *Aphelops* to Aceratheriini, as the taxon nests well within the clade. Against the Prothero (2005) assignment however, we also find *Teleoceras* to nest well within the Aceratheriini in all trees, and not with the tribe Teleocerini, despite that tribe being named for the North American genus. This suggests some of the gross morphological similarities used for the inclusion of Eurasian taxa are more likely to be environmentally plastic characters, rather than phylogenetically informative characters. Teleoceratini (as used in Pandolfi, 2015), or Teleoceratina in Antoine (2002), are characterized by a shortening of the skull and distal leg segments (Heissig, 1999, Prothero, 2005). However, this shortening of distal limb elements is also strongly shown in *Chilotherium*, as well as several other members of the Aceratheriini. Prothero (2005) further describes the metapodials as flattened, but as no postcranial elements were included in this study, this character is harder to discuss in the context of the Asian rhinocerotids. This character was also present in the Asian Shamsi taxon, and several species of *Chilotherium*. Prothero (2005) also lists a "U-shaped" nasal

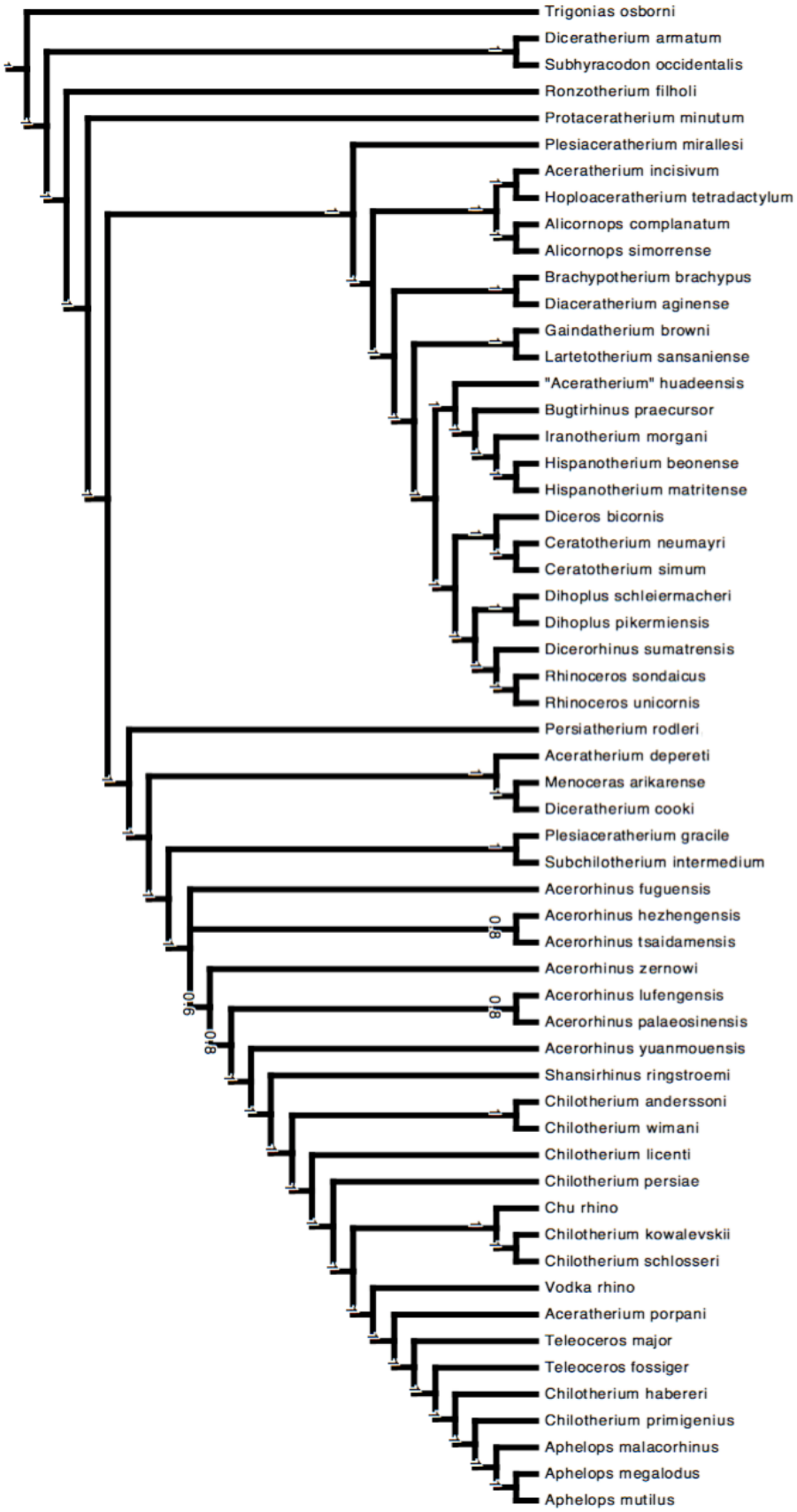

Figure 50: Consensus tree, of five returned trees. Numerical values on nodes are values that split was returned in the analysis. Note the non-monophyletic nature of both *Acerorhinus* and *Chilotherium*.

notch as a synapamorphy of the Teleoceratini, however this character is extremely common in Eurasian Aceratheres, yet again highlighting the need to examine rhinocerotids on a broader scale than single continents. Limb proportions change within genera, and thus may be more indicative of ecology than phylogeny as a result. The degree of skull shortening is also not more than seen *Chilotherium habereri*, and thus again may not be a synapamorphy.

I found the new Shamsi taxon distinct in enough characters to justify the description of a new taxon, although as this is a dissertation, designation of novel nomenclature will be left for the subsequent publication stemming from this work. The Shamsi taxon consistently nested with the genus *Chilotherium*, although the validity or organization of this genus is now questionable. Some previous authors (Qiu, Xie & Yan, 1987) have proposed the tribe Chilotheriini, with others following this assignment (Deng, 2006). However, the inclusion of *Acerorhinus* in any monophyletic group containing *Chilotherium* leads us to reject Chilotheriini as a tribe within Rhinocerotidae, and retain the assignment of *Chilotherium* to the tribe Aceratheriini as done by Pandolfi (2015). Our new taxon from the Vodka locality is therefore assigned to the tribe Aceratheriini, as it is included within the genus *Chilotherium* as it currently stands.

Despite incomplete character coding for the Chu Formation Kyrgyz rhinoceros (see Chapter 2 for description of material), the Chu taxon consistently nests near or with the Shamsi taxon within our analysis, although closer to two species of *Chilotherium*, *C. kowalevskii* and *C. schlosseri*. As the Chu Formation overlies the Shamsi Formation, the Chu taxon is undoubtedly younger, and therefore may represent a descendant of the Shamsi taxon. It is possible the Chu taxon may also represent a new species given its

placement in many of the analyses; however, the craniodental material is too incomplete and therefore prohibits a definitive assessment of the taxon. The Chu rhinoceros does not nest outside of *Chilotherium*, and therefore is retained as *Chilotherium* sp. in our phylogeny.

Paleoecology: The Shamsi taxon is a medium sized rhinocerotid, making the species certainly one of the larger taxa present in the Kyrgyz Miocene. While larger giraffids and pachyderms are possible, none have thus far been produced by the Vodka bone bed. By element representation (see McLaughlin Chapter 2) the Shamsi *Chilotherium* is the dominant taxon, represented by a MNI of three individuals. While this is not a sufficient sample to make substantial claims about behavior, the relative elemental abundance of the rhinocerotid taxon at least opens the possibility of herd behavior, as demonstrated in fossil rhinocerotids like *Teleoceras* (Prothero, 2005). Fossil rhinocerotids were likely more social than modern rhinocerotids, even exhibiting behaviors with no modern analogue (Milhbachler, 2005), although habitat fragmentation and decimated populations in modern rhinoceros make establishing possible ancestral behavioral traits more difficult. Tusked modern rhinoceros, like *Rhinoceros unicornis*, use their sexually dimorphic tusks in male-male displays (Laurie, 1982), which may have also been part of the function of tusks in the fossil taxa. The combination of the large body size and possible herding behavior made the Shamsi taxon potentially one of the dominant organisms in its ancient ecosystem (Figure 51).

While the dental material present at Vodka belonged to a presumably quite elderly individual, and therefore crown height could not be assessed, the teeth lack cementum, a

dental characteristic more commonly associated with grazing rhinoceros (Prothero, 2005). The wear pattern on the lower teeth is also very uneven, consistent with browsing or at least mixed-feeding. This jagged macrowear indicative of browsing was also present in the associated Hipparion horse teeth and the unidentified cervid. While the Kochkor Basin was lower elevation 8-9 million years ago than today, the initiation of uplift in the Oligocene-Miocene (Abdrakhmatov et al., 2001) implies the region was already quite mountainous by the late Miocene. Even in the intermontane basins, the habitat was likely lacking in dense vegetation and semi-open, consistent with browsing taxa as the predominant ungulates.

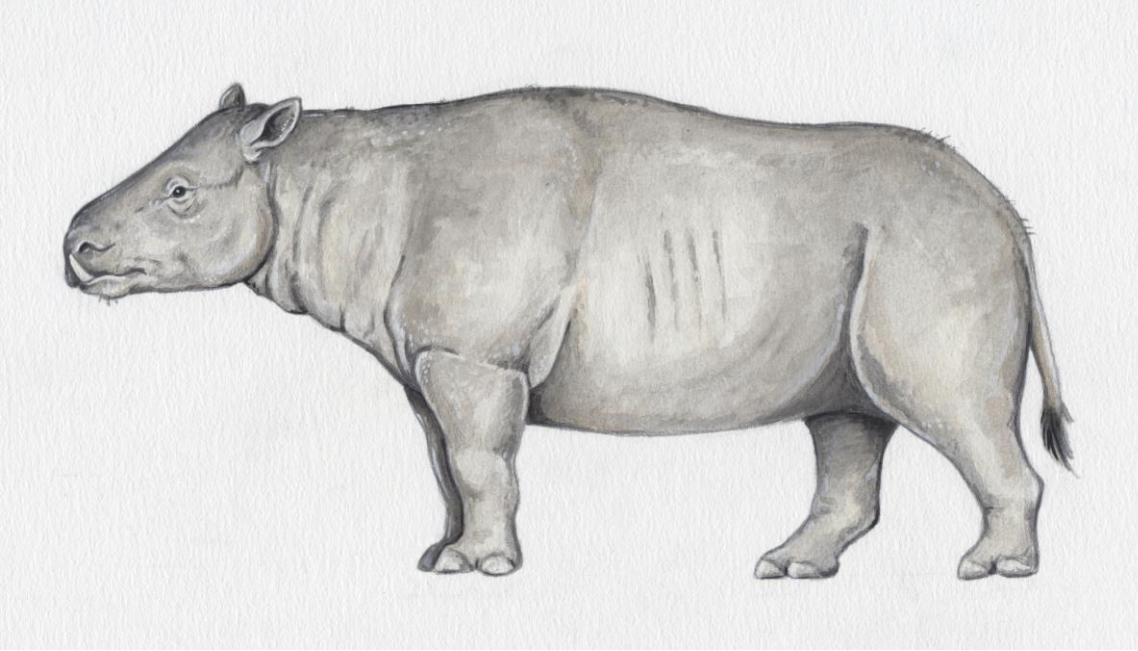

Figure 51: Life reconstruction of the Shamsi *Chilotherium*. Note the lack of horn, tusks, large body, and relatively gracile limbs.

The Shamsi rhinocerotid is produced from a fluvial sandstone to conglomerate. The clasts are subangular to subrounded, and frequently imbricate, with extensive cross bedding. Those sedimentary characteristics are consistent with braided river channels

emptying out of the uplifting mountain range to the south. The basin floor may have been wider in the past (Sobel et al., 2006), with high energy material being deposited in the valley floor, resulting in quick burial of carcasses. The rhinocerotids could have inhabited ranges throughout of the river profile, as discussed in the transport section of Chapter 2, ranging from the valley floors to foothills and even sub-alpine habitats. While significant uplift occurs from aproxematly 7 Ma to modern times, the Tien Shan were already at moderate elevations, with the Kochkor Basin likely greater than 700 m by the late Miocene (Chapter 3).

Conclusions

The Shamsi taxon is herein assigned to the genus *Chilotherium*, and represents a new species. This moderate sized, hornless and tusked rhinocerotid may have lived in moderately open habitats and been an abundant member of Late Miocene Central Asian endemic faunas. As the Greater Tibetan Plateau was already an area of moderately high elevation by 9 Ma (Sobel et al., 2006), this endemic taxon could reflect early sub-alpine to steppe habitats. Central Asia represents the obvious corridor for biotic interchange between much of Europe and Asia, yet transitional endemic faunas have received little attention previously. The new taxon, and its placement in a novel phylogenetic analysis, highlight the importance of Central Asia in both biogeographic and phylogenetic studies. While *Chilotherium* was previously reported from younger fossil beds (the Chu Formation) in Kyrgyzstan, we find the older Shamsi taxon to be distinctly different than the Chu Formation rhinocerotid.

The inclusion of North American taxa in the phylogenetic analysis displays the need for careful evaluation of what characters are taxonomically informative, rather than environmentally driven phenotypic response. Additionally, characters (like the shape of the nasal notch) may be consistent on a continent level, but not at an intercontinental level. *Teleoceras* and *Aphelops* are clearly derived from Asian taxa, as previously proposed, and further drive home the need to address taxonomic assignments and phylogenetic analyses on an intercontinental scale to truly sample biotic interchange and relatedness. Additional older North American and Eurasian taxa should be included in future analyses to establish the degree of interchange between North American rhinocerotids and Eurasian and African taxa, as well as examining the timing of intercontinental biotic interchange.

CHAPTER V

CONCLUSION

The fossils of Kyrgyzstan offer a wealth of information about changing landscapes, climate, and the biota inhabiting Central Asia. From ancient bones alone I can reconstruct an ancient ecosystem, full of a diversity of megafauna. This fauna changes through time in response to changing climate, much as the organisms of Kyrgyzstan are responding to modern climate change today. The climate change was driven by uplift, both locally in the Tien Shan, but also in the broader region in the Pamir, Himalayas, and the Greater Tibetan Plateau. Rapid uplift changed global atmospheric circulation, and regionally blocked the Indian monsoon from reaching Central Asia. Without the monsoonal signal, Kyrgyzstan became drier, forcing changes in the fauna.

Via magnetostratigraphy and biostratigraphy I have dated this tectonically driven climatic change to have occurred between 9-7 million years ago. This aligns with similar data from China, Pakistan, India, and Kazakhstan, suggesting uplift in the region reached a level sufficient to block the monsoon by the latest Miocene. In contrast to some other geologic work, I find that the modern uplift and shortening rates seem to be consistent throughout the history of Neogene uplift of the Tien Shan. The Tien Shan, and many of the specific geologic formations, are younger than some studies suggested.

On an evolutionary perspective, Central Asia lies at an important boundary between Europe and Asia, yet despite the importance to dispersal events, or the evolution of endemic faunas, little paleontological work in the region concentrates on the Neogene. I begin to tackle this issue by investigating the taxonomy, phylogeny, and

biogeography of the most common fossil animal of Kyrgyzstan's Neogene: a rhinoceros. I find there to be two species in the two different age formations included in this work, both of which are likely new species. The older species I find to be a new member of the genus *Chilotherium*, a barrel-bodied, hornless, tusked rhinocerotid. Importantly, this taxon shares phylogenetic similarities with several North American rhinocerotids, suggesting significant biotic interchange in the late Miocene.

Together the faunas and their geochronologic placement illustrate a time of rapid change, both biologically and physically, to the ecosystems of ancient Kyrgyzstan. As the geologic processes remain the same today, Kochkor Basin's ancient past can be an analogue for the future, both in terms of changing landscapes, but also the changes faced by a biota we are now part of.

APPENDIX A

VODKA BONE BED (UO-4603)

Specimen #	Locality #	Order	Family	Genus	element	L1	L2	L3
64560	UO-4603	Artiodactyla	Bovidae	Gazella?	mandible fragment with first two premolars (p2-3?)	22.62	14.99	5.82
64520	UO-4603	Artiodactyla	Cervidae		P4-M1	22.51	21.99	12.97
64532	UO-4603	Artiodactyla	Cervidae		1.5 teeth in jaw fragment of unknown cervid, m1-m2 or m2-m3	36.43	23.4	9.47
64533	UO-4603	Artiodactyla	Cervidae		mandible, p3-m3	80.49	36.4	13.5
64534	UO-4603	Artiodactyla	Cervidae		scapula	89.78	24.7	11.02
64535	UO-4603	Artiodactyla	Cervidae		metapodial	128.77	20.99	12.46
64536	UO-4603	Artiodactyla	Cervidae		phalanx	25.15	14.3	8.91
64537	UO-4603	Artiodactyla	Cervidae		proximal scapula	47.37	24.11	14
64538	UO-4603	Artiodactyla	Cervidae		proximal femur and partially articulated pelvis	46.93	23.87	21.57
64539	UO-4603	Artiodactyla	Cervidae		distal tibia	58.78	27.61	19.4
64517	UO-4603	Artiodactyla			distal radio/ulna	110.56	47.15	19.94
64524	UO-4603	Artiodactyla			skull bit, horn core	72.68	69.05	49.86
64553	UO-4603	Artiodactyla			sesamoid	16.69	10.35	5.69
64492	UO-4603	Perissodactyla	Equidae	Hipparion	R upper cheek tooth	46.37	22.97	20.55
64493	UO-4603	Perissodactyla	Equidae	Hipparion	mandible, w/ incisors and 6 cheek teeth	235	66.34	59.82
64521	UO-4603	Perissodactyla	Equidae		carpal sesamoid	40.81	27.08	10.79
70316	UO-4603	Perissodactyla	Equidae		tooth frag	11.71	10.8	1.19
64514	UO-4603	Perissodactyla	Rhinoceratidae		distal radius	111.77	82.55	30.9
64515	UO-4603	Perissodactyla	Rhinoceratidae		distal radius	105.76	80.54	38.39
64522	UO-4603	Perissodactyla	Rhinoceratidae		distal lateral metapodial	55.05	34.77	28.44
64523	UO-4603	Perissodactyla	Rhinoceratidae		tibia (whole)	282	103.09	40.45
64527	UO-4603	Perissodactyla	Rhinoceratidae		carpal	44	34.24	23.45
64529	UO-4603	Perissodactyla	Rhinoceratidae		tibia mid shaft	65.31	41	30.82
64530	UO-4603	Perissodactyla	Rhinoceratidae		calc frag	68.77	44.85	29.12

64534	UO-4603	Perissodactyla	Rhinoceratidae		thing	94.17	49.18	41.78
64537	UO-4603	Perissodactyla	Rhinoceratidae		astragalus	80.66	70.09	40.32
64551	UO-4603	Perissodactyla	Rhinoceratidae		tarsal	42.58	37.02	19.22
64552	UO-4603	Perissodactyla	Rhinoceratidae		distal humerus	146.18	124.08	55.31
64553	UO-4603	Perissodactyla	Rhinoceratidae		partial pelvis	152.86	84.41	37.83
64554	UO-4603	Perissodactyla	Rhinoceratidae		basacranium	101.57	65.4	16.74
64555	UO-4603	Perissodactyla	Rhinoceratidae	Chilotherium	complete radius, plus some little bits and pieces.	322	87.75	56.26
64556	UO-4603	Perissodactyla	Rhinoceratidae		proximal left tibia and associated frag	101.21	100.44	45.97
64557	UO-4603	Perissodactyla	Rhinoceratidae	Chilotherium	skull			
64558	UO-4603	Perissodactyla	Rhinoceratidae		acetabulum	83.29	60.6	27.91
64559	UO-4603	Perissodactyla	Rhinoceratidae	Chilotherium	distal lateral metapodial	54.05	33.09	27.19
64560	UO-4603	Perissodactyla	Rhinoceratidae		carpal	31.66	21.09	15.38
64561	UO-4603	Perissodactyla	Rhinoceratidae		carpal			
64562	UO-4603	Perissodactyla	Rhinoceratidae		tarsal, 1/2	38.04	25.68	24.87
64563	UO-4603	Perissodactyla	Rhinoceratidae		tarsal sesamoid	37.29	28.56	19.5
64564	UO-4603	Perissodactyla	Rhinoceratidae		sesamoid	29.57	26	23
64565	UO-4603	Perissodactyla	Rhinoceratidae		proximal meta tarsal			
64566	UO-4603	Perissodactyla	Rhinoceratidae		mid shaft of tibia	67.95	51	40.87
64567	UO-4603	Perissodactyla	Rhinoceratidae		distal metapodial	42.78	28.12	26.58
64568	UO-4603	Perissodactyla	Rhinoceratidae		carpal	69.63	55.14	34.64
64569	UO-4603	Perissodactyla	Rhinoceratidae		vertebra fragment	52.5	30.74	21.33
64570	UO-4603	Perissodactyla	Rhinoceratidae		fragment of humerus mid shaft, other fragment (?)	53.99	37.57	28.45
64571	UO-4603	Perissodactyla	Rhinoceratidae		pelvis fragments			
64572	UO-4603	Perissodactyla	Rhinoceratidae		ungal	42.51	38.81	19.07
64573	UO-4603	Perissodactyla	Rhinoceratidae		metapodial fragments	24.11	24.1	10.42
64574	UO-4603	Perissodactyla	Rhinoceratidae		metapodial, 3rd			
64575	UO-4603	Perissodactyla	Rhinoceratidae		tibia (whole)	275	119.59	44.1
64576	UO-4603	Perissodactyla	Rhinoceratidae		complete tarsal	47.46	46.61	17.52
64577	UO-4603	Perissodactyla	Rhinoceratidae		left fibula	148.89	34.68	19.42
64578	UO-4603	Perissodactyla	Rhinoceratidae		atlas fragment	60.04	47.07	28.88

64579	UO-4603	Perissodactyla	Rhinoceratidae	sesamoid	37.21	18.87	16.9
64580	UO-4603	Perissodactyla	Rhinoceratidae	tooth fragments	26.35	22.04	17.17
64581	UO-4603	Perissodactyla	Rhinoceratidae	thoracic vertebra process	65.75	34.85	32.77
70303	UO-4603	Perissodactyla	Rhinoceratidae	carpal	35.08	25.48	20.71
70304	UO-4603	Perissodactyla	Rhinoceratidae		86.91	38.05	36.26
70305	UO-4603	Perissodactyla	Rhinoceratidae	calcaneum	56.92	42.52	26.88
70306	UO-4603	Perissodactyla	Rhinoceratidae	calcaneum and other stuff	69.35	29.88	8.35
70307	UO-4603	Perissodactyla	Rhinoceratidae	5 bone scraps	20.87	12.02	7.25
70312	UO-4603	Perissodactyla	Rhinoceratidae	carpal	60.42	39.37	17.91
70314	UO-4603	Perissodactyla	Rhinoceratidae	whole metapodial	108.99	46.94	20.53
70318	UO-4603	Rodentia	Cricetidae	incisor	7.21	1.95	1.49
70319	UO-4603	Testudines		shell frag	30.19	16.43	8.46
64518	UO-4603			pelvis thing?	152.25	51.99	18.67
64519	UO-4603			small carpal fragment	31.5	16.47	8.16
64557	UO-4603			little rib bits, smaller animal	35.32	15.31	14.46
64558	UO-4603			crap	60.36	48.63	22.29
64559	UO-4603			bone frag	58.01	25.76	13.58
64560	UO-4603			bone frags	33.34	23.45	20.96
64561	UO-4603			frags of God only knows what	40.31	20.2	16.38
64562	UO-4603			pelvis frag? Maybe?	73.14	32.92	17.37
64563	UO-4603			proximal toe	14.77	12.92	10.95
64564	UO-4603			two complete podials, NOT rhino, smaller, shape doesn't seem to match	28.72	22.15	19.95
64565	UO-4603			rib fragment, not rhino, medium animal size			
64566	UO-4603			rib	77.28	15.55	14.97
64567	UO-4603			carpal?	30.9	29	20.73
64568	UO-4603			ribs?	54	8.12	4.19
64569	UO-4603			rib	85.25	36.47	32.55
64570	UO-4603			sesamoid?	28.75	20.06	19.62
64571	UO-4603			bone frags	15.05	11.94	9.04
64572	UO-4603			smallish animal bone bit?	20.43	17.44	11.47
70308	UO-4603			bone frag	17.96	10.03	7.37
70309	UO-4603			scapula	71.95	63.86	16.57

70310	UO-4603	pelvis	102.62	67.78	20.44
70311	UO-4603	bits	44.28	24.76	8.98
70313	UO-4603	frag	42.72	24.69	20.55
70315	UO-4603	frags	41.6	29.96	17.78
70317	UO-4603	indet	62.47	29.54	14.01
70319	UO-4603	frag	21.31	4.74	0.9

APPENDIX B

ORTOK BONE BED (UO-4605)

Specimen #	Locality #	Order	Family	Genus	element	L1	L2	L3
70325	UO-4605	Artiodactyla	Bovidae		distal metapodial	23.53	15.05	7.72
70327	UO-4605	Artiodactyla	Bovidae		right astragalus, small bovid munjack sized	22.42	12.03	11
70328	UO-4605	Artiodactyla	Bovidae		right astragalus, small bovid munjack sized	20.23	12.56	11.35
70329	UO-4605	Artiodactyla	Bovidae		distal 1st phalanx	20.45	8.51	6
70339	UO-4605	Artiodactyla	Bovidae	Gazella	horn core	50.79	24.7	20.45
70346	UO-4605	Artiodactyla	Bovidae		distal calcaneum, from very small bovid, muntjac in size	17.26	10.4	8.63
71406	UO-4605	Artiodactyla	Bovidae	Gazella	horn core	72.48	24.9	18.58
71407	UO-4605	Artiodactyla	Bovidae	Gazella	horn core	42.21	24.66	22.73
71408	UO-4605	Artiodactyla	Bovidae	Gazella	horn core	24.48	19.17	12.84
71409	UO-4605	Artiodactyla	Bovidae	Gazella	horn core	52.19	23.31	18.69
71410	UO-4605	Artiodactyla	Bovidae	Gazella	horn core	107.23	27.03	17.83
71411	UO-4605	Artiodactyla	Bovidae	Gazella	horn core	37.16	21.02	18.77
70333	UO-4605	Artiodactyla	Cervidae		two antler fragments	40.04	27.72	16.38
70334	UO-4605	Artiodactyla	Cervidae		antler pedicle	63.54	36.43	21.61
70356	UO-4605	Artiodactyla	Cervidae		antler fragment, base of branching tine	26.88	23.48	14.53
70380	UO-4605	Artiodactyla	Cervidae		antler fragments	62	22.67	16.68
70390	UO-4605	Artiodactyla	Cervidae		antler fragment	33.26	22.23	17.61
70423	UO-4605	Artiodactyla	Cervidae		radius	92	37.39	25.48

64478	UO-4605	Artiodactyla	Giraffidae	Samotherium	3 teeth	31.41	18.99	7.74
64481	UO-4605	Artiodactyla	Giraffidae	Samotherium	metapodial, articulating cubonavicular and other podial, associated distal tibia, other podial bits	366	62.29	35.33
67907	UO-4605	Artiodactyla	Giraffidae		ossicone frag	38.53	19.17	18.16
70341	UO-4605	Artiodactyla	Giraffidae		celene on tooth	12.03	9.97	7.84
70382	UO-4605	Artiodactyla	Giraffidae		distal metapodial frag	35.77	30.3	19.37
70400	UO-4605	Artiodactyla	Palaeomerycidae	palate	137.87	99.91	35.73	
70343	UO-4605	Artiodactyla			tooth frags	13.16	8.9	2.22
70364	UO-4605	Artiodactyla			calcaneum fragment	14.76	12.53	8.92
70372	UO-4605	Artiodactyla			distal toe frag	16.47	11.39	5.68
70384	UO-4605	Artiodactyla			astragalus fragment	24.43	17.49	16.29
	UO-4605	Perissodactyla	Equidae	Hipparion	complete mandible			
64481	UO-4605	Perissodactyla	Equidae	Hipparion	tooth frag	47.12	14.4	8.92
64482	UO-4605	Perissodactyla	Equidae	Hipparion	partial upper molar	29.2	19.91	9.27
64483	UO-4605	Perissodactyla	Equidae	Hipparion	1/2 astragalus	59.65	41.42	24.71
70323	UO-4605	Perissodactyla	Equidae		distal metapodial frag	33.3	18.46	13.72
70334	UO-4605	Perissodactyla	Equidae	Hipparion	distal metapodial frag	26.1	19.72	16.69
70338	UO-4605	Perissodactyla	Equidae	Hipparion	tooth frag	21.85	16.91	8.04
70355	UO-4605	Perissodactyla	Equidae		distal femur fragment	40.73	31.1	23.12
70373	UO-4605	Perissodactyla	Equidae		tooth frags	28.85	10.73	4.61
70381	UO-4605	Perissodactyla	Equidae	Hipparion	upper cheek tooth fragment	39.62	12.58	11.94
70396	UO-4605	Perissodactyla	Equidae	Hipparion	upper tooth row	90	25.16	17.59
70398	UO-4605	Perissodactyla	Equidae		incissors and frags	21.81	14.48	6.37

70424	UO-4605	Perissodactyla	Equidae		tooth frag	23.74	10.27	5.69
64479	UO-4605	Perissodactyla	Rhinoceratidae	Chilotherium	1 astragalus fragment	36.25	31.65	13.44
64480	UO-4605	Perissodactyla	Rhinoceratidae	Chilotherium	podial	75.61	38.59	21.77
64481	UO-4605	Perissodactyla	Rhinoceratidae	Chilotherium	tooth fragments	33.2	9.4	3.57
64482	UO-4605	Perissodactyla	Rhinoceratidae	Chilotherium	astragalus fragment	44.45	38.45	32.86
64483	UO-4605	Perissodactyla	Rhinoceratidae	Chilotherium	carpal?	46.6	35.95	32
64484	UO-4605	Perissodactyla	Rhinoceratidae	Chilotherium	tooth frag	34.82	20.18	4.75
64485	UO-4605	Perissodactyla	Rhinoceratidae	Chilotherium	1/2 astragalus	79.7	42.58	29.15
64486	UO-4605	Perissodactyla	Rhinoceratidae	Chilotherium	tooth bit	31.39	17.14	4.01
64487	UO-4605	Perissodactyla	Rhinoceratidae	Chilotherium	unworn tooth fragments	36.72	17.8	12.23
64488	UO-4605	Perissodactyla	Rhinoceratidae	Chilotherium	distal tibia fragment	37.5	23.06	13.06
64489	UO-4605	Perissodactyla	Rhinoceratidae	Chilotherium	tooth frags	21.29	9.56	1.98
70324	UO-4605	Perissodactyla	Rhinoceratidae	tooth frag	36.63	12.91	5.7	
70335	UO-4605	Perissodactyla	Rhinoceratidae	Chilotherium	humerus	281	101.03	64.85
70337	UO-4605	Perissodactyla	Rhinoceratidae	tooth frag	18.73	9.37	2.33	
70342	UO-4605	Perissodactyla	Rhinoceratidae	tooth frags	23.16	14.86	2.14	
70345	UO-4605	Perissodactyla	Rhinoceratidae	tooth frags	18.47	16.97	7.88	
70347	UO-4605	Perissodactyla	Rhinoceratidae	tooth frags	26.3	12.8	7.07	
70348	UO-4605	Perissodactyla	Rhinoceratidae	astragalus fragment	59.08	40.11	29.8	
70349	UO-4605	Perissodactyla	Rhinoceratidae	distal femur fragment	42.44	24.08	20.63	
70350	UO-4605	Perissodactyla	Rhinoceratidae	distal metapodial frag	34.26	27.2	19.83	
70351	UO-4605	Perissodactyla	Rhinoceratidae	carpal	39.75	27.18	15.31	
70354	UO-4605	Perissodactyla	Rhinoceratidae	astragalus fragment	31.22	29.78	22.53	

70357	UO-4605	Perissodactyla	Rhinoceratidae	proximal humerus fragent		44.08	27.67	22.73	
70359	UO-4605	Perissodactyla	Rhinoceratidae	tooth fragments		43.62	19.8	7.65	
70360	UO-4605	Perissodactyla	Rhinoceratidae	Chilotherium	radius		70.09	68.93	42.4
70362	UO-4605	Perissodactyla	Rhinoceratidae	ooth fragment		9.22	4.09	2.2	
70363	UO-4605	Perissodactyla	Rhinoceratidae	tooth frag		27.69	11.84	3.47	
70365	UO-4605	Perissodactyla	Rhinoceratidae	tooth frags		20.07	9.99	3.68	
70374	UO-4605	Perissodactyla	Rhinoceratidae	astragalus fragment		58.42	49.46	26.7	
70375	UO-4605	Perissodactyla	Rhinoceratidae	tooth frags		26.73	15.1	5.15	
70385	UO-4605	Perissodactyla	Rhinoceratidae	tooth fragments		34.23	13.58	4.69	
70386	UO-4605	Perissodactyla	Rhinoceratidae	proximal humerus fragent		60.54	42	38.31	
70387	UO-4605	Perissodactyla	Rhinoceratidae	bone frag		49.36	40.68	30.83	
70388	UO-4605	Perissodactyla	Rhinoceratidae	distal femur fragment		50.19	35.57	23.14	
70389	UO-4605	Perissodactyla	Rhinoceratidae	tooth frag		42.65	15.51	3.16	
70391	UO-4605	Perissodactyla	Rhinoceratidae	tooth frags		23.05	13.6	6.6	
70394	UO-4605	Perissodactyla	Rhinoceratidae	tooth fragments		30.37	13.78	6.84	
70395	UO-4605	Perissodactyla	Rhinoceratidae	radius		70.01	66.9	26.89	
70397	UO-4605	Perissodactyla	Rhinoceratidae	tooth frags		21.71	8.68	3.27	
70399	UO-4605	Perissodactyla	Rhinoceratidae	tooth fragments		16	6.4	2.96	
70401	UO-4605	Perissodactyla	Rhinoceratidae	tooth frag		23.54	9.41	4.59	
70402	UO-4605	Perissodactyla	Rhinoceratidae	distal femur frag		49.86	41.27	22.62	
70403	UO-4605	Perissodactyla	Rhinoceratidae	proximal femur frag		46.5	28.68	24.93	
70404	UO-4605	Perissodactyla	Rhinoceratidae	patella		68.89	46.86	29.89	
70405	UO-4605	Perissodactyla	Rhinoceratidae	calcaneum		81.74	55.66	36.89	

70406	UO-4605	Perissodactyla	Rhinoceratidae	podial		37.68	23.55	19.98
70407	UO-4605	Perissodactyla	Rhinoceratidae	podial		70.55	48.82	34.25
70425	UO-4605	Perissodactyla	Rhinoceratidae	tooth frags		22.06	10.3	3.18
70427	UO-4605	Perissodactyla	Rhinoceratidae	tooth frag		42.99	23.39	8.08
70344	UO-4605	Perissodactyla		tooth scraps		11.67	10.16	5.49
70353	UO-4605	Perissodactyla		distal tibia fragment		30.23	22.45	18.22
70368	UO-4605	Perissodactyla		carpal		31.55	21.06	10.78
70377	UO-4605	Perissodactyla		tooth frag		23.24	5.96	2.33
64482	UO-4605				bone frags			
64483	UO-4605				unidentified piece	46.87	46.26	21.41
64484	UO-4605				small mandible fragment	23.21	12.51	4.74
70330	UO-4605				carpal fragment	27.81	16.76	10.72
70331	UO-4605				periotic capsul fragment	20.68	17.03	9.8
70332	UO-4605				fragment	35.13	30.57	22.49
70336	UO-4605					62.29	31.45	14.03
70352	UO-4605				bone	33.32	20.75	12.7
70358	UO-4605				bone frag	50.57	30.23	17.51
70361	UO-4605				tooth scraps	18.18	14.61	6.7
70366	UO-4605				frag	29.35	22.52	12.18
70367	UO-4605				frag	35.54	27.62	7.31
70369	UO-4605				frag	31.95	17.24	17.01
70370	UO-4605				frag	28.74	23.12	15.49
70371	UO-4605				frag	31.49	22.86	11.96
70376	UO-4605				proximal metapodial	28.62	18.89	11.05
70378	UO-4605				proximal metapodial frag	21.6	14.04	9.22
70379	UO-4605				carpal fragment	19.44	13.39	12.34
70383	UO-4605				podial frag	24.9	22.92	19.42
70392	UO-4605				periotic capsul fragment	20.08	12.42	9.54

70393	UO-4605				43.18	31.93	21.71
70408	UO-4605			frag	38.61	30.39	18.51
70409	UO-4605			frag	55.54	38.88	30.93
70410	UO-4605			frag	38.24	25.37	15.63
70411	UO-4605			frag	51.48	38.6	26.17
70412	UO-4605			frag	39.75	38.81	17.25
70413	UO-4605			frag	65.17	52.44	27.14
70414	UO-4605			frag	38.88	33.84	24.33
70415	UO-4605			frag	34.61	27	17.25
70416	UO-4605			frag	53.97	29.43	19.79
70417	UO-4605			frag	28.25	19.25	10.25
70418	UO-4605			frag	49.42	28.18	17.65
70419	UO-4605			frag	36.75	21.08	12.38
70420	UO-4605			frag	46.05	38.67	27.85
70421	UO-4605			frag	51.61	22.02	8.65
70422	UO-4605			frag	20.09	16.76	13.96
70426	UO-4605			frag	61.71	24.62	13.9
70428	UO-4605			frag	48.82	40.34	31.28
70429	UO-4605			frag	46.37	28.57	16.44
70430	UO-4605			frag	31.3	21.54	17.83
67906	UO-4605	Carnivora		canine tooth	28.16	13.58	8.76

APPENDIX C

BONE HILL BONE BED (UO-4601)

Specimen #	Locality #	Order	Family	Genus	element	L1	L2	L3
64376	UO-4601	Artiodactyla	Bovidae			10.41	6.41	3.75
64384	UO-4601	Artiodactyla	Bovidae		"Ryan's area"	39.97	31.75	6.05
64373	UO-4601	Artiodactyla	Bovidae			48.02	25.99	6.54
70451	UO-4601	Artiodactyla	Cervidae		was with F-64372, but bone not near each other, so association unknown	17.61	14.89	9.16
64565	UO-4601	Artiodactyla	Cervidae			18.32	7.18	5.38
70458	UO-4601	Artiodactyla	Cervidae		was with 64484, no direct evidence of association	18.89	16.96	14.92
64443	UO-4601	Artiodactyla	Cervidae			20.86	20.36	8.53
70456	UO-4601	Artiodactyla	Cervidae			20.97	9.89	8.63
70471	UO-4601	Artiodactyla	Cervidae			25	16.77	14.13
64353	UO-4601	Artiodactyla	Cervidae			25.84	18.54	8.56
64445	UO-4601	Artiodactyla	Cervidae		"ankle Logan"	31	25.08	18.26
64402	UO-4601	Artiodactyla	Cervidae			32.09	16.86	12.2
70446	UO-4601	Artiodactyla	Cervidae		"toes from Ryan 9/18/14"	34.97	23.51	12.82
64372	UO-4601	Artiodactyla	Cervidae			35.33	14.66	8.54

64441	UO-4601	Artiodactyla	Cervidae	"Meaghan's tooth row"	35.72	32.33	20.29
70452	UO-4601	Artiodactyla	Cervidae	was with 64392, split because not associated	37.77	30.89	17.34
70463	UO-4601	Artiodactyla	Cervidae	"Ryan's gazelle jaw :(9/18/14"	39	23.28	9.6
70439	UO-4601	Artiodactyla	Cervidae	"box 2 of 3"	39.04	30.99	12.04
70457	UO-4601	Artiodactyla	Cervidae	was with 64484, no direct evidence of association	42.15	32.05	10.7
64392	UO-4601	Artiodactyla	Cervidae		44.08	24.67	16.47
64375	UO-4601	Artiodactyla	Cervidae	base of cervid antler	44.9	38.52	28.52
64346	UO-4601	Artiodactyla	Cervidae		49.7	14.17	8.63
64484	UO-4601	Artiodactyla	Cervidae	tooth impression Ryan's area	55.67	53.45	5
64488	UO-4601	Artiodactyla	Cervidae		61.16	19.18	16.08
64545	UO-4601	Artiodactyla	Cervidae		61.7	25.6	10.91
70454	UO-4601	Artiodactyla	Cervidae	artiodactyl metapodial	69.44	20.19	10.91
70443	UO-4601	Artiodactyla	Cervidae	"Logan sept 11"	76.76	24.93	12.28
64368	UO-4601	Artiodactyla	Cervidae	"Ryan's jaw 3"	90.31	30.09	9.73
64348	UO-4601	Artiodactyla	Cervidae		134	23.16	13.18
70432	UO-4601	Artiodactyla	Cervidae	"WNFM-K-o814-08 Box 3 of 3"	153	20.45	16.46
70474	UO-4601	Artiodactyla		same batch as X1 below	14.24	8.23	2.58
70482	UO-4601	Artiodactyla		X1	15.77	9.09	8.58

64350	UO-4601	Artiodactyla			Kyle bovid horn	136	22.07	17.27
70472	UO-4601	Perissodactyla	Equidae	Hipparion	kyles horse tooth bits 9/18/19	19	16.77	13.89
64548	UO-4601	Perissodactyla	Equidae	Hipparion		24.57	16.35	10.92
64538	UO-4601	Perissodactyla	Equidae	Hipparion		36.49	16.86	10.05
64608	UO-4601	Perissodactyla	Equidae	Hipparion		37.43	21.18	15.57
64609	UO-4601	Perissodactyla	Equidae	Hipparion	"horse jaw" from Bone Hill	93.73	45.15	17.82
70460	UO-4601	Perissodactyla	Equidae	Hipparion	all teeth by m3 erupted and in wear	190	73.87	63.75
64463	UO-4601	Perissodactyla	Equidae	Hipparion		238	21.82	6.21
64393	UO-4601	Perissodactyla	Equidae			18.05	7.23	4.46
70467	UO-4601	Perissodactyla	Equidae			19.41	18.43	9.22
64379	UO-4601	Perissodactyla	Equidae		"Ryan's podials"	31.72	23.58	16.08
70495	UO-4601	Perissodactyla	Equidae		"Kyle's pawny toof" 9/18/11	32.01	22.88	21.29
70465	UO-4601	Perissodactyla	Equidae			46.94	37.89	21.84
70492	UO-4601	Perissodactyla	Equidae			68.13	49.75	33.52
70444	UO-4601	Perissodactyla	Equidae		"Logan sept 11"	82.07	48.67	39.17
64425	UO-4601	Perissodactyla	Rhinoceratidae	Chilotherium		23.29	9.58	8.13
64428	UO-4601	Perissodactyla	Rhinoceratidae	Chilotherium		38.62	37.05	19.03
64493	UO-4601	Perissodactyla	Rhinoceratidae	Chilotherium		73.44	62.02	35.73

70503	UO-4601	Perissodactyla	Rhinoceratidae	Chilotherium	split off of 64554		79.28	58.86	52.59
70500	UO-4601	Perissodactyla	Rhinoceratidae	Chilotherium	split off of 64554		105.09	54.9	32.42
64614	UO-4601	Perissodactyla	Rhinoceratidae	Chilotherium			109.36	88.07	38.29
64554	UO-4601	Perissodactyla	Rhinoceratidae	Chilotherium			195	130.7	110.98
64371	UO-4601	Perissodactyla	Rhinoceratidae			13.8	12.26	7.1	
64397	UO-4601	Perissodactyla	Rhinoceratidae			19.56	10.29	7.44	
70447	UO-4601	Perissodactyla	Rhinoceratidae	"toes from Ryan 9/18/14"		22.4	8.32	4.4	
70499	UO-4601	Perissodactyla	Rhinoceratidae			23.29	16.26	8.41	
70469	UO-4601	Perissodactyla	Rhinoceratidae			29.02	19.92	13.66	
70466	UO-4601	Perissodactyla	Rhinoceratidae			29.16	17.43	15.77	
70478	UO-4601	Perissodactyla	Rhinoceratidae	X1		29.19	16.32	7.42	
70438	UO-4601	Perissodactyla	Rhinoceratidae	"Zack=h's rhino tooth w/ horse tooth"		36.89	31.99	27.37	
70433	UO-4601	Perissodactyla	Rhinoceratidae	"WNFM-K-o814-08 Box 3 of 3"		38.93	37.31	25.35	
64499	UO-4601	Perissodactyla	Rhinoceratidae			54.17	44.28	21.38	
70437	UO-4601	Perissodactyla	Rhinoceratidae	" o814-08 Box 3 of 3"		55.05	33.09	20.26	
70464	UO-4601	Perissodactyla	Rhinoceratidae	"9/18/14"		69.52	39.95	39.83	

70468	UO-4601	Perissodactyla	Rhinoceratidae			74.81	46.7	39.17	
70502	UO-4601	Perissodactyla	Rhinoceratidae	"tibia in five pieces"		153.53	70.42	45.96	
70442	UO-4601	Perissodactyla		"Logan sept 11"		280	55.57	25.52	
70498	UO-4601						2.74	2.59	0.2
70449	UO-4601				"toes from Ryan 9/18/14"		8.75	6.76	3.91
64439	UO-4601						9.52	5.8	3.94
70448	UO-4601				"toes from Ryan 9/18/14"		10.64	8.56	7.37
70487	UO-4601				X1		10.79	10.18	5.21
70485	UO-4601				X1		11.16	9.03	2
70486	UO-4601				X1		11.55	7.69	7.32
70481	UO-4601				X1		11.93	7.09	3.97
70488	UO-4601				X1		13.13	9.73	4.77
70483	UO-4601				X1		14.03	11.54	9.78
70484	UO-4601				X1		16.26	10.96	6.16
70470	UO-4601						18.21	15.31	7.24
70455	UO-4601				was with F-64402		20.86	13.69	8.16
70480	UO-4601				X1		21.13	16	14.12
70479	UO-4601				X1		22.01	20.7	12.93

70475	UO-4601	X1	22.2	14.24	11.36
70453	UO-4601	was with F-64350	24.12	9.3	3.92
70450	UO-4601	"toes from Ryan 9/18/14"	24.21	11.48	9.95
70493	UO-4601		25.57	24.3	11.54
64349	UO-4601		25.96	20.46	8.73
70496	UO-4601		29.57	18.35	8.67
70473	UO-4601	was with F-70472, not associated	30.07	17.82	8.13
70445	UO-4601	"Logan sept 11"	33.37	32.07	25.47
70494	UO-4601		33.91	24.68	23.64
70436	UO-4601	"WNFM-K-o814-08 Box 3 of 3"	35.06	23.43	13.07
70477	UO-4601	X1	35.55	31.04	9.16
70434	UO-4601	"WNFM-K-o814-08 Box 3 of 3"	35.65	26.53	17.88
70491	UO-4601	with last F#	39.01	38.67	17.34
70489	UO-4601	new batch	42.43	34.42	24.95
70435	UO-4601	"WNFM-K-o814-08 Box 3 of 3"	46.11	33.11	19.48
70490	UO-4601	with last F#	47.75	27.59	22.74
70497	UO-4601		55.36	40.12	19.51
70476	UO-4601	X1	60.97	46.52	26.94

70440	UO-4601				"box 2 of 3"	67.15	35.77	31.89
70441	UO-4601					142.59	69.65	17.5
64341	UO-4601	Squamata	Varanidae	Varanus	mandible	30.7	6.28	5.38

APPENDIX D

DAM SITE BONE BED (UO-4604)

Specimen #	Locality #	Order	Family	Genus	element	L1	L2	L3
64509	UO-4604	Artiodactyla	Bovidae	Gazella	base of horn core	31.88	24.71	21.33
64639	UO-4604	Artiodactyla	Bovidae	Gazella	partial jaw with 1 partial tooth	34.93	25.06	10.24
64618	UO-4604	Artiodactyla	Bovidae	Gazella	basal horn core	36.3	24.76	18.2
64457	UO-4604	Artiodactyla	Bovidae	Gazella	horn core	67.08	25.96	19.75
71402	UO-4604	Artiodactyla	Bovidae	Gazella	horn core	68.01	25.89	21.28
70340	UO-4604	Artiodactyla	Bovidae	Gazella	two horn cores and associated imprint. From bag “rhino radius and stuff”	69.8	24.01	20.5
64539	UO-4604	Artiodactyla	Bovidae	Gazella	two horn cores and associated imprint. From bag “rhino radius and stuff”	102.25	25.03	18.61
71404	UO-4604	Artiodactyla	Bovidae	Gazella	horn core	102.28	25.58	18.25
71403	UO-4604	Artiodactyla	Bovidae	Gazella	horn core	104.07	23.89	19.2
71405	UO-4604	Artiodactyla	Bovidae	Gazella	horn core	119.79	21.28	18.85
64462	UO-4604	Artiodactyla	Bovidae	Gazella	horn core	127.08	26.65	17.81
64463	UO-4604	Artiodactyla	Bovidae		tooth frag	8.52	6.93	3.58
70326	UO-4604	Artiodactyla	Bovidae		partial jaw w/ m3-m1	44.98	23.51	8.46

64542	UO-4604	Lagomorpha		tooth frag		5.49	3.03	2.01
70321	UO-4604	Lagomorpha		incissors		10.93	3.2	2.67
70320	UO-4604	Lagomorpha		partial skull, front w/incissors. Pika.		14.6	7.2	2.38
64363	UO-4604	Lagomorpha		bunny jaw		16.99	15.43	5.31
64460	UO-4604	Lagomorpha		two distal humeri, calcaneous, other bone bits		20.83	10.63	5.04
64452	UO-4604	Lagomorpha		small bones, mostly rabbit, but I think there is some rodent mixed in		77.12	14.28	4.36
64453	UO-4604	Perissodactyla	Equidae	Hipparion	jaw fragment with 4 teeth	99.98	56.92	13.48
64504	UO-4604	Perissodactyla	Equidae		distal tibia	59.39	36.87	28.44
64423	UO-4604	Perissodactyla	Rhinoceratidae	Chilotherium	rhino tooth bit	38.68	19.5	14.91
64540	UO-4604	Perissodactyla	Rhinoceratidae	Chilotherium	metacarpal bit and other bit	39.49	33.71	30.04
64544	UO-4604	Perissodactyla	Rhinoceratidae	Chilotherium	distal metapodial from bag “rhino radius and shit”	53.98	41.77	31.32
70462	UO-4604	Perissodactyla	Rhinoceratidae	Chilotherium	patella	93.12	81.24	19.8
64617	UO-4604	Perissodactyla	Rhinoceratidae	Chilotherium	ulna thing?	95.68	75.9	71.38

70461	UO-4604	Perissodactyla	Rhinoceratidae	Chilotherium	proximal radius	99.77	81.56	38.18
64637	UO-4604	Perissodactyla	Rhinoceratidae	Chilotherium	proximal tibia	115.24	106.35	85.29
64489	UO-4604	Perissodactyla	Rhinoceratidae	Chilotherium	distal radius with articulated carpals	149.44	79.85	48.82
64624	UO-4604	Perissodactyla	Rhinoceratidae	Chilotherium	distal tibia and tiny bit of astragalus	170	88.06	45.45
64526	UO-4604	Perissodactyla	Rhinoceratidae	Chilotherium	whole radius	253	88.03	30.99
64638	UO-4604	Perissodactyla	Rhinoceratidae	Chilotherium	proximal radius and ulna	262	89.37	36.13
70501	UO-4604	Perissodactyla	Rhinoceratidae	astragalus	62.21	42.12	32.71	
70502	UO-4604	Perissodactyla	Rhinoceratidae	proximal radius	96.41	83.7	32.08	
64557	UO-4604				small thing… rodent?	10.12	6.54	5.69
64620	UO-4604				composite of a lot of crap	40.79	34.53	31.52
64619	UO-4604				proximal metapodial	55.19	27.36	19.28
70322	UO-4604				little things, will be sorted more….			

APPENDIX E

UNCORRECTED STRIKE AND SUN COMPASS READINGS

Sample #	**Azimuth**	**Sun compass**	**Difference**	**Average error by section**
KSS-001	no Brunton	139.3		
KSS-002	no Brunton	157.6		
KSS-003	no Brunton	113.6		
KSS-011	160	89.4	70.6	
KSS-022	194	136.8	57.2	
KSS-023	181	135.6	45.4	
KSS-024	219	108	111	
KSS-025	168	178.5	10.5	
KSS-026	186	152.2	33.8	
KSS-028	181	178.9	2.1	
KSS-029	159	198.9	39.9	
KSS-030	178	201.6	23.6	
KSS-032	177	189.6	12.6	
KSS-033	249	141.6	107.4	
KSS-034	264	125.7	138.3	
				54.36666667
KDS-001	238	239.3	1.3	
KDS-002	240	242.4	2.4	
KDS-003	285	208	77	
KDS-004	252	240.3	11.7	
KDS-005	274	226.1	47.9	
KDS-006	242	261.3	19.3	
KDS-007	200	314	114	
KDS-008	180	324.8	144.8	
KDS-009	218	295.8	77.8	
KDS-010	254	242.9	11.1	
KDS-011	213	269.3	56.3	
KDS-012	256	270.7	14.7	
KDS-013	255	287.4	32.4	

KDS-014	258	286.4	28.4	
KDS-015	277	275.7	1.3	
KDS-016	9	4.1	4.9	
KDS-017	21	341.1	39.9	
KDS-018	21	21.1	0.1	
KDS-019	356	17.6	21.6	
KDS-020	354	24	28	
KDS-021	9	17.3	8.3	
KDS-044	144	229.8	85.8	
KDS-045	165	248.6	83.6	
KDS-046	213	245.4	32.4	
KDS-047	182	239	57	
KDS-048	210	218.8	8.8	
KDS-049	174	260	86	
KDS-050	155	274.2	119.2	
KDS-051	156	276.1	120.1	
KDS-052	110	14.4	95.6	
KDS-054	111	10.2	100.8	
				49.43548387
KO-009	100	102.9	2.9	
KO-010	101	105	4	
KO-011	112	95.5	16.5	
KO-012	102	109.5	7.5	
KO-013	131	82.8	48.2	
KO-014	110	108.3	1.7	
				13.46666667
KSU-011	207	169.7	37.3	
KSU-012	187	182	5	
KSU-013	190	182.3	7.7	
KSU-100	140	87.8	52.2	
KSU-101	137	87.7	49.3	
KSU-102	164	74.3	89.7	
KSU-103	155	79.5	75.5	
KSU-104	160	78.4	81.6	
KSU-105	128	99	29	
KSU-106	155	87.9	67.1	
KSU-107	157	95.7	61.3	
KSU-108	25	328	57	
KSU-109	10	75.2	65.2	

KSU-110	20	77.4	57.4	
KSU-020	135	148.8	13.8	
KSU-021	140	84.7	55.3	
KSU-022	139	86.9	52.1	
KSU-026	351	-35.6	44.6	
KSU-027	355	331.5	23.5	
KSU-028	0	-37.6	37.6	
KSU-029	129	181.6	52.6	
KSU-030	134	175	41	
KSU-031	136	185.8	49.8	
KSU-111	91	61.2	29.8	
KSU-112	111	35.7	75.3	
KSU-113	135	199.5	64.5	
KSU-114	166	172.8	6.8	
KSU-115	156	186.5	30.5	
KSU-116	173	171.9	1.1	
KSU-050	32	327.1	64.9	
KSU-051	35	95	60	
KSU-052	49	125.6	76.6	
KSU-053	64	132.2	68.2	
KSU-054	64	127.2	63.2	
KSU-055	79	123.4	44.4	
KSU-056	74	144.1	70.1	
KSU-057	74	126.1	52.1	
KSU-058	79	127.5	48.5	
KSU-059	96	107.8	11.8	
KSU-060	125	78.4	46.6	
KSU-061	122	79.5	42.5	
KSU-062	42	356.7	45.3	
KSU-063	53	345.6	67.4	
KSU-064	89	130.6	41.6	
KSU-065	19	106.2	87.2	
KSU-066	33	21.6	11.4	
KSU-067	41	25.4	15.6	
				48.5

APPENDIX F

P-MAG SAMPLE COLLECTION FIELD DATA

LOCATION	SAMPLE #	ROTATION	STIKE	DIP	LITHOLOGY
KSS	KSS-001	+1			siltstone below red layer
	KSS-002	+5			siltstone below red layer
	KSS-003	+3			siltstone below red layer
	KSS004	-5	S51E	50°	reddish siltstone
	KSS005	+3	S65E	35°	reddish siltstone
	KSS006	0	S47E	36°	reddish siltstone
	KSS007	+4	S57.5E	40°	2m up from red
	KSS008	-3	S71E	42.5°	2m up from red
	KSS009	+12	S48E	43.5°	2m up from red
	KSS010	-1	S19E	46°	mud stone with yellow altered material
	KSS011	+2	S20E	51°	mud stone with yellow altered material
	KSS012	+2	S24E	53°	mud stone with yellow altered material
	KSS013	+14	S15E	43.5°	slightly sand grey siltstone
	KSS014	-3	S64E	45°	slightly sand grey siltstone
	KSS015	-3	N75E	39°	slightly sand grey siltstone
	KSS016	+11	S24E	56.5°	red claystone thin band
	KSS017	-7	S22W	46.5°	grey claystone
	KSS018	-4	S34E	50°	grey claystone
	KSS019	0	S38W	67.5°	brick red paleosol
	KSS020	+6	S1E	49°	brick red paleosol
	KSS021	-5	S62W	45°	brick red paleosol
	KSS022	+8	S14W	50°	tannish grey siltstone
	KSS023	+17	S1W	48°	tannish grey siltstone
	KSS024	+3	S39W	55°	tannish grey siltstone
	KSS025	+2	S12E	57.5°	sandy siltstone
	KSS026	+25	S6W	47°	sandy siltstone
	KSS027	+10	S8E	44°	sandy siltstone
	KSS028	+23	S1W	45°	greyish greenish siltstone
	KSS029	+7	S21E	35°	greyish greenish siltstone
	KSS030A	+20	S30E	35°	greyish greenish siltstone
	KSS030	-10	S2E	52.5°	red sandy claystone
	KSS031	-5	240E	53°	red sandy claystone
	KSS032	+3	S3E	47°	red sandy claystone
	KSS033	+5	S69W	44°	dark red siltstone

	KSS034	-7	S84W	55°		dark red siltstone
	KSS035	0	N58W	47°		dark red siltstone
	KSS036	+17	S18W		58.5	sandy greyish tan layer
	KSS037	-3	S42W	65°		sandy greyish tan layer
	KSS038	-2	S54W	65°		sandy greyish tan layer
KDS	KDS-001	-17	S58W	36°		brown shaley layer below sandstone
	KDS-002	-20	S60W	52°		brown shaley layer below sandstone
	KDS-003	-13	N75W	45°		brown shaley layer below sandstone
	KDS-004	-9	S72W	30°		brown shaley layer below sandstone
	KDS-005	-15	N86W	38°		brown shaley layer below sandstone
	KDS-006	-18	S62W	63°		brown shaley layer below sandstone
	KDS-007	+3	S20W	54°		brown shaley layer below sandstone
	KDS-008	+5	S0	44°		brown shaley layer below sandstone
	KDS-009	+6	S38W	38°		brown shaley layer below sandstone
	KDS-010	-32	S74W	40°		brown shaley layer below sandstone
	KDS-011	-6	S33W	46.5°		brown shaley layer below sandstone
	KDS-012	-10	S76W	50°		brown shaley layer below sandstone
	KDS-013	+5	S75W	44°		brown shaley layer below sandstone
	KDS-014	-8	S78W	44°		brown shaley layer below sandstone
	KDS-015	0	N83W	39°		brown shaley layer below sandstone
	KDS016	+14	S9W	55°		red paleosol
	KDS017	+10	S21W	49°		red paleosol
	KDS018	+4	S21W	45°		red paleosol
	KDS-019	+1	S4E	43°		red paleosol
	KDS-020	+3	S6E	28°		red paleosol
	KDS-021	-4	S9W	30°		red paleosol
	KDS-022	+7	S60W	47°		red paleosol
	KDS-023	+1	S68W	34°		red paleosol
	KDS-024	+1	S50W	43°		red paleosol
	KDS-025	+13	S60W	37°		red paleosol
	KDS-026	+8	S47W	42°		red paleosol
	KDS-027	+8	S65W	35°		red paleosol
	KDS-028	+5	S0	64°		grey paleosol below a thick sandstone
	KDS-029	+3	S11E	62°		grey paleosol below a thick sandstone
	KDS-030	0	S24W	70°		grey paleosol below a thick sandstone
	KDS-031	+10	S86W	52°		reddish brown paleosol
	KDS-032	0	S62W	63°		reddish brown paleosol
	KDS-033	+10	N64W	46°		reddish brown paleosol
	KDS-034	-18	S9W	51°		greenish siltstone, fossil bed layer
	KDS-035	-20	S12E	49°		greenish siltstone, fossil bed layer

	KDS-036	-20	S2W	50°	greenish siltstone, fossil bed layer
	KDS-037	-4	S25W	62°	reddish clayey siltstone
	KDS-038	-9	S15W	60°	reddish clayey siltstone
	KDS-039	-6	S39W	52°	reddish clayey siltstone
	KDS-040	+18	N73W	45°	silty sandstone
	KDS-041	-11	N43W	46°	silty sandstone
	KDS-042	-3	N44W	62°	silty sandstone
	KDS-043	-11	S12E	56°	dark brown clayey paleosol
	KDS-044	-3	S6E	64°	dark brown clayey paleosol
	KDS-045	+5	S15E	68°	dark brown clayey paleosol
	KDS-046	-8	S33W	59°	brown paleosol
	KDS-047	+5	S2W	65°	brown paleosol
	KDS-048	0	S30W	60°	brown paleosol
	KDS-049	-4	S6E	47°	red brown blocky paleosol
	KDS-050	-1	S25E	59°	red brown blocky paleosol
	KDS-051	0	S24E	60°	red brown blocky paleosol
	KDS-052	-12	S70E	35°	red brown blocky paleosol
	KDS-053	+1	S68E	38°	red brown blocky paleosol
	KDS-054	+3	S69E	29°	red brown blocky paleosol
	KDS-055	-15	S12W	33°	reddish paleosol
	KDS-056	-4	S8W	44°	reddish paleosol
	KDS-057	-3	S44W	43°	reddish paleosol
	KDS-058	-9	S17E	29°	sandy silt layer
	KDS-059	0	S17W	30°	sandy silt layer
	KDS-060	0	S13W	44°	sandstone
	KDS-061	-3	S25W	34°	sandstone
	KDS-062	+1	S27W	39°	sandstone
	KDS-063	0	N1W	39°	reddish brown paleosol above sandstone
	KDS-064	-5	N3W	35°	reddish brown paleosol above sandstone
	KDS-065	+9	N4E	29°	reddish brown paleosol above sandstone
	KDS-066	0	N55E	29°	brownish tan paleosol
	KDS-067	-3	S60W	27°	brownish tan paleosol
	KDS-068	0	S70W	22°	brownish tan paleosol
	KDS-068A	-5	S41W	45°	sandy silt layer
KO	KO-001	+9	N34E	24°	tan siltstone
	KO-002	-3	N60E	29°	tan siltstone
	KO-003	-4	N67E	17°	tan siltstone
	KO-004	+15	S75E	48°	siltstone with some bands of oxidized material
	KO-005	+4	S83E	54°	siltstone with some bands of oxidized material
	KO-006	+3	279E	46°	siltstone with some bands of oxidized material

	KO-007	+4	S75E	57°	tan siltstone
	KO-007A	+4	S75E	57°	tan siltstone
	KO-008	-15	S88E	41°	tan siltstone
	KO-009	+8	S80E	58°	tan/grey siltstone with oxidized bands
	KO-010	-15	S79E	53°	tan/grey siltstone with oxidized bands
	KO-010A	-15	S79E	53°	tan/grey siltstone with oxidized bands
	KO-011	+10	S68E	51°	tan/grey siltstone with oxidized bands
	KO-011A	+10	S68E	51°	tan/grey siltstone with oxidized bands
	KO-012	+4	S78E	43°	tan/grey siltstone with oxidized bands
	KO-013	-18	S49E	49°	tan/grey siltstone with oxidized bands
	KO-014	0	S70E	48°	tan/grey siltstone with oxidized bands
	KO-015	-10	S74E	53°	tan/grey siltstone with oxidized bands
	KO-16	-10	S67E	49°	tan/grey siltstone with oxidized bands
	KO-17	-10	S76E	40°	tan/grey siltstone with oxidized bands
	KO-18	-20	S71E	44°	tan/grey siltstone with oxidized bands
	KO-19	-5	S68E	59°	tan/grey siltstone with oxidized bands
	KO-19A	-5	S68E	59°	tan/grey siltstone with oxidized bands
	KO-20	0	S72E	50°	tan/grey siltstone with oxidized bands
	KO-21	+17	S66E	53°	tan/grey siltstone with oxidized bands
	KO-22	-10	S74E	44°	tan/grey siltstone with oxidized bands
	KO-23	-8	S62E	41°	tan/grey siltstone with oxidized bands
	KO-24	-5	S69E	63°	tan siltstone with orange oxidized banding, platier peds
	KO-25	-10	S74E	50°	tan siltstone with orange oxidized banding, platier peds
	KO-26	+4	S70E	49°	tan siltstone with orange oxidized banding, platier peds
	KO-27	-16	S55E	45°	tan siltstone with some clastic material present
	KO-28	+5	S67E	29°	tan siltstone with some clastic material present
	KO-29	0	S70E	48°	tan siltstone with some clastic material present
	KO-30	+5	S81E	58°	tan siltstone, platy peds
	KO-31	-3	S72E	54°	tan siltstone, platy peds
	KO-32	0	S68E	38°	tan siltstone, platy peds
	KO-33	-12	S62E	64°	yellowish tan siltstone
	KO-34	-10	S54E	32°	yellowish tan siltstone
	KO-35	-4	S65E	47°	yellowish tan siltstone
	KO-36	+3	S66E	61°	yellowish silts with oxidized bands
	KO-37	0	S65E	54°	yellowish silts with oxidized bands
	KO-38	-15	S64E	45°	yellowish silts with oxidized bands
	KO-39	-9	S65E	48°	light brown siltstone
	KO-40	+5	S46E	40°	light brown siltstone
	KO-41	-10	S45E	46°	light brown siltstone

	KO-42	-6	S58E	44°	grey/tan/orange banded silts
	KO-43	-3	S69E	43°	grey/tan/orange banded silts
	KO-44	-4	S64E	68°	grey/tan/orange banded silts
	KO-45	-8	S51E	43°	grey/tan/orange banded silts
	KO-46	-5	S80E	44°	grey/tan/orange banded silts
	KO-47	-5	S81E	68°	grey/tan/orange banded silts
KU	KU-115	-2	S24E	38°	reddish siltstone
	KU-116	-2	S7E	37°	reddish siltstone
	KU-113	+13	S45E	37°	reddish siltstone
	KU-114	+1	S14E	33°	reddish siltstone
	KU-111	+10	S89E	39°	siltstone
	KU-112	-3	S69E	43°	siltstone
	KU-108	-3	N25E	56°	silt with granule sized clastic component
	KU-109	-5	N10E	54°	silt with granule sized clastic component
	KU-110	-10	N20E	45°	silt with granule sized clastic component
	KU-105	0	S52E	47°	sandy silt layer
	KU-106	+20	S25E	34°	sandy silt layer
	KU-107	0	S23E	36°	sandy silt layer
	KU-102	-8	S16E	48°	sandy silt layer
	KU-103	+8	S25E	50°	sandy silt layer
	KU-104	-10	S20E	42°	sandy silt layer
	KU-100	+9	S40E	41°	reddish sandy silt
	KU-101	0	S43E	40°	reddish sandy silt
	KU-101A	0	S43E	40°	reddish sandy silt
	KU-01	-10	N70W	58°	tan silt with abundant granule sized clastic material
	KU-02	-20	N43W	46°	tan silt with abundant granule sized clastic material
	KU-03	+8	N25W	48°	tan silt with abundant granule sized clastic material
	KU-04	-5	N29W	42°	tan silt with abundant granule sized clastic material
	KU-5	+5	S36W	48°	sandy silt inbetween two gravel layers
	KU-6	0	S6E	43°	sandy silt inbetween two gravel layers
	KU-7	-15	S16W	36°	sandy silt inbetween two gravel layers
	KU-8	+5	S12W	46°	sandy silt 1m above gravel layer
	KU-9	+10	S0	44°	sandy silt 1m above gravel layer
	KU-10	-15	S13W	47°	sandy silt 1m above gravel layer
	KU-11	+5	S27W	45°	sandy siltstone
	KU-12	-10	S7W	34°	sandy siltstone
	KU-13	+8	S10W	49°	sandy siltstone
	KU-14	+6	S24E	45°	sandy siltstone with some sand layers

	KU-15	-10	S10E	52°	sandy siltstone with some sand layers
	KU-16	-15	S25E	48°	sandy siltstone with some sand layers
	KU-20	0	S45E	36°	reddish sandy siltstone
	KU-21	-14	S40E	43°	reddish sandy siltstone
	KU-22	0	S41E	45°	reddish sandy siltstone
	KU-23	-18	N51E	55°	reddish paleosol
	KU-24	-10	N61E	50°	reddish paleosol
	KU-25	-20	N57E	45°	reddish paleosol
	KU-26	-20	N9W	57°	reddish paleosol
	KU-27	+8	N5W	49°	reddish paleosol
	KU-28	0	N	48°	reddish paleosol
	KU-29	+16	S51E	35°	siltstone at base of gravel
	KU-30	+6	S46E	34°	siltstone at base of gravel
	KU-31	0	S44E	28°	siltstone at base of gravel
	KU-50	+10	N32E	43°	reddish sandy siltstone
	KU-51	+8	N35E	57°	reddish sandy siltstone
	KU-52	0	N49E	78°	reddish sandy siltstone
	KU-53	-5	N64E	56°	brownish paleosol interbed
	KU-54	+3	N64E	57°	brownish paleosol interbed
	KU-55	+3	N74E	41°	brownish paleosol interbed
	KU-56	-2	N54E	41°	clayey silt, brown with green gley
	KU-57	+20	N74E	37°	clayey silt, brown with green gley
	KU-58	+3	N79E	48°	clayey silt, brown with green gley
	KU-59	+15	S84E	36°	sandy silts with carbonate nodules
	KU-60	-9	S55E	50°	sandy silts with carbonate nodules
	KU-61	+3	S58E	51°	sandy silts with carbonate nodules
	KU-62	+10	N42E	28°	poorly sorted orangish tan material with clay to sand
	KU-63	+25	N53E	31°	poorly sorted orangish tan material with clay to sand
	KU-64	+10	N89E	27°	poorly sorted orangish tan material with clay to sand
	KU-65	+17	N19E	39°	sandstone
	KU-66	+3	N33E	28°	sandstone
	KU-67	0	N41E	21°	sandstone
	KU-68	+2	N42E	46°	redish brown clay with metavolcanic components (Chu Like)
	KU-69	-3	N44E	50°	redish brown clay with metavolcanic components (Chu Like)
	KU-70	-5	N41E	58°	redish brown clay with metavolcanic components (Chu Like)
	KU-71	-13	N34E	48°	sandy siltstone
	KU-72	-30	N26E	40°	sandy siltstone

	KU-73	-15	N31E	42°	sandy siltstone
	KU-74	-1	N3E	34°	siltstone with clastic material
	KU-75	+15	N24E	29°	siltstone with clastic material
	KU-76	10	N52E	31°	siltstone with clastic material
	KU-77	+8	N40E	32°	siltstone with clastic material
	KU-78	+11	N34E	39°	siltstone with clastic material
	KU-79	0	N30E	38°	siltstone with clastic material
	KU-150	+20	S33W? 9wrong side)	42°	tan siltstone
	KU-151	+15	N62E	37°	tan siltstone
	KU-152	+6	N70E	38°	tan siltstone
	KU-153	+15	N77E	30°	sandy siltstone
	KU-154	+24	N84E	62°	sandy siltstone
	KU-155	+15	N74E	33°	sandy siltstone
	KU-156	+13	N40E	46°	red paleosol
	KU-157	+17	N57E	34°	red paleosol
	KU-158	+6	N73E	34°	red paleosol
	KU-159	+15	N61E	32°	reddish sandy siltstone
	KU-160	+8	N70E	48°	reddish sandy siltstone
	KU-161	-10	N86E	31°	reddish sandy siltstone
	KU-162	+30	N13E	22°	siltstone
	KU-163	-13	N66E	26°	siltstone
	KU-164	+15	N36E	33°	siltstone
	KU-165	+17	N26W	39°	reddish brown paleosol
	KU-166	+13	N9W	30°	reddish brown paleosol
	KU-167	-11	N44E	30°	brown siltstone
	KU-168	+13	N27E	29°	brown siltstone
	KU-169	+20	N32E	31°	brown siltstone

APPENDIX G

SQR FILE FOR ORTOK WITH RATINGS

#	Sample		path			degree	180	Geo	RATING	N/R
37	KO-001	L	int	189.8 -48.3 202.8 -41.0 D-I	6	14	X	9.8		
38	KO-001	L	pri	167.7 -82.6 230.5 -73.3 I-N	6	14.3	X	347.7	A2	R
39	KO-001	L	ovr	187.4 -44.1 199.1 -37.3 B-I	8	13.8	X	7.4		
40	KO-002	L	int	356.4 49.3 11.9 44.7 B-H	7	10.6				
41	KO-002	L	ovr	357.4 49.6 12.9 44.8 BCE-H	6	10.6				
42	KO-002	L	vrm	180.4 -56.5 199.3 -50.6 AB	2	0				
43	KO-002	L	pri	18.1 66.4 38.9 56.3 H-N	7	9.1			A1	N
44	KO-001	L	vrm	343.5 59.6 7.9 57.3 AB	2	0				
45	KO-003	L	vrm	152.1 -72.6 197.8 -70.3 AB	2	0				
46	KO-003	L	ovr	2.8 71.0 33.7 63.1 B-H	7	11.3				
47	KO-003	L	pri	318.6 70.1 3.2 71.8 H-MN	7	7.5			A1	N
48	KO-004	L	vrm	344.4 37.7 356.0 36.8 AB	2	0	X	164.4		
49	KO-004	L	ovr	207.5 5.4 205.5 14.1 B-F	5	7.1	X	27.5		
50	KO-004	L	pri	174.8 -7.8 176.5 -5.6 G-N	8	4.8	X	354.8	A2	N
51	KO-005	L	vrm	176.9 -35.5 186.6 -31.6 AB	2	0				
52	KO-005	P	ovr	61.8 27.3 63.3 12.4 B-F	5	7.5				
53	KO-005	L	pri	350.5 66.5 20.3 61.6 G-N	8	3.1			A1	N
54	KO-006	L	vrm	187.2 -44.1 198.9 -37.5 AB	2	0				
55	KO-006	L	ovr	10.2 48.6 22.9 40.6 B-G	6	10.6				
56	KO-006	L	pri	5.3 55.4 22.6 48.5 G-N	8	4.5			A1	N
57	KO-008	L	vrm	168.2 -48.2 184.2 -45.7 AB	2	0				
58	KO-008	P	ovr	175.4 48.8 157.8 48.8 B-H	7	15.7				
59	KO-008	L	pri	0.2 57.0 19.4 51.1 I-N	6	11.1			A1	N
60	KO-010	L	vrm	174.5 -37.8 185.3 -34.5 AB	2	0				
61	KO-010	P	ovr	87.0 -17.4 88.2 -32.5 B-GN	7	15.8				
62	KO-010	L	pri	3.2 21.8 8.2 17.0 G-N	8	6			A2	N
63	KO-010A	L	vrm	187.8 -37.0 196.9 -30.5 AB	2	0				
64	KO-010A	L	ovr	43.6 17.6 45.2 5.6 B-G	6	12.8				
65	KO-010A	P	pri	181.0 67.2 145.5 66.0 H-N	7	10				
66	KO-011A	L	vrm	236.8 -31.3 239.0 -17.1 AB	2	0				
67	KO-011A	P	ovr	352.2 48.2 8.0 45.1 B-F	5	9.6				

68	KO-011A	P	pri	318.5	20.8	324.6	27.2	I-N	6	11.7				B2		N
69	KO-011A	L	int	18.5	21.7	22.4	13.3	F-I	4	6.6						
70	KO-012	L	vrm	177.7	-45.9	191.4	-41.3	AB	2	0						
71	KO-012	P	ovr	170.8	47.2	155.8	46.9	B-G	6	9.8						
72	KO-012	P	int	59.2	-20.1	236.8	34.2	G-K	5	10.4						
73	KO-012	P	pri	356.5	-8.2	353.9	-10.4	K-N	4	18.2				B2		N
74	KO-014	L	vrm	241.8	-32.0	243.5	-17.5	AB	2	0						
75	KO-014	L	ovr	74.7	25.6	74.9	10.6	B-I	8	7						
76	KO-014	L	pri	72.7	39.6	73.3	24.7	G-N	8	15				A2		N
77	KO-015	L	vrm	179.5	-36.0	189.2	-31.5	AB	2	0						
78	KO-015	P	ovr	128.8	14.1	127.0	4.2	B-G	6	19.4						
79	KO-015	L	pri	347.6	41.5	0.3	39.7	G-N	8	10.1				A1		N
80	KO-017	L	vrm	141.0	-34.3	151.6	-39.6	AB	2	0						
81	KO-017	L	ovr	11.8	42.2	21.5	34.7	B-E	4	10.6						
82	KO-017	L	pri	305.0	51.2	323.5	59.5	FGI-N	8	8.8				A2		N
83	KO-018	L	vrm	173.2	-42.4	185.9	-39.1	AB	2	0						
84	KO-018	P	ovr	50.6	-30.3	47.2	-43.8	B-F	5	16.5						
85	KO-018	L	pri	352.2	36.9	2.8	34.2	G-N	8	4.8				A1		N
86	KO-19A	L	vrm	206.3	-30.4	211.6	-20.3	AB	2	0						
87	KO-19A	L	ovr	325.9	67.7	3.9	68.4	B-F	5	9.1						
88	KO-19A	L	pri	45.5	36.1	49.7	23.0	G-M	7	10.6				A2		N
89	KO-020	L	vrm	172.4	-35.8	182.6	-33.0	AB	2	0						
90	KO-020	L	ovr	358.1	39.3	9.2	35.1	B-H	7	10						
91	KO-020	L	pri	344.8	39.6	357.0	38.5	H-N	7	10				A1		N
92	KO-021	L	vrm	4.4	32.8	12.5	27.3	AB	2	0	X	184.4				
93	KO-021	L	ovr	222.3	25.0	216.6	37.0	B-G	6	11.1	X	42.3				
94	KO-021	L	pri	184.5	-24.4	190.1	-19.2	H-N	7	13	X	4.5		A3		N
95	KO-022	L	vrm	183.0	-45.5	195.8	-39.7	AB	2	0						
96	KO-022	L	ovr	183.6	-45.9	196.6	-40.0	A-F	6	2.7						
97	KO-022	L	pri	7.9	52.5	23.2	45.3	G-N	8	14.5				A1		N
98	KO-023	L	vrm	190.1	-50.2	203.9	-42.5	AB	2	0						
99	KO-023	L	ovr	8.3	60.1	27.7	52.3	B-GN	7	8.2						
100	KO-023	L	pri	2.2	56.3	20.6	49.9	G-KMN	7	8.4				A1		N
101	KO-024	L	nrm	18.2	27.7	23.6	19.3	AB	2	0	x	x				
102	KO-024	P	ovr	41.1	78.6	61.9	65.3	B-F	5	10.4	x	x				
103	KO-024	L	pri	185.8	6.5	183.6	11.1	H-N	7	14.5	x	5.8		A2		N
104	KO-025	L	vrm	184.5	-40.2	195.1	-34.3	AB	2	0						

105	KO-025	P	ovr	335.5	-16.1	331.3	-13.5	B-F	5	9		
106	KO-025	L	pri	2.5	37.6	12.4	32.3	G-N	8	4.7	A1	N
107	KO-026	L	vrm	202.0	-40.7	210.5	-31.2	AB	2	0		
108	KO-026	P	ovr	134.3	6.3	132.9	-5.2	B-F	5	15.6		
109	KO-026	L	pri	21.0	35.1	28.1	25.9	G-N	8	3.9	A2	N
110	KO-028	L	vrm	167.9	-56.2	188.8	-53.1	AB	2	0		
111	KO-028	P	ovr	296.0	49.9	311.6	60.4	B-E	4	8.4		
112	KO-028	L	pri	341.6	50.9	359.9	49.9	F-N	9	7	A1	N
113	KO-029	L	vrm	173.8	-37.4	184.5	-34.2	AB	2	0		
114	KO-029	P	ovr	97.1	2.7	98.9	-11.9	B-E	4	17.3		
115	KO-029	L	pri	353.4	38.0	4.3	35.0	F-N	9	10.9	A1	N
116	KO-031	L	vrm	173.6	-31.0	182.0	-28.2	AB	2	0		
117	KO-031	P	ovr	116.8	73.6	98.3	60.2	B-F	5	18		
118	KO-031	L	pri	342.9	50.3	0.6	49.0	G-N	8	6.7	A1	N
119	KO-032	L	vrm	195.0	-50.6	208.0	-41.9	AB	2	0		
120	KO-032	P	ovr	4.6	-23.4	357.7	-28.5	B-E	4	15.4		
121	KO-032	L	pri	13.2	56.5	29.3	48.0	F-N	9	6.4	A1	N
122	KO-035	L	vrm	151.0	-22.0	157.5	-25.3	AB	2	0		
123	KO-035	P	ovr	91.5	-42.5	276.7	56.8	B-DF	4	3.7		
124	KO-037	L	vrm	179.5	-31.5	187.6	-27.1	AB	2	0		
125	KO-037	P	ovr	115.9	54.7	106.5	43.0	B-FN	6	14.6		
126	KO-037	L	pri	1.5	15.9	5.1	11.7	G-N	8	7.9	A2	N
127	KO-040	L	vrm	188.6	-42.1	199.4	-35.3	AB	2	0		
128	KO-040	L	pri	14.8	41.3	24.4	33.2	G-N	8	12	A1	N
129	KO-041	L	vrm	195.2	-34.2	202.7	-26.1	AB	2	0		
130	KO-041	L	ovr	88.7	-32.2	91.5	-47.0	B-F	5	9.6		
131	KO-041	P	pri	72.0	-25.1	71.2	-40.0	H-LN	6	15.8	B2	N

132	KO-043	L	vrm	347.1	38.1	358.5	36.6	AB	2	0				
133	KO-043	L	ovr	193.5	-18.1	196.9	-11.1	B-F	5	11.3				
134	KO-043	P	pri	95.8	-16.2	97.9	-30.2	G-N	8	21			B2	N
135	KO-044	L	vrm	245.9	-17.8	246.4	-3.0	AB	2	0				
136	KO-044	L	ovr	83.2	-6.5	83.7	-21.5	B-F	5	8				
137	KO-044	L	pri	42.6	44.4	48.6	31.5	F-J	5	11.1			A2	N
138	KO-045	L	vrm	258.9	-40.0	258.7	-24.9	AB	2	0				
139	KO-046	P	ovr	4.0	-41.5	170.2	44.2	B-G	6	14.4				
140	KO-046	L	vrm	215.8	-42.4	222.6	-30.5	AB	2	0				
141	KO-047	L	vrm	227.0	-12.8	227.8	0.2	AB	2	0				
142	KO-047	L	ovr	340.9	20.2	346.5	21.2	B-G	6	13.1				
143	KO-047	P	int	128.8	-3.5	130.6	-12.7	G-J	4	4.5				
144	KO-047	L	pri	139.2	39.2	130.3	31.2	J-N	5	18.4	x	319.2	A2	N

APPENDIX H

SQR FILE FOR KOCHKOR EAST (KSS) WITH RATINGS

#	Sample						180?
33	KSS-003	L	vrm	251.1 45.5 214.1 52.4 AB	2	0	
34	KSS-003	L	ovr	307.7 53.7 286.7 85.3 B-H	7	4	
35	KSS-003	P	pri	350.1 7.7 358.1 31.4 H-NP	8	13.1	
36	KSS-004	L	ovr	211.8 -13.3 220.4 -16.1 C-H	6	9.4	X
37	KSS-004	P	pri	276.2 64.0 186.5 72.3 I-O	7	17.2	X
38	KSS-005	L	vrm	258.4 70.1 171.1 64.9 AB	2	0	
39	KSS-005	L	ovr	29.4 62.3 81.4 53.2 B-G	6	7.9	
40	KSS-005	P	int	46.1 -4.4 43.0 -6.4 H-K	4	12	
41	KSS-005	P	pri	312.4 28.5 313.6 60.4 L-P	5	14.7	
42	KSS-006	L	ovr	73.1 65.0 102.9 40.7 A-F	6	7.6	
43	KSS-006	P	pri	135.4 44.9 134.2 12.9 G-KP	6	13.6	
44	KSS-007	L	ovr	199.3 -64.1 261.0 -58.0 B-G	6	8.7	X
45	KSS-007	P	pri	20.5 -24.3 11.0 -10.4 I-KMP	5	17.2	X
46	KSS-008	L	vrm	309.6 31.7 308.0 63.9 AB	2	0	
47	KSS-008	P	ovr	12.6 -33.7 0.4 -15.1 B-GP	7	17.1	
48	KSS-008	P	pri	71.5 20.1 76.9 2.2 KLNO	4	13.7	
49	KSS-009	L	pri	40.1 28.9 56.6 24.6 F-LQ	8	12.3	
50	KSS-009	P	ovr	204.7 55.3 174.7 37.8 BD-GS	6	26.4	
51	KSS-009	L	vrm	332.8 1.0 336.0 31.0 AB	2	0	
52	KSS-010	P	ovr	350.5 34.2 16.3 54.7 A-F	6	16.3	X
53	KSS-010	P	pri	251.5 48.0 210.8 54.1 H-L	5	5.2	X
54	KSS-011	L	vrm	354.0 -28.2 348.1 -2.3 AB	2	0	
55	KSS-011	L	ovr	178.4 80.2 142.4 50.8 B-G	6	4.8	
56	KSS-011	L	int	154.6 -8.1 160.7 -36.9 G-K	5	9.4	
57	KSS-011	L	pri	155.6 -17.0 165.4 -45.1 G-KP	6	9.9	
58	KSS-012	L	nrm	98.0 -9.0 90.2 -35.5 AB	2	0	
59	KSS-012	L	ovr	101.8 73.1 120.1 42.7 B-F	5	7.9	
60	KSS-012	L	pri	151.0 28.0 148.6 -2.5 G-P	10	17.5	
61	KSS-014	L	vrm	103.2 13.7 102.9 -15.0 AB	2	0	
62	KSS-014	L	ovr	351.4 67.9 86.3 69.6 B-F	5	4.6	
63	KSS-014	L	pri	76.3 64.3 103.8 39.2 F-IK	5	11.6	
64	KSS-015	L	ovr	304.2 54.4 261.2 84.8 A-H	8	11.4	
65	KSS-015	L	int	211.5 65.4 168.3 47.3 H-LQ	6	15.7	
66	KSS-015	P	pri	333.9 35.0 354.6 62.4 M-Q	5	11.7	
67	KSS-017	P	ovr	97.1 -17.0 85.4 -41.9 B-J	9	14.4	
68	KSS-017	L	vrm	213.5 36.0 194.6 26.3 AB	2	0	
69	KSS-017	L	pri	75.6 83.3 121.6 53.7 J-LOP	5	9.7	

70	KSS-018	P	ovr	43.8	-29.5	26.5	-26.1	A-I	9	15.8		
71	KSS-018	L	pri	137.9	52.1	135.5	20.3	I-MOP	7	12.1		
72	KSS-020	L	ovr	335.5	30.4	353.0	57.6	B-G	6	5.7		
73	KSS-020	L	vrm	296.4	-25.6	297.0	5.4	AB	2	0		
74	KSS-020	L	pri	274.8	50.2	225.6	67.8	H-Q	10	13.6		
75	KSS-021	L	vrm	199.0	9.0	199.0	-2.7	AB	2	0		
76	KSS-021	L	ovr	69.2	78.8	115.0	51.6	BCE-L	10	5.5		
77	KSS-021	L	pri	0.3	58.2	62.8	64.5	L-P	5	5.1		
78	KSS-022	L	ovr	324.5	39.9	342.3	70.0	A-E	5	9.1	X	
79	KSS-022	L	pri	322.8	34.1	334.4	64.8	F-P	11	9.5	X	
80	KSS-024	L	vrm	198.6	-0.9	202.5	-12.5	AB	2	0		
81	KSS-024	L	ovr	299.5	59.7	201.8	83.8	B-G	6	5.9		
82	KSS-024	L	pri	281.6	38.6	253.8	62.9	H-P	9	5.1		
83	KSS-026	P	ovr	63.4	-15.5	52.0	-25.0	A-D	4	1.2		
84	KSS-026	P	pri	334.3	34.1	354.2	61.5	D-GKMNP	8	15.2		
85	KSS-027	P	ovr	94.4	-22.5	258.9	45.8	A-F	6	9.3		
86	KSS-029	L	ovr	23.5	67.6	88.5	57.8	A-G	7	13.9		
87	KSS-029	P	pri	25.1	-23.0	15.6	-11.4	G-P	10	16.3		
88	KSS-030A	L	vrm	27.6	-7.9	25.5	0.2	AB	2	0		
89	KSS-030A	L	ovr	271.8	62.7	190.4	70.2	B-F	5	3.9		
90	KSS-030A	L	pri	322.9	44.6	345.0	74.7	F-OP	11	3.9		
91	KSS-031	L	vrm	63.1	1.1	61.6	-9.9	AB	2	0		
92	KSS-031	P	ovr	50.2	-44.0	20.1	-40.5	B-I	8	13.7		
93	KSS-031	P	pri	32.1	-36.3	13.2	-25.8	H-P	9	22.5		
94	KSS-032	L	vrm	338.1	32.0	357.7	58.2	AB	2	0		
95	KSS-032	L	ovr	92.2	62.9	110.6	34.5	B-H	7	7.9		
96	KSS-032	P	pri	59.0	-0.5	56.2	-9.8	I-O	7	8.3		
97	KSS-034	L	ovr	49.8	60.9	88.7	44.9	A-F	6	3.5		
98	KSS-034	L	pri	338.9	48.4	23.1	71.0	F-P	11	7.7		
99	KSS-035	L	vrm	268.7	-17.0	271.0	7.3	AB	2	0		
100	KSS-035	P	ovr	88.1	14.8	88.7	-9.5	B-EG	5	4.8		
101	KSS-035	P	pri	60.5	4.2	59.9	-6.5	FH-P	10	13.5		
102	KSS-037	L	ovr	241.6	79.6	150.8	60.2	A-H	8	12.6		
103	KSS-038	L	ovr	68.4	74.9	110.3	48.9	A-E	5	4.3		
104	KSS-038	L	pri	347.2	31.5	9.7	53.8	F-Q	12	7.7		

APPENDIX I

DAM SITE (KDS) FIELD DATA AND RATINGS WITH FOLD TEST

#	Sample								plastic	Geo Correct	RATING	N/R
41	KDS-029	L	ovr	22.6	74.9	169.8	41.5	B-F	5	8.2		
42	KDS-029	L	pri	5.9	30.2	107.7	82.7	G-MN	8	2.9	A2	N
43	KDS-030	L	pri	13.9	8.0	37.9	65.0	F-N	9	9.3	A2	N
44	KDS-030	L	ovr	112.1	59.3	149.5	12.7	A-E	5	3.6		
45	KDS-032	L	ovr	300.9	74.8	193.6	35.4	B-G	6	5		
46	KDS-032	L	pri	348.3	33.3	233.1	80.1	G-N	8	4.3	A2	N
47	KDS-032	L	vrm	92.1	23.0	110.4	6.9	AB	2	0		
48	KDS-033	L	ovr	315.5	45.4	228.8	52.3	A-G	7	6.2		
49	KDS-033	L	pri	333.2	11.5	298.4	61.5	G-N	8	2.4	A3	N
50	KDS-035	L	vrm	62.8	-27.8	58.5	9.1	AB	2	0		
51	KDS-035	L	ovr	354.9	39.1	190.8	78.7	B-F	5	6		
52	KDS-035	L	pri	15.9	9.6	43.8	65.0	F-N	9	4.2	A2	N
53	KDS-036	L	vrm	321.1	64.1	199.0	46.9	AB	2	0		
54	KDS-036	L	ovr	43.7	4.0	67.6	40.4	B-G	6	10		
55	KDS-036	L	pri	19.6	-7.4	31.6	48.9	G-N	8	5	A3	N
56	KDS-038	L	ovr	34.2	25.8	92.5	57.7	A-G	7	7.9		
57	KDS-038	L	pri	8.1	-26.7	8.9	34.5	G-N	8	6.6	A3	N
58	KDS-039	L	vrm	79.8	-0.4	82.9	6.4	AB	2	0		
59	KDS-039	L	ovr	48.9	13.7	82.0	40.7	B-G	6	7		
60	KDS-039	L	pri	12.0	-6.0	21.8	53.4	G-N	8	5.8	A3	N
61	KDS-041	L	vrm	162.7	53.0	170.5	-8.1	AB	2	0		
62	KDS-041	L	ovr	299.5	75.6	192.9	34.7	B-G	6	5.3		
63	KDS-041	L	int	3.8	45.8	164.9	71.7	G-J	4	5.3		
64	KDS-041	L	pri	5.8	1.3	15.0	62.3	J-N	5	4.9	A2	N

65	KDS-042	L	vrm	152.5 35.6 155.3 -22.1 AB	2	0							
66	KDS-042	L	ovr	349.0 79.4 180.1 38.4 B-G	6	2.9							
67	KDS-042	L	int	337.1 22.2 280.7 70.3 G-J	4	9.3							
68	KDS-042	L	pri	359.6 -21.2 360.0 40.8 J-N	5	8.7						A3	N
69	KDS-043	L	ovr	221.3 -13.3 257.0 -47.2 A-E	5	4.8	X		41.3				
70	KDS-043	L	int	211.9 -13.1 249.7 -55.1 E-I	5	11	X		31.9				
71	KDS-043	L	pri	180.5 -7.3 185.1 -69.3 JKMN	4	13.2	X		0.5	A3	N		
72	KDS-044	L	ovr	30.2 62.6 155.7 49.4 A-E	5	11.4							
73	KDS-044	L	pri	350.0 52.3 189.6 65.0 FH-M	7	9.1						A1	N
74	KDS-045	P	ovr	319.9 -37.8 328.3 14.7 A-E	5	12.7							
75	KDS-045	L	pri	18.7 14.7 57.7 66.7 G-N	8	11.4						A2	N
76	KDS-047	L	ovr	32.0 48.1 134.6 56.9 B-G	6	10.7							
77	KDS-047	L	pri	354.9 -12.5 353.2 49.3 G-N	8	4.3						A3	N
78	KDS-048	L	vrm	80.7 -37.7 50.2 -11.6 AB	2	0							
79	KDS-048	L	ovr	15.8 66.5 167.0 49.9 B-G	6	4.3							
80	KDS-048	L	pri	1.4 -9.5 3.5 52.3 G-N	8	6.7						A3	N
81	KDS-049	L	vrm	129.2 -13.0 95.9 -42.2 AB	2	0	X		309.2				
82	KDS-049	L	ovr	206.7 -2.2 229.0 -52.4 B-E	4	7.5	X		206.7				
83	KDS-049	L	int	239.2 -4.8 258.2 -27.6 E-I	5	13.9	X		239.2				
84	KDS-049	L	pri	154.6 30.1 155.3 -27.8 I-N	6	15.1	X		334.6	A2	N		
85	KDS-050	L	vrm	188.5 53.0 184.4 -8.5 AB	2	0							
86	KDS-050	L	ovr	1.2 52.0 173.2 66.0 B-G	6	2.2							
87	KDS-050	L	pri	338.4 19.8 288.4 70.4 G-LN	7	6.1						A2	N
88	KDS-051	L	ovr	29.2 70.4 164.1 44.1 A-G	7	4.4							
89	KDS-051	L	pri	2.7 28.5 96.4 85.8 G-N	8	6.5						A2	N
90	KDS-053	L	ovr	3.6 51.3 169.4 66.3 A-E	5	3.9							
91	KDS-053	L	int	355.6 14.7 348.2 76.5 E-I	5	22.5							
92	KDS-053	L	pri	352.5 -19.9 351.0 41.8 IK-N	5	8.6						A3	N

93	KDS-054	L	ovr	26.9 61.0 155.7 51.7 A-H	8	4							
94	KDS-054	L	pri	44.2 27.7 98.8 49.4 F-N	9	11.5					A2	N	
95	KDS-055	L	pri	168.2 -30.7 68.1 -81.1 H-O	8	10.3	X		348.2		A3	N	
96	KDS-055	L	vrm	114.6 -28.4 70.6 -34.2 BC	2	0	X		294.6				
97	KDS-055	L	ovr	257.6 -37.9 299.5 -24.5 C-H	6	5.2	X		77.6				
98	KDS-056	L	ovr	19.3 54.5 153.9 59.4 B-G	6	8.5							
99	KDS-056	L	pri	7.4 9.7 25.6 69.6 G-O	9	3.2					A2	N	
100	KDS-057	L	vrm	97.2 -18.5 76.5 -16.8 AB	2	0							
101	KDS-057	L	ovr	56.1 60.9 145.6 39.7 B-G	6	7.3							
102	KDS-057	L	pri	28.8 14.1 68.5 58.2 G-N	8	3.9					A3	N	
103	KDS-059	L	vrm	130.2 75.7 167.4 17.9 AB	2	0							
104	KDS-059	L	ovr	26.0 65.8 161.1 48.4 B-G	6	7.8							
105	KDS-059	P	pri	326.4 -32.2 329.2 22.7 GI-N	7	16.6					B1	N	
	KDS-059	L	ps	348.9 55.8 188.8 61.5	2	0							
	KDS-059	L	pf	303.8 35.1 244.9 43.9	2	0							
10	KDS-058	L	vrm	96.4 19.8 110.1 1.6 AB	2	0							
11	KDS-058	L	ovr	2.8 64.0 174.4 53.9 B-H	7	16.1							
12	KDS-058	L	pri	195.2 37.6 192.6 -22.4 H-JLN-P	7	31.5					A3	N	
21	KDS-068A	P	ovr	329.0 -1.7 310.2 49.2 A-F	6	4.2	X						
22	KDS-068A	P	int	55.9 15.5 88.0 35.3 F-J	5	7.6	X						
23	KDS-068A	L	pri	309.3 56.7 214.0 45.5 I-N	6	10.4	X		129.3		A2	N	
13	KDS-060	L	ovr	23.4 66.1 162.6 48.9 A-E	5	6.9							
14	KDS-060	L	int	68.0 -21.9 59.2 6.0 E-G	3	5.5							
15	KDS-060	L	pri	350.3 24.5 292.7 82.3 G-O	9	10.1					A2	N	
106	KDS-061	L	ovr	67.9 69.1 154.3 33.1 A-E	5	3							
107	KDS-061	L	pri	15.6 20.4 66.4 72.3 E-N	10	6.6					A2	N	
108	KDS-062	L	ovr	329.0 68.1 193.1 46.4 A-G	7	6.2	X						
109	KDS-062	L	pri	327.7 20.1 277.2 61.4 G-M	7	8.8	X		147.7		A3	R	

16	KDS-063	L	over	42.7	82.6	171.9	33.2	A-E	5	7.1		
17	KDS-063	L	int	357.4	69.0	178.2	49.1	E-H	4	11.3		
18	KDS-063	L	pri	19.9	45.0	138.2	65.6	G-Q	11	10.8	A1	N
110	KDS-064	L	over	87.4	60.4	145.1	24.2	A-E	5	6.9		
11	KDS-064	L	pri	47.2	31.7	105.4	47.5	F-N	9	10.2	A2	N
12	KDS-065	L	over	12.7	48.7	153.7	66.4	A-F	6	8.2		
13	KDS-065	L	int	33.7	8.5	65.1	51.0	G-J	4	9		
14	KDS-065	L	pri	27.9	-29.6	26.7	25.8	I-N	6	17.4	A3	N
19	KDS-066	P	over	28.6	41.7	124.7	61.9	A-F	6	6		
20	KDS-066	L	pri	220.4	30.4	216.0	-19.0	FGI-Q	11	8.4	A3	N

more fold test samples below

1	KDS-006	L	vrm	256.3	66.3	201.8	20.6	AB	2	0		
2	KDS-006	L	over	46.9	49.4	131.8	47.3	B-H	7	5.9		
3	KDS-006	L	pri	17.7	-21.4	21.2	37.0	IJL-P	7	11.6		
4	KDS-008	L	vrm	36.0	-19.0	40.3	30.3	AB	2	0		
5	KDS-008	L	over	285.1	65.5	206.0	32.3	B-G	6	10.7		
6	KDS-008	L	pri	343.6	39.6	220.3	73.4	F-O	10	14.3		
7	KDS-012	L	vrm	261.1	29.7	238.5	8.1	AB	2	0		
8	KDS-012	L	over	19.8	68.1	166.1	47.8	B-H	7	4.4		
9	KDS-012	L	pri	18.8	5.2	42.7	59.8	I-O	7	13		

APPENDIX J

KARA SUU (KSU) FIELD DATA AND RATINGS

#	Sample						180?	Corrected geographic	RATING	N/R	
105	KU-116	L	ovr	213.4 -1.4 214.1 -20.1 A-H	8	6.4	X	33.4			1
106	KU-116	L	pri	61.7 -39.4 54.9 -23.8 I-P	8	10.2	X	241.7	A2	R	
107	KU-115	L	vrm	123.2 -20.8 115.7 -22.9 BC	2	0	X	303.2			
108	KU-115	L	ovr	228.7 -13.6 232.3 -30.5 C-I	7	10.1	X	48.7			
109	KU-115	L	pri	19.8 -5.7 19.7 13.3 IKMNP	5	12.9	X	199.8	A2	R	
110	KU-114	L	vrm	139.6 -13.5 134.0 -21.4 AB	2	0	X	319.6			2
111	KU-114	L	pri	27.6 -6.3 27.7 12.6 L-P	5	4.3	X	207.6	A2	R	
112	KU-113	L	pri	28.8 -1.1 29.2 17.8 K-P	6	8.6	X	208.8	A3	R	
113	KU-113	P	ovr	311.6 50.5 287.1 53.0 A-EHP	7	17.1	X	131.6			
114	KU-112	L	ovr	327.9 53.3 300.5 60.6 B-F	5	10.8	X	147.9			3
115	KU-112	L	pri	262.5 65.0 239.2 51.8 F-HJ-P	10	11.4	X	82.5	A2	N	
116	KU-111	L	vrm	266.7 -14.2 272.0 -21.9 AB	2	0	X	86.7			
117	KU-111	P	ovr	12.9 -11.5 13.1 7.4 B-H	7	5.8	X	192.9			
118	KU-111	L	pri	137.6 -75.2 70.5 -71.5 I-P	8	7.1	X	317.6	A1	R	
119	KU-110	P	ovr	22.5 -21.4 22.3 -2.5 A-G	7	12.9					4
120	KU-110	P	pri	66.6 -18.0 64.1 -3.9 HJ-P	8	14			B3	R	
	KU-110	L	pf	344.6 15.1 339.4 29.5	2	0					
	KU-110	L	pl	103.7 -41.7 88.8 -36.1	2	0					
121	KU-109	L	vrm	195.9 56.8 199.1 37.9 AB	2	0					
122	KU-109	L	ovr	349.3 62.3 309.7 74.3 B-L	11	7.6					
123	KU-109	P	pri	242.7 42.9 54.6 -27.6 L-P	5	5.9			B2	N	
	KU-109	L	pri	355.4 22.6 349.6 39	5	11.7			A2	N	
	KU-109	L									
124	KU-108	L	vrm	238.7 -49.5 259.3 -63.4 AB	2	0	X	58.7			

125	KU-108	L	over	149.2 14.0 151.4 2.3 B-G	6	4.3	X	329.2							
126	KU-108	L	pri	185.7 -21.4 182.0 -39.4 I-P	8	6.8	X	5.7	A3	N					
127	KU-107	L	vrm	293.3 56.6 266.9 52.7 AB	2	0					5				
128	KU-107	L	over	26.8 29.1 28.0 48.0 B-J	9	8									
129	KU-107	L	pri	15.4 23.1 13.6 41.9 J-P	7	7.4			A2	N					
130	KU-106	L	vrm	186.3 -21.0 183.5 -37.9 AB	2	0									
131	KU-106	P	over	117.9 25.6 126.1 22.6 B-K	10	11.2									
132	KU-106	L	pri	339.0 43.3 321.3 55.0 K-P	6	9.3			A2	N					
133	KU-104	P	over	312.1 -41.7 325.9 -33.2 A-H	8	12.2					6				
134	KU-104	L	pri	327.3 30.3 315.5 39.4 I-P	8	10.5			A2	N					
135	KU-103	L	over	358.0 74.1 258.8 81.9 A-H	8	6.6									
136	KU-101A	L	vrm	190.8 66.0 196.2 47.5 AB	2	0					7				
137	KU-101A	L	over	6.0 53.8 350.3 71.3 B-H	7	6.2									
138	KU-101A	L	pri	338.4 43.2 320.7 54.7 I-P	8	6.5			A2	N					
139	KU-101	L	vrm	266.8 19.2 267.1 7.5 AB	2	0									
140	KU-101	L	over	339.2 60.2 302.2 69.7 B-J	9	8.6									
141	KU-101	L	pri	340.7 43.2 323.3 55.3 J-P	7	7.6			A1	N					
41	KU-009	L	vrm	200.7 42.9 199.8 24.2 AB	2	0					8				
42	KU-009	L	over	341.1 57.3 309.4 67.7 B-G	6	11.4									
43	KU-009	L	pri	333.4 60.6 295.6 68.0 H-Q	10	4.4			A1	N					
44	KU-010	L	vrm	237.8 35.3 232.1 19.5 AB	2	0									
45	KU-010	P	over	118.8 39.3 133.0 35.1 B-L	11	6.8									
46	KU-010	L	pri	348.0 32.9 337.6 47.5 J-Q	8	5.5			A2	N					
47	KU-12	L	over	324.5 69.2 269.7 70.8 A-F	6	6.8					9				
48	KU-12	L	pri	350.1 51.2 328.6 65.2 C-Q	15	11.7			A1	N					
49	KU-013	L	over	356.7 83.7 215.1 76.3 A-F	6	6.9									
50	KU-013	L	pri	8.5 55.0 354.1 72.8 F-KM-P	10	11.2			A1	N					

51	KU-15	P	ovr	311.9 -25.0 319.0 -17.6 A-F	6	10.5									10
52	KU-15	L	pri	347.7 17.5 342.2 32.5 F-Q	12	6.5						A2		N	
53	KU-16	L	ovr	21.7 53.4 20.5 72.3 A-G	7	13.7									
54	KU-16	P	pri	258.6 75.3 227.6 60.1 G-KM-OQ	9	21						B3		N	
55	KU-20	P	ovr	324.7 -13.9 326.9 -3.5 A-G	7	13.1									11
56	KU-20	L	pri	249.1 -33.5 261.5 -45.3 G-Q	11	3						A2		R	
57	KU-22	L	ovr	138.5 38.3 149.3 28.4 A-G	7	13.7									
58	KU-22	L	pri	265.3 -10.0 269.6 -18.2 G-Q	11	6.8						A3		R	
59	KU-24	L	ovr	212.2 -28.6 215.1 -47.7 B-F	5	10.8									12
60	KU-24	L	pri	192.7 -56.8 180.6 -75.1 G-Q	11	5.1						A1		R	
61	KU-25	L	ovr	353.4 36.6 342.9 52.3 A-E	5	7									
62	KU-25	L	pri	321.4 17.1 314.7 25.1 M-Q	5	6						A3		N	
63	KU-27	L	ovr	349.2 52.1 326.8 65.8 A-E	5	7.2									13
64	KU-27	L	pri	352.3 46.7 335.5 61.6 L-Q	6	11.1						A1		N	
65	KU-28	L	ovr	354.3 64.1 311.2 77.2 AF-M	9	9.4									
66	KU-28	L	pri	7.2 56.4 350.1 74.0 M-OSTV-	8	5.8						A1		N	
67	KU-30	P	ovr	69.2 -1.5 70.2 11.9 A-F	6	14.7									14
68	KU-30	L	pri	123.3 -50.4 100.1 -50.0 F-Q	12	11.4						A2		R	
69	KU-31	L	ovr	56.3 75.1 151.6 79.7 A-G	7	6									
70	KU-31	L	pri	149.4 -36.4 134.7 -45.8 G-LN	7	7.3						A2		R	
71	KU-50	L	ovr	102.1 4.9 104.1 8.1 A-H	8	19.7	X	282.1							15
72	KU-50	L	int	27.9 45.6 30.8 64.5 H-L	5	12.3	X	207.9							
73	KU-50	L	pri	265.0 36.4 255.2 26.0 M-Q	5	4.4	X	85				A3		N	
74	KU-52	P	ovr	131.1 49.8 328.5 -40.8 A-EH	6	11.6									
75	KU-52	L	int	176.1 -38.7 165.2 -54.8 H-L	5	3.9									
76	KU-52	L	pri	185.4 -34.6 179.0 -52.5 M-Q	5	7.4						A1		R	
77	KU-54	L	vrm	146.9 26.6 152.7 15.2 AB	2	0	X	326.9							16

78	KU-54	L	ovr	52.7 73.2 140.7 80.7 B-EGH	6	14.2	X	232.7						
79	KU-54	P	pri	92.5 -8.8 90.8 -1.9 H-MO-Q	9	13.4	X	272.5	B3		R			
80	KU-55	P	ovr	312.8 -15.7 316.7 -9.1 C-H	6	13.6								
81	KU-55	L	pri	191.9 -11.7 190.3 -30.4 H-Q	10	9.1			A2		R			
82	KU-57	L	ovr	276.9 73.3 238.9 61.4 B-H	7	10.3	X	96.9						17
83	KU-57	L	pri	344.4 72.5 267.7 78.0 H-Q	10	5.1	X	164.4	A2		N			
84	KU-58	L	ovr	177.3 39.6 181.9 22.2 A-EG	6	6.5								
85	KU-58	L	pri	183.1 -25.8 178.0 -43.4 F-Q	12	6.2			A2		R			
86	KU-60	L	pri	96.5 35.4 110.8 38.6 N-R	5	4.6	X	276.5	A3		N			18
87	KU-60	L	ovr	5.1 38.6 357.3 56.3 A-K	11	12.6	X	185.1						
88	KU-61	L	ovr	42.9 64.0 80.5 79.9 A-G	7	12								
89	KU-61	L	pri	178.5 -54.4 157.5 -70.3 H-JM-Q	8	9.9			A1		R			
90	KU-62	P	ovr	66.9 -21.4 63.8 -7.3 A-F	6	9.6	X	246.9						19
91	KU-62	L	pri	2.9 57.1 341.1 73.7 F-Q	12	4.2	X	182.9	A3		N			
92	KU-64	P	ovr	219.2 39.6 36.3 -21.4 B-H	7	17.8								
93	KU-64	L	pri	155.5 -36.9 141.2 -48.0 H-Q	10	7.3			A2		R			
94	KU-66	P	ovr	174.0 41.6 359.4 -24.7 A-F	6	14.5	X	354			?			20
95	KU-69	L	ovr	139.8 17.2 143.5 8.0 A-F	6	8.6	X	319.8						21
96	KU-69	L	pri	336.2 81.2 229.7 75.5 G-N	8	18.9	X	156.2	A2		N			
97	KU-70	P	ovr	66.9 -6.2 67.0 7.5 A-F	6	17.8								
98	KU-71	L	ovr	326.4 26.8 316.0 36.0 C-J	8	13.7	X	146.4						21
99	KU-71	L	pri	325.2 28.3 314.3 37.0 J-Q	8	6.7	X	145.2	A3		N			
100	KU-73	P	ovr	314.4 -35.2 325.9 -26.3 C-G	5	21.4								
101	KU-73	L	pri	162.0 -67.5 106.7 -75.4 H-NP-R	10	3.7			A1		R			
102	KU-74	L	ovr	290.0 15.0 285.3 13.3 B-EGH	6	18	X	110						23
103	KU-74	L	pri	317.3 38.1 301.4 43.5 JKM-OQ	6	19.7	X	137.3	A3		N			
104	KU-76	P	ovr	338.3 -32.7 344.5 -18.4 A-F	6	14								

105	KU-76	P	pri	63.3 -11.3 62.5 3.3 G-IL-NQ	7	17.8			A3	R		
106	KU-77	L	vrm	174.7 63.0 185.5 44.4 AB	2	0	X	354.7				24
107	KU-77	L	ovr	180.1 -49.9 164.0 -66.3 B-F	5	6	X	0.1				
108	KU-77	L	pri	191.8 -65.0 162.6 -82.8 G-Q	11	3.8	X	11.8	A2	R		
109	KU-79	L	ovr	348.9 51.8 326.4 65.3 B-DFH	5	16.3						
110	KU-79	L	pri	346.2 41.1 331.3 54.9 H-OQ	9	11.1			A2	N		
111	KU-150	L	ovr	180.0 -58.3 154.2 -74.2 B-G	6	7.4	X	0				25
112	KU-150	L	pri	128.8 -69.9 79.7 -66.7 I-NQ	7	13.6	X	308.8	A2	R		
113	KU-152	L	ovr	19.5 28.1 18.5 47.1 B-F	5	6.5						
114	KU-152	L	pri	3.6 -15.4 4.3 2.6 G-Q	11	8.3			A2	N		
115	KU-153	P	ovr	253.2 56.7 237.9 42.6 A-F	6	13	X	73.2				
116	KU-155	L	ovr	1.3 40.5 351.4 57.7 A-F	6	7.5						
117	KU-155	L	pri	343.2 30.6 332.8 44.2 F-NPQ	11	8.8			A2	N		
118	KU-156	L	vrm	154.9 20.6 158.9 6.8 AB	2	0	X	334.9				
119	KU-156	L	ovr	186.3 -41.0 178.3 -58.9 B-G	6	5.4	X	6.3				
120	KU-156	L	pri	179.3 -50.6 162.5 -67.0 G-Q	11	5.1	X	359.3	A3	R		
121	KU-158	L	ovr	6.1 50.0 353.7 67.6 A-E	5	9.1						
122	KU-158	L	pri	355.4 37.4 344.9 53.5 M-Q	5	8.5			A2	N		
123	KU-160	L	ovr	173.8 -19.4 168.8 -35.6 A-E	5	5.3	X	353.8				
124	KU-160	L	pri	171.7 -52.4 149.7 -66.8 M-Q	5	6	X	351.7	A3	R		
125	KU-162	P	ovr	236.5 44.1 49.6 -27.7 A-F	6	13.6	X	56.5				
126	KU-162	P	pri	262.2 74.9 229.8 60.5 L-Q	6	17.8	X	82.2	A2	N		
127	KU-164	L	vrm	274.6 34.5 263.9 26.4 AB	2	0						
128	KU-164	L	ovr	8.1 33.6 2.7 51.8 B-G	6	8.2						
129	KU-164	L	pri	335.8 33.3 323.3 44.7 G-Q	11	10.2			A2	N		
130	KU-165	L	vrm	71.8 44.8 92.3 55.3 AB	2	0	X	251.8				
131	KU-165	L	ovr	118.5 7.1 120.5 4.8 B-F	5	9.7	X	298.5				

13	KU-			137.8	-7.5	134.2	-15.0	1							
2	165	L	pri	G-Q				1	6.9	X		317.8	A3	N	

APPENDIX K

SOURCES FOR MATERIAL INCLUDED IN COMPARISONS AND PHYLOGENETIC ANALYSIS

Institutional Abbreviations—NMNH, Smithsonian Natural History Museum, Washington D.C., U.S.A.; UONMCH, University of Oregon Museum of Natural and Cultural History, Eugene, Oregon, U.S.A., MGUH, Uppsala Museum, Uppsala Sweden.

Sources for the taxa used in morphological comparisons and the phylogenetic analysis. Underlined taxa included in the phylogenetic analysis. If bold, data taken directly from reference and not the fossil material

Taxon	Collection/Institution	Reference
Persiatherium huadeensis		**Pandolfi, 2015, Lu, 2013**
Aceratherium depereti		**Pandolfi, 2015**
Aceratherium incisivum		**Pandolfi, 2015**
Aceratherium porpani		**Pandolfi, 2015**
Acerorhinus fugensis		**Pandolfi, 2005**
Acerorhinus hezhengensis		**Pandolfi, 2015, Lu, 2013**
Acerorhinus lufengensis		**Pandolfi, 2015**
Acerorhinus palaeosinensis		**Pandolfi, 2015, Ringström, 1924, Lu, 2013**
Acerorhinus tsaidamensis		**Pandolfi, 2015, Lu, 2013**
Acerorhinus yuanmouensis		**Pandolfi, 2015, Lu, 2013**
Acerorhinus zernowi		**Pandolfi, 2015, Antoine et al., 2003**
Alicornops complanatum		**Pandolfi, 2015, Antoine et al., 2003**
Alicornops laogouense		**Pandolfi, 2015**
Alicornops simorrense		**Pandolfi, 2015**
Aphelops malacorhinus	NMNH	Prothero, 2009
Aphelops megalodus	NMNH	Prothero, 2009
Aphelops mutilus	NMNH	Prothero, 2009
Brachypotherium brachypus		**Pandolfi, 2015, Guérin, 1980**
Brachypotherium goldfussi		**Pandolfi, 2015, Guérin, 1980**
Bugtirhinus praecursor		**Pandolfi, 2015, Antoine et al., 2010**
Ceratotherium simum	MNCH	Pandolfi, 2015, Guérin, 1966
Ceratotherium neumayri		**Pandolfi, 2015**

Chilotherium anderssoni	MGUH	Pandolfi, 2015, Ringström, 1924, Deng, 2006
Chilotherium habereri	MGUH	Pandolfi, 2015, Schlosser, 1903, Ringström, 1924
Chilotherium kiliasi		**Pandolfi, 2015**
Chilotherium kowalevskii		**Pandolfi, 2015**
Chilotherium licenti		
Chilotherium persiae		**Pandolfi, 2015**
Chilotherium primigenium		**Deng, 2006**
Chilotherium samium		**Pandolfi, 2015**
Chilotherium schlosseri	MGUH	Pandolfi, 2015
Chilotherium wimani	MGUH	Pandolfi, 2015, Deng, 2006, Ringström, 1924
Diceratherium aginense		**Pandolfi, 2015, Antoine et al., 2010**
Diceratherium armatum		**Pandolfi, 2015, Antoine et al., 2010, Prothero, 2009**
Dicerorhinus sumatrensis		**Pandolfi, 2015, Guérin, 1980, Antoine et al., 2010**
Diceros bicornis		**Pandolfi, 2015, Guérin, 1980, Antoine et al., 2010**
Dihoplus pikermiensis		**Pandolfi, 2015**
Dihoplus schleirmacheri		**Pandolfi, 2015, Guérin, 1980**
Gaindatherium browni		**Pandolfi, 2015, Antoine et al., 2010**
Hispanotherium beonense		**Pandolfi, 2015, Antione, 2002, Antoine et al., 2010**
Hispanotherium matritense		**Pandolfi, 2015**
Hoploaceratherium tetradactylum		**Pandolfi, 2015, Guérin, 1980**
Iranotherium morgani		**Pandolfi, 2015, Antoine, 2002**
Lartetotherium sansaniense		**Pandolfi, 2015, Guérin, 1980, Antoine, 2002**
Menoceras arikarense	NMNH	Pandolfi, 2015, Prothero, 2009, Antoine et al., 2010
Plesiaceratherium gracile		**Pandolfi, 2015, Lu, 2013**
Plesiaceratherium mirallesi		**Pandolfi, 2015, Antoine et al., 2010**
Protoceratherium minutum		**Pandolfi, 2015, Antoine et al., 2010**

Rhinoceros sondaicus		**Pandolfi, 2015, Guérin, 1980, Antoine et al., 2010**
Rhinoceros unicornis		**Pandolfi, 2015, Guérin, 1980, Antoine et al., 2010**
Ronzotherium filholi		**Pandolfi, 2015, Antoine et al., 2010**
Shansirhinus ringstroemi		**Pandolfi, 2015, Deng, 2005, 2006**
Subchilotherium intermedium		**Pandolfi, 2015**
Subhyracodon occidentalis	NMNH	Pandolfi, 2015, Prothero, 2009, Antoine et al., 2010
Trigonias osborni	NMNH	Pandolfi, 2015, Prothero, 2009, Antoine et al., 2010
Teleoceras fossiger	NMNH	Prothero, 2009
Teleoceras major	NMNH, MNCH	Prothero, 2009

APPENDIX L

PHYLOGENETIC CHARACTERS AND DESCRIPTIONS

List and description of the 214 characters included in the phylogenetic analysis as used in by Pandolfi (2015), with characters modified in most cases from Lu (2012) and Antoine (2002)

Skull

1. Nasal: lateral apophysis = 0, absent; 1, present

    -Posterior end of the nasal is significantly wider that anterior end, on the order of twice as broad. Nasal constricts suddenly, leaving the nasals with two lateral bulges.

2. Nasal: dorsal profile: 0, straight; 1, undulated; 2, dorsally arched; 3, upturn

    -Profile of the nasal bone is primarily referring to the anterior portion of the nasal bone where it is not in contact with other facial bones. Starting just behind the nasal opening, the dorsal most profile of the nasal bone is (0) roughly straight, (1) dished before turning ventrally in the anterior most portion, (2) a smooth curve, with the highest point mid nasal bone, or (3) dished with the anterior most portion pointing dorsally.

3. Nasal: anterior end: 0, at the level of DP1 or after DP1: 1, before the DP1 without over the premaxillae; 2, before premaxillae

    -Anterior most tip of nasal bone, when viewed laterally, is (0) even or posterior to the first deciduous premolar, (1) anterior to the first deciduous premolar but posterior to the anterior most projection of the premaxillae, or (2) projects anterior to the anterior most projection of the premaxillae.

4. Maxillary: foramen infraorbitalis = 0 above premolars; 1, above molars

    - When viewed laterally, the entirety to majority of the infraorbital foramen is situated above the premolars (0), or the entirety or majority of the infraorbital foramen is dorsal to the molar teeth (1), if the occlusal surface of the upper dentition is aligned flat as a plane.

5. Infraorbital foramen: 0, behind the nasal notch; 1, below the nasal notch

-When viewed laterally, the posterior most opening of the external naras opening, ventral to the projecting portion of the nasal bones. The infraorbital foramen is situated ventral to the afore described feature (1), or with the anterior most edge of the infraorbital foramen situated posterior to the posterior most edge of the nasal notch opening.

6. Infraorbital foramen: 0, one; 1, two–three

-Generally clumped closely together is there are more than one (1), otherwise, the single standard infraorbital foramen.

7. Nasal notch = 0, above P1–3; 1, above P4–M1

The posterior most portion of the nasal notch, when the skull is leveled so that the upper tooth row forms a plane, is dorsal to the P1-3 (0) or is dorsal to the P4-M1 (1)

8. Nasal notch: 0, U–shaped; 1, V–shaped

The posterior portion of the nasal notch, as is "pointing" posteriorly, forms a broad U-shape (0), or narrows to more of a point in a V-shape (1)

9. Nasal notch: distance to the orbit/length of the skull: 0, long (>17%); 1, short (≤17%)

-From the most posterior point of the nasal notch opening measured directly posterior (with the upper tooth row flat for a plane) measured to the most anterior portion of the opening of the orbit. This first measurement is then compared to the length of the skull, with the skull again leveled so that the upper tooth row is flat. The anterior most portion may be the nasals or the premaxilla.

10. Nasal septum = 0, never ossified; 1, ossified (even sometimes)

-This feature is most typified in woolly rhinos, in the broad ossification of the nasal septum extending from the posterior of the nasal notch, far anterior, leaving opening on either side with a boney median.

11. Nasal septum: ossified = 0, partially; 1, totally

-ossification extends to some median point between the most posterior opening of the

nasal notch to the anterior tip of the nasal bone (0), or extends fully to the anterior tip of the nasal bone (1). If character 10 was a 0 than this character is a -.

12. Nasal/lacrymal: contact = 0, long; 1, punctual or absent

-The contact between the lacrimal bone and the posterior portion of the nasal bone connects unevenly or over a very short distance of roughly ~1cm (1), or the contact between the two bones is longer and continuous, and is greater than 1cm of contact.

13. Orbit: anterior border = 0, above P4–M2; 1, above M3; 2, behind M3

-With the skull aligned with the upper dentition as a plane, the anterior most border of the orbit is directly dorsal to the P4-M2 (0), M3 (1), or posterior to the M3 (2).

14. Lacrymal: processus lacrymalis = 0, present; 1, absent

-The lacrimal process in rhinos is anterior in the orbit, just above the median anterior-posterior division of the orbit to slightly more dorsal. The process usually projects posterior-laterally. If the process is present (0), if process is absent (1).

15. Frontal: processus postorbitalis = 0, present; 1, absent

-The post orbital process projects ventrally from the frontal bone forming the rear of the orbit. No rhinocerotid taxa form a complete post orbital bar, however some taxa pocess a significant process. Any degree of process is coded as the process being present (0) in this case, while a total absence is (1).

16. Maxillary: anterior base of the processus zygomaticus maxillari = 0, high; 1, low

-Where the zygomatic arch joins into the maxillary bone, does the suture extend the connection of the maxillary bone all the way to the orbit (0) or terminate before reaching the orbit (1).

17. Zygomatic arch = 0, low; 1, high; 2, very high

-The median portion of the Zygomatic arch dips ventrally towards the tooth row (0), is relatively flat lying, without any portion extending ventrally (1), or extends dorsally in the medial most portion (2).

18. Zygomatic arches: dorsoventral depth: 0, shallow (<75mm); 1, deep (≥75mm)

-in the median to anterior portion of the zygomatic arch, when viewed laterally, the dorsoventral depth is shallow(1) or deep(1).

19. Zygomatic arches: depression at the external surface of the anterior part: 0, absent; 1, present

-A concave portion of the anterior most edge of the zygomatic arch is present (0) as compared to the entire anterior portion of the arch structure is convex (1).

20. Zygomatic ach: constriction of the ventral edge anterior to the temporal condyle: 0, present; 1, absent

-The anterior most portion of the zygomatic arch, where it curves medially, constricts on the ventral edge where the edge moves dorsally (0). If no constriction is present (1).

21. Zygomatic arches: process on the posterior end of the dorsal edge: 0, present; 1, absent

-When present (0) this is generally a small cone-shaped protrusion on the posterior most dorsal surface of the zygomatic arch. If not present (1) the dorsal margin of the zygomatic arch maintains a smooth profile. See supplemental figure Character 21.

22. Zygomatic arch: processus postorbitalis = 0, present; 1, absent

-Again, while no included taxa form a post orbital bar, the post orbital process is the ventral portion, where part of the zygomatic bone extends dorsally. This is most commonly in the form of a small cone shaped structure in the medial most portion of the zygomatic arch (0). If not present (1) the medial portion of the zygomatic arch maintains a smooth dorsal profile. See also supplementary figure Character 23 for an example from Chilotherium licenti.

23. Zygomatic arch: processus postorbitalis = 0, on jugal; 1, on squamosal

-If a post orbital process is present (0 on character 22), it is more anterior and forms on the jugal (zygomatic) bone (0) or is more posterior and forms on the squamosal bone (1). See supplemental figure Character 23.

24. Jugal/squamosal: suture = 0, smooth; 1, rough

-In the portion of the zygomatic arch where the jugal and squamosal bone suture, does the suture form a smooth extended “S” shape (0), or does it have a rougher, more goniatic, suture (1).

25. Skull: dorsal profile = 0, flat; 1, concave; 2, very concave

-If the skull is viewed laterally, the profile from the posterior most portion of the occipital bone to the anterior most portion of the nasal bone forms roughly a straight line (0), is concave with the nasals and occipital slightly more dorsal than the median portion of the skull (1), or the nasals and occipital are so raised compared to the median portion of the profile that the skull is dish shaped (2). See supplemental figure for an example of Character 24 in state 2.

26. Sphenoid: foramen sphenorbitale and f. rotundum = 0, distinct; 1, fused

-When viewed looking at the ventral surface of the skull, the sphenoid bone has 1-2 foramen. If these foramen merge across the median axis on the palate, then the character state is (1), whereas if two distinct foramen persist then (0). As this bone is extremely thin, this feature is not preserved in most specimens to an extent that allows the character to be coded.

27. Squamosal: area between temporal and nuchal crests = 0, flat; 1, depression

-When viewing the skull laterally, the nuchal crest connects to the temporal crest at the posteriodorsal most point. If this area outlines by the afore mentioned features form a depression than (1), whereas if the crest rise above an area that is flat in the central portion and then steeply rises into the crests (0).

28. External auditory pseudo–meatus = 0, open; 1, partially closed; 2, closed

-The external auditory meatus is formed from two bones closing to form a tube shape. In many rhinos this is still two separate bones, with each bone forming a lunate shape when viewed laterally, connected on the dorsal side (0). If the ventral opening, when viewed laterally, is showing contact between the two bones, it is considered partially closed (1). Both sides must be fused forming a tube (2) to be considered closed. See Supplementary figure Character 28 for an example of character state 2 from Chilotherium habereri.

29. Occipital side = 0, inclined forward; 1, vertical; 2, inclined backward

-When viewed laterally, with the molar portion of the tooth row leveled, the

posterior most visible portion of the occipital bone is inclined forward (0), vertical (1), or backwards (2). For an example of character state 2 see Chilotherium primigens in the Supplemental Figures Character 29.

*This character was removed for later analyses. This character seems to variable within species, when larger sample sizes are examined (such as Subhyracodon and Teleoceras) and can also be hard to separate from diagenic alteration.

30. Occipital: ventral end of the paraoccipital process relative to the postglenoid process: 0,

under; 1, above; 2, nearly equal

-The paraoccipital process and the post glenoid process together form two finger-like projections ventrally, when viewed laterally. When the skull is leveled relative to the molar portion of the tooth row, the two processes may be level in maximum extent (2), or have the posterior of the two processes, the paraoccipital extend farther ventrally than the post glenoid process (0), or the postglenoid process extend ventrally to the paraoccipital process (1).

31. Occipital: ventral end of the paraoccipital processes: 0, inclined anteriorly; 1, inclined posteriorly; 2, straight

-The paraoccipital process, the posterior of the two ventrally projecting processes, when the skull is leveled relative to the molar portion of the tooth row, projects forward (0), is vertical (1), or projects posteriorly (2).

32. 20 Occipital: nuchal tubercle = 0, little developed; 1, developed; 2, very developed

-A projecting tubercle off of the nuchal crest on the occipital bone when viewed from the posterior. If absent (0), or a slight thickening of the profile of the crest (1), if a pronounced cone-shaped protrusion (2). See Supplemental Figure Character 32 for an example of a state 2 as shown in Chilotherium primigens.

33. Skull: back of teeth row = 0, in the posterior half; 1, restricted to the anterior half

-If the skull, viewed in lateral view, is leveled given the occlusal surface of the molars, the posterior edge of M3 is before the anteroposterior midpoint of the skull (1), or is posterior to the midpoint of the skull (0).

34. Pterygoid: posterior margin = 0 nearly horizontal; 1, nearly vertical

-The pterygoid bone, where it projects posterior to the M3, points out posteriorly when viewed laterally (0), or curves upwards sharply posterior to the M3 (1).

35. Skull = 0, dolichocephalic; 1, brachycephalic

-Brachycephalic, defined as a foreshortened skull compared to the norm, is herein defines as a skull that is broad compared to the overall length, when comparing the maximum width across the posterior edge of the zygomatic arches. Teleoceras fossiger would be an example of a brachycephalic skull, whereas Subhyracodon copei would be an example of dolichocephalic.

36. Skull: narrowing of dorsal surface anterior the orbit: 0, gradual; 1, abrupt

-The skull narrows, angled at roughly around 45 degrees, in toward the median line when viewed from above (1), as compared to the skull continuing posteriorly at roughly the same thickness to a slight narrowing (0). See the two supplemental figures, Character 36A is Chilotherium primigens (state 1) and Character 36B Chilotherium licenti (state 0).

37. Skull: widest part of the dorsal surface: 0, at level of postorbital process area; 1, at level of supraorbital process

-The postorbital process area sits just posterior to the orbit, regardless of is the taxon possesses postorbital processes or not. The supraorbital process sits in the front third of the orbit region. The skull of Chilotherium primigens has red bars drawn on both sites, with the supraorbital process site being the widest (1) (Supplemental Figure Character 37).

38. Nasal bones: rostral end = 0, narrow; 1, broad; 2, very broad

-The rostral, or anterior, end of the nasal bones end in a narrow point (0), is relatively blunt and rounded on the anterior end (1), or is thickened and almost hammer-like (2).

39. Nasal bones = 0, totally separated; 1, anteriorly separated; 2, fused

-At the anterior portion of the nasal bones are the separate (0), touching but with a distinct separation at the anterior tip (1), or fully fused together (2).

40. Nasal bones = 0, long; 1, short; 2, very long

-Long nasals are generally also narrow. Short nasals tend to form more a triangular shape than the long or very long nasals, which poses roughly parallel lateral outlines.

41. Median nasal horn = 0, absent; 1, present

-While the horn is not preserved, the rugose texture of the nasal bone indicates presence of a horn. A median nasal horn span the suture in the nasal bone.

42. Median nasal horn = 0, small; 1, developed

-Developed refers to the diameter of the rugose area relative to the size of the skull.

43. Paired nasal horns = 0, absent; 1, present

-As seen in Menoceras, two distinct areas of rugosity on either side of the suture in the median of the nasal bone.

44. Paired nasal horns = 0, terminal bumps; 1, lateral crests

45. Frontal horn = 0, absent; 1, present

-A more posterior horn, in contact with the frontal bone and not just the nasal bones.

46. Frontal horn = 0, small; 1, huge

47. Orbit: lateral projection = 0, absent; 1, present

-When viewed from dorsally, the orbits project out laterally noticeably away from the skull (1). In taxa lacking this trait, the exact position of the orbits is not visible from a dorsal view. (0)

48. Zygomatic width/frontal width = 0, less than 1.5; 1, more than 1.5

-When measured from a dorsal view, the width across the widest portion of the zygomatic arches is 1.5 times or less the width of the frontal bone at the same position (0). Shown in Supplemental Figure Character 48 on Chilotherium sp. nov. character state 1.

49. Frontal–parietal = 0, sagittal crest; 1, close frontoparietal crests; 2, distant crests

-A sagittal crest (0) in a single structural feature running along the median of the skull. Close frontoparietal crests are nearly fused into one structure, but have a crack or slot between the two parallel ridges (1). Distinct crest have a flattened area between the distinct crests, which may or may not be directly parallel to each other or slightly concave towards the median line (2).

50. Occipital crest: transverse expansion: 0, narrow; 1, wide

-The occipital crest, Or the most central portion of the nuchal crest connecting the sagittal crest may narrowly connect to the posterior most portion of the sagittal crest (0) or have a broad connection (1).

51. Parietal crest: dorsal surface: 0, concave; 1, prominent

-The parietal crest, or posterior portion of the sagittal crest, when viewed in profile is slightly curved downwards (0) or is strongly pronounced and either level or projecting slightly upwards (1). The structure most form a notable crest, and not just be an upturning of the entire posterior of the skull.

52. Occipital crest = 0, concave; 1, straight; 2, forked

-When viewed from the posterior, the occipital crest forms the dorsal most outline of the skull. If this is shallowly concave, with a general U-shaped curve, then (0). If the profile is straight across (1), and if it forms a steeply sided fork ending in a V-shape as the base, then (2).

53. Maxillary: processus zygomaticus maxillari, anterior tip = 0, progressive; 1, brutal

-Where the zygomatic arch connects into the maxillary bone is a small cone-shaped bump. If this process is smooth and angled somewhat anteriorly, it is progressive (0), whereas is its roughened and almost rugose in texture, while projecting primarily laterally, it is brutal (1).

54. Vomer = 0, acute; 1, rounded

-If the vomer projects as a very thin ridge and narrows quickly, it is acute (0), if it tapers more gradually into the palate, than it is rounded (1).

55. Squamosal: articular tubercle = 0, smooth; 1 high

-The articular tubercle, on the posterior ventral most surface of the zygomatic

arch, may either be low in profile and smooth (0), or project out noticeably from the rest of the zygomatic (1).

56. Squamosal: transversal profile of articular tubercle = 0, straight; 1, concave

-When viewed from the ventral surface, the articular tubercle is deeply grooved with a concave surface (1), or presents more as a flat shelf, with no internal groove (0).

57. Squamosal: foramen postglenoideum = 0, distant from the processus postglenoidalis; 1, close to it

-When viewing the skull from the ventral surface, the postglenoid foramen is situated posterior to the glenoid fossa. It can either be relatively lateral near the postglenoid process (1), or displaced more medially, away from the postglenoid process (0).

58. Squamosal: processus postglenoidalis = 0, flat; 1, convex; 2, dihedron

-When viewing the anterior and ventral surfaces of the postglenoid process, it can form a small plateau, with a level ventral surface (0), a small hook shape with the hook opening towards the anterior (1), Or have steeply sloping sides with distinct ridges making a dihedron shape when viewed ventrally (2).

59. Basioccipital: foramen nervi hypoglossi = 0, in the middle of the fossa; 1 shift antero-externally

-The hypoglossal canal sits just inside or just externally of the foramen magnum.

60. Basioccipital: sagittal crest on the basilar process = 0, absent; 1, present

-Looking directly at the foramen magnum, the basilar process sits directly ventral to the opening. A sagittal crest is usually a small ridge initiating within a centimeter of the foramen magnum and extending anteriorly along the basilar process when present (1). When absent, the whole basilar process is smooth and convex in profile (0).

61. Squamosal: posterior groove on the processus zygomaticus = 0, absent; 1, present

-The posterior edge of the zygomatic process has a mediolateral groove (1), or presents are a straight vertical surface to a convex surface when viewed laterally (0).

62. Squamosal–occipital: processus posttympanicus and processus paraoccipitalis = 0,

fused; 1, distant

-The post tympanic process is present in basal rhinocerotids, as well as the teleoceracid lineages. It forms a thin wing-like projection when not connected to the paraoccipital process (1).

63. Squamosal: processus posttympanicus = 0, well developed; 1, little developed; 2, huge

-only if present in the last character can this character be well developed or huge.

64. Occipital: processus paraoccipitalis = 0, well developed; 1, little developed

-The process just anterior to the lateral margin of the occipital condyles. Well developed (0) it is very robust, as opposed to the more finger-like nature of a little developed paraoccipital process (1).

65. Nuchal face: outline: 0, bell–shaped; 1, trapezoidal; 2, square

-Viewing the skull from the posterior, the main face of the back of the skull, outlines by the nuchal crests, form a bell shape (0), a trapezoid with the smaller limb across the top (1), or a square (2).

66. Magnum foramen: dorsal incision: 0, absent; 1, present

-The dorsal incision, when present, is a small notch extending dorsally from the otherwise ovate foramen magnum. In some literature, this is referred to as being “onion shaped”.

67. Occipital: foramen magnum = 0, circular; 1, subtriangular

-The foramen magnum can be either circular (0) or somewhat triangular, with rounded edges and the ventral portion being wider that the narrow dorsal portion (1).

68. Basioccipital: median ridge on the condyle = 0, absent; 1, present

-the most median edge of the occipital condyle forms a ridge before opening to the foramen magnum.

69. Basioccipital: medial truncation on the condyle = 0, absent; 1, present

-The condyle truncates abruptly before the opening to the foramen magnum (1),

or the surface of the condyle smoothly wraps anteriorly into the foramen magnum (0).

70. Basioccipital: medial truncation on the condyle = 0, present at juvenile stage; 1, still present at adult stage

-If last character was a 1, then character 70 can be coded as a (1) even without juvenile material available. If no juvenile material is available, and last character was a (0), then this character is left (?)

Mandible

71. Symphysis = 0, very upraised; 1, upraised; 2, nearly horizontal

-Very upraised, is when the posterior/dorsal surface of the symphysis is almost facing directly posterior (0), upraised is when the posterior/dorsal surface forms a distinct slope, increasing in height anteriorly (1), and nearly horizontal is when the symphysis projects anteriorly almost as a shelf (2).

72. Symphysis = 0, spindly; 1, massive; 2, very massive

-Spindly is a very narrow anteroposterior connection (0), whereas massive is a much thicker connection, and very massive is a symphysis that extends far beyond the tooth row and is around 50% of tooth row length or greater.

73. Symphysis: ventral surface: 0, flat; 1, concave

74. Symphysis: constriction before the lower cheek teeth row: 0, absent; 1, present

-When viewed from above, the bone of the mandible forms a “chromosome shaped” X, with the limbs of the X being the tooth row and then extending out on the mandibular symphysis to tusks.

75. Symphysis: crest along the diastema: 0, slender; 1, stout

-stout is defined as both vertical and horizontal robustisity.

76. Symphysis: posterior margin = 0, in front of p2; 1, level of p2–4

- When viewed from above, the posterior most edge of the symphysis is either in front of the teeth of behind the teeth.

77. Foramen mentale = 0, in front of p2; 1, level of p2-4

78. Corpus mandibulae: lingual groove = 0, present; 1, absent

79. Corpus mandibulae: lingual groove = 0, still present at adult stage; 1, present at juvenile stage only

80. Corpus mandibulae: base = 0, straight; 1, convex; 2, very convex

-Basically, how strongly curved is the base of the jaw? An example of character state 2 would be Aphelops megalodus

81. Mandible: orientation of row of lower cheek teeth: 0, not parallel to long axis of mandible; 1, parallel to long axis of mandible

-When viewed from dorsally, does the tooth row follow the line of the mandible or not?

82. Ramus = 0, vertical; 1, inclined forward; 2, inclined backward

-Is the anterior most edge of the ascending ramus, when viewed laterally, vertical (0), or inclined in either direction?

83. Ramus: processus coronoideus = 0, well developed; 1, little developed

-When little developed, the dorsal most portion of the coronoid process comes to a sharp tip, rather than a blunt and rounded feature in (0)

84. Foramen mandibulare = 0, below the teeth neck; 1, above the teeth neck

Teeth

85. Compared length of the premolars/molars rows = 0, (100 x LP3–4/LM1–3) > 50; 1, 42 < (100 x LP3–4/LM1–3) < 50; 2, (100 x LP3–4/LM1–3) < 42

86. Cheekteeth: enamel foldings = 0, absent; 1, weak; 2, developed; 3, intense

87. Cheekteeth: cement = 0, absent; 1, present

88. Cheekteeth: cement = 0, weak or variable; 1, abundant

89. Cheekteeth: shape of enamel = 0, wrinkled; 1, wrinkled and corrugated; 2, corrugated and arborescent

-Corrugated is the extention of “wrinkles” most of the crown height of the tooth.

Arborescent is complicated branching patterns in the textured enamel of the crowns. Most apparent on the labial surface typically.

90. Cheekteeth: crown = 0, low; 1, high

91. Cheekteeth: crown = 0, high; 1, partial hypsodonty; 2, subhypsodonty; 3, hypsodonty

92. Cheekteeth: roots = 0, distinct; 1, joined; 2, fused

-Often related to the degree of hypsodonty, more hypsodont teeth form less distinct roots. Roots that are distinct also typically angle out from the enamel dentine juncture to an extent.

93. I1 = 0, present; 1, absent

94. I1: shape of the crown (cross section) = 0, almond; 1, oval; 2, half moon

95. I2 = 0, present; 1, absent

96. I3 = 0, present; 1, absent

97. C1 = 0, present; 1, absent

98. i1 = 0, present; 1, absent

99. i1: crown = 0, developed, with a pronounced neck; 1, reduced

100. i2 = 0, present; 1, absent

-If present, usually the protruding tusk in the lower dentition.

101. i2: shape = 0, incisor–like; 1, tusk–like

-Earlier rhinos retained more incisors, and were more likely to have canines present. In most of the "tusked" rhinocerotids, the tusks are formed by the i2. If the i2 is greatly enlarged AND projects at a different angle than i1, it would be considered tusk-like (1).

102. i2: orientation = 0, parallel; 1, divergent

-If tusks are present, do they project forwards in a continuation of the tooth row angle (0), or do they angle laterally (1).

103. i2: upturning of the internal edge: 0, absent; 1, present

-Forms a flange on the median edge of the tusk (1), or tusk is ovate or conical in cross section (0).

104. i3 = 0, present; 1, absent

105. c1 = 0, present; 1, absent

106. Upper cheek teeth: lingual rim of row of cheek teeth: 0, arched; 1, always straight

107. Upper cheek teeth: branch of the crochet and crista: 0, always absent; 1, occasionally present; 2, always present

108. Upper cheek teeth: protocone constricted: 0, anteroposteriorly; 1, just anteriorly

109. Upper cheek teeth: expansion of the lingual cusps: 0, absent; 1, present

110. Upper cheek teeth: crista: 0, one; 1, always doubled

111. Upper premolars: V-shaped incision on the lingual cingulum around the entrance of the median valley: 0, absent; 1, present

112. Upper premolars: labial cingulum = 0, always present; 1, usually present; 2, usually absent; 3, always absent

113. P2–4: crochet = 0, always absent; 1, usually present; 2, always present

114. P2-4: crochet = 0, always simple; 1, usually simple; 2, usually multiple

115. P2–4: metaloph constriction = 0, absent; 1, present

116. P2–4: lingual cingulum = 0, always present; 1, usually present; 2, usually absent; 3, always absent

117. P2–4: lingual cingulum = 0, continuous; 1, reduced

118. P2-4: postfossette = 0, narrow; 1, wide; 2, posterior wall

119. P2-3: antecrochet = 0, always absent; 1, usually absent; 2, usually present; 3, always present

120. P1 (in adults) = 0, always present; 1, usually present; 2, always absent

121. P1: antero–lingual cingulum = 0, present; 1, absent

122. P2 = 0, present; 1, absent

123. P2: protocone and hypocone = 0, fused; 1, lingual bridge; 2, separated; 3, lingual wall

124. P2: metaloph = 0, hypocone posterior to metacone; 1, transverse; hypocone anterior to metacone

125. P2: lingual groove = 0, present; 1, absent

126. P2: protocone = 0, equal or stronger than the hypocone; 1, less strong than the hypocone

127. P2: protoloph = 0, present; 1, absent

128. P2: protoloph = 0, joined to the ectoloph; 1, interrupted

129. P3–4: medifossette = 0, always absent; 1, usually absent; 2, usually present; 3, always present

130. P3–4: constriction of the protocone = 0, always absent; 1, usually absent; 2, usually present; 3, always present

131. P3–4: protocone and hypocone = 0, fused; 1, lingual bridge; 2, separated; 3, lingual wall

132. P3–4: metaloph = 0, transverse; 1, hypocone posterior to metacone; 2, hypocone anterior to metacone

133. P3: protoloph = 0, joined to the ectoloph; 1, interrupted

134. P3: crista = 0, always absent; 1, usually absent; 2, usually present; 3, always present

135. P3: pseudometaloph = 0, always absent; 1, sometimes present

136. P4: antecrochet = 0, always absent; 1, usually absent; 2, usually present; 3, always present

137. P4: hypocone and metacone = 0, joined; 1, separated

138. Upper molars: labial cingulum = 0, always present; 1, usually present; 2, usually absent; 3, always absent

139. Upper molars: antecrochet = 0, always absent; 1, usually absent; 2, usually present; 3, always present

140. Upper molars: base of the antecrochet spread toward the entrance of the median valley: 0, absent; 1, present

141. Upper molars: crochet = 0, always absent; 1, usually absent; 2, usually present; 3, always present

142. Upper molars: crista = 0, always absent; 1, usually absent; 2, usually present; 3, always present

143. Upper molars: medifossette = 0, always absent; 1, usually absent; 2, usually present

144. Upper molars: lingual cingulum = 0, always present; 1, usually present; 2, usually absent; 3, always absent

145. M1–2: constriction of the protocone = 0, always absent; 1, usually absent; 2, usually present; 3, always present

146. M1–2: constriction of the protocone = 0, weak; 1, strong

147. M1–2: paracone fold = 0, present; 1, absent

148. M1–2: paracone fold = 0, strong; 1, weak

149. M1–2: metacone fold = 0, present; 1, absent

150. M1–2: metastyle = 0, short; 1, long

151. M1–2: metaloph = 0, long; 1, short

152. M1–2: posterior part of the ectoloph = 0, straight; 1, concave

153. M1–2: cristella = 0, always absent; 1, usually present; 2, always present

154. M1–2: posterior cingulum = 0, continuous; 1, low and reduced

155. M1: metaloph = 0, continuous; 1, hypocone isolated

156. M1: antecrochet-hypocone = 0, always separated; 1, sometimes joined; 2, always joined

157. M1: postfossette = 0, present; 1, usually absent

158. M2: protocone, lingual groove = 0, always absent; 1, usually absent; 2, always present

159. M2: metaloph = 0, continuous; 1, hypocone isolated

160. M2: mesostyle = 0, absent; 1, present

161. M2: mesostyle = 0, weak; 2, strong

162. M2: antecrochet and hypocone = 0, separated; 1, joined

163. M3: ectoloph and metaloph = 0, distinct; 1, fused (ectometaloph)

164. M3: shape = 0, quadrangular; 1, triangular

165. M3: constriction of the protocone = 0, always absent; 1, usually absent; 2, always present

166. M3: protocone = 0, trefoil–shape; 1, indented

167. M3: protoloph = 0, transverse; 1, lingually elongated

168. M3: posterior groove on the ectometaloph = 0, present; 1, absent

169. p2-3: vertical external rugosities = 0, absent; 1, present

170. Lower cheekteeth: external groove = 0, developed; 1, smooth, U-shaped; 2, angular, V-shaped

171. Lower cheekteeth: external groove = 0, vanishing before the neck; 1, developed until the neck

172. Lower cheekteeth: paralophid: 0, nearly reach the lingual rim; 1, away from the lingual rim

173. Lower cheekteeth: occlusal outline of the trigonid basin: 0, U-shaped; 1, V-shaped

174. Lower cheekteeth: trigonid = 0, angular; 1, rounded

175. Lower cheekteeth: trigonid = 0, obtuse or right dihedron; 1, acute dihedron

176. Lower cheekteeth: metaconid = 0, joined to the metalophid; 1, constricted

177. Lower cheekteeth: entoconid = 0, joined to the hypolophid; 1, constricted

178. Lower premolars: lingual opening of the posterior valley = 0, U-shape; 1, narrow, V-shape

179. Lower premolars: lingual cingulum = 0, always present; 1, usually present; 2, usually absent; 3, always absent

180. Lower premolars: lingual cingulum = 0, reduced; 1, continuous

181. Lower premolars: labial cingulum = 0, present; 1, absent

182. Lower premolars: labial cingulum = 0, continuous; 1, reduced

183. d1/p1 (in adults) = 0, always present; 1, usually present; 2, usually absent; 3, always absent

184. d1: 0, always two-rooted; 1, usually two-rooted; 2, always one-rooted

185. p2 = 0, always present; 1, usually present; 2, always absent

186. p2: paralophid = 0, isolated, spur-like; 1, curved, without constriction

187. p2: paraconid = 0, developed; 1, reduced

188. p2: posterior valley = 0, lingually open; 1, usually closed; 2, always closed

189. Lower molars: lingual cingulum = 0, always present; 1, usually present; 2, usually absent; 3, always absent

190. Lower molars: lingual cingulum = 0, reduced; 1, continuous

191. Lower molars: labial cingulum = 0, always present; 1, usually present; 2, usually absent; 3, always absent

192. Lower molars: labial cingulum = 0, continuous; 1, reduced

193. Lower molars: hypolophid = 0, transverse; 1, oblique; 2, almost sagittal

194. m2-3: lingual groove of the entoconid = 0, absent; 1, present

195. dI1 = 0, present; 1, absent

196. dI2 = 0, present; 1, absent

197. D2: mesostyle = 0, present; 1, absent

198. D3-4: mesostyle = 0, absent; 1, present

199. D2: lingual wall = 0, absent; 1, present

200. D2: secondary folds = 0, absent; 1, present

201. D2: mesoloph = 0, absent; 1, present

202. di1 = 0, present; 1, absent

203. di2 = 0, present; 1, absent

204. Lower milk teeth: constriction of the metaconid = 0, present; 1, absent

205. Lower milk teeth: constriction of the entoconid = 0, absent; 1, present

206. Lower milk teeth: protoconid fold = 0, present; 1, absent

207. d1 (in juveniles) = 0, present; 1, absent

208. d2-3: vertical external roughnesses = 0, absent; 1, present

209. d2-3: ectolophid fold = 0, present; 1, absent

210. d2: anterior groove on the ectolophid = 0, absent; 1, present

211. d2: paralophid = 0, simple; 1, double

212. d2: posterior valley = 0, always open; 1, usually open; 2, usually closed; 3, always closed

213. d3: paralophid = 0, double; 1, simple

214. d3: lingual groove on the entoconid = 0, always absent; 1, usually absent; 2, always present

REFERENCES CITED

Abdrakhmatov, K., H.B. Havenith, D. Delvaux, D. Jongmans, & P. Trefois. 2003. Probabilistic PGA and arias intensity maps of Kyrgyzstan (Central Asia). Journal of Seismology, 7(2): 203-220.

Abdrakhmatov, K., R. Weldon, S. Thompson, D. Burbank, C. Rubin, M. Miller, and P. Molnar. 2001. Onset, style and current rate of shortening in the central Tien Shan, Kyrgyz Republic. Russian Geology and Geophysics, 42(10); 1585-1609.

Abdrakhmatov, K., S.A. Aldazhanov, B.H. Hager, M.W. Hamburger, T.A. Herring, K.B. Kalabaev, V.I. Makarov, P. Molnar,S.V. Panasyuk, M.T. Prilepin, R.E. Reilinger, I.S. Sadybakasov, B.J. Souter, Y.A. Trapeznikov, V.Y. Tsurkov, and A.V. Zubovich. 1996. Relatively recent construction of the Tien Shan inferred from GPS measurements of present-day crustal deformation rates. Nature, 384; 450–453.

Abdrakhmatov, K.Ye. 1988. Quaternary tectonics of the Chu Basin. Ilim, Frunze (Bishkek), p. 1-118. (in Russian)

Abrajevitch, A. 2008. Magnetic memory of rocks: the Kazakhstan orocline and climatic record of the Indian monsoon. Doctoral dissertation, The University of Michigan.

Andersson, K., and L. Werdelin. 2005. Carnivora from the Late Miocene of Lantian, China. Vertebrata Pal Asiatica 43(4); 256-271.

Antoine, P.O. 2002. Phylogénie et evolution des Elasmotheriina (Mammalia, Rhinocerotidae). Mémoires du Muséum National d'Histore Naturelle 188, 1-359.

Antoine, P.O., Downing, K.F., Crochet, J.Y., Duranthon, F, Flynn, L.J., Marivaux, L., Métais, G., Rajpar, A.R., and Roohi, G. 2010. A revision of Aceratherium blanfordi Lydekker, 1884 (Mammalia, Rhinocerotidae) from the Early Miocene of Pakistan: Postcranials as a key. Zoological Journal of the Linnean Society 160; 130-194.

Antoine, P.O., Duranthon, K.F., and Welcomme, J.L. 2003. Alicornops (Mammalia, Rhinocerotidae) dans le Miocène supérieur des collines Bugti (Balouchistan, Pakistan): implications phylogénétiques. Geodiversitas 25; 575-603.

Aslan, A., and A.K. Behrensmeyer. 1996. Taphonomy and time resolution of bone assemblages in a contemporary fluvial system: the East Fork river, Wyoming. PALAIOS 11; 411-421.

Averianov, A.O., A.A. Bakirov, T. Martin. 2007. First definitive stegosaur from the Middle Jurassic of Kyrgyzstan. Paläontologische Zeitschrift, 81(4): 440-446.

Averianov, A.O. and M. Godinot. 2005. Ceratomorphs (Mammalia, Perissodactyla) from the early Eocene Andarak 2 locality in Kyrgyzstan. Geodiversitas, 27(2); 221-237.

Averianov, A. and M. Godinot. 1998. A report on the Eocene Andarak mammal fauna of Kyrgyzstan. In Dawn of the Age of Mammals, Beard and Dawson, eds. Bulletin of Carnegie Museum of Natural History 34; 210-219.

Averianov, A. and I. Danilov. 1996. Agamid lizards (Reptilia, Sauria, Agamidae) from the Early Eocene of Kyrgyzstan.

Azanza, B., G.E. Rössner, E. Ortiz-Jaureguizar. 2013. The early Turolian (late Miocene) Cervidae (Artiodactyla, Mammalia) from the fossil site of Dorn-Dürkheim 1 (Germany) and implications on the origin of crown cervids. Palaeobiodiversity and Palaeoenvironments 93(2); 217-258.

Badgley, C. 1986. Taphonomy of mammalian fossil remains from Siwalik rocks of Pakistan. Paleobiology 12(2); 119-142.

Barry, J.C., M.E. Morgan, L.J. Flynn, D. Pilbeam, A.K. Behrensmeyer, S.M. Raza, I.A. Khan, C. Badgley, J. Hicks, and J. Kelley. 2002. Faunal and environmental change in the late Miocene Siwaliks of northern Pakistan. Paleobiology 28(sp3); 1-71.

Batsch, A.J.G.K. 1788. Versuch einer Anleitung zur Kenntniß und Geschichte der Thiere und Mineralien: Allgemeine Geschichte der Natur, besondre der Säugthiere, Vögel, Amphibien und Fische, Volume 1. Akademische Buchhandlung, pp. 528.

Bayshashov, B.U. 1982. A new rhinoceros species of the genus Chilotherium from Pavlodar. In Mezozoic and Cenozoic Vertebrate Fauna and Flora of North-Eastern and Southern Kazakhstan. Academy Natural Kazakhstan, Alma-Ata (Almaty); 8; 72-83, 1Pl.

Behrensmeyer, A.K., S.M. Kidwell, and R.A. Gastaldo. 2000. Taphonomy and Paleobiology. Paleobiology, 26(4); 103-147.

Behrensmeyer, A.K. 1991. Terrestrial vertebrate accumulations. Taphonomy: releasing the data locked in the fossil record, in P.A. Allison and D.E.G. Briggs (eds.), Topics in Geobiology, v.9, Plenum Press, New York, p. 291-335.

Behrensmeyer, A.K., and A.P. Hill. 1980. Fossils in the making; Vertebrate taphonomy and paleoecology. The University of Chicago Press, Chicago IL.

Behrensmeyer, A.K. 1978. Taphonomic and ecological information from bone weathering. Paleobiology 4(2); 150-162.

Belyaeva, E.I. 1962. First record of a tapiromorph in the Eocene of Middle Asia. Byuleten' Moskovskogo Obschestva Ispytatelei Prirody, Otdel Geologicheskii 37(5); 142-145 (in Russian).

Belyaeva, E.I. 1948. Katalog Mestonakhozhdenii Tretichnykh Nazemnykh Mlekopitayushchikh na Territorii SSSR [Catalogue of the Localities of Finds of Tertiary Terrestrial Mammals on USSR Territory] (in Russian). Trudy Paleontologicheskogo Instituta AN SSSR. 1948; 36-114.

Berger, J., S. Dulamtseren, S. Cain, D. Enkkhbileg, P. Lichtman, Z. Namshir, G. Wingard, and R. Reading. 2001. Back-casting sociality in extinct species: new perspectives using mass death assemblages and sex ratios. Proceedings of the Royal Society of London 268; 131-139.

Bernor, R.L., Z. Qiu, and L.C. Hayek. 1990. Systematic revision of Chinese *Hipparion* species described by Sefve, 1927. American Museum Novitates 2984; 60 pp.

Beziehung auf die Gattung Castor. Mémoires de l'Academie impériale des sciences de Saint-Pétersbourg, sixième série Sciences Mathematiques, Physiques et Naturelles, seconde partie, Sciences Naturelles 7; 127-365.

Blob, R.W. and A.R. Fiorillo. 1996. The significance of vertebrate microfossil size and shape distributions for faunal abundance reconstructions: a Late Cretaceous example. Paleobiology 22; 422-435.

Boaz, N.T. and A.K. Behrensmeyer. 1976. Hominid taphonomy: transport of human skeletal parts in an artificial fluviatile environment. American Journal of Physical Anthropology 45; 53-60.

Böhme, W. 2003. Checklist of the living monitor lizards of the world (family Varanidae). Zoologische verhandelingen / uitgegeven door het Rijksmuseum van Natuurlijke Historie te Leiden (Ministerie van Cultuur, Recreatie en Maatschappelijk Werk) 341; 1-43.

Bowditch, T.E. 1821. An analysis of the natural classification of Mammalia for the use of students and travelers. John Smith, Paris, France, 115 pp.

Brandt, J.F. 1855. Untersuchungen über die Craniologischen Entwickelungsstufen ung die davon herzuleitenden Verwandtschaften und Classification der Nager der Jetztwelt mit besonderer Beziehung auf die Gattung Castor. Mémoires de l'Academie impériale des sciences de Saint-Pétersbourg, sixieme série Sciences Mathmatiques, Physiques et Naturelles, seconde partie, Sciences Naturelles 7; 127-365.

Breda, M. 2001. The holotype of Cervalces gallicus (Azzaroli, 1952) from Sénèze (Haute-Loire, France) with nomenclature implications and taxonomical-phylogenetic accounts. Rivista Italiana di Paleontologia e Stratigrafia 107(3); 439-449.

Burbank, D.W., J.K. McLean, M. Bullen, K.Y. Abdrakhmatov, and M.M. Miller. 1999. Partitioning of intermontane basins by thrust-related folding, Tien Shan, Kyrgyzstan. Basin Research 11; 75-92.

Burgette, R.J., R.J. Weldon, K.Ye. Abdrakhmatov, C. Ormukov, L.A. Owen, and S.C. Thompson. 2017. Timing and process of river and lake terrace formation in the Kyrgyz Tien Shan. Quaternary Science Reviews 159; 15-34.

Calede, J.J. 2016. Comparative taphonomy of the mammalian remains from the Cabbage Patch beds of western Montana (Renova Formation, Arikareean): contrasting depositional environments and specimen preservation. PALAIOS 31;497-515.

Cande, S.C. and D.V. Kent. 1995. Revised calibration of the geomagnetic polarity timescale for the Late Cretaceous and Cenozoic. Journal of Geophysical Research, Solid Earth 100(B4); 6093-6095.

Cardoso, H.F.V., A. Santos, R. Dias, C. Garcia, M. Pinto, C. Sérgio, and T. Magalhães. 2010. Establishing a minimum postmortem interval of human remains in an advanced state of skeletonization using the growth rate of bryophytes and plant roots. International Journal of Legal Medicine 124(5); 451-456.

Chainey, A., W.F.F. McLaughlin, E.B. Davis, S.S.B. Hopkins. (in prep) New methods for geometric and statistical differentiation of *Gazella* horn cores, with comments on new material from Kyrgyzstan.

Chediya, O.K. 1986. Morphology and neotectonics of the Tien Shan. Ilim, Frunze (Bishkek), p. 313. (in Russian)

Chen, S., T. Deng, S. Hou, Q. Shi, and L. Pang. 2010. Sexual dimorphism in perissodactyl rhinocerotid Chilotherium wimani from the late Miocene of the Linxia Basin (Gansu, China). Acta Palaeontologica Polonica 55(4); 587-597.

Chinsamy, A. 1997. Assessing the biology of fossil vertebrate through bone histology. Palaeontologis Africana 33; 25-39.

Christol, J. de. 1832. Description of *Hipparion*. Annales Science I'Industrie du midi de la France; 180-181.

CIA World Fact Book: Kyrgyzstan (https://www.cia.gov/library/publications/the-world-factbook/geos/kg.html) Accessed, November 17, 2017.

Coombs, M.C. and W.P. Coombs. 1997. Analysis of the geology, fauna, and taphonomy of Morava Ranch Quarry, early Miocene of northwest Nebraska. PALAIOS 12;165-187.

Danilov, I.G., A.O. Averianov, P.P. Skutchas, and A.S. Rezvyi. 2006. "Kirgizemys (Testudines, 'Macrobaenidae'): new material from the lower Cretaceous of Buryatia (Russia) and taxonomic revision" in: Danilov I.G. and Parham J.F. (eds.), Fossil Turtle Research, Vol. 1, Russian Journal of Herpetology, 13(Supplimental), pp. 46-62.

Deng, T., X. Wang, M. Fortelius, Q. Li, Y. Wang, Z.J. Tseng, G.T. Takeuchi, J.E. Saylor, L.K. Säilä, G. Xie. 2011. Out of Tibet: Pliocene woolly rhino suggests high-plateau origin of ice age megaherbivores. Science, 333:1285-1288.

Deng, T. 2006. Neogene rhinoceroses of the Linxia Basin (Gansu, China). CFS Courier Forschungsinstitut Senckenberg 256; 43-56.

Deng T. 2006. Paleoecological comparison between late Miocene localities of China and Greece based on *Hipparion* faunas. Geodiversitas 28(3); 499-516.

Deng, T. 2005. New discovery of Iranotherium morgani (Perissodactyla, Rhinocerotidae) from the Late Miocene of the Linxia Basin in Gansu, China, and its sexual dimorphism. Journal of Vertebrate Paleontology 25; 442-450.

Deng, T. 2002. Limb bones of Chilotherium wimani (Perissodactyla, Rhinocerotidae) from the Late Miocene of the Linxia Basin in Gansu, China. Vertebrata PalAsiatica 40(4); 305-316.

Deng, T. 2001. New material of Chilotherium wimani (Perissodactyla, Rhinocerotidae) from the Late Miocene of Fugu, Shaanxi. Vertebrata Palasiatica 39; 129-138.

Deng, T., X. Wang, M. Fortelius, Q. Li, Y. Wang, Z.J. Tseng, G.T. Takeuchi, J.E. Saylor, L.K. Säilä, G. Xie. 2011. Out of Tibet: Pliocene woolly rhino suggests high-plateau origin of ice age megaherbivores. Science, 333:1285-1288.

Ding, Z.L., S.F. Xiong, J.M. Sun, S.L. Yang, Z.Y. Gu, and T.S. Liu. 1999. Pedostratigraphy and paleomagnetism of a ~7.0 Ma eolian loess-red clay sequence at Lingtai, Loess Plateau, north-central China and the implications for paleomonsoon evolution. Palaeogeography, Palaeoclimatology, Palaeoecology 152(1-2); 49-66.

Dollo, L. 1885. Rhinocéros vivants et fossils. Revue des Questions Scientifiques 17:293-299.

Dong, W. 1993. "The fossil records of deer in China" in Deer of China. N. Ohtaishi and H.-I. Sheng, editors. Elsevier Science Publishers B. V. pg. 95-102.

Dudley, J.P., G.C. Craig, D.ST.C. Gibson, G. Haynes, and J. Klimowicz. 2001. Drought mortality of bush elephants in Hwange National Park, Zimbabwe. African Journal of Ecology 39(2); 187-194.

Erfurt, J., A.O. Averianov, J. Buchantschenko, A.B. Fortuna. 1999. Rediscovery of the Eocene mammal site Toru Ajgyr (Kyrgyzstan). Hallesches Jahrbuch Geowissenschaften 21; 107-127.

Faith, J.T., and A.K. Behrensmeyer. 2006. Changing patterns of carnivore modification in a landscape bone assemblage, Amboseli Park, Kenya. Journal of Archaeological Sciences 33; 1718-1733.

Famoso, N.A., and D. Pagnac. 2011. A comparison of the Clarendonian equid assemblages from the Mission Pit, South Dakota and Ashfall Fossil Beds, Nebraska. Transactions of the Nebraska Academy of Sciences 32; 98-107.

Fischer von Waldheim, G. 1817. Adversaria zoological. Mémories de la Société Impériale des Naturalistes de l'Université Impériale de Moscou 5; 368-428.

Flora, H., W.N.F. McLaughlin, S.S.B. Hopkins, E.B. Davis. (in prep for Journal of Vertebrate Paleontology). A description of lagomorph material from Kyrgyzstan, with the first occurrence of leporids.

Flynn, L.J., A.J. Winkler, M. Erbaeva, N. Alexeeva, U. Anders, C. Angelone, S. Čermák, F.A. Fladerer, B. Kraatz, L.A. Ruedas, I. Ruf, Y. Tomida, K. Veitschegger, and Z. Zhang. 2013. The Leporid Datum: a late Miocene biotic marker. Mammal Review 44(3-4); 164-176.

Fortelius, M., K. Hessig, G. Sarac, and S. Sen. 2003. Rhinocerotidae (Perissodactyla). In M. Fortelius, J.W. Kappelman, S. Sen, and R.L. Bernor (eds). Geology and paleontology of the Miocene Sinap Formation, Turkey. Columbia University Press. pp.282-307.

Geyer, G., J.S. Peel, M. Streng, and S. Voigt. 2014. A remarkable Amgan (Middle Cambrian, Stage 5) fauna from the Sauk Tanga, Madygen region, Kyrgyzstan. Bulletin of Geosciences, 89(2): 375-400.

Global Seismic Hazard Assessment Program. 1999. GSHAP Region 8, Eastern Asia. (http://static.seismo.ethz.ch/GSHAP/eastasia/) Accessed January 2018.

Goloboff, P.A., and S.A. Catalano. 2016. TNT version 1.5, including a full implementation of phylogenetic morphometrics. Cladistics 32(3); 221-238.

Gray, J.E. 1821. On the natural arrangement of vertebrose animals. London Medical Repository 15:296-310.

Gubanov, A.P., R.B. Blodgett, V.N. Lytochkin. Early Devonian (Pragian) gastropods from Kyrgyzstan (Central Asia). Journal of Paleontology 69(3); 431-440.

Guérin, C. 1980. Les rhinoceros (Mammalia, Perissodactyla) du Miocène terminal au Pleistocène supérieur en Europe occidentale: comparaison avec les espèces actuelles. Documents du Laboratoire de Géologie de la Faculté des Sciences de Lyon 79; 1-1182.

Güleç, E.S., A. Sevim, C. Pehlevan, F. Kaya. 2007. A new great ape from the late Miocene of Turkey. Anthropological Science 115(2); 153-158.

Halvorson, S.J. & J.P. Hamilton. 2007. Vulnerability and the erosion of seismic culture in mountainous Central Asia. Mountain Research and Development, 27(4); 322-330.

Hanson, C.B. 1980. Fluvial taphonomic processes: models and experiments. In Fossils in the Making, A.K. Behrensmeyer and A.P. Hill eds. University of Chicago Press, Chicago IL, 156-181.

Haynes, G. 1988. Mass deaths and serial predation: Comparative taphonomic studies of modern large mammal death sites. Journal of Archaeological Science 15(3); 219-235.

Hessig, K. 1999. Family Rhinocerotidae; pp. 175-188 in G.E. Rössner and K. Heissig (eds.), The Miocene Land Mammals of Europe. Pfeil, Munich.

Heissig, K. 1996. The stratigraphic range of fossil rhinoceroses in the late Neogene of Europe and the eastern Mediterranean. In: Bernor, Fahlbusch, & Mittman (eds) The Evolution of Western Eurasian Neogene Mammal Faunas. Columbia University Press, New York. 339-347 pp.

Hunt Jr., R.M. 1990. Taphonomy and sedimentology of Arikaree (Lower Miocene) fluvial, eolian, and lacustrine paleoenvironments, Nebraska and Wyoming: A paleobiota entombed in fine-grained volcaniclastic rocks. Special Paper of the Geological Society of America 244; 69-111.

Hutchins, M. and M.D. Kreger. 2006. Rhinoceros behavior: implications for captive management and conservation. International Zoo Yearbook, 40(1); 150-173.

Kaiser, T.M., D.W.H. Müller, M. Fortelius, E. Schulz, D. Codron, M. Clauss. 2013. Hypsodonty and tooth facet development in relation to diet and habitat in herbivorous ungulates: implications for understanding tooth wear. Mammal Review 43(1); 34-46.

Kirschbaum, D.B., R. Adler, Y. Hong, S. Hill, A. Lerner-Lam. 2010. A global landslide catalog for hazard applications: method, result, and limitations. Natural Hazards, 52(3); 561-575.

Kirschvink, J.L. 1980. The least-squares line and plane and the analysis of the paleomagnetic data: examples from Siberia and Morocco. Geophysical Journal of the Royal Astronomical Society 62; 699-718.

Kostopoulos, D.S. 2009. The late Miocene mammal faunas of the Mytilinii basin, Samos Island, Greece: new collection. 2. Giraffidae. Beiträge zur Paläontologie 31; 345-389.

Koufos, G.D. 2003. Late Miocene mammal events and biostratigraphy in the Eastern Mediterranean. Natuurhistorisch Museum Rotterdam 10(1); 343-372.

Kuznetsov, V.D., K.K. Karabalaev, and I.M. Ibragimov. 1964. The fossil land tortoise from Kyrgyzstan. Materials on the geology of the Tien Shan. Ilim Publishing house, Frunze, pp. 135-146 (in Russian).

Kyrgyz National Census "Национальный состав населения (оценка на начало года, человек)". stat.kg. (http://www.stat.kg/ru/opendata/category/312/) Accessed, November 17, 2017.

Laurenti, J.N. 1768. Specimen medicum, exhibens synopsin Reptilium emendatam cum experimentis circa venena et antidota Reptilium Austriacorum. 214 pp. J.T. de Trattern, Wien.

Laurie, A. 1982. Behavioral ecology of the Greater one-horned rhinoceros (Rhinoceros unicornis). Journal of Zoology (196)3; 307-341.

Levy, D., R. Giustetto, and A. Hoser. 2012. Structure of magnetite (Fe_3O_4) above the Curie temperature: a cation ordering study. Physics and Chemistry of Minerals 39(2); 169-176.

Linnaeus, C. 1758. Systema naturae per regna tria naturae, secundum classis, ordines, genera, species cum characteribus, differentiis, sunonyms locis, 10^{th} revides edition, Volume 1. Laurentii Salvii, Stockholm, 824 pp.

Lloveras, L., M. Moreno-García, and J. Nadal. 2012. Accessing the variability in taphonomic studies of modern leporid remains from Eagle Owl (*Bubo bubo*) nest assemblages: the importance of age of prey. Journal of Archaeological Science 39; 3754-3764.

Lu, X. 2013. A juvenile skull of Acerorhinus yuanmouensis (Mammalia: Rhinocerotidae) from the Late Miocene hominid fauna of the Yuanmou Basin (Yuannan, China). Geobios 46; 539-548.

Macaulay, E.A., E.R. Sobel, A. Mikolaichuk, M. Wack, S.A. Gilder, A. Mulch, A.B. Fortuna, S. Hynek, and F. Apayarov. 2016. The sedimentary record of the Issyk Kul basin, Kyrgyzstan: climatic and tectonic inferences. Basin Research 28; 57-80.

Maldonado, V., L.G.M. Monteiro, A. Rotti, C. Pereira, H.I. de Araújo-Júnior, and L. dos Santos Avilla. 2016. Taphonomic aspects of deer (Mammalia, Cetartiodactyla, Cervidae) remains from a Quaternary cave deposit in Northern Brazil. Journal of Sedimentary Environments 1(2); 234-248.

Makarov, V.I. 1990. Late Cenozoic orogens, their structure and geodynamics. Scientific report for Doctor of Geological and Minerological Sciences, Geological Institute Russian Academy of Science, p.1-57. (in Russian)

Makorov, V.I. 1977. Neotectonic structures of the central Tien Shan. Order of the Red Banner Geology Institute, Akad. Sci., Moscow, Vol. 307, p. 1-171. (in Russian)

Martin, T., and A.O. Averianov. 2004. A new docodont (Mammalia) from the Middle Jurassic of Kyrgyzstan, Central Asia. Journal of Vertebrate Paleontology 24(1): 195-201.

Merrem, B. 1820. Versuch eines systems der Amphibien, Vol. 8. J.C. Krieger, Marburg, xv + 191 pp.

Miao, Y., M. Herrmann, F. Wu, X. Yan, and S. Yang. 2012. What controlled Mid-Late Miocene long-term aridification of Central Asia?-Global cooling or Tibetan Plateau uplift: a review. Earth Science Review 112; 155-172.

Mihlbachler, M.C. 2005. Linking sexual dimorphism and sociality in rhinoceroses: insights from Teleoceras proterum and Aphelops malacorhinus from the Late Miocene of Florida. Bulletin of the Florida Museum of Natural History 45(4); 495-520.

Mikolaichuk, A.V., F.Kh. Apayarov, M.F. Buchroithner, Z.I. Chernavskaja, L.I. Skrinnik, M.D. Ghes, A.V. Neyevin, and T.A. Charimov. 2008. Geological Map of Khan Tengri Massif, Explanatory Note. ISTC Project No. #KR-920, Bishkek, Kyrgyzstan.

Molnar, P. 2005. Mio-pliocene growth of the Tibetan plateau and evolution of east Asian climate. Palaeontologia Electronica 8(1); 2A:23p.

Moore, J.R. and D.B. Norman. 2009. Quantitatively evaluating the sources of taphonomic biasing of skeletal element abundances in fossil assemblages. PALAIOS 24;591-602.

Nakaya, Hideo. 1994. Faunal change of Late Miocene Africa and Eurasia: Mammalian fauna from the Namurungule Formation, Samburu Hills, Northern Kenya. African Study Monographs, Suppl. 20;1-112.

Nikonorov, V.V., J.V. Karaev, F.I. Borisov, T.S. Zamaletdinov, T.V. Larina, V.I. Tolsky. 2017 Mineral resources map of Kyrgyz Republic. Computer version compiled by T.E. Nogaev, N.A. Polovinskaja.

The NOW Community [2017]. New and Old Worlds Database of Fossil Mammals (NOW). Licensed under CC BY 4.0. Release [4.0], retrieved [September-December 2017] from http://www.helsinki.fi/science/now/.

Oppel, M. 1811. Die Ordnungen, Familien und Gattungen der Reptilien als Prodrom einer Naturgeschichte derselben. Joseph Lindauer, Munich, 87 pp.

Owen, R. 1845. Odontography or a treatise on the comparative anatomy of the teeth, their physiological relations, mode of development, and microscopic structure, in the vertebrate animals: 665 S.; London (Balliète).

Owen, R. M. 1848. Description of teeth and proportion of jaws of two extinct Anthracotherioid quadrupeds (Hyopotamus vectianus and Hyopotamus bovinus) discovered by the Marchioness of Hastings in the Eocene deposits on the N.W. coast of the Isle of Wight: with an attempt to develop Cuvier's idea of the classification of pachyderms by the number of their toes. Quarterly Journal of the Geological Society of London 4; 103-141.

Paleobiology Database, data downloaded in December, 2017, using the following parameters: time interval = Neogene, region = Central Asia, Kyrgyzstan.

Palmqvist P., B. Martinez-Navarro, and A. Arribas. 1996. Prey selection by terrestrial carnivores in a lower Pleistocene paleocommunity. Paleobiology 22; 514-534.

Pandolfi, L. 2015. Persiatherium rodleri, gen. et. sp. nov. (Mammalia, Rhinocerotidae) from the Upper Miocene of Maragheh (Northwestern Iran). Journal of Vertebrate Paleontology 36(1); e1040118.

Parker, T.J. and W.A. Haswell. 1910. A text-book of zoology: Volume 2. Macmillan and co., limited, London, United Kingdom. 714 pp.

Paulson, K. 2013. Generation of structural relief by fault propagation folding, Tien Shan, Kyrgyzstan. Master's thesis, University of Oregon, Eugene, Oregon.

Petronio, C., T. Krakhmalnaya, L. Bellucci, G. Di Stefana. 2007. Remarks on some Eurasian pliocervines: Characteristics, evolution, and relationships with the tribe Cervini. Geobios 40;113-130.

Pitra, C., J. Fickel, E. Meijaard, and P.C. Groves. 2004. Evolution and phylogeny of old world deer. Molecular Phylogenetics and Evolution 33; 880-895.

Prothero, D.R. 2005. The evolution of North American rhinoceroses. Cambridge University Press, Cambridge, United Kingdom. 218 pp.

Purdue, J.R. 1983. Epiphyseal closure in white-tailed deer. The Journal of Wildlife Management 47(4); 1207-1213.

Qiu, Z., W. Huang, and Z. Guo. 1987. Chinese hipparionines from the Yushe Basin. Palaeontologica Sinica, series C 175(25); 1-250.

Qiu, Z.X., J.Y. Xie, and D.F. Yan. 1987. A new chilothere skull from Hezheng, Gansu, China, with special reference to the Chinese "Diceratherium". Scientia Sinica, Series B 30; 545-552.

Quade, J., T.E. Cerling, and J.R. Bowman. 1989. Development of Asian monsoon revealed by marked ecological shift during the latest Miocene in northern Pakistan. Nature 342; 163-166.

Rage, J-C. and S. Bailon. 2005. Amphibians and squamate reptiles from the late early Miocene (MN 4) of Béon 1 (Montréal-du-Gers, southwestern France). Geodiversitas 27(3); 413-441.

Retallack, G.J. 2008. Soils of the past; An introduction to paleopedology. Wiley. 403 pp.

Ringström, T. 1924. Nashorner der Hipparion-fauna Nord-Chinas. Palaeontologia Sinica C 1(4) (4); 1-159.

Ríos, M., I.M. Sánchez, and Jorge Morales. 2017. A new giraffid (Mammalia, Ruminantia, Pecora) from the late Miocene of Spain, and the evolution of the sivathere-samothere lineage. PLoS ONE 12(11); e0185378.

Ríos, M., M. Danowitz, and N. Solounias. 2016. First comprehensive morphological analysis on the metapodials of Giraffidae. Palaeontologia Electronica 19.3.50A;1-39.

Robson, S., W.N.F. McLaughlin, J. Tseng, S.S.B. Hopkins. (in prep) A new species of hyenid from the Kochkor Basin, Kyrgyzstan.

Rowley, D.B. 1996. Age of initiation of collision between India and Asia: A review of stratigraphic data. Earth and Planetary Science Letters 145(1-4); 1-13.

Sadybakasov, I. 1990. Neotectonics of high Asia. Nauka, Moscow, pp. 1-176. (in Russian)

Sánchez, I.M., J.L. Cantalapiedra, M. Ríos, V. Quiralte. 2015. Systematics and Evolution of the Miocene Three-Horned Palaeomerycid Ruminants (Mammalia, Cetartiodactyla). PLoS ONE 10(12): e0143034.

Schlosser, M. 1903. Die fossilen Säugethiere Chinas nebst einer Odontographie der recenten Antilopen. Abh Bayer Akad Wiss 22;1-221.

Sen S. 1990. Hipparion datum and its chronologic evidence in the Mediterranean area. In: Lindsay E.H., Fahlbusch V., Mein P. (eds) European Neogene Mammal Chronology. NATO ASI Series (Series A: Life Sciences), vol 180. Springer, Boston, MA.

Shannon, L.M., R.H. Boyko, M. Castelhano, E. Corey, J.J. Hayward, C. McLean, M.E. White, M.A. Said, B.A. Anita, N.I. Bondjengo, J. Calero, A. Galov, M. Hedimbi, B. Imam, R. Khalap, D. Lally, A. Masta, K.C. Oliveira, L. Pérez, J. Randall, N.M. Tam, F.J. Trujillo-Cornejo, C. Valeriano, N.B. Sutter, R.J. Todhunter, C.D. Bustamante, & A.R. Boyko. 2015. Genetic structure in village dogs reveals a Central Asian domestication origin. Proceedings of the National Academy of Sciences of the United States of America, 112(44); 13639-13644.

Shipman, P. 1981. Life history of a fossil; An introduction to taphonomy and paleoecology. Harvard University Press, Cambridge, MA.

Shotwell, J.A. 1955. An approach to the paleoecology of mammals. Ecology 36(2);327-337.

Shrader, A.M. and N. Owen-Smith. 2002. The role of companionship in the dispersal of white rhinoceroses (Ceratotherium simum). Behavioral Ecology and Sociobiology 52(3); 255-261.

Silver, I.A. 1963. 26 The aging of domestic animals. Science in Archaeology: a comprehensive survey of progress and research. 250 pp.

Smith, D.R. 1995. Environmental security and shared water resources in Post-Soviet Central Asia. Post-Soviet Geography 36(6); 351-370.

Sobel, E.R., M. Oskin, D. Burbank, and A. Mikolaichuk. 2006. Exhumation of basement-cored uplifts: Example of the Kyrgyz Range quantified with apatite fission track thermochronology. Tectonics 25(2); 1-17.

Sobel, E.R., and T.A. Dumitru. 1997. Thrusting and exhumation around the margins of the western Tarim Basin during the India-Asia collision. Journal of Geophysical Research 102; 5043-5063.

Sotnikova, M.V., A.E. Dodonov, and A.V. Pen'kov. 1997. Upper Cenozoic bio-magnetic stratigraphy of Central Asian mammalian localities. Palaeogeography, Palaeoclimatology, Palaeoecology 133; 243-258.

Southern Asia (Political) map. 2004. Perry-Castañeda Library Map Collection, The University of Texas at Austin, University of Texas Libraries. Accessed September 2014.

Stilson, K.T., S.S.B. Hopkins, and E.B. Davis. 2016. Osteopathology in Rhinocerotidae from 50 million years to the present. PLOS ONE 11(8): e0160793.

Tapio, M., N. Marzanov, M. Ozerov, M. Cinkulov, G. Gonzarenko, T. Kiselyova, M. Murawski, H. Viinalass, J. Kantanen. 2006. Sheep mitochondrial DNA variation in European, Caucasian, and Central Asian areas. Molecular Biology and Evolution, 23(9); 1776-1783.

Tarasov, S.A. 1970. Cenozoic geology and neotectonics of the Tien Shan (in Russian): Frunze (Bishkek), Ilim, 211 p.

Thompson, S.C., R.J. Weldon, C.M. Rubin, K. Abdrakhmatov, P. Molnar, G.W. Berger. 2002. Late Quaternary slip rates across the central Tien Shan, Kyrgyzstan, central Asia. Journal of Geophysical Research 107(B9); 2203.

Turner, A., M. Antón, and L. Werdelin. 2008. Taxonomy and evolutionary patterns in the fossil Hyaenidae of Europe. Geobios 41(5); 677-687.

Valli, A.M.F. 2005. Taphonomy of the late Miocene mammal locality of Akkaşdağı, Turkey. In Sen S. (ed.), Geology, mammals and environments at Akkaşdağı, late Miocene of Central Anatolia. Geodiversitas 27(4); 793-808.

Van Valkenburgh, B. 1988. Trophic diversity in past and present guilds of large predatory mammals. Paleobiology 14(2); 155-173.

Vislobokova, I., M. Sotnikova, and A. Dodonov. 2003. Bio-events and diversity of the Late Miocene-Pliocene mammal faunas of Russia and adjacent areas. In: Distribution and Migration of Tertiary Mammal in Eurasia, DEINSEA 10; 563-574.

Voorhies, M.R. 1969. Taphonomy and population dynamics of an early Pliocene vertebrate fauna, Knox County, Nebraska. Rocky Mountain Geology 8;1-69.

Wack, M.R., S.A. Gilder, E.A. Macaulay, E.R. Sobel, J. Charreau, A. Mikolaichuk. 2014. Cenozoic magnetostratigraphy and magnetic properties of the southern Issyk-Kul basin, Kyrgyzstan. Tectonophysics 629; 14-26.

Wang, Y., T. Deng, and D. Biasatti. 2006. Ancient diets indicate significant uplift of southern Tibet after ca. 7 Ma. Geology 34(6); 309-312.

Weldon, R.J. 1986. The late Cenozoic geology of Cajon Pass: Implications for tectonics and sedimentation along the San Andreas fault, Ph.D. thesis, 400 pp., California Institute of Technology, Pasadena, California.

Zabelina, I.V., I.Y. Koulakov, and M.M. Buslov. 2013. Deep mechanisms in the Kyrgyz Tien Shan orogeny (from results of seismic tomography). Russian Geology and Geophysics, 54(7); 695-706.

Zdansky, O. 1925. Fossil Hirsche Chinas. Palaeontologia Sinica C 2; 1-94.

Zhang, Z-Q. and R. Yang. 2016. Morphology and taxonomy of *Gazella* (Bovidae, Artiodactyla) from the Late Miocene Bahe Formation, Lantian, Shaanxi Province, China. Vertebrata PalAsiatica 54(1);1-20.

Zhu, Y., L. Zhou, D. Mo, A., Kaakinen, Z. Zhang, and M. Fortelius. 2008. A new magnetostratigraphic framework for late Neogene Hipparion Red Clay in the eastern Loess Plateau of China. Palaeogeography, Palaeoclimatology, Palaeoecology 268(1-2); 47-57.